Retrospective and Emergency Dosimetry in Response to Radiological Incidents and Nuclear Mass-Casualty Events: A Review

I.K. Bailiff[1], S. Sholom[2] and S.W.S. McKeever[2]

[1] Department of Archaeology, University of Durham, Dawson Building, South Road, Durham, DH1 3LE, UK.
[2] Department of Physics, Oklahoma State University, Stillwater, OK 74078, USA.

HIGHLIGHTS

Review of the use of luminescence and electron paramagnetic resonance in retrospective and emergency dosimetry.

Optically stimulated luminescence (OSL), thermoluminescence (TL) and Electron Paramagnetic Resonance (EPR) results on biological and physical materials.

Descriptions of use in emergency and retrospective dosimetry, following large-scale radiological events.

ABSTRACT

This paper reviews recent research on the application of the physical dosimetry techniques of electron paramagnetic resonance (EPR) and luminescence (optically stimulated luminescence, OSL, and thermoluminescence, TL) to determine radiation dose following catastrophic, large-scale radiological events. Such data are used in dose reconstruction to obtain estimates of dose due to the exposure to external sources of radiation, primarily gamma radiation, by individual members of the public and by populations. The EPR and luminescence techniques have been applied to a wide range of radiological studies, including nuclear bomb detonation (e.g., Hiroshima and Nagasaki) nuclear power plant accidents (e.g., Chernobyl), radioactive pollution (e.g., Mayak plutonium facility), and in the future could include terrorist events involving the dispersal of radioactive materials. In this review we examine the application of these techniques in 'emergency' and 'retrospective' modes of operation that are conducted on two distinct timescales. For emergency dosimetry immediate action to evaluate dose to individuals following radiation exposure is required to assess deterministic biological effects and to enable rapid medical triage. Retrospective dosimetry, on the other hand, contributes to the reconstruction of doses to populations and individuals following external exposure, and contributes to the long-term study of stochastic processes and the consequential epidemiological effects. Although internal exposure, via ingestion of radionuclides for example, can be a potentially significant contributor to dose, this review is confined to those dose components arising from exposure to external radiation, which in most studies is gamma radiation.

The nascent emergency dosimetry measurement techniques aim to perform direct dose evaluations for individuals who, as members of the public, are most unlikely to be carrying a dosimeter issued for radiation monitoring purposes in the event of a radiation incident. Hence attention has focused on biological or physical materials they may have in their possession that could be used as surrogate dosimeters. For EPR measurements, in particular, this includes material within the body (such as bone or tooth biopsy) requiring invasive procedures, but also materials collected non-invasively (such as clippings taken from finger- or toenails) and artefacts within their personal belongings (such as electronic devices of which smart phones are the most common). For luminescence measurements, attention has also focused on components within electronic devices, including smartphones, and a wide range of other personal belongings such as paper and other polymer-based materials (including currency, clothing, bank cards, *etc.*). The paper reviews progress made using both EPR and luminescence techniques, along with their current limitations.

For the longer-established approach of retrospective dosimetry, luminescence has been the most extensively applied method and, by employing minerals found in construction materials, it consequently is employed in dosimetry using structures within the environment. Recent developments in its application to large-scale radiation releases are discussed, including the atomic bomb detonations at Hiroshima and Nagasaki, fallout from the Chernobyl reactor and atmospheric nuclear bomb tests within the Semipalatinsk Nuclear Test Site and fluvially transported pollution within the Techa River basin due to releases from the Mayak facility. The developments made in applying OSL and TL techniques are discussed in the context of these applications. EPR measurements with teeth have also provided benchmark values to test the dosimetry models used for Chernobyl liquidators (clean-up workers), residents of Semipalatinsk Nuclear Tests Sites and inhabitants of the Techa River basin.

For both emergency and retrospective dosimetry applications, computational techniques employing radiation transport simulations based on Monte Carlo code form an essential component in the application of dose determinations by EPR and OSL to dose reconstruction problems. We include in the review examples where the translation from the physical quantity of cumulative dose determined in the sampled medium to a dose quantity that can be applied in the reconstruction of dose to individuals and/or populations; these take into account the source terms, release patterns and the movements of people in the affected areas. One role for retrospective luminescence dosimetry has been to provide benchmark dose determinations for testing the models employed in dose reconstruction for exposed populations, notably at Hiroshima and Nagasaki. The discussion is framed within the context of the well-known radiation incidents mentioned above.

1. Introduction

1.1. Disasters and mass-casualty events

Hurricanes and tornadoes, floods and tsunamis, earthquakes and volcanic eruptions, nuclear power station accidents and terrorist events – mass-casualty disasters affecting modern society come in many different guises and afflict all countries. Social scientists, scientists and politicians alike are being forced to study and examine societies' vulnerabilities, preparedness and response to such events in attempts to mitigate effects and improve community resilience. Since such events appear to be increasing in frequency, whether via natural forces or man-made efforts, communities throughout the world are taking seriously all possible scenarios in efforts to be prepared (NRC, 2006 and Kohn et al., 2012).

Independent of the cause of a disaster there are several common aspects of all mass-casualty events that shape how the event and the response to it unfold, and which have led to numerous specialist research areas (Fig. 1). The overlap between understanding a community's vulnerability and how it can subsequently respond to the incident leads to an assessment of how prepared the community is to cope with the event.

FIG. 1

Some disasters, however, present certain considerations that are not seen in all disaster types - specifically, the preparedness and response necessary for radiological or nuclear disasters (Jaworska, 2009 and Coleman et al., 2015). Such events, although fortunately rare, can present major consequences that confound the normal response planning and compound the difficulties presented to emergency responders and medical personnel. Although an "all-hazards" response is necessary, coping with physical trauma and infrastructure destruction, emergency responders and medical personnel also have to deal with the effects of the potential exposure to radiation by citizens and the possibility of persistent elevated levels of above-background radiation due to contamination (e.g., Grace et al., 2011). Therefore, in addition to the adverse physical and psychological effects resulting from the traumatic event of the disaster itself, those affected have the induced stress and potential medical complications caused by the possibility of radiation exposure, both during and after the event. A recent example is the disaster that befell the citizens of northeast Japan caused by the Great East-Japan Earthquake of March 11th, 2011. The citizens of the Tohoku district of the Japanese main island suffered a triple blow from the original earthquake, the resulting tsunami, and the destruction of the Fukushima Daiichi Nuclear Power Plant with subsequent widespread release of radioactive contaminants (e.g., Report, 2011, von Hippel, 2011, Hirose, 2012,

Ohnishi, 2012 and Eisler, 2013; Tominaga et al., 2014). While the debate over the vulnerability assessment and preparedness concerning the Fukushima disaster continues, the response to the disaster has been closely monitored and is well documented (e.g., Eisler, 2013 and Dauer et al., 2014).

The types of mass casualty event involving large-scale exposure of the population are described in several publications. For example, Jaworska (2009) and Waller and van Maanen (2015) discuss possible terrorist-related events, including Improvised Nuclear Devices (INDs), Radiological Dispersive Devices (RDDs) and Radiological Exposure Devices (REDs). Additionally, one might have accidents caused by abandoned or orphaned radiological sources (e.g., from radiotherapy sources from hospitals, or industrial sources; Lubenau and Strom, 2002). Finally, there are large-scale nuclear power plant accidents (Three Mile Island, Chernobyl and Fukushima) and, of course, many lessons have been learned with respect to dosimetry from the intentional use of nuclear weapons at Hiroshima and Nagasaki.

While the details depend upon the situation, in principle the dosimetry requirements are the same in each of the above scenarios. In both the short-term and long-term aftermaths of any radiological or nuclear disaster, an assessment of the dose received by individuals is essential. In the immediate period following the event the most urgent radiological assessment requirement is triage in which the "worried-well" can be separated from those who require more detailed medical attention and, possibly, intervention. In the long-term, longitudinal health monitoring of the exposed members of the population, i.e., those exposed either during or after the initial radiation release, is required both for reasons of health care to the individual and for epidemiological studies of the long-term health consequences of radiation exposure. Since it is highly unlikely that members of the public will be equipped with individual radiation dose monitors or dosimeters, innovative efforts are required to assess individual, population and environmental radiation exposure. This can be done in one of two principal ways. Although both may be classed as "retrospective dosimetry", for the purposes of the present discussion we define two categories of retrospective dose assessment, namely:

- Emergency dosimetry: the immediate evaluation of dose to individuals. The targets in emergency dosimetry are deterministic effects and rapid triage. The main component of dose is due to external exposure.
- Retrospective dosimetry: reconstruction of dose weeks-to-years (tens of years) after exposure. The targets in retrospective dosimetry are stochastic effects and epidemiology. Both external and internal (due to consumption of food and drink contaminated by radionuclides) exposures may contribute to the cumulative doses; we deal here only with the component

due to external exposure. Because many individual dosimetric techniques cannot be used significant times after exposure due to fading of corresponding radiation-induced signals, the special peculiarity of retrospective dosimetry is reconstruction of spatial patterns of dose in the exposed environment via assessment of doses to buildings and structures, with accompanying modelling to take account of population movement and behavior.

We might note also that the target doses for two types of dosimetry are quite different: viz. ~2 Gy (or a range 0.5–10 Gy) for emergency dosimetry and much lower levels of dose for retrospective dosimetry. Other similar but slightly different definitions may be used elsewhere (e.g., Swartz et al., 2007 and Ainsbury et al., 2011).

A "Top Ten" list of radiation protection challenges for 2011 included several that impinge upon emergency management during a large-scale radiological event, namely Dose Reconstruction and Epidemiology, Calculation Dosimetry, Nuclear Terrorism and Biological Dosimetry (McDonald, 2010). Similarly, a 'table-top' exercise dealing with exposure of the public caused by a hypothetical release of radioactive cesium in Toronto, Canada, listed the "requirement for rapid identification of casualties and assessment of the severity/dose" and the "need for guidance of dose dependent triage protocols" among the identified gaps in the community's ability to respond (Wilkinson et al., 2010). As pointed out by González (2007), the potential for overexposure of individuals, either intentional or accidental, has generated the need for capabilities to determine absorbed dose to those individuals following such events.

1.2. Emergency dosimetry

Numerous reports, publications and guidelines emphasize the need for the availability of dose assessment tools, and their rapid deployment, immediately following a radiological or nuclear event. Specifically required are "Tools to rapidly triage individuals needing medical attention and to intelligently direct medical treatment to those needing immediate care …. " (JIWG, 2005). The numbers of people to be assessed in this way may be in the many thousands, or even millions. When coupled with the general population's fear of radiation this would present a significant problem to medical authorities. Psychological factors such as fear of radiation also extends to emergency personnel who may make incorrect or inappropriate decisions based on their lack of understanding of radiation contamination and exposure and its effect on human health. If not addressed, hospitals and other first-responder medical-care units may be overwhelmed or be made ineffective as a result of an inundation of patients wishing to be assessed for

radiation exposure. To counter this, as noted in the JIWG (2005) report and in more recent summaries (Coleman et al., 2015), the development of methods of radiation exposure triage or screening for deployment in community health-care facilities is critical in order to separate the worried well from those more seriously affected.

Surviving populations following radiological or nuclear mass-casualty events may exhibit a range of radiation exposure health symptoms, such as psychological distress, acute radiation syndrome (ARS), and more serious, life-threatening problems, all compounded by the possibility of physical injury. The purpose of the triage is therefore to separate the "worried well" from those who require some degree of medical intervention. The US Department of Homeland Security (DHS) describes multiple scenarios involving radiological exposure of the public and estimate that the ratio of the worried well to those whose health is actually compromised may vary from approximately 5:1 to 10:1.

Table 1

The required triage levels have been discussed in multiple publications and reports (JIWG, 2005, Alexander et al., 2007, Simon et al., 2007, Rea et al., 2010, Jaworska et al., 2014a and Jaworska et al., 2014b). For this paper we adopt the levels described in the MULTIBIODOSE project, as shown in Table 1. In reviewing Table 1 it is clear that the most critical triage dose level is 2 Gy, above which it is advised that individuals be referred for follow-up medical care and possible intervention. Below 2 Gy, individuals may be advised to return home for the time being. In this way critical medical facilities will be free to treat patients with more severe and/or critical injuries. The selection of 2 Gy as the critical triage level is supported by data from the Chernobyl victims. Guskova et al. (1988) report that of 31 patients with an evaluated dose of <2.1 Gy, no deaths were recorded. However, for doses >2.1 Gy, the number of deaths progressively increased as the dose increased (1 death for doses 2.2–4.1 Gy; 7 deaths for 4.2–6.4 Gy; and 20 deaths for 6.1–16.0 Gy).

Sullivan et al. (2013) describe an idealized model for triage and high-throughput screening of patients after a large-scale radiological incident. The scheme described by these authors is illustrated in Fig. 2. In this model, two screening levels are conceptualized – so-called Point-of-Care (PoC) screening, followed by a High-Throughput (HT) screening for those individuals identified in the PoC process to have been potentially exposed to a dose >2 Gy. Technical requirements of the two screening levels have been proposed by the US Department of Health and Human Services, Biomedical Advanced Research and Development Authority (BARDA) and are described in Table 2.

Table 2

The characteristics of the PoC and HT emergency dosimetry methods to be used after a radiological incident are described by Sullivan et al. (2013) and include simple sample collection and preparation, field-ready, short time to result, high capacity, standardized method (easily comparable across laboratories; not experimental), radiation-specific (not affected by confounding environmental elements), low inter- and intra-variation, low uncertainty, stable, and inexpensive. Finding a dosimetry system that complies with all these characteristics is a non-trivial task. Indeed, as discussed by Flood et al. (2014), while it is feasible to systematically triage such large numbers of people, the overall task is daunting.

In the search for processes that comply with these requirements a variety of dosimetry methods have been proposed. These include both physical dosimetry and biological dosimetry. Swartz et al. (2011) note that both techniques have the ability to assess absorbed dose at the level of the individual but bring different advantages and disadvantages.

Physical dosimetry methods discussed here are electron paramagnetic resonance (EPR), thermoluminescence (TL) and/or optically stimulated luminescence (OSL). The basic principle of each of these assessment methods is that with certain materials (primarily insulating materials) the energy absorbed from exposure to radiation creates electron-hole pairs within the material and these subsequently become localized ("trapped") at atomistic or molecular defects. In the case of EPR trapped electrons with unpaired spins result in a radiation-induced EPR signal. In favorable circumstances, the induced-EPR signal is stable (long-lived) and its intensity is proportional to the dose received.

In TL and OSL, electrons trapped at one defect site may be induced to recombine with holes trapped at a different site by the application of external energy – i.e., heat with TL; light with OSL. Luminescence results when the recombination process is radiative. If conditions are favorable, the luminescence signal (TL or OSL) is stable, and the intensity is proportional to the absorbed radiation dose. Thus, with EPR, TL or OSL one has the opportunity to evaluate the dose of radiation absorbed by examining EPR, TL or OSL signals from materials that may be found on an individual or in their personal belongings. A great deal of research in this area has been performed to find suitable materials for these applications. EPR dosimetry has focused primarily, but not exclusively, on biological matter. The most studied is tooth enamel while other research has examined clippings from human fingernails and/or toenails. In some cases, the EPR signals from personal belongings have been assessed, for example, from the glass screen of a smart phone.

TL and OSL techniques have also occasionally been applied to human tooth enamel and nails, with less success than EPR. However, the main focus of these methods has

been on non-biological materials that may be found on a person. Example materials include items of clothing, shoes, contents of wallets and purses, electronic and other components from personal electronic devices (e.g., phones).

Biologically based dosimetry relies upon identification and quantification of induced biological effects (biomarkers) in an individual as a result of radiation exposure. It has the potential advantage over physical dosimetry in that it measures a biological effect of the absorbed dose, not just the absorbed dose. However, such effects may vary from individual to individual despite exposure to the same level of radiation. The targets used to quantify the effects of the radiation include chromosomal aberrations due to DNA single- and double-strand breaks, protein cross-links, etc. Most of this type of damage can be repaired by the body's own repair mechanisms but, if miss-repaired, chromosomal aberrations can result. Methods to assess such biological damage include dicentric chromosome aberrations (DCA; often referred to as "the gold standard"), translocation analysis using painting techniques (fluorescence in-situ hybridization, FISH), and premature chromosome condensation and cytokinesis-block micronuclei (CBMN) assay (Blakely et al., 2005, Alexander et al., 2007, Simon et al., 2010, Ainsbury et al., 2011, Crespo et al., 2011, Fenech, 2011 and Wilkins et al., 2011) among others. Recent studies have also examined the potential of an assay based on protein expression in peripheral blood serum (Deperas-Kaminska et al., 2014), with particular interest in skin irradiation as an indication of partial body exposure. In Europe, a large, multi-technique approach has been adopted with a network of biodosimetry and physical dosimetry labs being established. The network is called RENEB (Realizing the European Network of Biodosimetry) and its purpose is to provide standardized dosimetry service for emergency situations (Kulka et al., 2012).

The purpose of this paper is to review of the physical dosimetry techniques for use in emergency (and retrospective) dosimetry applications. Biological dosimetry is not discussed further.

1.3. Retrospective dosimetry

The roots of retrospective luminescence dosimetry lie in work dating back to the early 1960s when it was realized that granular quartz within fired ceramic roof tiles exposed to gamma radiation from the Hiroshima and Nagasaki bombs could be used as a tool for performing dosimetry many years after the exposure event had occurred (Higashimura et al., 1963). This seminal work laid the foundations, not only for radiological application, but also in leading to the identification of dosimeter minerals that subsequently proved to be of central importance to the development of luminescence dating (Aitken, 1985, Aitken, 1998 and Bötter-Jensen et al., 2003). As discussed in more detail below, the application of luminescence as a retrospective

dosimetry technique has made important contributions to the testing of computational dosimetry models developed for the Hiroshima and Nagasaki bomb detonations, and this role has been replicated in subsequent investigations of significant radiological events affecting human populations and where the physical scale of the events extended from the regional (the Nevada and Semipalatinsk Nuclear Test Sites and the Mayak Plutonium Facility) to the global (Chernobyl and potentially the Fukushima reactors) via, in the case of fallout, the transfer of radionuclides carried by atmospheric transport mechanisms (Bennett, 2002 and Simon and Bouville, 2002). The basis of retrospective EPR dosimetry techniques also originated in the 1960s with the pioneering work of Swartz and colleagues (Swartz, 1965 and Brady et al., 1968) who observed stable radiation-induced EPR signals in calcified tissues exposed to ionizing radiation doses. EPR tooth dosimetry research started to grow rapidly after the Chernobyl accident in 1986 (Aldrich and Pass, 1988, Shimano et al., 1989 and Ikeya and Ishii, 1989), which resulted in maturation of the EPR technique with tooth enamel. The technique has been verified through several intercomparisons (Chumak et al., 1996, Wieser et al., 2000a, Wieser et al., 2000b, Wieser et al., 2005, Wieser et al., 2006, Hoshi et al., 2007, Ivannikov et al., 2007 and Fattibene et al., 2011) and was applied for dose reconstruction of A-bomb victims (Ikeya et al., 1984 and Nakamura et al., 1998), Chernobyl liquidators (Chumak et al., 2005, Chumak et al., 2007 and Chumak et al., 2008), the population in territories contaminated due to the Chernobyl accident (Skvortzov et al., 1995, Skvortzov et al., 2000, Ivannikov et al., 1997, Ivannikov et al., 2004b and Ivannikov et al., 2014), residents near the Semipalatinsk Nuclear Test Site (SNTS, Kazakhstan) (Zhumadilov et al., 2006, Zhumadilov et al., 2007, Zhumadilov et al., 2009, Zhumadilov et al., 2011a, Zhumadilov et al., 2011b, Zhumadilov et al., 2013 and Zhumadilov et al., 2016; Ivannikov et al., 2002, Ivannikov et al., 2006, Pivovarov et al., 2002, Pivovarov et al., 2007 and Sholom et al., 2007a), and the inhabitants of the Techa River basin affected by the operation of the Mayak Production Association (Romanyukha et al., 1996, Degteva et al., 2005, Degteva et al., 2015, Volchkova et al., 2011 and Shishkina et al., 2011).

In the application of luminescence, samples for testing have been obtained mostly, but not exclusively, from buildings that were present at the time of the onset of exposure to radiation from radionuclides introduced to their environment and which subsequently remained intact and in a fixed location. In concluding a previous review (Bailiff, 1997), the potential for validating computational dosimetry models applied in dose reconstruction had been exemplified by the Hiroshima and Nagasaki study, but in the case of Chernobyl and Techa River studies recently underway at that time, it had been recognized that the largely ad hoc experimental procedures that had been applied required underpinning by an agreed

methodology. Since there are relatively few laboratories engaged in experimental retrospective dosimetry research, and the number of potential applications small, the body of literature is not large. Thus, for the application of luminescence techniques, an emphasis is placed in this review on samples from fixed structures and, in particular, to studies during the last decade that have advanced the integration of the basic techniques of absorbed dose determination to fulfil the aim of developing a set of deployable tools for use in dose reconstruction (ICRU, 2002). Such contributions are being made in major studies related to Hiroshima and Nagasaki, Chernobyl, Techa River and the Semipalatinsk Nuclear Test Site, and application to the Fukushima accident is now on the horizon. The methodological developments brought about in each of the main applications mentioned are discussed in the context of contributing to the broader research questions set by the needs of dose reconstruction.

EPR dosimetry with teeth is discussed relative to two possible applications. In the first case, the EPR technique estimates the dose to an individual, which can be used directly in epidemiological and other radiation-related studies. Also, EPR dosimetry may be used to provide benchmark values of dose that check the analytical methods of dose reconstruction (Chumak et al., 2005 and Degteva et al., 2015).

1.4. Measured quantities in emergency and retrospective dosimetry

In emergency situations the primary concerns are deterministic effects, characterized by clinical reaction of cells and tissue to absorbed radiation. As expressed in NCRP Report 132 (NCRP, 2000) effective dose (in Sieverts, Sv) is not the appropriate quantity for assessing deterministic effects. Instead the radiation protection quantity of interest is the gray-equivalent (Gr,t), defined as the absorbed dose, D$_{r,t}$ (i.e., the energy per unit mass imparted to the tissue t), modified by the dimensionless relative biological effectiveness (RBE, R$_{r,t}$). The RBE is defined as the ratio of the dose of radiation of type r that yields the same biological effect as a reference dose. Hence, R$_{r,t}$ is both radiation type and tissue dependent. Normally low linear energy transfer (LET) radiation such as ^{60}Co gamma or 250 kVp x-rays is used to provide the reference exposure. Thus, the gray-equivalent for tissue t absorbing dose D$_{r,t}$ for radiation of type r is:

$$G_{r,t} = R_{r,t}D_{r,t}, \qquad (1)$$

where, G$_{r,t}$ is the quantity measured by biodosimetry methods and D$_{r,t}$ is the quantity measured by physical dosimetry methods. However, for the radiation types mostly of interest in emergency dosimetry, R$_{r,t}$ = 1 and thus Gr,t and Dr,t are equivalent and are both expressed in units of gray (Gy). For R$_{r,t}$ ≠ 1, R$_{r,t}$ depends on the biomarker or biological end-effect of concern, as well as the radiation type. For

some radiation emergencies neutrons may be an important component of the radiation field (for example, in an improvised nuclear device, IND). With the exception of neutron irradiation and assuming penetrating (low-LET) radiation, however, an approximation to gray-equivalent can be made by considering absorbed dose only.

It is important to realize that in physical dosimetry the measured quantity is the dose absorbed by the physical dosimeter, $D_{r,P}$. What is really needed for triage, however, is the "whole-body averaged" absorbed dose (or gray–equivalent). For this purpose a whole-body averaged absorbed dose, $D_{r,WB}$, can be defined as:

$$D_{r,WB} = (\Sigma_t D_{r,t})/N, \qquad (2)$$

where, $D_{r,t}$ is the dose absorbed by a certain tissue t within the body and the sum is over N such tissues, yielding a "whole-body average". In practice the chosen points could be critical, radiation-sensitive organs as listed by ICRP Report 103 (ICRP, 2007). In any case, what is needed is the ability to convert the cumulative dose measured using physical dosimetry $D_{r,P}$, to the whole-body dose $D_{r,WB}$, using dose conversion coefficients Cr, namely:

$$D_{r,WB}=C_r D_{r,P.} \qquad (3)$$

Critical organs include the blood forming organs, reproductive organs, thyroid, and others (ICRP, 2007). The dose thresholds in Table 1 refer to whole-body dose and not organ-specific dose for which the triage levels could be different.

There have been some attempts to determine organ doses $D_{r,t}$ and whole-body dose $D_{r,WB}$ from physical dosimetry measurements, $D_{r,P}$, using Monte Carlo calculations. For example, photon dose conversion coefficients C were calculated for doses in human teeth by Ulanovsky et al., 2005, Takahashi et al., 2001 and Takahashi et al., 2002 and Takahashi and Sato (2012). Khailov et al. (2015) performed similar calculations of conversion coefficients for doses to human fingernails. Similar calculations to obtain the dose to ceramic components within personal electronic devices for a particular external exposure have been performed by Eakins and Kouroukla (2015) and Eakins et al. (2016). Generally, all these authors use a virtual, computerized phantom and Monte Carlo methods to simulate the dose absorbed by, for example, teeth, fingernails or components of a smart phone, and the doses absorbed by various critical internal organs under a variety of exposure conditions. The indications from these simulations are that particular organs can receive doses higher than or less than (C > 1, or <1) the recorded physical dose (in teeth, fingernails or in electronic components), depending on the specific circumstances of the exposure and locations of the teeth/nails/electronic devices. Eakins and Kouroukla (2015) noted that isotropic irradiation, which may be the most realistic case, gave the

closest agreement between surface dose (as calculated for a smart phone on the surface of the person's body) and the average, whole-body dose. Similar results were found for the simulations of the whole-body dose and dose to teeth (Takahashi et al., 2001 and Takahashi et al., 2002; Takahashi and Sato, 2012), and fingernails (Khailov et al., 2015).

For retrospective dosimetry, the measurement data are to be applied ultimately to the study of stochastic effects (e.g., cell mutation, cancer induction) in individuals (EPR) or populations (luminescence). While the measured quantity of interest for these applications is absorbed dose (in Gy), the total absorbed dose, D_T, registered by minerals within a ceramic building material or by a tooth within an individual's mouth is the dose due to natural and artificial sources of radiation. For these minerals, the total dose, D_T, is the sum of: (a) the cumulative 'background' dose, D_{BG}, arising from radiation emitted by lithogenic radionuclides (i.e., ^{238}U, ^{235}U, ^{232}Th and progeny, and ^{40}K) within the surrounding media, including, as a relatively minor contributor, incident cosmic radiation, and (b) a cumulative dose, D_X, arising from radiation emitted by radionuclides introduced artificially into the local environment (e.g., from a nuclear device or fallout). The quantity D_T can be determined by applying established dose evaluation procedures to luminescent minerals such as granular quartz extracted from ceramic building material (e.g., brick and tile) and teeth in the case of EPR (ICRU, 2002, Chap. 3).

In the case of luminescence techniques applied to ceramic materials, the cumulative background dose, D_{BG}, is the product of the age, A, of the ceramic material since manufacture and the combined effective annual dose-rate to coarse quartz grains arising from beta and gamma radiation emitted by the lithogenic radionuclides and from cosmic radiation. In most applications the use of coarse quartz grains (e.g., >100 μm diameter, etched in HF acid) to determine D_T is preferred because it improves the resolution of D_X by reducing the proportion of D_T contributed by D_{BG} and it also avoids the effects of athermal fading exhibited by other minerals, notably members of the feldspar group that are commonly present in ceramics. The stability of trapped charge in quartz at ambient temperatures (20 °C) far exceeds the requirements needed for the timescale of retrospective dosimetry (ICRU, 2002), providing the ceramic was not subsequently heated to elevated temperatures (>100 °C) for prolonged periods following the start of exposure to artificial radionuclide sources.

The dose-rate associated with the lithogenic radionuclides within the environment is determined using a combination of experimental measurement and calculation (ICRU, 2002), and it typically amounts to several tens of mGy per decade. Consequently the age of the building selected affects the precision with which D_X can be determined, particularly where it is less than D_{BG} (Fig. 45 in ICRU, 2002).

Once subtracted from the total dose, D_T, the cumulative dose due to artificial sources of radiation, D_X, is obtained where,

$$D_X = D_T - D_{BG.} \qquad (4a)$$

If coarse quartz grains, treated to remove their outer layer, are used to determine DT, the alpha dose can be neglected (Aitken, 1985) and,

$$D_{BG} = A \, (\dot{D_\beta} \; + \; \dot{D_\gamma} \; + \dot{D_c} \,), \qquad (4b)$$

where, A represents the age of the ceramic and the other terms represent the effective dose rate components (β, γ and cosmic, as indicated by the subscripts) to coarse grains. Natural quartz typically contains very low quantities of lithogenic radionuclides, usually giving rise to a contribution of less than 0.05 mGy a^{-1}, but this may not always be the case. The components of Equation (4b) are calculated as average values to the mineral grains extracted from a defined sample volume and location (e.g., a slice of brick located in a wall between 2 and 3 cm beneath the external face of the brick at a height of 1 m above ground level). Providing there is a measurable difference between D_T and D_{BG}, Equation (4a) provides an estimate of cumulative dose, D_X, in the sampled volume since the onset of exposure to radiation from artificial sources. Various terms have been adopted in the literature to describe D_X, including 'transient' dose, 'anthropogenic' dose and 'accident' dose.

When the determinations of D_X are made using relatively thin samples taken at progressively greater depths into a brick or wall, a depth-dose profile can provide information related to the time-averaged source energy if the source geometry is known (the form of the profile depends on both source energy and geometry; Meckbach et al., 1996). If samples can be obtained at different elevations above ground level (e.g., 10m), information on source configuration can also be gleaned (Bailiff, 1999 and Bailiff and Stepanenko, 2001).

To make use of determinations of D_X in dose reconstruction studies, in particular for application to populations inhabiting land contaminated by fallout, the values of dose are translated to a more suitable quantity, usually as air kerma at a Reference Location. This translation is obtained by the application of a conversion factor CRL, the calculation of which is formulated to suit the particular application, as discussed further below. For a brick sample taken from a wall facing uniformly contaminated flat ground, C_{RL} is expected, in the simplest case, to have a value of about 2 at the surface, arising from the shielding by the wall of half of an infinitely extended source. Its value increases with sample depth (in the wall) as a consequence of the effects of attenuation, although in the sub-surface layers its value is expected to fall below 2 depending on the proportion of dose carried by photons of energy less than

~100 keV (where quartz exhibits an over-response with respect to the response at higher energies).

For application to dose reconstruction in urban environments contaminated by fallout, Jacob and Meckbach (1987) introduced the "Reference Location" as a point 1m above undisturbed ground containing a homogeneous distribution of artificial radionuclide sources, and this provides a point of comparison for cumulative dose estimates obtained using different methods. In addition, Meckbach and Jacob (1988) defined a location factor, f, as the quotient of the values of exposure dose at a specified location and at the Reference Location to account for modifications in fallout distribution that occur within a built environment and the effects of shielding, and they were calculated by performing Monte Carlo simulations for various environments (e.g., interior of buildings, etc.) and source distributions (e.g., on walls, tree foliage, etc.). The location factors were applied when using deterministic models (Jacob and Likhtarev, 1996, Golikov et al., 2002 and ICRU, 2002) to calculate the cumulative dose based on historic data derived from radionuclide concentration and/or dose rate measurements. By calculating the cumulative dose at the Reference Location, the models form a starting point for input to dose reconstruction models that ultimately take into account both dynamic human behavioral and environmental factors and apply computational modelling to obtain cumulative dose estimates to populations or cohorts living and moving within a built environment (e.g., Chumak et al., 1998).

For tooth enamel, the total dose is also the sum of several components, namely: (a) the background dose D_{BG} caused by environmental exposure, (b) an accidental dose D_X, (c) a dose D_{UV} arising from possible exposure to the UV component of solar light and (d) a dose D_{X-ray} caused by possible diagnostic and medical dental procedures. An extra dose component was detected in the teeth of some Techa Riverside residents; it was caused by ^{90}Sr incorporated in tooth tissue during the period 1949–1956 when significant radioactive releases into the Techa River from the Mayak Production Association (MPA) took place.

Equations (4a) and (4b) can be rewritten in the following way:

$$D_X = D_T - D_{BG} - D_{UV} - D_{X-ray} \qquad (5a)$$

$$D_{BG} = A_{te}\dot{D}_{BG} \qquad (5b)$$

where, A_{te} is the tooth enamel age and View the MathML source $\dot{D}_{BG}$ is the dose rate of the environmental exposure. The UV dose D_{UV} is usually observed in buccal parts of the front teeth (Ivannikov et al., 1997, Nakamura et al., 1998 and Sholom et al., 2000b), and this was a reason why only lingual parts of front teeth were

recommended to be used for dose reconstruction (IAEA, 2002). In the case of the X-ray dose, D_{X-ray}, two approaches have been proposed to account for this component. According to the first approach (Sholom et al., 1997, Sholom et al., 2000b and Aragno et al., 2000), the X-ray dose to a tooth is calculated as the product of the number of X-ray examinations delivered to the tooth and the mean dose deposited per examination. This approach requires knowledge of the mean dose in each case, which depends on operational parameters of the specific X-ray dental machine (high voltage, current, filtration, etc.) and may differ according to the machine used and the individual teeth. Examples of values of mean dose measured for typical dental X-ray machines used in Ukraine and Italy are given in Sholom et al. (1997) and in Aragno et al. (2000), respectively; similar mean doses may be obtained for dental X-ray machines used in other countries. However, the main drawback of this approach is that information about the number and type of lifetime-dental-X-ray examinations delivered to a specific tooth is not always available. Another approach (Sholom et al., 2002 and Sholom et al., 2007b) to overcome this possible issue relies on the fact that most dental X-ray machines produce photons with energy of a few tens of keV, which are attenuated significantly when passing through a tooth. However, the X-ray dental dose may be estimated by using a separate measurement of tooth lingual and buccal parts followed by applying a correction coefficient, if a difference in dose for the two parts of the tooth is detected.

More discussion about possible UV and X-ray dose components is provided in Section 2.1.2.2 below and further discussion can be found in the review by Fattibene and Callens (2010).

2. Physical dosimetry for emergency response

2.1. Electron paramagnetic resonance

The application of electron paramagnetic resonance to organic materials (biologically derived or synthetic) has been used as an emergency dosimetry tool for several decades (e.g. Nakajima, 1986 and Ikeya and Ishii, 1989). Indeed, electron paramagnetic resonance (EPR; also known as electron spin resonance, ESR) of biological materials (bone, tooth enamel and finger/toenails) has been a suggested method for retrospective assessment of absorbed dose to radiation accident victims almost since the beginning of the nuclear age (see Regulla, 2005). EPR detects the presence of unpaired electron spins within a substance. With bone, tooth enamel and finger/toenails, unpaired spins occur in the form of free radicals following the trapping of delocalized electrons induced by exposure to ionizing radiation. For example, in calcium-based biogenic material carbonate radicals of the type CO_2^- are generated during exposure to ionizing radiation giving rise to the opportunity to

detect such radiation-induced species using EPR to use this as a measure of the absorbed dose.

In the absence of a magnetic field the unpaired electrons populate an energy state corresponding to trapping by the free radical. In the presence of a strong magnetic field, however, the energy state splits corresponding to those states in which the electron spin is parallel (lower energy state) or anti-parallel (higher energy state) to the applied field. The degree of splitting is dependent upon the strength of the applied magnetic field. By application of a microwave field of the required frequency, transitions between the states can be induced with the consequent absorption of microwave power. At a fixed microwave frequency, one can scan the magnetic field until the energy separation between the lower and higher states is in resonance with the microwave energy, whereupon microwave absorption is observed. The strength of the absorption is related to the concentration of unpaired spins. Thus, by irradiating a specimen one can generate a radiation-induced microwave absorption signal the intensity of which is related to the absorbed dose. Normally, the first derivative of the absorption band is recorded as the magnetic field is swept. This is the EPR signal of interest (such as Fig. 3).

Fig. 3

In the materials of interest for EPR dosimetry it is often the case that the radiation-induced signal (RIS) has to be distinguished from any pre-existing background (BG) signals, and any signals induced by mechanical sampling (a mechanically induced signal, MIS). As a result, much of the developmental work on EPR of biological materials for retrospective dosimetry has concerned the identification of the RIS, BG and MIS, generating an understanding of the processes that cause variability of these signals, and developing processes by which they can be reliably separated from each other. The intensive work on the EPR of tooth enamel has led to this material becoming the leading candidate for EPR dosimetry in many accident situations (e.g., Kleinerman et al., 2006, Alexander et al., 2007, Gougelet et al., 2010, Nicolalde et al., 2010, Fattibene et al., 2011, Ainsbury et al., 2011 and Flood et al., 2014).

When applying EPR techniques to mass casualty events experience with and lessons learned from dose assessment in cases of small-scale radiation accidents, where just one or two people were exposed, provides information pertinent to applications of the same techniques to large-scale accidents. One of the earliest materials to be examined with EPR in this context is bone.

2.1.1. EPR of bone

The EPR spectra of bone have been studied for several decades. Sixty-seventy percent of bone mineral is carbonated calcium hydroxyapatite $Ca_{10}[(PO_4)_{6-x}(CO_3)_x$

][$(OH)_{2-y}$ $(CO_3)_y$], the hydroxyl end-member of the apatite group (Fattibene and Callens, 2010). The main EPR signals from this material, in the X-band (9 GHz), are shown in Fig. 3. The spectrum consists of an asymmetrical RIS signal, with amplitudes A1 and A2, and a highly variable, non-radiation-induced BG signal (Ciesielski et al., 2016). Also shown are the reference lines from Mn^{2+} (Ciesielski et al., 2014). The RIS is anisotropic (Brik et al., 2000) and is mainly caused by a CO_2^- radical, typical of calcified natural and synthetic bio-minerals (Callens et al., 1998).

2.1.1.1. Radiation-induced radicals

Among the other radicals that form in calcified tissue, in addition to CO_2^-, are included CO−, CO_3^{3-}, and CO_3^{3-} . More than one species can occur, but CO_2^- dominates after irradiation at room temperature. The signal is anisotropic and for the free radical typical g-tensor values are g_x = 2.0030 (x perpendicular to the molecular plane), g_y = 1.9970 (y parallel to the O-O axis), g_z = 2.0015 (z is the C_{2v} -symmetry axis). These values are fairly constant, independent of the crystalline environment surrounding the radical (Callens et al., 1998). The similarity of the g-values means that they overlap in the X-band producing a broad signal, with g-tensors perpendicular and parallel to the applied field being observed (A1 and A2, respectively, in Fig. 3). Greater resolution can be obtained by making measurements in the Q-band (Strzelczak et al., 2007).

The CO2− radicals can be found on hydroxyl (OH^-) sites, phosphate (PO_4^{3-}) sites, or surface sites (Callens et al., 1998) and each contribute to the net EPR signal. The same is true for all the other carbonate radicals noted above. Romanyukha et al. (2005) speculate that the radicals associated with the three different sites may have different dose dependences and therefore contribute to the complex, sample-dependent, dose dependencies sometimes observed in biogenic hydroxyapatites.

The dominance of the radiation-induced CO_2^- in the X-band EPR spectrum from bone allows this material to be used as dosimeter. This was first recognized by Brady et al. (1968) following the initial observation of EPR from bone by Gordy and colleagues a decade earlier (Gordy et al., 1955). Since those early publications the application of EPR to bone has been developed as a dosimetric method, especially in accident dosimetry (e.g., Desrosiers, 1993, Wieser et al., 1994, Breen and Battista, 1995, Pass, 1997 and Desrosiers and Schauer, 2001).

2.1.1.2. Use in accident dosimetry

EPR techniques have been applied to bone for the dosimetry of patients undergoing radiotherapy (e.g., Krefft et al., 2014) but it has also been used to assess the radiotherapy doses received in cases of accidental overexposure. An example of the latter application was described by Trompier et al. (2007a) in which the authors

examined pieces of rib bone removed from breast-cancer patients who had each experienced over-exposure (60–80 Gy) during radiotherapy, caused by faulty equipment.

Fig. 4(a) shows a typical EPR spectrum obtained with rib bone from one of the patients, clearly showing a strong RIS. Fig. 4(b) illustrates typical dose response curves for the RIS, for ^{60}Co gamma photons and 9 MeV electrons. The Institute for Radiological Protection and Nuclear Safety (IRSN) in France has specialized in this type of accident assessment and several example studies are available in the literature (e.g., Clairand et al., 2006 and Clairand et al., 2008). A similar accident assessment applying EPR to bone was carried out by Schauer et al. (1996) for an individual overexposed in a 3 MeV electron beam.

Fig. 4

Kinoshita et al. (2003) used bone from an amputated finger to assess the dose received by an accident victim exposed to ^{60}Co gamma radiation from a radiotherapy machine, revealing a received dose of around 20 Gy. In general, EPR measurements with bone are able to determine absorbed doses from 1-2 Gy, and above.

2.1.2. EPR of teeth

Although much has been learned from the EPR analysis of radiation-induced radicals from bone and its application in accident dosimetry, extraction of bone samples for analysis is a significantly invasive procedure and alternative biomaterials have been examined. Foremost among these in terms of application and technique maturity is the EPR of tooth enamel.

Hydroxyapatite constitutes 95–97% of tooth enamel and 70–75% of dentin (Desrosiers and Schauer, 2001), and the EPR signal from teeth is due to the same induced CO_2^- radicals as in bone (Zdravkova et al., 2005). The signal increases with absorbed radiation dose and is the main signal used in dosimetry. There are no known dose rate effects and the signal is reported to be very stable at room and body temperatures. The EPR spectrum from teeth is identical to that shown for bone in Fig. 3 and early challenges in the development of the EPR as a dosimetric method centered on reproducibility, sample preparation and measurement techniques, and the ability to identify and separate the BG and RIS components (e.g., Romanyukha and Regulla, 1996, Straume et al., 1997, Hayes et al., 1998, Sholom et al., 1998b, Sato et al., 2007, Romanyukha et al., 2000a and Lanjanian et al., 2008). As applications in retrospective dosimetry progressed (e.g., Ishii et al., 1990, Serezhenkov et al., 1992, Romanyukha et al., 1994, Straume et al., 1997, Chumak et al., 1999, Wieser et al., 2000b and Williams et al., 2007), so too did technique development. EPR of teeth is now a well-established method for evaluating absorbed doses to individuals under

many circumstances (Egersdorfer et al., 1996, Pass, 1997, IAEA, 2002, Simon et al., 2007, Trompier et al., 2010a, Fattibene and Callens, 2010, Ainsbury et al., 2011, Sullivan et al., 2013 and Degteva et al., 2015). The method has been tested against biodosimetry methods (e.g., Nakamura et al., 1998, Kleinerman et al., 2006 and Khvostunov et al., 2015) and conventional dosimeters (e.g., Romanyukha et al., 2000b), and in multiple inter-laboratory comparisons (e.g., Chumak et al., 1996, Wieser et al., 2000a, Wieser et al., 2005, Hoshi et al., 2007, Ivannikov et al., 2007 and Fattibene et al., 2011).

Most of the developments in EPR dosimetry of teeth were for purposes of retrospective dose evaluation and epidemiology. In more recent years, however, attention has turned to its value as an emergency dosimeter, and in this section we shall focus our attention on this application.

2.1.2.1. Radiation-induced radicals

Since the main mineral present in tooth enamel and dentine is the same as that in bone, i.e., carbonated calcium hydroxyapatite, radiation-induced CO_2^- radicals dominate (Fig. 5), with similar sample-dependent dose dependencies as found for bone (Desrosiers and Schauer, 2001, Romanyukha et al., 2000a and Romanyukha et al., 2005). Also, as discussed in a very detailed and useful review by Fattibene and Callens (2010), radiation-induced carbonate radicals (CO^-, CO_3^{3-}, and CO_3^-), oxygen radicals (O^-, O_2^-, and O_3^-) and phosphate radicals (PO_4^{2-}) can be expected.

Fig. 5

Teeth can be grouped into molars (including wisdom teeth), premolars, incisors and canines. Not all are equally suitable for EPR dosimetry. The outer layer of teeth is characterized by a thin layer of enamel in which the hydroxyapatite crystals grow perpendicularly from the dentin-enamel interface (Fattibene and Callens, 2010). Dentin consists of approximately 70% mineral and the rest is pulp, containing blood vessels and nerves. For this reason, the sensitivity of EPR from dentine is lower than that of enamel and dosimetry has centered on the enamel portion only. The organic material is usually removed mechanically with a dental bur or by chemical treatment before measurement.

As with bone, there are two main EPR signals from tooth enamel, namely the anisotropic signal from radiation-induced radicals (RIS; as discussed above) and a dose-independent, isotropic (g-value approximately 2.0045) background (BG) or native signal (Fig. 6). It is observed in the EPR spectra from both enamel and dentin (Pass et al., 1990). The origin of the native signal is unclear but may be related to organic material. Some authors (e.g., Sholom et al., 2000a and Romanyukha et al., 1999) have suggested a relationship between the native signal and carious (diseased)

material within the teeth. However, independent of its origin, chemical treatment during sample preparation has been shown to reduce the native signal in most cases.

Fig. 6

Most measurements for EPR dosimetry are performed in the X-band (9 GHz). Although finer resolution of the various components of the spectrum can be obtained with the higher-frequency Q-band (35 GHz), the loss of sensitivity caused by the use of smaller samples does not lead to an obvious advantage of Q-band over X-band. Lower-frequency L-band measurements have been adopted for in-vivo measurements, as described in a later section.

2.1.2.2. Confounding effects

There several potentially confounding effects that need to be accounted for when performing EPR dosimetry of teeth, some of which have already been alluded to. They include:

The native (background) signal: As noted, the native, or background, signal ($g = 2.0045$) appears to be related to the organic component in that it is decreased following removal of the organic material (Romanyukha et al., 2000a). However, other authors have also indicated that crushing to produce a finer grain size increases the strength of what appears to be the same BG signal (Haskell et al., 1997) leading some to suggest that whatever the origin of the native signal it appears to be related to the surface of the enamel (e.g., Romanyukha et al., 2000a). Others have observed a larger BG signal in diseased teeth suggesting a relationship with tooth caries (Sholom et al., 2000a and Romanyukha et al., 1999).

Organic material: Organic material contributes to the native signal. Dentine contains most of the organic material and clean separation of the enamel from the dentine is critical. Furthermore, the enamel itself contains a few percent of protein and other organic matter (Fattibene and Callens, 2010). Removal of the organic material can be achieved with chemical treatment. A typical treatment would involve mechanical separation using orthodontic tools in combination with treatment with a 5M–8M NaOH alkaline solution. Some researchers use an ultrasonic bath to speed up the treatment. Additionally, etching the surface of the enamel using acid (e.g., 20% acetic acid solution) along with frequent washing to remove residues is recommended to avoid parasitic EPR signal from surface impurities. All treated samples must be thoroughly dried to avoid microwave absorption by water. Other variants of these methods can be found in the literature, as thoroughly reviewed by Fattibene and Callens (2010).

Light and UV effects: The effect of UV light on the EPR signal from teeth has been studied by several authors (Liidja et al., 1996 and Sholom et al., 1998a). UV exposure produces a signal of significant strength (depending on wavelength) and of the same form as that produced by ionizing radiation (Fig. 7; Rudko et al., 2007). UV exposure produces different intensity native signals (i.e., the background signal, at g = 2.0045) compared with gamma irradiation (El-Faramawy, 2005). UVC (100–280 nm) radiation induces the strongest signal, but even UVB (280–315 nm) and UVA (315–400 nm), to which front teeth may be exposed during normal daily activities or during usage of UV lamps, can induce significant signals (Nilsson et al., 2001). UV dental instruments are an additional possible source of UV-induced signals. The UV-induced signals are complex (Sholom et al., 1998a and Jiao et al., 2007) and consist of stable and unstable components (Liidja et al., 1996, Nilsson et al., 2001 and Rudko et al., 2007). The unstable component can be removed by heating, while etching of the enamel surface can help remove the stable component since the UV penetration depth is small compared with that of ionizing radiation. However, as a result of these considerations, the outer parts (i.e., buccal sides) of the incisors and canines may be unsuitable for EPR dosimetry.

Fig. 7

The contribution of UV exposure to the radiation-induced signal can be as large as ~200 mGy equivalent per sunny day for the buccal sides of the front teeth (the "UV equivalent dose"; Sholom et al., 1998a). Notwithstanding that avoidance of the buccal side of the front teeth is advisable, and common practice, UV effects on all teeth have not been fully characterized. Sholom et al. (2010) observed three UV-related EPR signals (denoted R1, R2 and R3) that are induced only by UV exposure. These authors proposed that R1 (g = 2.011) be used to assess and account for the UV equivalent dose and they demonstrated the use of the method with teeth from Semipalatinsk-area inhabitants.

Energy Response and Medical X-rays: Desrosiers and Schauer (2001) discussed the photon energy dependence of tooth enamel and dentine and indicated that for photon energies of less than 0.1 MeV the relative response (compared with soft tissue) can be as high as 10.9 for enamel. Actual correction factors, however, will be significantly dependent upon incident photon energy and tooth location. Several research groups have calculated dose conversion coefficients for various photon energies for teeth, dependent upon where the tooth is located in the mouth (Takahashi et al., 2001 and Takahashi et al., 2002; Takahashi and Sato, 2012; Ivannikov et al., 2000, Ivannikov et al., 2004a, Wieser et al., 2002 and Ulanovsky et al., 2005).

Since teeth are several millimeters thick and of mineral composition one can expect a decrease in dose due to photon attenuation, from the outside to the inside (buccal to lingual), to a degree dependent upon the energy of the photon source. This has been examined by several authors (e.g., Schauer et al., 1994 and Sholom et al., 2007b and in the review by Fattibene and Callens, 2010).

Sholom et al. (2007b) obtained EPR depth-dose profiles following irradiation with a variety of photon sources, including low-to mid-energy X-rays and ^{60}Co and ^{137}Cs gamma sources, which (Fig. 8) indicate attenuation of the lower-energy photon sources, as expected. This raises the question of how irradiation with medical X-rays can be distinguished from irradiation with higher-energy photons, as might be expected during an accident. Aragno et al. (2000) averaged the signal from the entire tooth (including buccal and lingual parts) and estimated that a typical dental X-ray source, of 65 kVp, delivered the gamma-equivalent of ~2 mGy per exposure. Wieser et al. (2011) (see also Wieser, 2012) evaluated doses from medical X-rays to workers from the Mayak facility and found an average of ~10 mGy per medical examination, being higher (20–40 mGy) for examinations before 1970, compared to after 1970 (10–20 mGy). Sholom and Chumak (2008) estimate that a cumulative medical X-ray dose for a cohort of 65–75 year age group of Ukrainian residents, could be as high as 300–400 mGy. However, as shown by Sholom et al. (2007b), the absorbed dose in the buccal face was significantly higher than that in lingual face with, for example, 60% attenuation buccal-to-lingual for H60 X-rays. Similar observations were made by Wieser et al. (2011). Data from Sholom and Chumak (2008) indicate medical X-ray exposures of 400 mGy for the buccal face versus 250 mGy for the lingual face in the cohort of 65–75 year old Ukrainian residents. Thus, the best way to distinguish medical exposures from accidental, higher-energy exposures is to evaluate the depth-dose profile, even in the presence of a mixed signal (i.e., gamma exposure superimposed on a medical X-ray exposure). These doses are to be compared with the doses of interest for emergency triage, which are >0.5 Gy.

Fig. 8

Tooth disease: Since teeth are extracted for ex-vivo EPR analysis, it is necessary to be aware of the reason for the extraction. Diseased teeth can produce anomalous results and, as noted above, the presence of caries appears to increase the size of the BG signal (Sholom et al., 2000a and Romanyukha et al., 1999).

2.1.2.3. Non-X-band EPR dosimetry

Aside from X-band microwave measurements (9 GHz) several efforts have examined the use of higher-frequency Q-band (35 GHz) EPR spectroscopy. Such examples are not common, however, owing to the lack of availability of these more-expensive

spectrometers. The EPR spectra show improved resolution (Fig. 9) of the individual radicals but with greater complexity of the EPR spectra (e.g., Vanhaelewyn et al., 2002 and Strzelczak et al., 2007). Greater sensitivity potentially enables EPR measurements of small (2–10 mg) tooth fragments or powder removed from the patient by biopsy (Romanyukha et al., 2007a and De et al., 2013).

Fig. 9

The usefulness of the K-band (24 GHz) was examined by Santos et al. (2005), the rationale being that it was intermediate in frequency between the Q- and X-bands and may therefore retain some of the higher resolution of the former and the sensitivity of the latter, which was shown to be the case.

So far, however, there is little development in the use of K- or Q-bands in emergency dosimetry. The same cannot be said for the L-band, however, as described in the next section.

2.1.2.4. In vivo dosimetry

Despite the extensive work performed with X-band EPR dosimetry, the major drawback for emergency assessment purposes is the requirement to perform the measurements ex vivo, thereby requiring invasive tooth extraction. To overcome this problem there has been an extensive effort, especially by the group at Dartmouth College (USA), to develop in-vivo EPR dosimetry using the L-band (1.2 GHz). The L-band is necessary for in vivo dosimetry in order to reduce the large background microwave absorption due to moisture in the mouth. The concept of in vivo L-band EPR dosimetry was first mooted by Miyake et al. (2000) following experiments with mice. The first prototype demonstrated for use with humans was by Iwasaki, Swartz and colleagues (Iwasaki et al., 2005a and Iwasaki et al., 2005b). Since that time there have been significant developments in technique and equipment aimed at improving the signal-to-noise, increasing the sensitivity, and developing field-deployable, portable in vivo equipment.

The major developments have concerned the design of the resonator, along with tuning electronics. Tooth size, shape and overlap with other teeth all compromise the signal and thus resonator design has to be robust enough to account for, or minimize the effects of, these variations. While molar, pre-molar and canine teeth are all potential targets for in vivo dosimetry, practical developments have focused on incisors. Developments in both technique and equipment have been described in several summary documents (e.g., Swartz et al., 2007, Williams et al., 2010, Williams et al., 2011, Williams et al., 2014 and Sirota et al., 2013; Ivannikov et al., 2016; Guo et al., 2016 and Schreiber et al., 2016). Demidenko et al. (2007) examined the standard error induced by state-of-the-art in vivo (in 2007) measurements using ex vivo

irradiated teeth placed in the mouth of a volunteer in a gap in the dentition. Other studies included radiotherapy patients. Williams et al. (2007) examined reproducibility of the technique, primarily due to tooth placement within the resonator cavity. Measurements on volunteer patients who had not undergone irradiation and patients that had undergone total body irradiation treatments have produced encouraging results (Williams et al., 2014) and development of this approach continues. Possible confounding factors like EPR signals caused by tooth restorations or whitening treatments still have to be tested (Desmet et al., 2016).

Although all early developments were in laboratory settings, field-deployable spectrometer designs are emerging (Williams et al., 2011 and Williams et al., 2014). Nevertheless, the current equipment is large and likely to be expensive. To overcome this there is a recent design movement away from CW L-band EPR measurements to pulsed X-band measurements. Ikeya and Ishii (1989) proposed an early design of an X-band in vivo EPR spectrometer for teeth but the use of pulsed microwaves reduces the size of the probehead significantly (Sirota et al., 2013). The latest developments on these lines use a probehead (for insertion in the mouth) of just 30 mm with a mass of 220 g (Woflson et al., 2015; see Fig. 10).

Fig. 10

2.1.2.5. Sensitivity and minimum measurable dose

EPR sensitivity is governed by several factors, including the size of the tooth, the location in the mouth, the health of the tooth, and the energy of the incident radiation. Additionally, numerical procedures designed to separate the accident-induced signal from unwanted signals (including native signals but also natural radiation-induced and UV-induced signals), and procedures to minimize noise, etc., all play a part (e.g., Demidenko et al., 2007, Wieser et al., 2008, Sholom et al., 2010 and Ivanov et al., 2014). Finally, the linearity of the dose response and the interpolation procedures used to determine the unknown dose each contribute to the uncertainty and ultimately to the lowest dose that can be measured. Thus, the minimum doses published in the literature vary with circumstances. Ex vivo X-band dosimetry has developed sufficiently to the point that a typical minimum measureable dose (MMD) as low as 100 mGy can be achieved (e.g., Güttler and Wieser, 2008 and Wieser, 2012), with claims of MMD lower still in some cases (Desrosiers and Schauer, 2001 and Khvostunov et al., 2015). In vivo L-band dosimetry can produce sensitivities of around a few hundred mGy to 1 Gy (e.g., Swartz et al., 2007).

2.1.2.6. Use in dosimetry

Several protocols for the preparation of tooth enamel for ex vivo EPR dosimetry have been recommended. All have a similar outline and a typical procedure is illustrated in Fig. 11. The procedures can be lengthy, thereby reducing the utility as a triage method. Additionally, of course, the technique relies upon invasive procedures to extract a tooth. Perhaps as a result of this, there have been very few examples of emergency dosimetry using the EPR from tooth enamel ex-vivo using the general procedures as described above to separate the RIS. Rossi et al. (2000) applied EPR dosimetry to teeth from five victims of the Goiânia, Brazil, accident, evaluating doses that ranged from approximately 1 Gy to >16 Gy. Clairand et al. (2008) determined doses from radiation accidents in Dakar and Abidjan by taking biopsies of enamel from the molars of three patients involved in accidental exposure to 192Ir, and these indicated exposures of several Gy to the teeth and jaws. Ciesielski et al. (2007) examined tooth enamel from extracted teeth of radiotherapy patients and reconstructed doses using ex-vivo EPR dosimetry and modelling, obtaining values of dose ranging from <1 Gy to >70 Gy.

Fig. 11

2.1.3. EPR of finger and toe nails

Despite the extensive literature on EPR from teeth and bone, neither method has yet to overcome the problem of the need for invasive surgery to remove suitable biomaterial. In vivo L-band EPR dosimetry holds that promise but, despite exciting progress, is yet to be fully realized. As a result, practitioners of EPR dosimetry have also focused on a type of biomaterial that is significantly easier to extract without causing the patients discomfort or subjecting them to invasive procedures – namely finger- and toenail clippings.

2.1.3.1. Radiation-induced radicals

Although the use of fingernails as potential radiation dosimeters was suggested as early as the late 1980s (Chandra and Symons, 1987 and Dalgarno and McClymont, 1989) it is only in more recent years that significant effort has been devoted to the development of an EPR technique for fingernails as an emergency dosimetry method, especially through the work of Trompier, Romanyukha and others (e.g., Trompier et al., 2009a, Trompier et al., 2009b, Trompier et al., 2014a, Reyes et al., 2009 and Black and Swarts, 2010. See also a recent review by Marciniak and Ciesielski, 2016.). As with bone and tooth enamel, human fingernails are characterized by radiation-induced signals (RIS), mechanically induced signals (MIS), and dose-independent background signals (BG). Both unstable and stable signals are to be found.

Fig. 12 shows the main three components observed in the EPR spectra of finger- or toenails. They may be described as the singlet, doublet and triplet signals, the latter being found to be slightly anisotropic. These three components appear in both the RIS and MIS spectra – i.e., the same radicals are generated whether the nails are subjected to mechanical stress (MIS) or radiation (RIS). All three signals can be removed by soaking of the nails in water for long periods. What remains is called the background (BG) signal. The BG signal has the same form as the singlet, but is a non-zero, quasi-stable signal that cannot be entirely removed. BG may be a native signal observed, to greater or lesser extents, in all human nails. (Some authors, however, claim the BG signal is introduced by cutting; e.g., Reyes et al., 2008.) It is observed to grow with subsequent drying of the sample under ambient conditions and is also affected by exposure to room lighting or natural sunlight.

Fig. 12

The MIS is induced following mechanical stress caused by, for example, clipping of the fingernails or by the application of non-cutting mechanical pressure (i.e., squeezing). It consists of the three different MIS components observed in Fig. 12, but the strength of each component depends the severity of the pressure applied and the method for cutting or clipping the nails. They are unstable in water or a humid atmosphere and may be removed by soaking. The MIS shown in Fig. 12 can be observed, to greater or lesser degrees, immediately after clipping an unirradiated fingernail.

The RIS also consists of the same multiple signals. The anisotropic triplet signal is observed only in highly irradiated samples and may be observed, for example, following clipping and soaking, and irradiating with a high dose (hundreds of Gy) to clearly show the signal shape. The X-band RIS is also unstable with storage in humid conditions and can be removed by soaking.

Q-band spectrometry may provide greater resolution for some of these signals. In a detailed analysis by Trompier et al. (2014a), using X- and Q-band spectrometry at different microwave powers and measurement atmospheres, the multiple MIS and RIS components were analyzed. These authors claim four MIS components (labeled MIS1, MIS2, MIS3 and MIS4). MIS1 has components at $g_1 = 2.055$, $g_2 = 2.024$ (0.85 mT splitting), and $g_3 = 1.998$, corresponding to the triplet seen in Fig. 12; MIS2 at $g = 2.004$; MIS3, also at $g = 2.004$, but with 2 mT splitting – which may be the doublet observed in Fig. 12; and MIS4 at $g_1 = 2.025$, $g_2 = 2.008$ (1.5 mT separation) and $g_3 = 2.003$, which is not obvious from Fig. 12 but may be contributing to the triplet signal. These features observed by Trompier et al. (2014a) are seen in Fig. 13, in the Q-band.

Fig. 13

Similarly, Trompier at al. (2014a) decomposed the RIS signal (see Fig. 14) into RIS1 at $g_1 = 2.055$, $g_2 = 2.023$ (0.85 mT splitting) and $g_3 = 1.998$ (the triplet); RIS2 at $g = 2.005$ (the singlet); RIS3 at $g = 2.004$ (2 mT splitting – the doublet); RIS4 at $g_1 = 2.025$, $g_2 = 2.008$ (1.5 mT) and $g_3 = 2.003$ (same as MIS 4); and RIS5 at $g = 2.004$ (possibly the same as RIS2).

Fig. 14

Finally, the BG signal is observed at $g = 2.004$. Similar signals are reported by Black and Swarts (2010). These features are seen in Fig. 14, in the X-band.

The similarity of the EPR spectra for RIS and MIS suggests a similar origin for the signals; that is, they may originate from the same radicals but produced by different mechanisms. The origins of the EPR signals are discussed in terms of R-group sulfur radicals (where R represents an alkyl group of the type C_nH_{2n+1}, for example). Finger- and toenails are made up of the protein α-keratin, which consists of three right-handed α-helical peptide chains, twisted into a left-handed coil with disulfide S-S cross-links from the amino acid components, cystine and cysteine. The similarity of the MIS with the RIS components can cause significant difficulties when attempting to extract the radiation-induced component only. Black and Swarts (2010) identify the EPR feature at $g_1 = 2.056$, $g_2 = 2.021$ and $g_3 = 1.999$ (RIS1 and/or MIS1) with either perthyl or sulfuaranyl radicals. Trompier et al. (2014a) propose that the RSSR group may be cut to form an RSS° radical (identified with MIS1) and an RSO° radical (identified with MIS4). Alternatively, the RSSR group may be ionized by radiation to again form the RSS° radical (identified with RIS1), the RSO° radical (RIS4) and an RSO2° radical (RIS2 and possibly RIS5).

Strzelczak et al. (2013) propose that exposure to ionizing radiation generates free thiyl radicals by either breakage of the S-H bond in cysteine or the S-S bond in cystine. Subsequent reaction of the thiyl radicals with cysteine molecules creates perthinyl radicals. The perthinyl radicals so-formed generate the RIS EPR ($g = 2.004/5$) signal, which is unstable under ambient conditions. The BG signal, however, also at $g = 2.004/5$, is said to be generated by radiolysis of melanin, producing a semiquinone radical. This can also be generated by UV or sunlight exposure and is ever-present in all fingernails, even without radiation. The semiquinone radical is more stable under ambient conditions than the RIS signal. This model may also explain why the BG signal grows during storage under ambient lighting.

Although different stimuli (stress, radiation, UV) may induce the same radicals, the behavior of the induced signals is not the same. For example, many authors observe that both MIS and RIS fade at room temperature in humid conditions. However, it is

also observed that the fading rates are different (e.g., Trompier et al., 2009b and Black and Swarts, 2010). The dependence on microwave power is also different (e.g., Reyes et al., 2008, Black and Swarts, 2010 and Trompier et al., 2014a). Furthermore, the BG signal increases with time after cutting under ambient conditions, rather than decreasing (e.g., Reyes et al., 2008). Thus the connection of various signals with the same radicals is only part of the picture. For example, perhaps radiation induces signals throughout the bulk of the material but cutting produces signals originating only along the cut edge. The latter may therefore be more sensitive to humidity than the former.

2.1.3.2. Protocols for dose assessment

The complexity of the RIS and MIS from fingernails and, in particular, their instability with respect to moisture content and storage conditions has not yet enabled a generally accepted or consistent protocol for dose assessment. It is clear that significantly more work on these issues is required (Marciniak and Ciesielski, 2016). Several attempts to remove the MIS while leaving the RIS intact (or, at least, to find a stable component of the RIS not affected by moisture) have been attempted. For example, Romanyukha et al. (2007b) subjected cut fingernails to several chemicals for various lengths of time to observe the decrease in the MIS signal with treatment time. All were seen to reduce the MIS signal. Trompier et al. (2009b) observed that "painting" the edge of the cut fingernail with water significantly, but not completely, reduced the MIS. Soaking in water has been adopted by many authors (Reyes et al., 2008, Reyes et al., 2009 and Romanyukha et al., 2011).

Difficulties with assessing the hydration levels of fingernail clippings, and the uncertainties that subsequently result when measuring MIS and RIS, led Wilcox et al. (2010) to advocate the unusual approach of increasing the MIS signal by an additional cut of the fingernails, thereby clearly demonstrating the shape of the MIS signal which may then be subtracted from the RIS + MIS signal to reveal the RIS.

The shape of the dose response curves is dependent on whether the nail clippings are analyzed following water (or similar) treatments or not. Generally, "stressed" nails (without post-clipping water treatment) show linear dose response curves, whereas "unstressed" (water soaked) nails yield non-linear, saturating dose response curves (e.g., Reyes et al., 2009 and Romanyukha et al., 2010). As a result, a variety of protocols has been proposed for dose determination, as described, for example, by Trompier et al., 2007b, Reyes et al., 2009, He et al., 2011, Romanyukha et al., 2014, Trompier et al., 2014a and He et al., 2014 and Wang et al. (2015), to name a few. As pointed out by Wilcox et al. (2010), humidity during sample storage is a confounding factor. Results obtained with uncertain humidity levels and storage conditions must be questioned. Storage at low (sub-zero) temperatures appears to

provide some stability to the signals and this may be the result of reduced humidity in the freezer during storage. Furthermore, even if one knows the humidity levels, and the times between exposure and cutting, and cutting and measurement, it is not certain what to do with this information – i.e., how to correct the results for the different conditions.

In Trompier et al. (2014a) the stable Q-band signal, denoted by these authors as RIS5, was used in dose assessment. However, this component is weak and could be used in dose evaluations only for doses significantly higher than those relevant for emergency triage. RIS2 is the more sensitive component. However, as demonstrated in all published studies, this radiation sensitive component is unstable under humid conditions and cannot be easily used. Sholom and McKeever (2016) observed that if the irradiated samples are stored in dry, vacuum conditions at room temperature following irradiation, RIS2 is stable, over a period of at least 7 days. Although the effect of oxygen (or lack of it) in the stabilization of the RIS signal is not yet known (if there is any effect), Sholom and McKeever (2016) posit that the stability is due to storage in a dry (zero humidity) vacuum.

Fig. 15 shows the stability of the three main signals observed by Sholom and McKeever in the X-band at g = 2.005 (and separated using the procedures described above with respect to Fig. 12). The Figure contrasts the stability of the RIS, MIS and BG signals if stored in a vacuum (Fig. 15(a), (c) and (e)) with that observed for storage under ambient humidity (62% in this case; Fig. 15(b), (d) and (f)). The stability of the RIS signal during vacuum storage versus ambient conditions is clear. By isolating the signals in this way, and by stabilizing RIS, the dose response observed by Sholom and McKeever (2016) was linear (Fig. 16). The intercept was found to depend on the time between irradiation and nail harvesting, increasing with time. This observation is consistent with those of other research groups (e.g., Reyes et al., 2009 and Romanyukha et al., 2010).

Fig. 15

Fig. 16

Fig. 17

Following the observations of Fig. 15 and Fig. 16, Sholom and McKeever (2016) proposed a specific protocol for determination of absorbed dose with fingernails. The protocol is described in Fig. 17. The authors note that the "extra-cut" step in the protocol should be made as soon as possible after the initial cut in an attempt to ensure that the extra cut is made under the same ambient conditions as the initial cut.

Application of this protocol to recover absorbed doses delivered in the laboratory was successful in recovering the doses (between 0 Gy and 10 Gy), with standard deviations of several tenths of a gray.

2.1.3.3. In vivo analysis

In view of the difficulties and uncertainties caused by the mechanical harvesting of finger- and toenails the development of an in vivo evaluation technique would be valuable. As a step towards this, He et al. (2011) described two possible resonator designs for potential measurement of X-band EPR signals in vivo, without cutting the fingernails. The main challenge is to measure EPR signals in the nails while limiting the penetration of the microwave power into the lossy tissue beneath the nail. Surface aperture and coil resonator designs are proposed to address this issue (see also Grinberg et al., 2016 and Petryakov et al., 2016). The challenge of calibration of the fingernails in vivo has not yet been addressed, and questions concerning the effect of the degree of hydration of the in vivo nail, and the stability of the radiation-induced signal while the nail is in vivo also have to be addressed.

2.1.3.4. Applications in accident dosimetry

It is perhaps not surprising given the practical difficulties described above that EPR dosimetry of nails has not yet been widely applied in real situations. One exception is the work of Trompier et al. (2014b). These authors applied EPR techniques on fingernails from victims of three separate accidents (in Gabon, Tunisia and Peru) with 192Ir sources used in gamma radiography. RIS5 measured in the Q-band was used as the radiation signature, as described in Trompier et al. (2014a). The method used is an additive-dose procedure where two nail samples are compared, one with the accident dose, and one (from the same individual) that has not been exposed (from the opposite hand, or from the victim's feet, for example). Comparison of the two dose response curves, using storage at ambient conditions yields an estimate for the accident dose. For the victims studied, the nail doses varied from as low as ~18 Gy to as high as ~45 Gy. RIS5 could be used in these assessments, despite its low sensitivity, because the doses were high and much greater than those targeted in triage applications (<2 Gy).

2.1.4. Hair

Human hair contains the same protein, α-keratin, as finger- and toenails, so it is understandable that some effort has been devoted to an analysis of human hair for emergency dosimetry applications. Trevedi and Greenstock (1993) attempted to use the EPR signals from hair in this manner but the radiation-induced signals were confounded by a high non-radiation induced background, possibly related to mechanical effects similar to those observed by Chandra and Symons (1987), but also

possibly related to melanin (Çolak and Özbey, 2011). Melanin, as has been shown by Strzelczak and others (Strzelczak et al., 2013) generates an EPR signal following exposure to sunlight. Different colored hair contains variable amounts of melanin, but in all cases a large BG signal results. RIS signals are observed following irradiation of hair, but the significant and color-dependent BG signal due to melanin has, so far, confounded attempts to use EPR of hair as a dosimetry method (Çolak and Özbey, 2011 and Tepe Çam et al., 2014).

2.1.5. Other materials used in EPR dosimetry

The invasive nature of the extraction of biodosimetry materials, such as bone and teeth, and the problems with dose estimation using nails, has led to studies of other materials that may be carried by the exposed person, either in or close to the body. Several efforts have examined the EPR signal from various sugars and quite an extensive literature exists (e.g., Trevedi and Greenstock, 1993, Wieser et al., 1996, Fattibene et al., 1996, Yordanov and Georgieva, 2014, Da Costa et al., 2005, Hervé et al., 2006 and Desrosiers and Wadley, 2006, among others). However, as pointed out by Trompier et al. (2010a), the availability of sugar as a personal emergency dosimetry material is limited due to the unlikelihood that individuals would routinely carry such materials.

Clothing is an obvious material to be found on individuals and there have been some, but a limited number of, EPR studies of various textile materials for this application. Some studies of EPR from cotton and polypropylene have been published with a view to development of the technique for emergency dosimetry (Kamenopoulou et al., 1986, Barthe et al., 1989, Barthe et al., 1992 and Viscomi et al., 2011). In general, the EPR signals are consistent with previously reported EPR signatures from cellulose, but dose responses and sensitivity characteristics did not reveal a sensitivity high enough for triage.

Other likely materials present themselves, namely materials found in modern electronic and personal items (e.g., from smartphones, watches, credit cards, etc.). The target material in these cases might include, for example, glasses and plastics, and some research has been undertaken on these materials to evaluate their usefulness as emergency EPR dosimeters. Trompier et al., 2009a and Trompier et al., 2010a summarize their EPR studies of liquid crystal displays (LCDs) in which the investigated material is a silico-sodo-calcic glass. In high-OH^- glasses the radiation-induced EPR signal is from a non-bonding oxygen center while for low-OH^- glass the signal is due to a peroxy radical. Borosilicate glasses did not produce a RIS signal. Fading of the RIS was observed to be between 15% and 35% over the first 24 h, with very slow decay thereafter, depending on the glass type (Bassinet et al., 2010a). So-called glasses "Types I-V" (Trompier et al., 2012), were observed, based

on the shape of the obtained EPR spectra. The RIS for "Type I" is shown in Fig. 18. The RIS dose response is linear (Trompier et al., 2011).

Fig. 18

Following on from this work and as part of the MULTIBIODOSE project, Trompier et al. (2012) and Fattibene et al. (2014) published summaries of comprehensive inter-comparisons between EPR laboratories in order to examine the procedures, methods and resulting uncertainties of using EPR from smartphone glass as a dosimetry method. The glass chosen in the latter work is known commercially as Gorilla® Glass from Corning®. This type of glass is used extensively for smartphone touch-screens. For those participants who used glass from the same batch, stored under controlled conditions, smaller errors (between the evaluated doses and the administered doses) were observed compared with those participants using glass from different phones and stored in different conditions (light, temperature, etc.,). The former group was able to determine the administered blind doses within a 95% confidence interval. However, the second group did not fare so well in the intercomparison, with none of the members of this group being able to report correct doses near 1 Gy, in the range needed for reliable triage dosimetry. The study revealed potential pitfalls that need to be addressed if routine and reliable dosimetry is to be found.

Watch glass gives similar EPR properties to those reported for LCD glass. The gamma dose response is linear (Wu et al., 1995 and Bassinet et al., 2010a), whereas 6 MV photons and 10 MeV electrons appear to give non-linear dose responses for similar soda-lime watch glasses (Marrale et al., 2011). Modern eye-glass material is generally plastic, for example, polycarbonate. Trompier et al. (2010b) report the EPR dose response from eye-glass plastic as being non-linear, but the dose response from some eye-glass material can be approximated to a linear response over a limited dose range. The signal is unstable, however, and to date there is insufficient sensitivity to warrant popular use.

Trompier et al. (2010b) and Sholom and Chumak (2010) studied other plastic materials, obtained from various sources. The EPR dose responses were all non-linear and sensitivities varied according to the source of the material. Although unstable, some plastics displayed sufficient sensitivity to warrant continued study. A potentially confounding factor, however, is the sensitivity of the radiation-induced EPR signal to ambient light (Sholom and Chumak, 2010).

2.2. Luminescence techniques

The complexity of the EPR signals found in polymeric and glassy materials have prompted others to examine an entirely different measurement modality – namely

luminescence. Two measurement modes have been adopted for a wide array of materials, both synthetic and natural. These are thermoluminescence and optically stimulated luminescence.

2.2.1. Thermoluminescence

Thermoluminescence (TL) has been used in radiation dosimetry for many decades (McKeever, 1985). It was recognized early on as being a very sensitive technique and with the right materials is able to detect trapped electrons at levels as low as 109 (total) within a specimen (Townsend and Kelly, 1973). Such sensitivity has given TL a leading position in the field of radiation dosimetry and many synthetic materials have been produced for use as personal dosimeters (McKeever et al., 1995). It is not surprising then that TL has been examined as a potential technique for use in emergency triage dosimetry, using either biomaterials or fortuitous material on or near an individual's body.

The TL process relies upon initial ionization by radiation absorption and the subsequent creation of free electrons and holes. Subsequent trapping of these electronic species at defects within the material leads to the storage of a portion of energy from the incident radiation field that is proportional to the dose of radiation absorbed (Fig. 19). Upon heating the material, electrons and/or holes are thermally released from their traps and recombine with charges of the opposite sign. If the recombination process is radiative, luminescence (i.e., TL) is emitted from the material. For good dosimetry materials the signal is stable over the time delay between irradiation and heating, and the signal measured (TL intensity) is proportional to the absorbed dose.

Fig. 19

In practical measurements, the TL intensity is plotted as a function of the temperature to which the sample is heated, and a series of TL emission peaks – the "glow-curve" - is recorded. Each peak corresponds to a different species of trap releasing its trapped charge at a temperature related to the energy with which the charge is bound to the trap, i.e., the "trap depth" or the potential barrier that the trapped species has to overcome to be released into the appropriate delocalized energy band (conduction band for trapped electrons; valence band for trapped holes). Since some of the binding energies are small ("shallow traps"), the trapped charge may be released at quite low temperatures (say, 100 °C or less). Such trapped charge is usually unstable at room temperature and can leak away during the period between irradiation and heating (TL readout). Therefore, for dosimetry, higher temperature TL peaks are preferred and these can be stable for years following the irradiation.

Materials for TL dosimetry include synthetic compounds - e.g., LiF:Mg,Ti, CaF$_2$:Mn, CaSO$_4$:RE (RE = rare earth) and many others (McKeever et al., 1995). However, the technique has also become very popular in retrospective dosimetry applications using natural minerals found, for example, in building items (see other sections of this review paper and also Simon et al. (2006) for summaries). The search for materials that are suitable for emergency triage dosimetry focuses on those with TL glow curves displaying high-temperature, stable peaks, and high-enough sensitivity such that TL can easily be measured following exposure to doses as low as a few tens or hundreds of mGy. In this regard, the wavelength of the emitted TL is important since a measurement system that is optimized to the right wavelengths becomes necessary in order to maximize sensitivity (TL intensity per unit dose).

2.2.2. Optically stimulated luminescence

Related to TL is the technique of optically stimulated luminescence (OSL). Here the stimulus to release the trapped charge comes from the absorption of light, not heat, following the irradiation (Fig. 19; see also Yukihara and McKeever, 2011). Again, it is important to find stable signals – or signals with sufficient stability that they can be measured accurately over a period of days following the irradiation. OSL has become a very popular dosimetry technique. Personal dosimetry employs synthetic compounds (e.g., Al$_2$O$_3$:C, BeO) while retrospective dosimetry (see other sections of this paper, and Bøtter-Jensen et al., 2003) has centered on the use of natural minerals found in building materials. Key considerations in the measurement of OSL for emergency triage dosimetry include sensitivity, which in this case is not only governed by the wavelength of the luminescence emission but also by the wavelength of the stimulating light. Both need to be optimized for maximum sensitivity. Furthermore, since the light-sensitive traps may not be the same as those that participate in TL, the thermal stability of the OSL signals needs to be monitored and stable signals identified.

The usual procedure for measuring OSL is to illuminate the sample with a constant-intensity stimulation source and measure the subsequent luminescence (known as CW-OSL). The OSL signal reaches a maximum emission almost immediately after the stimulation light is turned on and thereafter decays with an exponential-like decay as the traps are emptied (Yukihara and McKeever, 2011).

2.2.3. Biological materials

2.2.3.1. Teeth

In an attempt to circumvent the issue of invasive procedures to extract teeth from individuals for EPR dosimetry (notwithstanding the efforts already noted to develop in situ EPR dosimetry), Godfrey-Smith and Pass (1997) proposed the use of OSL to

determine absorbed dose in teeth. The ultimate goal is to develop a small, high-sensitivity, portable system that could be used for tooth dosimetry in vivo.

Early studies of TL from tooth enamel and dentin revealed a radiation sensitive TL signal, but with associated problems caused by triboluminescence (caused by grinding the samples) and chemiluminescence (caused by the presence of organic material; e.g., Jasińka and Niewiadomski, 1970 and Christoudlides and Fremlin, 1971). The luminescent material in tooth enamel and dentin is hydroxyapatite and in order to eliminate the chemiluminescence effect the material has to be deproteinated, for example using NaOH (Kolberg et al., 1974). The difficulties with chemiluminescence and the necessity for deproteination, however, led Godfrey-Smith and Pass (1997) to try a non-heating method, namely OSL. A signal from undeproteinated and irradiated tooth enamel was observed from extracted teeth when stimulated with infra-red (IR) light. Either IR or green light could stimulate OSL when using deproteinated teeth. Yukihara et al. (2007) followed up this observation using a high-sensitivity OSL reader and were able to measure IR-, green- and blue-light-stimulated OSL from undeproteinated teeth, with a minimum detection limit of 4–6 Gy. Further developments by Godfrey-Smith, 2008 and DeWitt et al., 2010 and Yüce et al. (2010) pushed the MMD to as low as 1.5–4 Gy, approaching the limits required for triage. However, these results were only obtained on extracted, deproteinated teeth using high-sensitivity apparatus and blue stimulation.

One potential method for enhancing the sensitivity is to measure the OSL at an elevated temperature. Soni et al. (2014) examined the so-called "thermally assisted" OSL response from dental enamel and, using small samples, were able to maximize the sensitivity by performing the OSL measurement at 250 °C. Clearly this can only be performed with ex vivo samples. The same authors also showed that the maximum OSL excitation is observed at a stimulation wavelength of 324 nm, while the emission maximum is 412 nm. Thus, additional sensitivity increase should be possible through optimization of the stimulation and emission optics.

Fig. 20(a) shows typical OSL decay curves for irradiated tooth enamel. The OSL curve shape is compared for three types of irradiation – beta (^{90}Sr:^{90}Y), 302 nm UV and 254 nm UV. Although each curve can be fitted with the sum of two exponentials, different decay time constants are observed for the beta (0.14 s and 3.2 s) and for the UV (1 s and 16 s) (Sholom et al., 2011a). By using a high sensitivity system and multiple teeth, MMD values of <0.5 Gy could be measured. Although adequate for triage these low MMDs could only be observed with multiple teeth, placing stringent requirements on the design of potential apparatus for the eventual

goal of in vivo dosimetry. Fig. 20(b) shows a typical dose response, as a function of beta dose.

Fig. 20

Sholom et al. (2011a) investigated UV effects at two wavelengths (302 nm and 254 nm) for potential use of these irradiations as an in situ calibration source. However, as indicated in Fig. 20(a), the UV irradiation seems to stimulate different OSL traps from the beta irradiation. Further work on UV effects is required.

One problematic issue with the OSL signal from teeth is that it fades with time after irradiation. This is in contrast with the RIS EPR signal from these materials, which was discussed in an earlier section to be from CO2− radicals. The fading can be significant; 98% of the samples studied by Sholom et al. (2011a) demonstrated monotonic fading, as illustrated Fig. 21. As a result, fading corrections need to be made. The fading curve illustrated can be fitted by the sum of two exponentials, with time constants of 0.19 h and 14 h. As a result, as noted by Sholom and Desrosiers (2014), the MMD increases from approximately 0.2 Gy to approximately 1 Gy after a 24-hour delay between irradiation and OSL measurement.

Fig. 21

Since the EPR RIS component due to CO_2^- does not fade, a comparison of the OSL and EPR results from the same sample is of interest. This was carried out by Sholom and Desrosiers (2014) who noted that as long as corrections for fading of the OSL are made, using an algorithm obtained from fitting the experimental fading curve (Fig. 21), excellent agreement between the EPR recovered dose and the OSL recovered dose can be obtained. These authors further illustrated that the fading of the OSL signal correlated well with the fading of the EPR signal caused by radiation-induced CO_3^- radicals (g = 2.0115).

Another potential problem for the eventual development of an in vivo OSL measurement technique is that when tooth enamel is irradiated in moist conditions, as would be found in the mouth, the resulting OSL signal is significantly weaker than when irradiated in dry conditions (Geber-Bergstrand et al., 2012). Although results were found by these authors to vary depending on dose and sample, the conclusion was that if the emergency dose is delivered in moist conditions, but the calibration performed in dry condition (ex vivo), the recovered dose will be underestimated by a factor of two or more. Stated differently, if the calibration is also performed under moist conditions, mimicking those in the mouth, a sensitivity loss of more than a factor of two will result, adversely affecting the MMD. Clearly this important observation requires further research.

One encouraging observation by Geber-Bergstrand et al. (2012), however, is that dental repair ceramics did not suffer from this effect, leading to the suggestion that such materials may be used reliably. Bailiff et al., 2002 and Veronese et al., 2010 and Ekendahl et al. (2013) also studied the OSL (and TL) properties of a wide range of dental repair ceramics for potential use in dosimetry, following earlier work by Davies (1979) using only TL. Dental ceramics for tooth prosthetics come in various chemical forms, including alumina-based (porcelain), zirconia-based, glass and feldspathic ceramics (Veronese et al., 2010). Although these are not biological materials they are included in this section because of their importance in dentistry.

Typical TL glow curves from the four main types of dental ceramic are shown in Fig. 22 (a–d). Similarly, typical OSL curves from the same materials are illustrated in Fig. 23 (a–d). The signals (both TL and OSL) fade with storage time after irradiation, but in a predictable and monotonic manner, allowing correction algorithms to be applied. Dose response curves are linear and the sensitivity sufficient for MMDs from a few mGy to several tens of mGy. An example dose response is shown for fluorapatite glass dental ceramic in Fig. 24, with a value for MMD of about 5 mGy (Ekendahl et al., 2013). These authors also studied the fading characteristics and the energy response.

Figs 22-24

From the point of view of sensitivity, ease of fading correction and insensitivity to moisture, OSL from dental ceramics holds some promise for the development of an in vivo emergency dosimetry technique.

2.2.3.2. Nails and hair

Although the EPR properties of finger- and toenails have been, and are being, studied extensively it is perhaps surprising that the OSL properties of this material have not been examined. One exception is the work of Sholom et al. (2011b) who examined the OSL response from human nails (finger and toe) and compared the potential of this material for recovering an administered dose using OSL with that of other possible emergency dosimetry materials. Materials examined included nails, teeth, plastic buttons and business cards. All materials, including nails, showed the ability to determine the delivered dose accurately, with a value for MMD for nails of 0.1–5.0 Gy immediately after irradiation. Fading of the signal (in the dark) meant that the MMD increased to 0.2–10.0 Gy after 24 h. It could not be excluded that the OSL signal might originate not from the nail material itself, but from silicate contaminants embedded in the surface of the nail.

One additional possible difficulty is that in reality fingernails, in particular, will be exposed to natural or artificial light after irradiation, thereby potentially bleaching

any radiation-induced OSL signal. In view of the scarcity of results on OSL from nails, it is perhaps even more surprising that a patent exists using OSL from this material for the determination of radiation dose to which an individual may have been exposed (Moscovitch, 2012).

2.2.4. Commonplace materials

An important requirement for an emergency triage dosimeter is widespread occurrence. This is certainly satisfied with teeth and nails, both of which are biomaterials, but other, non-biological, materials have also been examined, with some success. Clearly, the materials chosen must be commonplace. Studies have included personal items that an individual might be wearing (e.g., clothing, jewelry) or might have on their person (electronic devices, money, etc.). In the following sections we discuss the luminescence properties of some commonplace materials and personal items that have been proposed as emergency dosimeters.

2.2.4.1. Clothing

The most extensive study to date of luminescence from clothing is that by Sholom and McKeever (2014a), following initial studies by Sholom et al. (2011b). Clothing is made up either of natural or synthetic long-chain polymers such as cotton (cellulose), polyester (polyethylene teraphthalate), PVC (polyvinyl chloride), polyurethane, and ethylene vinyl acetate. Such materials can be found in modern clothing and shoe fabrics. The structure of many of these compounds shows short-range crystallinity, although this is not essential for observation of TL or OSL. Clearly, since most melt or decompose at relatively low temperatures, OSL is preferred over TL. OSL can also be observed from plastic buttons (Sholom et al., 2011b). Most fabrics also contain dust particle contamination, mainly of silica-based minerals, and these too can give rise to OSL signals following irradiation.

Fig. 25 and Fig. 26 show some representative OSL signals from specimens of clothing and shoes after irradiation, when stimulated with blue light (Fig. 25) or green light (Fig. 26). Signals before irradiation (the initial "native" signals) are not shown in Fig. 25 and Fig. 26, but they were observed to be strong with blue stimulation and almost negligible for green stimulation.

Figs 25-26

A difficulty with these materials, however, is that each shows a non-radiation-induced "native signal". In a real situation this native signal would be superimposed on the radiation-induced signal and would require a method in which the two signal types can be separated. Fortunately, the shapes of the native and radiation-induced

OSL signals are different, enabling separation of the two via a deconvolution method described in detail by Sholom and McKeever (2014a).

After accounting for the native signal the dose response curves for fabrics were found to be linear, with MMD values ranging from 45 mGy to 1.2 Gy, depending on sensitivity. Of the clothing materials examined by Sholom and McKeever (2014a), materials extracted from shoes were the most sensitive with MMD values in the range 50–550 mGy.

All radiation-induced signals were unstable, up to 7 days after irradiation. However, for most materials sufficient signal exists even after 7 days delay between irradiation and analysis. Furthermore, the fading is monotonic and can be described by simple functions. Interestingly, the rate of fading fell into one of two categories, termed "fast" and "moderate", presumably depending on some unknown characteristic of the polymer material being used (Fig. 27). Either "fast" or "moderate" fading signals, however, can be used to recover unknown doses as long as the appropriate fading correction is applied.

Fig. 27

2.2.4.2. Personal items

In the same study and using similar methods and procedures, Sholom and McKeever (2014a) also studied OSL from credit cards, business cards and money (both paper and coin) from different countries. In all cases, some native signals were observed, although larger in some materials (e.g., some examples of plastic cards and paper money) than in others (other examples of plastic cards). In each case, the native signal shape was found to be different from the radiation-induced OSL shape, allowing separation of the two signals. As with the polymer materials from clothing, the polymers examined from plastic cards, business cards and paper money were all found to display unstable OSL after irradiation (fading), albeit with a monotonic decrease allowing for corrections using simple mathematical algorithms.

Sensitivities varied across the materials studied, with the sensitivity of plastic cards also being affected by the transmission properties of the plastics used, some of which were more transparent than others. Dose response curves, however, were linear and MMD values typically varied from 40 mGy to 240 mGy for paper money (with values as low as 20 mGy being achieved in one case and as high as 1.5 Gy in another). Plastic card MMDs varied typically between 8 mGy and 1.5 Gy (with two outliers of 2 Gy). Examples of the dose response from paper bills and plastic cards are shown in Fig. 28.

Fig. 28

The OSL signal from metal coins was found to be dominated by microscopic dust particles embedded in the surface. The particles (examined by scanning electron microscopy) were found to be Al-silicates, possibly feldspars. As with other examples of feldspar, fading was observed. After correction, MMD values were found to range from 30 mGy to as high as 2 Gy.

Bortolin et al., 2010 and Bortolin et al., 2011 conducted a more detailed study of the luminescence properties of dust to be found on personal objects using TL. Specifically, dust from coins, keys, jewelry and tobacco from cigarettes was examined to determine the dose response and sensitivity. Procedures for obtaining the dust from the surface of or embedded within the materials are described by these authors and a typical set of TL glow curves from the extracted dust is shown in Fig. 29. The TL shapes are different, depending on the origin of the dust. These preliminary studies indicate sensitivities in the range 100 mGy to 5 Gy.

Fig. 29

2.2.4.3. Electronic components

By far the most numerous luminescence studies have been on the TL and/or OSL from electronic components from personal electronic devices, watches, etc. and some overviews have been published (Woda et al., 2009a and Pradhan et al., 2014). In what follows we review the important results from the various studies.

Glasses: Following studies of EPR from smartphone and watch glass, several research groups have examined the TL signals from these same materials, building on earlier work demonstrating that glass in general can be used as an accident dosimeter using TL (e.g., Narayan et al., 2008). Thus, Bassinet et al. (2010a) compared the TL and EPR signals from both watch glass and glass from various touch-screen phones. The TL curves are broad and typical of amorphous, glassy materials. For many of the glasses studied, however, a large pre-irradiation, native signal was observed. Insufficient information is available about the glasses studied to call this a non-radiation-induced signal; all that can be stated is that the signal exists even before irradiation in the laboratory. To be noted, however, is the fact that it is not present in all of the glasses studied. Discher et al. (2016) chemically analyzed several glasses from the same phone manufacturer and determined that high TL sensitivity, and a high sensitivity for the pre-irradiation signal, is related to the presence of Al and K. Glass with low Al and K showed no sensitivity to TL and no pre-irradiation signal. Whatever its cause, this pre-existing signal acts as interference to the TL signal induced by laboratory irradiation. The latter is characterized by a main TL peak near 200 °C, with a lower-temperature shoulder near 100 °C (which is missing

from the pre-existing signal, presumably due to thermal fading). Typical TL glow curves for various glasses are demonstrated in Fig. 30.

Fig. 30

Although the examined dose response curves were found to be linear over a wide dose range, the sensitivity is only just sufficient for triage dosimetry (near 1 Gy), in agreement with other reports for TL from watch glass (Teixeira et al., 2008). Later studies, examined the pre-existing, native TL signal. Discher and Woda (2013) concluded that it is due to prior irradiation of the sample, either by UV or natural background irradiation, or both. They determined the pre-irradiation signal equivalent dose for 29 such samples and concluded that they ranged from as low as 7 mGy to as high as almost 900 mGy, with a mean of 46 mGy. The presence of this signal is said to limit the MMD to no less than 340 mGy. However, further work by this team (Discher et al., 2013) demonstrated that the pre-irradiation signal could be removed entirely by etching the surface of the glass before TL analysis. Using HF acid they were able to reduce the pre-existing native signal by up to 90%, indicating that the unwanted signal is a surface effect only. Furthermore, the inside of the glass displays a much weaker native signal than the outside. This observation led the authors to suggest a protocol for determining an unknown dose and using it were able to push the detection limit down to ~80 mGy.

The group from IRSN followed this observation with a suggestion of mechanically grinding the surface layer to remove the native signal (Bassinet et al., 2014a). This too led to a reduced background signal and a similar lowering of the MMD. Using these procedures both Discher et al. (2013) and Bassinet et al. (2014a) were able to recover administered doses with reasonably small standard deviations. However, to do so each had to apply corrections for fading. TL from glassy materials is often observed to fade. Part of the fading is thermal, while part is athermal, or "anomalous" - possibly caused by tunneling or localized electronic transitions between centers (McKeever, 1985 and Chen and McKeever, 1997). Both Discher et al. (2013) and Bassinet et al. (2014a) observed similar fading curves characteristic of anomalous processes. However, the fading curves are monotonic and corrections are simple to apply. Mrozik et al. (2014a) made similar observations.

An additional feature studied by the group from the Helmholtz Zentrum München (Discher and Woda, 2013, Discher and Woda, 2014, Discher et al., 2013 and Discher et al., 2016) was the effect of exposure to light on the TL curve. Clearly, the glass will inevitably be exposed to sunlight following irradiation. Discher and Woda (2103) observed that part of the TL glow curve is sensitive to light, whereas part (at higher glow-curve temperatures) is insensitive. This leads to the requirement of a "pre-bleach" of the specimen following irradiation and before TL analysis. Not all phone

glass is equally sensitive, however, with boron-silicate glass being more optically sensitive than lime-aluminosilicate glass (Discher and Woda, 2014). Discher et al. (2016) tested the pre-bleach protocol (using 470 nm light from blue LEDs) and found disappointing results in that the pre-bleach seems to lead to an underestimation of the delivered dose. Discher and Woda (2014) also describes the TL emission spectra of these glasses, showing that the former emits mostly in the red region of the spectrum (with a peak near 605 nm), while the latter emission peaks at 380 nm and 465 nm. Not surprisingly, the latter is more sensitive (TL signal/unit dose) than the former.

The photon energy dependence of phone glass was examined by Bassinet et al. (2014a) and Discher et al. (2014), showing a peak response at about 50 keV, as expected from consideration of the mass-energy absorption coefficients for these materials. The over-response, with respect to soft tissue, begins below ~150 keV, reaching a maximum of about a factor of ~5 at ~50 keV. Thus correction would be required in the estimation of tissue dose if the individual were subjected to such low-energy photons. The response to other forms of irradiation was studied by Bartolotta et al. (2011) and Marrale et al. (2013) using high-energy photons (6 MV), electrons (10 MeV) and protons (62 MeV), indicating acceptable accuracy for photon dose recovery, but less so for electrons and protons. The latter irradiation types, however, are likely to have limited interest for emergency triage applications.

Resistors, Capacitors, Inductors: Target components for potential dosimetry applications have included ceramic surface-mounted resistors (SMRs), capacitors and inductors. Surface-mount resistors have been the subject of most research (Fig. 31). The reason for this lies in the alumina substrates from which these devices are made. Alumina (Al_2O_3) is the material most used for OSL dosimetry using synthetically grown material and is the component of commercial dosimetry systems (Yukihara and McKeever, 2011). One might expect, therefore, to see similar behavior and properties for OSL from SMR substrates – an expectation that has proven to be only partially fulfilled.

Fig. 31

Inrig et al. (2008) were the first to propose the use of SMRs in emergency dosimetry. These authors examined OSL and TL from alumina substrates from mobile phones and demonstrated a number of important properties. The dose response was found to be linear over a wide range (10 mGy–100 Gy) with little change of sensitivity observed over multiple cycles. A value for the MMD of <10 mGy was found to be typical (Fig. 32). A key feature of the OSL properties of the material was fading of the OSL signal during the period between irradiation and OSL readout. Inrig et al., 2008 and Inrig et al., 2010 analyzed the fading curves and found them to be

primarily athermal – i.e., not temperature dependent – and that the fading followed a predictable t^{-1} law (where t = the time between irradiation and OSL readout) characteristic of quantum mechanical tunneling. Such behavior is not observed in commercial Al_2O_3 OSL dosimeters (Yukihara and McKeever, 2011). Woda et al. (2010) also examined the fading of OSL from these materials and noted a change in shape of the OSL decay curve after a long storage time, indicating that the most light-sensitive part of the OSL signal faded first such that care must be taken when comparing the OSL signal from an accident dose obtained several days after the irradiation event with that obtained during calibration procedures in the laboratory.

Fig. 32

Most authors (e.g., Inrig et al., 2008, Inrig et al., 2010, Woda et al., 2010, Bassinet et al., 2010b, Ekendahl and Judas, 2012 and Kouroukla et al., 2014) consistently observe the hyperbolic fading behavior of the OSL from the SMR alumina substrates, but fading that did not follow this law has also been observed. Beerten et al. (2011) could not describe the fading using a t^{-1} law and instead found that the fading could be described as the sum of three exponentials, plus a constant. Using this model they attempted to find a "universal" decay behavior that described the fading in the samples they examined and which could then be applied to all alumina substrate components. However, since the behavior observed does not conform to the norm, it remains to be seen if this approach will become of widespread use. Eakins et al. (2016) described the fading by a sum of exponentials. One possibility for the discrepancy between the observations of Beerten et al. (2011) and others may be a contribution to the fading from thermal decay processes (e.g., Kouroukla et al., 2014). Beerten et al. (2011) did not use a pre-heat (after irradiation and before OSL measurement). Others (e.g., Inrig et al., 2010 and Woda et al., 2010) have observed that a preheat can have a small effect in reducing the fading rate, suggesting a component of the fading may indeed be thermal. As such, this component would likely follow an exponential decay law.

Estimates of the MMD vary, but are generally in the range of a few tens of mGy (e.g., Inrig et al., 2008, Inrig et al., 2010 and Kouroukla et al., 2014), even after correction for fading. Analysis of published uncertainties in the estimation of the dose using OSL from SMRs reveals an expected uncertainty of ~±20%, consistent with the uncertainties from other suggested emergency dosimetry methods (McKeever and Sholom, 2016).

Lee et al. (2016) examined the residual TL following OSL readout from phone resistors and inductors. For inductors in particular, the TL is characterized by two, well-separated glow peaks, only the lower-temperature one of which is sensitive to light during the OSL procedure. This leaves the high-temperature TL peak to be

used for a second estimation of the dose after the first estimate using OSL. For resistors, the second peak is partially bleached during the OSL process, but enough remains to enable a second dose estimate to be made. By comparing the doses obtained with OSL and then TL, for resistors and inductors, Lee et al. (2016) conclude that a second estimation of dose is possible using the residual TL following the first OSL measurement. Data published by these authors are encouraging for inductors, but less so for resistors.

Following the initial observations of Inrig et al. (2008), several research groups have examined SMRs and other components from various electronic devices. Components studied include alumina-components from USB memory sticks (Beerten and Vanhavare, 2008, Beerten and Vanhavare, 2010 and Beerten et al., 2009), resonators and inductors (Beerten et al., 2009, Fiedler and Woda, 2011 and Lee et al., 2015), and capacitors (Beerten et al., 2009, Bassinet et al., 2010b and Pascu et al., 2013) from mobile phones. However, SMRs seem to be the most stable, sensitive and reproducible, lending themselves to emergency dosimetry albeit with necessary correction due to fading. In an international, inter-laboratory comparison of dose evaluation using OSL of SMRs from mobile phones, within the framework of the MULTIBIODOSE project, Bassinet et al. (2014b) demonstrated the potential of the method. Two protocols were adopted – one a "fast-mode" process not involving a preheat, and one a "full-mode" process including a pre-heat. With both cases, however, one calibration dose only was used to assess the unknown pre-delivered doses. Low doses (<1 Gy), medium doses (1–2 Gy) and high doses (>2Gy) were delivered and recovered with 90% confidence.

The photon energy dependence of OSL from SMRs has been examined by several authors (Beerten and Vanhavare, 2010, Ekendahl and Judas, 2012 and Eakins et al., 2016). The conclusion emerging is that knowledge of the energy spectrum of the source, and the precise geometric conditions for exposure are needed for good dosimetry.

One aspect of using components from mobile phones that has needed assessment is the potential effect of heating of the OSL material while the device is in use, leading to a reduction in the signal and a subsequent under-response. Mrozik et al. (2014b) examined this possibility by comparing the results from pre-irradiated phones which were left switched on and used in cellular communications, phones left in stand-by mode, and phones switched off. The latter two recovered the same unknown doses accurately, whilst the first showed only a 10% under-response.

Integrated Circuits: Among the largest and easiest-to-extract components on a smartphone circuit board are the integrated circuits (ICs; see Fig. 31). The notion is not to use the semiconductor material within the IC but instead to use the epoxy

encapsulation. The latter is always black and therefore one might expect low luminescence sensitivity (TL or OSL) but experience shows that the sensitivity is in fact sufficient to extract meaningful signals and desirable MMD values. Bassinet et al. (2010b) compared the TL and OSL signals from ICs with other electronic components and found a lower sensitivity of OSL as compared with SMRs and capacitors (as expected) and furthermore could not find any usable TL signal. In contrast, Sholom and McKeever (2014b) revealed a usable TL signal. Although experiments with different pre-heat temperatures showed that the OSL signal (stimulated using 470 nm light-emitting diodes) was quite stable up to ~140 °C, and no gain in sensitivity was encountered. Similarly, variation of the stimulation temperature showed that 25 °C was the best temperature at which to stimulate the samples. As with SMRs, the fading of the signal appeared to follow a t^{-1} law, but they also concluded that a thermal component to the fading is present.

Bassinet et al. (2010b) show a non-linear, saturating type dose response for ICs, with approximate linearity at low doses. Pascu et al. (2013) report a cubic dose response (although no data are shown). Sholom and McKeever (2014b) examined OSL and TL from ICs from a variety of mobile phone manufacturers and found similar properties for all manufacturers examined. Typical OSL and TL curves are shown in Fig. 33. The OSL (470 nm stimulation) is characterized by a rapid depletion of the signal (<2 s at the stimulation powers used in this work). The TL demonstrates a TL glow curve typical of amorphous materials with a signal extending over a wide temperature range. Plateau tests show that the signal is thermally stable up to a glow curve temperature of ~140 °C.

Fig. 33

The dose response curves are quite different, with TL displaying a saturating curve shape and the OSL dose response displaying upward curvature (Fig. 34). The non-linearity and non-reproducibility of the dose response are reflections of sensitivity changes during OSL and/or TL measurement. Sholom and McKeever (2015) examined this further and found that, for OSL, by extending the OSL measurement to as long as 600s during stimulation, the subsequent dose response curves are linear, and reproducible. The inference is that there are deep, slow-to-bleach traps that contribute to the next OSL measurement thus apparently increasing OSL sensitivity. Removal of these by prolonged bleaching solves the problem.

Fig. 34

Both the TL and OSL signals from ICs fade. A significant part of this appears to be due to thermal fading since, when the specimens are preheated, after irradiation and prior to OSL readout, the TL and OSL signals can be stabilized, showing only 10%

fading for OSL over 1 week and negligible fading for TL over the same period. However, in contrast to the observations of Bassinet et al. (2010b), loss of sensitivity for both OSL and TL occurs as a result of the pre-heat. Sholom and McKeever (2014b) selected a compromise pre-heat temperature of 130 °C. However, adding a pre-heat step and inclusion of a 600 s stimulation period, means that the overall measurement is lengthy per sample, a disadvantage for triage. To attempt to accommodate for this, Sholom and McKeever (2015) eliminated the pre-heat step and simply corrected for the observed fading. This procedure allowed detection of MMDs of 0.17 ± 0.03 Gy for different samples of the same IC, 0.13 ± 0.05 Gy for different ICs within the same phone, and 0.26 ± 0.19 Gy for different ICs from different phones. The uncertainty increases if measured on ICs from different phones. On a comparative test of 12 different ICs, using a delivered dose of 0.4 Gy, the recovered dose was 0.37 ± 0.05 Gy using a single point calibration for the sake of rapid triage.

Chip Cards: In Europe, but less so in North America, electronic chip modules are being increasingly used in identity cards, credit cards, bank cards, etc. The front side is covered by metal contacts to allow reading of the electronic information. However, the reverse side, often covered by a plastic laminate, can be used for OSL dosimetry after extraction of the chip from the card. The chip is usually covered in an epoxy cover (Göksu, 2003 and Mathur et al., 2007; see also Fig. 35) and experiments have revealed that it is the silicate materials added to the epoxy that are the main source of the OSL signal potentially useful for dosimetry (Göksu et al., 2007 and Barkyoumb and Mathur, 2008).

Fig. 35

Göksu (2003) examined TL and infra-red-stimulated luminescence (IRSL) from the epoxy-encapsulated memory chips from over 200 chip cards. The TL measured exhibited a strong native signal, which precluded its use in dosimetry. However, IR-stimulated OSL showed only a weak (~100 mGy equivalent) "zero-dose" signal. Although the IR-OSL signal was generally unstable after irradiation, a stable component could be identified by performing a preheat to about 40 °C. Furthermore, a sensitivity change was observed following re-use of the material, indicating that this needs to be eliminated or accounted for in order to perform accurate dosimetry.

Mathur et al. (2007) followed up this initial work and confirmed the large "zero-dose" signal for TL, but extended the study to blue-light-stimulated OSL in addition to IR-OSL. Blue-stimulated OSL curves and the dose response are shown in Fig. 36. Blue-stimulated OSL was shown to have a significantly higher sensitivity than IR-OSL and MMDs of ~20 mGy were demonstrated. The dose response is linear over the range of interest in triage. The signal, however, is unstable, but a strong and

stable component was observed after the unstable component was allowed to decay (over approximately 1 h at ambient conditions).

Fig. 36

Barkyoumb and Mathur (2008) confirmed these results and examined different types of silica epoxy filler, concluding that not all chip card epoxies could be useful in dosimetry. Fused silica filler was shown to give the best results. Studies by Woda and Spöttl (2009) and Woda et al. (2012) led to an inference that the "zero-dose" signal is related to UV-curing of the epoxy, with the temperature at which the curing occurs being critical in dictating the strength of the "zero-dose" signal. These authors also examined the fading properties of the OSL signal and determined that it is a mix of thermal and athermal fading. They further recommend not using a pre-heat before OSL measurement. In this fashion they were able to demonstrate MMDs as low as 3 mGy if the measurement is performed immediately after exposure and ~20 mGy if performed as long as 10 days after exposure. Beerten and Vanhavare (2010) showed that the OSL signal has a strong photon energy dependence below a few hundred keV. Pascu et al. (2013) investigated chip modules from SIM cards with similar results to those reported by Mathur et al. (2007).

2.2.5. Summary of EPR, TL and OSL dosimetry

Table 3 summarizes the main features and conclusions, along with some representative citations, for all materials mentioned in this review which have been studied using EPR, TL or OSL for possible use in emergency triage dosimetry.

Table 3

2.2.6. Other methods

The above methods are not the only ones that have been suggested for emergency physical dosimetry. Cogliati et al. (2014) (see also Derr et al., 2012) thoroughly tested the properties of complementary metal-oxide-semiconductor (CMOS) sensors in modern cell phones as potential gamma detectors. As discussed by Cogliati et al. (2014), CMOS devices work via the photoelectric effect, generating electron-hole pairs for every incident photon. Separation of the electron and hole occurs in the depletion region of the device allowing the charges to be collected as a current. At higher photon energies, as with radiation sources, Compton scattering effects create multiple electrons per photon, potentially saturating the pixels of the device, especially at high dose rates. Further, the packaging and filters within the CMOS detector make energy spectrum analysis difficult.

Nevertheless, these devices have been demonstrated to be useful at detecting the presence of radiation at low dose rate levels and low doses and therefore may be of

some utility as general public radiation monitors. Several software packages (apps) are available to convert cell phone cameras into radiation detectors and are available commercially, as listed by Cogliati et al. (2014).

An alternative proposal by Ishigaki et al. (2013) is not to use the camera sensor on the phone itself, but rather to use a p-i-n diode module separately from the phone, but linked to the phone in order to display the radiation dose and geographical information. As with CMOS sensors, the device is a dose-rate meter, but can obviously be used in integrating mode to determine dose. Dose-rate detection as low as 0.05 mSv/h was possible in the lab (using ^{60}Co). The system was field tested in the Fukushima Prefecture of Japan.

Wagner et al. (2016) have also reviewed several CMOS cameras and external detectors, and their relevant apps, for use with smart phones and have examined their applicability in radiation detection by the public. Each device reviewed has its constraints in terms of dose range, dose-rate range and energy dependence and the authors conclude that such devices have some, but limited applicability for emergency dosimetry.

2.3. Whole-body and organ dose estimates

Determination of absorbed dose using physical dosimetry yields a dose to the object under study (teeth, nails, electronic component, etc.) and not the dose to the body and/or its internal organs. There have been some attempts to determine, using Monte Carlo radiation transport simulations, organ doses $D_{r,t}$ and whole body dose $D_{B,r}$ from physical dosimetry measurements, $D_{r,P}$. Ulanovsky et al., 2005, Takahashi et al., 2001 and Takahashi et al., 2002 and Takahashi and Sato (2012) used Monte Carlo techniques to estimate whole-body doses from absorbed dose to teeth, leading to dose conversion coefficients Cr. Khailov et al. (2015) performed similar calculations to determine whole-body and organ doses from doses to fingernails, for a variety of radiation scenarios. Additionally, there have been attempts to evaluate internal organ doses and determine dose conversion factors for personal electronic devices carried by individuals given a particular external exposure (Eakins and Kouroukla, 2015). The indications from these simulations are that particular organs can receive doses higher than, or less than, the recorded physical dose (in teeth, fingernails, or electronic components), depending on the specifics of the exposure and location of the teeth/electronic device. Eakins and Kouroukla (2015) showed that isotropic irradiation, which may be the most realistic case, gave the closest agreement between surface dose (as calculated for a smart phone on the surface of the person's body) and the average, whole body dose. For the particular case of penetrating radiation (e.g., gamma), the surface dose measured ($D_{r,P}$) and the calculated whole-body dose ($D_{r,WB}$) were statistically the same.

3. Retrospective dosimetry with luminescence techniques

3.1. Luminescence techniques for absorbed dose determination

The experimental techniques applied to determine the cumulative absorbed dose in building ceramics have recognizable roots in procedures developed in the 1960s and 1970s, primarily for application to archaeological dating (Aitken, 1985 and Aitken, 1998). While techniques based on the measurement of thermoluminescence (TL) continue to be applied in several of the large dosimetry studies discussed below, they are being increasingly replaced, or accompanied by, the use of optically stimulated luminescence (OSL) techniques, including single-grain measurement procedures (Bøtter-Jensen et al., 2003). Coarse quartz grains (i.e., ~ >50 μm nominal diameter) have been the generally preferred mineral for cumulative dose determinations and further details of techniques adapted specifically for application to retrospective dosimetry using quartz can be found, for example, in publications by Bailiff et al., 2000, Banerjee et al., 1999 and Bøtter-Jensen et al., 2000 and Thomsen et al. (2005). Details of the techniques applied are usually provided in application papers, making reference to the underlying methodology from which they are drawn. Aspects of OSL and TL techniques that are relevant to the applications are discussed herein.

In the case of TL measurements, two peaks in the glow curve of quartz are suitable for dose evaluation, generally referred to as the '210 °C' and '325 °C' TL peaks. Portions of grains of several mg (referred to as aliquots) are sufficient to enable absorbed doses of tens of mGy to be determined with the 210 °C TL peak. The 325 °C TL peak, on the other hand, has significantly lower sensitivity (photon yield per unit dose per unit weight) due to the effects of thermal quenching (McKeever, 1985), and it is more usually used to determine doses above ~10 Gy. The mean lifetime of traps associated with these TL peaks at ambient temperatures (~20 °C) is sufficient for dosimetry on the timescale of interest in retrospective dosimetry. There have been several investigations of the mean life-time of the 210 °C TL peak (Petrov and Bailiff, 1997, Veronese et al., 2004a and Veronese et al., 2004b). A recent study (Woda et al., 2011b) with quartz extracted from bricks of the Urals region (Techa River) has shown that at the higher ambient temperatures encountered in this central mid-Eurasian region (Mokrov, 2004, has suggested that the surface temperature of bricks in south-facing walls of the Metlino mill may have reached 50–60 °C during the summer months), the mean lifetime of the 210 °C TL peak can be considerably shortened, to less than 100 years, depending on the location of the bricks in the structure and the levels of direct insolation incident on their exposed surfaces. Hence, while this TL peak has been found to be generally very sensitive, it is susceptible to thermal fading of trapped charge at elevated ambient temperatures. Although long-established, the

pre-dose technique (Bailiff, 1994 and Bailiff, 1997), which employs a sensitization effect exhibited by the 110 °C TL peak of quartz and is capable of evaluating absorbed dose of ~10 mGy, has tended to be applied less frequently because of the complex measurement procedure, but it has provided an important adjunct to the conventional 'high temperature' TL measurement techniques applied in the Hiroshima and Nagasaki dosimetry studies (Young and Kerr, 2005) and was applied in earlier dosimetry studies (Southern Utah; Haskell et al., 1994).

In some earlier studies (e.g., Göksu et al., 1996) dose determinations were performed with the 'fine-grain' fraction of the ceramic matrix (~4–11 μm dia.). Unless chemical treatments are applied during preparation of the sample (Mauz and Lang, 2004), luminescence from all minerals present within the measurement sample are potentially detected, including feldspar which commonly exhibits athermal fading (Aitken, 1985). Although this may not be a significant factor for measurements on the timescale of interest in retrospective dosimetry, additional experimental checks are required to establish the rate of loss of trapped charge (Huntley and Lamothe, 2001). Also, when using this size fraction there is a substantial increase in D_{BG} caused by the registration of alpha dose in grains that are of size less than the average range of the alpha particles emitted by lithogenic radionuclides present in the ceramic, and this may affect the precision with which DX can be determined when it falls within a low dose range (i.e., <100 mGy) (Bougrov et al., 1998).

OSL techniques have sufficient sensitivity to enable absorbed dose of less than 100 mGy to be determined with granular quartz, and OSL has the advantage of being produced by the release of charge from deeper traps that have a mean lifetime comparable to that of the 325 °C TL peak (>106 a) and avoiding the effect of thermal quenching that strongly attenuates TL above ~ 200 °C. A variant of the single aliquot regeneration (SAR) procedure (Wintle and Murray, 2006) is usually employed to obtain dose determinations based on OSL measurements with aliquots each containing at least several tens of individual grains. In most cases the OSL decay curve observed is likely to be dominated by the 'fast' component (Bailey et al., 1997, Jain et al., 2003 and Bos and Wallinga, 2012), but occasionally samples may exhibit an 'ultra-fast' component that requires removal by the application of tailored preheat treatments (Jain et al., 2008 and Fujita et al., 2011). In the single-grain technique, similar measurement procedures are applied to individual grains (Bøtter-Jensen et al., 2003), enabling the absorbed dose to be determined for individual grains. Although developed primarily for dating applications, this experimental approach is of interest if grains used for dosimetry were not uniformly 'reset' during the manufacture of the building material, as is the case with cementitious materials such as concrete and mortars, which are discussed further below.

In the dose reconstruction studies conducted so far using bricks, the sample matrix is disaggregated to extract the minerals of interest. By preparing cut slices of a ceramic building material the integrity of the matrix is retained and this provides the opportunity to obtain spatially resolved determinations of absorbed dose on a sub-mm scale where measurements are performed on individual grains. By cutting slices orthogonal or parallel to the exposed surface such measurements could be used to obtain a depth-dose profile and examine spatial heterogeneity, respectively, in the case of external beta sources. This capability has been demonstrated in principle (Bailiff, 2006) using an OSL scanning technique (Bailiff and Mikhailik, 2004) that enables the absorbed dose to be determined for selected individual grains exposed within the cut surface of a ceramic and also is able to distinguish between quartz and feldspar emissions by measurement of time-resolved luminescence using a Q-switch laser (10 ns). Kim et al. (2015) proposed a rapid-assessment technique for the determination of absorbed dose using slices of drilled core of ceramic in which they used a pulsed blue LED stimulation source (10 μs width) to detect quartz OSL and discriminate against feldspar emission. Detector systems based on an electron multiplication CCD camera (Thomsen et al., 2015) currently under development for low-level luminescence detection are also obvious candidates for this approach. The main features of the method applied to retrospective dosimetry are summarized in Table 4.

Table 4

3.2. Materials

In the retrospective studies discussed below, ceramic building materials in the form of fired-clay brick and tile have provided the mainstay medium for dosimetry measurements and extracted from granular natural quartz has been the preferred mineral for dose determinations. Porcelain (e.g., tiles or electrical insulators) is also a potentially suitable material (Bailiff, 1997) and although it has yet to be deployed and tested more widely, its methodological development as a dosimeter has continued (Hübner and Göksu, 1997, Göksu et al., 1998 and Oks et al., 2011). To widen the range of materials available for dosimetry beyond ceramics, the potential of cementitious materials and calcium silicate bricks has been investigated and they are briefly reviewed in this section; although tested for their dosimetry potential, they have yet to be deployed in a major dose reconstruction effort.

3.2.1. Cementitious building materials

Given that many building structures, both civil and industrial in function, have exterior surfaces constructed of concrete, or have an outer layer of render, or where mortar binds non-ceramic building blocks, then various forms of cementitious

material are of interest as alternatives to ceramic building materials (CBM). Materials of this type commonly incorporate aggregates containing fine-to-coarse granular quartz and the usual accessory minerals. The concept of performing dosimetry using concrete had been demonstrated by Kitis et al. (1993), who applied TL procedures to barites extracted from concrete shielding in a synchrotron facility, although at very high levels of dose (1 kGy). The determination of much lower doses (~100 mGy), presents a number of technical challenges. For cementitious materials fabricated at ambient temperatures, a resetting mechanism is required where exposure to natural or artificial light fully depletes the residual trapped charge before the registration of the exposure of interest commenced, as employed in the dating of (unheated) sedimentary deposits (Aitken, 1998). However, the mixing process of aggregates with cement in concrete and mortar (and also when preparing plaster), is unlikely to thoroughly expose quartz grains contained within the mix to daylight, giving rise to individual grains with differing histories of exposure to light and hence differing degrees of resetting before their incorporation in the building material. A closer inspection of the luminescence from granular quartz reveals that the emission detected originates from only a small proportion of the grains, and this commonly occurs with quartz of sedimentary origin, whether heated or unheated. This characteristic has become the keystone of techniques that evaluate the absorbed dose where not all grains were completely reset. Using instrumentation developed for the measurement of OSL from individual mineral grains (Bøtter-Jensen and Murray, 2001) and the determination of absorbed dose using single-grain techniques, Thomsen et al., 2002 and Thomsen et al., 2003 found that by measuring a large number of individual grains (i.e., >104) extracted from concrete, a small fraction had been sufficiently reset by exposure to daylight and they were able to determine absorbed doses of less than 100 mGy. However, application of the technique to concrete is likely to be better suited to significantly higher levels of dose, as demonstrated in the case of a radioactive waste storage facility (Jain et al., 2002), and for such work the recent advances in statistical models developed for the analysis of single-grain dose distributions are relevant (Galbraith and Roberts, 2012). The luminescence characteristics of Portland Cement (PC), which is a key ingredient of modern concrete, has also been investigated (Göksu et al., 2003). After undergoing strong thermal treatment during manufacture, cement contains, in its hydrated form, complex calcium silicates and aluminates, but little quartz. Measurement of the OSL response of the hydrated PC produced a linear OSL response with dose to ~100 Gy, but weak luminescence emission limited its lower dose range to a few Gy.

Although OSL techniques are suitable for application to cement-based mortars, applied as a render or as the binding layer for ceramic bricks (Bøtter-Jensen et al., 2000), Göksu et al. (2003) applied an alternative measurement technique to quartz

based on the measurements of TL peaks (<200 °C) that are relatively shallow, but with mean-lifetimes long enough for application to retrospective dosimetry (i.e., less than 100 years) yet with sufficient thermal loss of charge from the traps at ambient temperatures to maintain a relatively low quantity of trapped charge arising from natural background radiation. Large coarse quartz grains (>350 μm diameter) extracted from ready-mixed mortars were found to exhibit a TL peak located at ~170 °C (at 5 °Cs^{-1}) that could be used for absorbed dose determinations above 100 mGy. This TL peak is often present in the quartz glow curve and located between the prominent and widely studied '110 °C' and '210 °C' TL peaks (Petrov and Bailiff, 1997 and Veronese et al., 2004a). Using this approach, application to the investigations of a clandestine X-ray irradiation alleged by inmates of Gera prison in the former GDR and the potential of using sun-dried adobe brick are discussed by Göksu and Bailiff (2006). However, to further develop this approach for wider application, a TL measurement procedure applied either to individual large coarse quartz grains, or to aliquots containing multiple grains and with a spatially resolved photon detector (e.g., a CCD) may be required to obtain the necessary discrimination in identifying a population of grains with negligible trapped charge at the time of fabrication.

While quartz has been the favored mineral for dose determinations, the quantity of material available in a sample may be insufficient or, when extracted, the luminescence characteristics may be unsuitable. In these circumstances, feldspar is a potential alternative mineral to use for dosimetry. The luminescence characteristics of feldspar present additional experimental issues, in particular, a loss of trapped charge via athermal fading mechanisms (anomalous fading; Aitken, 1998), which is not exhibited by quartz, a generally lower rate of optical bleaching under exposure to daylight compared with quartz and, in the case of potassic feldspar, the presence of ^{40}K within grains which increases D_{BG}. However, these factors may not necessarily present a significant obstacle in all applications and there is a considerable body of literature on the procedures developed for absorbed dose determination using feldspar extracts for dating applications (Bøtter-Jensen et al., 2003).

3.2.2. Calcium silicate bricks

Calcium silicate brick (CSB) was introduced and became widely used for the construction of houses in rural areas of the Former Soviet Union (FSU), and they are also manufactured in Europe and North America. The bricks, made with sand and lime, are treated in a super-heated steam atmosphere during manufacture, reaching temperatures of 200 °C for several hours (Bailiff and Mikhailik, 2004). Quartz extracted from three different types of CSB was found to be potentially suitable for retrospective dosimetry by performing measurements using the quartz 210 °C TL

peak. The currently developed OSL techniques are unsuitable because the OSL signal observed is dominated by luminescence associated with the stimulation of a reservoir of charge in deep traps accrued over a geological timescale and only partially depleted during the manufacturing process. The low concentration of lithogenic radionuclides in CSB gives rise to a significantly lower value of background dose rate than is the case for typical clay bricks. However, in terms of doses from the lower dose range, the resolving power of the technique is dependent on the effectiveness of the removal of trapped charge during the curing process. The results obtained from CSB from a 21-year-old building in a Ukrainian settlement downwind of the Chernobyl NPP illustrate the capability of the technique. An average value of 20 ± 4 mGy was obtained for D_X after subtraction of D_{BG} (11 ± 2 mGy), and this compares well with the estimate for D_X of 18 ± 7 mGy that had been obtained previously with samples of fired clay brick from the same building (Jacob, 2000). Although not all types of CSB may have similarly favorable characteristics and the technique has yet to be independently tested on a larger scale, it appears to be an alternative material for studies in settlements that lack buildings constructed of fired clay brick.

3.3. Applications to dose reconstruction

3.3.1. Hiroshima and Nagasaki

The survivors of the Hiroshima and Nagasaki atomic bomb detonations form a unique cohort for radiation epidemiological study. The cohort comprises several hundred thousand individuals of both genders with a wide range of ages who were acutely exposed to direct radiation emitted within several seconds following detonation, the events in each city being separated by 3 days. The primary source of radiation was localized to the bomb at its point of detonation and at Hiroshima and Nagasaki this occurred in the atmosphere at heights of ~600 and 500 m above the hypocenter, respectively (Young and Kerr, 2005). Depending on the distance from the hypocenter at the time of detonation and the extent of shielding, the dose received by survivors extended across the full range of epidemiological interest, from fatal to negligible. A high proportion of the survivors for whom detailed histories of movement are available were located within 2 km of the hypocenter and a major part of the epidemiological study of the survivors has focused on the Life Span Study (LSS) that comprises some 93,000 individuals who were located within 10 km of the hypocenter at the time of detonation (Ozasa et al., 2012). The relationship between dose and distance from the hypocenter forms an essential component of a study of this nature, and it has been progressively constructed as part of the dosimetry system for each city using a combination of computational and experimental techniques. The latter include luminescence techniques to measure the

cumulative gamma dose and accelerator mass spectrometry (AMS) to measure neutron activation products, both of which have played a pivotal role in developing and testing the robustness of the dosimetry system. Cullings et al. (2006) provide an informative overview of the key stages of the evolution of the dosimetry system (DS), and details of these are given in a series the published reports, including the initial tentative dosimetry system T65D (Milton and Shohoji, 1968), DS86 (Roesch, 1987) and the current system, DS02 (Young and Kerr, 2005). A series of interleaved workshops have served to review and develop agendas for further improvement of the dosimetry system (Kerr et al., 2015 and Kerr et al., 2013).

The results of the formative luminescence work (Higashimura et al., 1963) were available during the development of the first dosimetry model, TD65, and they included determinations of cumulative gamma dose obtained with roof tiles. Although ceramic tiles were used widely on the roofs of traditional Japanese houses, and consequently distributed across residential areas, very few were suitable for dosimetry measurements (Ichikawa et al., 1966) because of the heating they experienced before and after roof collapse during the conflagration that followed bomb detonation, particularly at Hiroshima. Alternative ceramic samples were available in the form of façade and decorative tiles fastened to concrete buildings, albeit at fewer locations. The availability and survival of such tiles was sporadic at Hiroshima, and more so at Nagasaki, restricting the range of ground distances from the hypocenter at which dose determinations could be obtained. Tiles also necessarily limited the depth to which dose determinations were measured, compared with a solid brick wall, for example. None the less, the results of experimental measurements from a much wider range of standing buildings located at different ground ranges were available for comparison with calculated values obtained with a computational model developed using Monte Carlo radiation transport simulations (Roesch, 1987 and Maruyama et al., 1987). Although good agreement between calculated and measured values of gamma dose was obtained at Hiroshima and Nagasaki with DS86 over a wide span of ground range, there were indications at Hiroshima of the registration in ceramic samples of a gamma dose in excess of the calculated values, by ~100–200 mGy, at a ground range of ~1.5 km.

During the decade following the publication of DS86, further experimental data produced from luminescence and AMS measurements became available. Determination of the gamma dose to tiles from buildings at a ground range of ~1.6 km at Hiroshima (Nagatomo et al., 1992, Nagatomo et al., 1995 and Hoshi et al., 1989) broadly supported the observation of an excess dose at this ground range, although the estimates had not been converted to free field tissue kerma by the application of the radiation transport modelling developed for DS86. Gold (1995) also suggested that the large dispersion evident in luminescence estimates of dose at

a ground range of ~2 km (Hoshi et al., 1989) was the result of a strongly anisotropic gamma radiation fluence, which would have been coupled to a similar anisotropy in the neutron field. Further measurements performed to determine thermal neutron activated products at Hiroshima (Straume et al., 1992) indicated levels that were significantly higher than the DS86 calculated values at distances greater than 1 km from the hypocenter and lower than the calculated values at the hypocenter. This gave rise to a distance versus activation relationship calculated by DS86 that was at odds with the experimentally derived data, in contrast to the generally good fit obtained when making an equivalent comparison for gamma rays. While over 95% of the radiation dose to survivors was attributed to gamma radiation, the neutron discrepancy raised persistent doubts within the radiation risk community regarding the overall accuracy of the DS86 calculations (Cullings et al., 2006).

3.3.1.1. Current dosimetry system, DS02

The airing of the neutron and, to a lesser extent, gamma dose issues provided sufficient impetus to re-examine the neutron dosimetry derived from the DS86 computational model, and examine a spatially broader range of locations and samples to obtain experimental determinations of gamma dose and concentrations of neutron activated products. The revised dosimetry system, published in 2005 (DS02; Young and Kerr, 2005), produced a more detailed explanation of the origin of the fluences of neutrons and gamma rays following detonation and fission of the bomb materials and the debris they produced. It provided estimates of cumulative free-in-air (FIA) kerma to a distance of ~2 km from the hypocenter that arose from the direct exposure to gamma (and neutron) radiation that was delivered within a few minutes of detonation.

The re-evaluation of the neutron fluences in DS02 included some 300 measurements of fast-neutron-activation products (^{32}P in porcelain insulators, ^{63}Ni in copper artefacts) and thermal-neutron-activation products (^{152}Eu and ^{38}Cl in rocks and roof tiles; ^{60}Co, in iron and steel artefacts) and a complete recalculation of the radiation output and radiation transport for the Hiroshima and Nagasaki bombs. An exhaustive evaluation of the results (Young and Kerr, 2005; chaps 8–10) led to the conclusion that the enhanced values of thermal neutron activation observed beyond 1 km were due to a background activity in the measurements that had not been accounted for previously, and a slight underestimation of the burst height of the detonation accounted for the lower measured values. When applied, the adjustments resulted in good agreement between measured and calculated values of activation across the range of distances of interest - and hence the neutron discrepancy was considered to have been resolved.

The formulation of DS02 also included the additional luminescence determinations of cumulative gamma dose to ceramics that had been obtained after the publication of DS86, and various aspects of earlier measurements were re-examined (Cullings et al., 2005 and Maruyama et al., 2005), including the early work by Ichikawa et al. (1966) that had provided key data at distances of less than 1 km from the hypocenter in both cities. The measurement data had been subject to screening, with samples selected on the basis of minimal shielding and where the age of the building was known. This work also included the testing of ceramics from a heavily shielded location in a building of known construction date to check the experimental procedures for cumulative background dose estimation, and tiles were tested for secondary heating during the fires that spread within the cities. In total, the distance vs measured gamma dose relationship was produced using 125 and 60 determinations of dose to directly exposed ceramic samples in Hiroshima and Nagasaki, respectively. As for DS86, TL high temperature and pre-dose measurement techniques were applied to HF-etched quartz coarse grains to determine the cumulative dose. The techniques used to determine the background dose are discussed in detail in the DS02 report.

The radiation transport calculations employing forward-adjoint Monte Carlo coupling techniques had been applied in DS86 to obtain calculated values of gamma fluence and subsequently the dose to quartz was calculated for specified ceramic sample locations. Similar calculations of the in-situ dose to quartz were not performed for DS02, but transmission factors (Egbert et al., 2007) were applied to the experimental values to obtain free-in-air kerma at each sampled location (Young and Kerr, 2005). The level of agreement between the DS02 calculated and experimental values of gamma dose at both Hiroshima and Nagasaki was judged to be good overall, although expressed only in qualitative terms. The production of a single figure of merit was considered to be problematic due to issues related to the weighting of individual dose determinations and the presence of unquantifiable errors, particularly those associated with the dose determinations obtained in the early testing work, for the very wide range of dose values (~100–0.1 Gy) under consideration (Cullings et al., 2005 and Young and Kerr, 2005, p451). While the agreement was deemed to be particularly good near the hypocenter at Hiroshima, it was conceded that at larger distances (>~1 km), the background dose in the case of ceramic samples may have been underestimated, giving rise to the apparent excess dose suggested in the earlier publications referred to above. At Nagasaki significant differences in the values of cumulative dose at several locations between ~520 and 660 m from the hypocenter were attributed to the limited number of measurement locations compared with Hiroshima and uncertainties related to the calculation of the transmission factor at these locations (Cullings et al., 2005, p.450). Hence,

whereas the level of agreement between measurement and calculation was regarded as good overall, conclusions regarding the significance of indicated differences were equivocal. Nonetheless, while the revised estimates of gamma dose produced by DS02 did not substantially alter those of DS86, the work undertaken largely resolved the reported contradictions in the assessment of dose arising from thermal neutron activation and endorsed the underlying basis for the assessment of radiation risk arising from exposure of workers to gamma rays that had been recommended (ICRP, 2007).

3.3.1.2. DS02 follow-up

Further examination of the differences between measured and calculated values of gamma dose was undertaken at two recent workshops (Kerr et al., 2013 and Kerr et al., 2015). Notwithstanding the overall agreement obtained between the luminescence and calculated values of free-in-air kerma with ground distance over a range of three orders of magnitude of dose (Fig. 37), discrepancies within this range formed the focus of further scrutiny, in particular at a ground range of ~1500 m at Hiroshima and at greater distances where the dose was below 1 Gy. As argued by Egbert and Kerr (2012), possible causes of these differences included 'residual' sources of radiation comprising: (a) neutron activated products in environmental materials such as soils and building materials, and (b) weapon debris comprising radioactive fallout, nuclear fuel (U/Pu) and neutron activated products from the weapon. Although 'residual' radiation had been assessed as a contributor whole body dose in the development of DS86 and DS02, it had been concluded that it was likely to be a minor factor.

Fig. 37

An accurate assessment of the size of any additional exposure dose to survivors arising from the 'residual' sources requires knowledge of the activities and distribution of each type. Although the largest potential reservoir of sources is considered to be contained within the cap of the nuclear cloud, the sources were in the form of sub-micron particulate debris within fallout that was dispersed and transported eastwards far beyond the sites of detonation due to a very slow rate of descent. However, there is evidence of some sporadic deposits of fission products reported within several km west of the hypocenter at Hiroshima.

3.3.1.3. Transported residual sources

In the formulation of DS02, various forms of fallout and in-situ neutron activation within environmental and building materials had been taken into account as potential contributors to the production and dispersal of radioactive sources. Close to the hypocenter where proximal survivors were located in both cities, the main

residual sources were neutron-activated radionuclides in soil and building materials that had been lofted into the trailing stem and then re-deposited, giving rise to a heterogeneous pattern of deposition. Environmental factors relating to atmospheric conditions further extended the distribution, precipitation causing wet deposition in some areas, and leading to greater penetration in the ground. Flooding at the Hiroshima site also created additional deposition pathways over a greater area and ultimately into the estuarine river systems leading to the sea. On the basis of ground-level activity monitoring data, these sources were estimated to contribute dose at levels that were one or two orders of magnitude lower than the cumulative dose measured in ceramic samples between 1 and 2 km from the hypocenter, although it had been recognized that the dose attributed to neutron activation was subject to significant uncertainty caused by factors related to its production (Cullings et al., 2006). Subsequent investigation of this issue (Egbert and Kerr, 2012) suggested a potential correlation of the spatial patterning of elevated levels of localized fallout and the excess dose indicated by the ceramic measurements, the former drawing on the radiation survey monitoring data obtained at ground level in 1945, subsequent ^{137}Cs measurements in soil and modelled 'black spot' rain patterns. The original monitoring at ground level identified areas of relatively high concentration of fallout, but the uncertainty in the quantities and spatial and temporal distribution of fission product fallout at Hiroshima was considered to be significant.

A rapid downward percolation of fallout products in soil following the heavy rains during typhoon conditions that prevailed during the middle of September 1945 has been suggested (Egbert and Kerr, 2012) as one of the possible causes of the significant mismatch in dose estimates obtained from the two approaches of survey measurements and ceramic dosimetry; the largest differences occur in Hiroshima, but some are also evident in Nagasaki. To investigate these enigmatic differences further Egbert and Kerr argue that a more detailed understanding of spatial variation of cumulative dose would be obtained by testing ceramic building materials in areas of high and low fallout. The objective of such measurements would be to estimate the proportion of the total dose attributable to fallout that had been received by distal and proximal survivors and to compare the spatial correlation of luminescence determinations and fallout with that predicted by a computational model for the trajectory of fallout and its evolution with time. In such work it would be important that the ceramic materials selected were of contemporary manufacture in 1945 to minimize the cumulative background dose (D_{BG}).

3.3.1.4. Future work

An indication of the potential for luminescence techniques to yield further information on the sources of residual radiation at Hiroshima has been provided by the measurement of high resolution depth-dose profiles (Fig. 38) reported at the 59th Annual HPS Meeting in Baltimore, MD and accompanying 2014 Workshop (Stepanenko et al., 2014). A single grain measurement procedure was applied to coarse quartz grains extracted from thin slices cut at progressively increasing depths in black-glazed ceramic tile; the depth-dose profile obtained provided evidence of a substantial beta dose registered in the sub-surface layers. The tile had been located in the roof eaves of the Old Hiroshima University building H-4 at a ground range of 1324 m (Young and Kerr, 2005). After deconvolution of the depth-dose profile, the value of external beta dose in the subsurface (~1Gy) was reported to be consistent with an estimate of several hundred mGy above neutron-activated soil at the Hiroshima hypocenter (Kerr et al., 2015). The average dose (depth range 2–22 mm) is 7% larger than the value adopted at this location in the DS02 model (measurements by Ichikawa et al., 1987), but given the combination of the use of two different measurement techniques (TL multiple grain and OSL single grain) and the differences in instrumentation during the intervening 30 years, this represents a very good level of agreement for dosimetry based on measurements with quartz. As noted by Kerr et al. (2015), the significant difference between the end-point energies of beta emitters associated with the main neutron-activated products in soil (all less than 3 MeV; [28]Al, [56]Mn, [24]Na and [46]Sc) and in the brackish waters of the river system ([38]Cl; 4.9 MeV) may provide the opportunity to establish the contribution of the latter in areas of the site affected by flooding by deconvolution of the beta particle depth-dose profiles obtained using a slice and single grain measurement technique. Also, if building structures with sufficiently thick ceramic layers are available (i.e., >10 cm), and preferably samples from locations with comparable source geometries, there is the opportunity to test the current interpretation of the physical dosimetry that the average energy of gamma photons increased linearly with ground range, from 2.4 MeV at 500 m to 4 MeV at 2200 m at both Hiroshima and Nagasaki (Egbert et al., 2007). For reliable measurement of beta depth-dose profiles within a depth range of ~5 mm using OSL techniques it will be essential that the outer surface is covered by an opaque layer and that the surface was not subject to flash heating following the onset of exposure to radiation from fallout. The expertise developed in the study of various Eurasian sites, discussed further below, which were characterized by issues of heterogeneous deposition of fallout, is of particular relevance to the research questions now being formulated to investigate the issue of residual radiation at the Japanese sites.

Fig. 38

One of the conclusions reached by the 2014 Workshop was that a more precise picture of the distribution and nature of the sources of residual radiation could help to resolve differing views on the potential effects on Hiroshima survivors located between ~800 and 2200 m from the hypocenter. On the one hand it can be argued (RERF, 2012) that within this ground range the health effects do not indicate a substantial underestimate of the dose and, close to the hypocenter, where ground activation was high, survivors could not gain access because of the physical destruction and conflagration. A differing view advanced, based on a multi-step cancer model (Kerr et al., 2015) is that a dose of ~1–2 Gy arising from exposure to sources of residual radiation would be required to match the prediction of the model and this would be comparable to the initial radiation dose (DS02) at ~500 m from the hypocenter (~1350–1450 m at Hiroshima; ~1450–1550 m at Nagasaki), making it a significant contribution at distances where many survivors were located, and thus representing an important departure in the currently adopted physical model for the dosimetry.

3.3.2. Chernobyl

The fallout from the Chernobyl nuclear power plant (NPP) was dispersed and deposited heterogeneously, the most heavily contaminated regions located sporadically across hundreds of kilometers within the Ukraine, Belarus and Russia (UNSCEAR, 2000). Luminescence retrospective dosimetry is not suited as a survey method on a large-scale because of the experimental effort required to apply it at any given location. The potential role that emerged for luminescence was the provision of benchmark values of cumulative dose for comparison with dose estimates produced by the deterministic models employed in dose reconstruction (Chumak, 2012). Although some exploratory retrospective work commenced within areas heavily contaminated by fallout from the Chernobyl reactor within five years after the accident (Bailiff, 1997), the work to obtain closer integration of luminescence techniques with the established approaches of dose reconstruction only commenced several years later. In an initiative that formed part of the Chernobyl Sasakawa Health and Medical Foundation Project (Hoshi et al., 1994) a joint Japanese–Belarusian team undertook fieldwork to sample buildings in 14 contaminated settlements Belarus (Sato et al., 2002). Working independently from the effort underway in Belarus, a collaborative group of institutes from the EU states, the Ukraine and Russia undertook fieldwork in three settlements in the Ukraine and Russia (Bailiff et al., 2004a and Bailiff et al., 2005). This research developed from a series of broad-ranging programs supported by the Commission of the European Communities (CEC) to investigate the radiological consequences of the Chernobyl accident (e.g., Karaoglou et al., 1996). Also, in a later study in Russia, a building in a

very highly contaminated forested recreational area was examined by Ramzaev et al. (2008).

3.3.2.1. Settlements in Belarus

The study undertaken during 1994 in Belarus by the Japanese-Belarusian team (Sato et al., 2002) examined one building in each of 5 settlements within the 30 km Exclusion Zone and 9 settlements located in a NNE direction between ca 150 and 250 km from the NPP in the Mogilev oblast (Supplementary Material, Fig. SM1), and it appears to be the only published report of a multi-settlement study of settlements in Belarus. Within the proximal region, the official (^{137}Cs) contamination levels for four of the settlements ranged from ~6000 to 15,400 kBq m^{-2} and, within the distal region they ranged from ~1100 to 1300 kBq m^{-2}. In each of these regions an additional settlement was selected with relatively low levels of contamination for comparison (up to ~100 kBq m^{-2}; locations G5 and M5 in Fig. SM1, Supplementary Materials). The objective of the work was to examine the relationship between the cumulative dose registered in brick and: (a) the contemporary dose rate recorded using dosimeters, and (b) the measured contamination activity levels in soil. For each building, TL phosphor and glass (radiophotoluminescence, RPL) dosimeters were implanted for a year to record the contemporary dose rate at each exterior and interior sample location, and the dose rate was also measured using a survey meter; in the case of wooden buildings the interior brick samples were taken from the typical rural brick-encased stoves. The survey monitoring and dosimeter measurements performed at the sample locations produced self-consistent results and at the interior locations they confirmed dose rates significantly higher than those typically obtained due to the presence of lithogenic radionuclides in the building materials alone (these were accounted for, but not included in the paper).

Although a detailed approach was taken in the fieldwork procedures, the cumulative dose determinations obtained with brick, DX, (denoted D_n in Sato et al., 2002), particularly from interior locations of sampled buildings, presented inconsistencies and difficulties in interpretation that limited the extent to which they could be applied more generally to settlements with lower levels of contamination (i.e., <1000 kBq m^{-2}). The main difficulty encountered in the Belarus study was finding that the cumulative dose to brick located within the interior of most of the buildings was significantly higher than expected for contamination deposited externally on the ground. For seven of twelve buildings where both exterior and interior bricks were sampled, the cumulative dose to the interior brick exceeded, or was comparable to, that registered by the exterior brick and, in all cases except one, the cumulative dose registered in the interior brick was at least 200 mGy, the highest being 700 mGy (see Supplementary Material, Table SM1). The brick buildings

selected were between ~10 and 20 years old and judged to have been constructed with new brick stock. The shielding provided by a single and double wythe brick wall (~10 and 20 cm thick, respectively) is expected by calculation to result in an reduction in dose to 30% and 10%, respectively, of that at the exposed face of the external brick (Bailiff, 1999). While two of the buildings exhibiting this 'reversal' were constructed in wood (mounted on a plinth containing brick), the others were constructed of brick. For example, in one building (G3, brick, double wythe), the dose at the surface of the interior brick was some three times larger (244 ± 144 mGy) than that at the exposed surface of the exterior brick (67 ± 14 mGy), albeit with a large uncertainty. In this case the dose registered in the exterior brick was not significantly lower than that expected on the basis of the measured ^{137}Cs contamination in soil, although for dose determinations below ~100 mGy, the generally high uncertainty in the measurement results limits the scope for a more detailed analysis. The authors suggest that the anomalously large dose values registered by the interior bricks could have been the result of strong sources that had been present inside the buildings.

The form of the depth-dose profiles obtained for walls of three buildings (Fig. 39; G4, distal settlement; G6, proximal settlement) have gradients significantly less than that expected (indicated by broken line) for ^{137}Cs sources (662 keV) distributed externally on flat ground adjacent to a structural wall (Bailiff, 1999). In the case of building G6, the measured value of D_x at the exterior surface is 1.45 ± 0.20 Gy and at the interior surface of the 2nd wythe (presumed 20 cm depth) it is 0.34 ± 0.09 mGy; the depth-dose profile indicates that at the intermediate depth of 10 cm the value of D_x is ~0.7 Gy. These determinations are to be compared with values of ~0.48 Gy (0.3 D_x) and ~0.15 Gy (0.1 D_x) at depths of 10 and 20 cm respectively, predicted by Monte Carlo simulations for a ground source, indicating an excess dose of 0.19 Gy at the interior surface.

Fig. 39

If a sufficiently strong concentration of sources was present within the interior of the building, a 'counter' gradient would be present, giving rise to a composite depth-dose profile. Although the buildings at locations G4 and G6 appear to be single storey dwellings (3–3.5 m height, Sato et al., 2002), the roof, unless flat, would have been unlikely to have retained a concentration of sources sufficient to give rise to a strong 'counter' gradient (see also discussion in Section 3.3.2.5 and Fig. 45). Although the form of the measured depth-dose profiles provides some qualitative support for such a combination of source configurations, the values of the dose determinations for the interior samples (presumed to be at ca 20 cm depth for the double wythe walls in these three buildings) appear to be too low to account for the

sustained level of dose observed in the middle of the wall. Noting that the form of the profiles is dependent on both source energy and source configuration, the relatively shallow gradients of the depth-dose profiles for these three locations (G6 and G9 being proximal and G4 distal) correspond closer to a calculated profile for a source energy in the region of ~1600 keV (e.g., the deposition of ^{140}Ba/^{140}La), but this is unlikely on the basis of the published fallout inventories in that region (UNSCEAR, 2000). Consequently aspects of the dose determinations obtained with the ceramics remain enigmatic.

Notwithstanding these problems at a detailed level, Sato et al. (2002) extract a form of dose conversion factor from a plot of the values of D_x for external brick vs the official settlement areal ^{137}Cs activity (Fig. 12 in Sato et al., 2002). For the period extending from the onset of delivery of fallout to the middle of 1994, when the samples were extracted, a value of ~0.1 mGy per kBq kg^{-1} for the cumulative gamma dose was derived, noting that the calculation is based on a dose value at the exposed brick surface. It is interesting to note that the value of this conversion factor, when doubled (to adjust for the shielding of the building, as discussed in Section 1.4), is broadly consistent with the dose conversion factor for the period 1986–1997 employed in the deterministic model developed by Likhtarev et al. (1996), which is discussed in the context of the retrospective dosimetry work conducted in the Ukraine (Section 3.3.2.2).

Using the dose rates recorded by the RPL dosimeters, and correcting for decay over 9 years assuming the sources were dominated by ^{137}Cs, the calculated values of cumulative dose since the onset of delivery of fallout were compared with the measured values of D_X at exterior and interior locations, respectively, where results were available. In the plot obtained (Supplementary Material, Fig. SM2), the trend line shown is reported to be the regression line fitted to the data obtained for the exterior locations, with a gradient of 1.5, and this is interpreted to indicate that about half the dose registered in the bricks arises from sources other than ^{137}Cs. While this is an interesting application of the dosimeter data, the apportionment appears to be high when compared with the proportion of cumulative dose arising from all radionuclides except ^{137}Cs and ^{134}Cs during the first year which is estimated to be ~12% in the deterministic dose model developed for use in the Russian territories (Golikov et al., 2002). Also, it is not clear whether, at the time of brick sampling, soil activity profiles had been measured to examine for evidence of decontamination (i.e., removal of soil) or the downward migration of the long-lived radionuclides in soil, both of which would affect the contemporary dosimeter measurement.

The Belarus project serves to illustrate the difficulties often encountered in fieldwork of this type, conducted in restricted areas where the opportunities to return to the field to resolve issues revealed by subsequent laboratory testing may be very limited. Consequently, one of the main objectives of formative methodological work of this type is the identification of conditions in the field that will potentially enable a relatively direct conversion from dose estimates in ceramic to a quantity suitable for use in dose reconstruction and reduce the risk that the investigation is drawn into resolving complexities of dosimetry of the building. This can be difficult to achieve on a short timescale, and it is worth noting that the Hiroshima/Nagasaki and Techa River studies have evolved over several decades of research.

3.3.2.2. Settlements in the Ukraine and the Russian Federation

For the purposes of developing a methodological basis for further work, direct comparisons of dose estimates produced by luminescence and the deterministic models were performed for settlements that were: (a) highly contaminated and promptly evacuated, and (b) contaminated but continuing to be inhabited. To investigate the first category, a program of fieldwork was completed in two highly contaminated settlements (with official levels of ^{137}Cs > 2000 kBq m^{-2} in 1986), one in each of two widely separated locations downwind of the reactor (Fig. 40), in Ukraine (Vesnianoje) 35 km W and the other in Russia (Zaborie) 220 km NNE of the reactor (Bailiff et al., 2004a). These settlements, having been evacuated at an early stage following the accident, were expected to have been relatively undisturbed by restorative counter-measures, such as the removal of contaminated soils. The participation of six laboratories, each applying their preferred measurement procedure (TL or OSL) to determine the cumulative dose at seven sampled external locations on six brick buildings, provided a test of the robustness of the experimental procedures for general use. Working with quartz extracted from a common depth range (5–25 mm depth from the exposed surface), the group achieved a level of agreement in the measured values of D_T across all the locations tested (14% relative standard deviation). This is considered good given that no restrictions were imposed on the experimental procedure, apart from participation in a beta source inter-calibration (Göksu et al., 1995). The depth-dose profiles obtained indicated consistency with a calculated profile (using Monte Carlo radiation transport simulations) for sources of energy of 662 keV (^{137}Cs) uniformly distributed to a depth of 5 g cm^{-2} within the ground adjacent to the sampled wall (Meckbach et al., 1996 and Bailiff, 1999). After subtraction of the background dose (~9–30% D_T), D_{BG}, the values of D_X ranged from ~100 to 300 mGy in Zaborie and ~450–780 mGy in Vesnianoje.

Fig. 40

The kerma in air at the Reference Location (RL), RLDX, was obtained by applying the conversion factor, CRL, where,

$$_{RL}D_X = C_{RL}D_X. \tag{6}$$

The value of CRL, which is the inverse of the ratio of the absorbed dose in brick to the air kerma at the Reference Location, was calculated for each sample location by performing radiation transport Monte Carlo (MC) simulations using a specified source energy (662 keV) and source geometry (Bailiff et al., 2004a and Bailiff and Slim, 2008). The MC simulations indicated that while the value of CRL does not vary greatly with changes in the depth-activity profile in soil, it is more sensitive to local variation in areal source activity (e.g., mBq m^{-2}), with, not unexpectedly, fallout closer to the structure having the greatest influence on the dose measured in brick. Sources distributed within 20 m of a wall location, for example, account for some 60% of the dose in the sub-surface of the wall at a height of 1 m (Bailiff et al., 2004a). To obtain reliable estimates of the cumulative dose at the Reference Location on the basis of measurements with bricks within the sampled wall(s), the effect of local heterogeneity in fallout density was removed to avoid overestimation or underestimation of $_{RL}D_X$. The former arises, for example, where fallout is washed by rainfall from a roof lacking guttering onto the ground surface below giving rise to a halo of increased activity. Conversely, if more heavily contaminated soil is removed and replaced with uncontaminated soil, a deficit in activity relative to the surrounding ground would be created.

To adjust for local variations in the distribution of fallout, a heterogeneity correction factor F_h was introduced to the calculation of $_{RL}D_X$. By performing radiation transport simulations for sources located within areas of the adjacent ground divided into a grid, the relative weighting of contributions from each element of the grid to the absorbed dose registered in a wall were calculated (Bailiff et al., 2004a). An above-ground survey of the activity performed adjacent to a sampled wall using a portable Geiger-Müller radiation monitor, coupled with gamma spectrometric analysis (^{137}Cs) of sections of cored soil sampled from within the same area (up to ~12 m from the wall), provided data for mapping the spatial variation in activity. Calculation of the weighted effect of an excess/deficit in activity within each area relative to the average activity more distant from the wall yielded the correction factor required to remove the effect of the local heterogeneity.

By applying the results of the two simulation exercises, the value of kerma in air at the Reference Location were obtained for each sampled location (at a specified sample depth) by application of the conversion factor C_{RL} and the additional

heterogeneity factor, F_h, to correct for the effects of local spatial variation in ^{137}Cs deposition in the ground adjacent to the sampled location where,

$$_{RL}D_X = C_{RL}F_hD_X. \qquad (7)$$

3.3.2.3. Comparison with deterministic models

The deterministic models employed in dose reconstruction developed (Jacob and Likhtarev, 1996) to calculate the cumulative external gamma dose at the Reference Location, employ historical data derived from periodic monitoring measurements of activity in soil. These models take into account the identification of the contributing radionuclides and also the measurement of dose-rate at a location judged to be consistent with that required for a Reference Location. The conversion of measured ^{137}Cs (and ^{134}Cs) areal activity (as kBq m^{-2}) to cumulative kerma in air, is obtained using an equation of the form:

$$_{RL}D_{cal} = D_\Sigma A_a, \qquad (8)$$

where, the coefficient D_Σ (mGy per Bq m^{-2}) is calculated for a required time interval and Aa (Bq m^{-2}) is the average ^{137}Cs areal activity in soil at the Reference Location, adjusted to the time of cessation of the delivery of fallout in 1986. For the Zaborie/Vesnianoje study, three deterministic models were applied for comparison with luminescence, two in Zaborie (Golikov et al., 1999 and Golikov et al., 2002; and an unpublished model described in Bailiff et al., 2004a) and one in Vesnianoje (Likhtarev et al., 2002). The calculation of $_{RL}D_{cal}$ is sensitive to variation in activity-depth profiles in soil and the two published models apply further adjustments to account for percolation of radionuclides in soil with time.

The plot of $_{RL}D_X$ versus $_{RL}D_{cal}$ is shown in Fig. 41 and represents the first systematic application and comparison of the two approaches in contaminated settlements. The average value of the ratio $_{RL}D_X$ /$_{RL}D_{Cal}$ (0.95; range, 0.72–1.12 for Zaborie and 1.07; range 0.80–1.36 for Vesnianoje) indicates overall agreement between the two systems of dose estimation within margins of ±25%. While the uncertainty in the values of D_X, as estimated by the laboratories, ranged between ±10% and ±13%, variation in the ^{137}Cs areal activity of the soil adds a comparable level of dispersion, increasing the overall uncertainty in ($C_{RL}F_h$) to between ±15 and ± 25% (1σ). These levels of uncertainty in $_{RL}D_X$ for settlements selected to have the least post-accident modification of their soils consequently provided an indicative baseline for inhabited settlements where modification of soils is more likely to have occurred. The overall agreement between the two sets of results supports the assumption made in the deterministic models that the relative contribution to the gamma dose arising from short-lived isotopes delivered during the immediate post-accident period and prior

to monitoring measurements that are unaccounted for in the model was relatively minor, although this is clearly a limited test.

Fig. 41

3.3.2.4. Populated settlement study

The methodology developed for the highly contaminated evacuated settlements was applied to a populated settlement in Russia, Stary Vishkov, located 175 km NNE of the reactor (Fig. 40), where the official average contamination was lower than in Zaborie and Vesnianoje, but nonetheless significant (1470 kBq m^{-2} ^{137}Cs in 1986). Since Stary Vishkov has remained populated since the accident it is of greater relevance to epidemiological studies. Ten brick buildings within the settlement, built between 1961 and 1978 were sampled and the measured cumulative dose due to fallout (5–15 mm depth in brick), D_X, ranged from 50 to 180 mGy. In this case the average ratio of D_{BG}/D_X was relatively high (mean: 1.1; range: 0.5–2.8) and the uncertainty in D_X is more sensitive to uncertainty in the estimation of D_{BG} compared with the two sites discussed above. As a means of checking the reliability of the determination of D_{BG}, and also the assumptions regarding the time-averaged source energy, the depth-dose profile (Fig. 42) obtained is consistent with the presence of an external (gamma) source of energy of 662 keV and confirms, for the most heavily shielded sample, a value of D_T that is in agreement with the value of D_{BG} calculated using Equation (4b).

Fig. 42

Of the ten locations in the settlement selected for brick sampling, measurements of the 137Cs activity of soil with depth had indicated evidence of disturbance at six of the locations and beyond 10 m the extent remained too high to obtain reliable estimates of cumulative dose at the Reference Location. However, values of $_{RL}D_X$ were calculated for the remaining four buildings where the disturbance was sufficiently constrained and these are plotted against the average areal ^{137}Cs activity for the ground adjacent to each wall location in Fig. 43(a), where the correction for heterogeneity, F_h, had been applied in each case. The results indicate an overall concordance of dose estimates produced by luminescence and the deterministic model as indicated by the broken line in the plot. As for the highly contaminated settlements, the relatively large uncertainties in $_{RL}D_X$ and $_{RL}D_{cal}$ reflect the local spatial variation in the measured areal ^{137}Cs activity. The pattern of fallout distribution obtained for one of the buildings (location #55) illustrates the main features of variation often observed: a downward percolation of ^{137}Cs in the soil depth-activity profiles (Fig. 44(a)) and an increase in areal activity close to the building arising from roof wash-off in the absence of a rainwater collection system

(Fig. 44(b)). While in this example there is a significant drop in areal ^{137}Cs activity within 10 m from the sampled wall, the much lower rate of change prevailing at greater distances (Fig. 44(c)) justified the calculation of C_{RL} to enable conversion to the Reference Location.

Fig. 43

Fig. 44

Fig. 45

For the six buildings where the extent of disturbance in the soils beyond 10 m was significant, a conversion factor was calculated for a more restricted 'local' environment, extending to 25 m from the sampled wall, C_{25m}. The values of $_{25m}D_X$ obtained for these locations are plotted against the average ^{137}Cs areal activity in Fig. 43(b), where the broken line corresponds to the values calculated using the deterministic model and a dose coefficient calculated for the period of exposure ($D\Sigma$ = 0.16 mGy a^{-1} per kBq at the Reference Location). Conversion of D_X to cumulative kerma in air for the local area, enabled measured values of the location factor, f, (as $_{25m}D_X/_{RL}D_X$) to be calculated. The measured values of f for Stary Vishkov ranged from 0.3 to 1.1 and this is a significantly wider range than had been proposed previously for outside locations in Russian settlements (0.4–0.5; Golikov et al., 1999). The data obtained from this study suggest that, in addition to obtaining benchmark values of cumulative dose at the Reference Location, a further potential validation role in dose reconstruction could include the measurement of location factors for a range of environments within a settlement.

3.3.2.5. Forested environment study

Ramzaev et al. (2008) present the results of a study undertaken in a forested environment, based on an examination of two brick-built structures within the recreational area of Novie Bobovichi, located 20 km NW of Novozybkov in Bryansk Oblast, and ~180 km NE of the Chernobyl NPP. The fallout deposition in the pine-forested recreational area was both heterogeneous and heavy, with an official 137Cs contamination level of 1.1 MBq m^{-2} in 1986, and the penetration of ^{137}Cs in soil was relatively shallow (reported to be within 4 cm). This study is interesting because the presence of a tree canopy gives rise to a more complex distribution of contamination compared with that obtained in the more open landscapes of Zaborie and Stary Vishkov. Also, Ramzaev et al. (2008) based their dose conversion factor on relative gamma dose rate measurements rather than computational modelling. In their radiation transport model for urban environments Meckbach and Jacob (1988) examined the effect of fallout retention within tree canopies and found a potential increase in dose rate within buildings. However, Golikov et al. (1999), in calculating

the effect of deposition within forested areas containing a dense tree canopy found that the external dose rate could be, depending on the height of the canopy, 2–3 times less than obtained with a source distribution on the ground.

In the Novie Bobovichi study, four brick samples were tested, two collected from exposed walls (one middle and one corner) of a small hut (2.2 × 1.6 m by ~2 m height) located within a forest setting, and two from an interior shielded location of the brick basement of a nearby wooden house; the age of the buildings was estimated to be 21 ± 2 years at the time of sampling (2004). The small hut, constructed of a 1-wythe (single skin) brick wall (~12 cm thick), was roofed with asbestos-cement sheet that, in 2004, was covered in a thick layer of forest litter (and presumed here to have a single low pitch). The cumulative dose due to fallout was determined using an experimental methodology similar to that discussed above (given in detail in Ramzaev et al., 2008), and included the application of an OSL SAR procedure to granular quartz extracted from the brick. The brick samples were cut to enable depth-dose profiles to be produced for the shielded basement bricks and the hut bricks (Fig. 45); polynomial curves were fitted to the measured profiles and extrapolated to zero depth to obtain values of a surface cumulative dose; 145 mGy at the mid 'wall' and 171 mGy at the 'corner' brick locations of the hut. The gamma dose rate was measured at the two hut sample locations and at the selected reference location (1 m above ground level and at least 2 m from the nearest tree); the dose rates at the reference location and the hut mid-wall location were 783 ± 95 and 457 ± 39 nGy h^{-1}, respectively. The ratio of these two dose rates, 1.71 ± 0.25, was applied to the determination of cumulative dose in brick (145 mGy) as the dose conversion factor, resulting in an estimate of the cumulative dose in air of 248 mGy. Following a similar calculation, the estimate of 228 mGy, obtained by employing the data for the corner brick, yielded a consistency that is encouraging. However, it should be noted that the internal dose profile within a brick at the corner of a building is complex where sources are distributed on the surrounding ground facing both walls. Consequently a building corner is usually not an optimum position for sampling (LUMINATE, 2003), as reflected in the measured depth-dose profile for the corner brick in the case of the hut (Fig. 45).

The measured depth dose profiles for both hut bricks appear to be complex when compared with a calculated profile for sources distributed on the ground (Meckbach et al., 1996). By speculatively applying (using the general purpose modelling tool described in Bailiff and Slim, 2008) a simple combination of calculated profiles for sources uniformly distributed on the ground facing the wall and on the roof, a surprisingly good match with the measured profile was obtained (Fig. 45). Although

in this case the calculated profiles for sources distributed on the floor of the interior and on the roof are expected to be similar, the roof appears to be the more likely location of the sources. In which case, apart from the issue of the equivalence of the instrument used to measure the gamma dose rate and quartz grains in brick at the sample location, the calculation of the dose conversion factor using the measured dose rate ratio, as applied in this study, assumes that the relative areal activities of the sources on the ground and on the roof have remained unchanged. With a relatively thin wall (single wythe, or single skin), these profiles illustrate the potential for a contribution to the extrapolated external surface dose from sources other than those distributed on the ground, reducing the value to be used to calculate the dose at the reference location (in this case a relatively modest ~10 mGy is indicated).

Ramzaev et al. (2008) also calculated the cumulative dose using a deterministic model by applying an initial ground contamination of 1.1 MBq m^{-2} for Novie Bobovichi to the estimated dose coefficient (216 mGy per MBq m^{-2}). The value of 238 mGy obtained compares very well with the values obtained at the reference location derived from the two brick determinations. Since the dose coefficient for the period 1986–2004 was based on a coefficient for the period 1986–1997 that had been calculated for a general rural, rather than forested, environment in Bryansk (Bailiff et al., 2004a), this agreement is interesting, and an examination of the soil contamination profiles within the ground adjacent to the sampled walls may cast further light on the reason for this equivalence.

3.3.3. Techa River

Discharges of radioactive waste (100 PBq; Trapeznikov et al., 1993) into the Techa River system from the Mayak Nuclear Materials Production Complex facility between 1949 and 1956, which peaked during the period 1950–51, gave rise to a potentially serious radiological hazard to populations of riparian settlements located downstream of the facility. In particular, the closest settlement through which the river flowed, Metlino, was located only 7 km from the point of release, and the riverbanks, contaminated with ^{90}Sr, ^{137}Cs and other radionuclides, were frequently used as a recreation area (Degteva et al., 1994). Radiation monitoring did not commence until the middle of 1951 and it was not until 1956 that the population of Metlino was relocated, by which time some seven years of potential exposure to radiation had occurred. Following evacuation, most of the settlement was destroyed, although several substantial, but partly demolished, buildings constructed of brick were left standing. The latter comprised a mill, a granary and a church sited between Metlinsky pond and Reservoir 10 (Fig. 46), the latter having been created during the autumn of 1956 by demolishing and then flooding what remained of the settlement.

Luminescence techniques were applied to the three surviving brick buildings in Metlino, with the objective of providing values of cumulative dose that could be used to reconstruct the kerma free in air dose at a reference location within the riverbank zone during the period 1949–1956 for comparison with the predictions of the Techa River Dosimetry System (TRDS; Degteva et al., 2000, Degteva et al., 2006, Degteva et al., 2012 and Shagina et al., 2012). The TRDS was developed to support a long-standing epidemiological study of the affected populations of the Techa River region and included a cohort of 30,000 individuals. In addition to the study in Metlino, bricks from a mill and associated buildings on the banks of the Techa River in Musylmovo located some 70 km further downstream were obtained for the dosimetry intercomparison.

Fig. 46

A slightly different radiological issue related to atmospheric releases from the MPA facility has also been investigated. Brick samples from several buildings in the city of Ozyorsk, located 8–10 km downwind from the release points, were tested to establish the potential exposure of inhabitants to radiation from releases of radioactive argon, krypton and xenon within the period 1948–1956 (Woda et al., 2009b).

3.3.3.1. Metlino

Uncertainties in the timing and nature of changes in the distribution of the radionuclide sources relative to the location of the three brick structures standing in Metlino (Fig. 46) have made the study of this site a challenging test of the coupled application of luminescence and radiation transport modelling. Of primary interest is whether the reliability of dose estimates for the period 1949–1956 can be improved by judicious choice of sample locations, the selection of which is expected to be sensitive to changes in source geometry. Fortunately, although published relatively late in the sequence of experimental work (Bougrov et al., 1995, Bougrov et al., 1998, Degteva et al., 2000, Göksu et al., 2002a, Jacob et al., 2003 and Tarenenko et al., 2003), more detailed information regarding the hydrological history and management of the fluvial system became available (in Russian) in 2005, and Degteva et al. (2008) clarify how the changes to water management affect the interpretation of results from the earlier work (see caption to Fig. 46).

Dose determinations were obtained with brick samples taken from various parts of the fabric of the Old Mill and the Granary (locations 1–6 in Fig. 46(b)) and also the Church. Initial work by Bougrov et al. (1995) had shown that the levels of cumulative dose registered in bricks from the Old Mill, ranged from 1 Gy (walls facing land) to 5 Gy (walls facing the reservoir), and that the cumulative background

dose was ~0.5 Gy arising from the substantial age of the buildings. The latter was checked by dating brick from a heavily shielded location in the mill and the resulting luminescence age of 129 ± 14 years was consistent with available documentary evidence (Bougrov et al., 1998). Although the NNW facing walls of the Old Mill and the Granary are of particular interest because part of the settlement was distributed around the shores of Metlinsky Pond, more recent work has focused on the SW wall of the Old Mill (Fig. 46, Loc #1). By obtaining measured values of dose in brick for samples at different heights, the results have the potential to inform the appropriate choice of source geometry model (Meckbach et al., 1996 and Göksu et al., 2002a), and consequently the calculation of a dose conversion factor. Estimation of the cumulative dose at a reference location for the period of interest (1949–1956) requires the separation of the contributions to the cumulative dose made before (1949–1956) and after the creation of Reservoir 10 during the autumn of 1956. Advancing the earlier work of Bougrov et al., 1998 and Tarenenko et al., 2003 constructed a 2-stage model for radiation transport simulations based on 'river' and 'reservoir' configurations of sources, corresponding to the pre- and post-evacuation stages. A calculated estimate of 0.35 Gy (2σ range, 0.2–0.6 Gy) was obtained for the cumulative dose during the post-evacuation period (1957–1997) using contemporary and historic monitoring and sediment radioactivity data for the reservoir floor and river channel deposits.

When examining the values of DX (Jacob et al., 2003, Tarenenko et al., 2003 and Bougrov et al., 1998) obtained for the SW wall of the Old Mill for the same depth range (10 ± 5 mm) and the same height, an overdispersion (ca 15–20%) was observed, unexpected given the relative proximity (several m) of the sampled locations. Jacob et al. (2003) concluded that, although not significantly affecting the median value of DX calculated for each height, some of the overdispersion could be attributed to systematic errors arising from one of the techniques applied. However, more recent work on bricks from Muslymovo (Woda et al., 2011a), has shown that elevated ambient temperatures in this region may cause the cumulative dose to be underestimated due to thermal fading of the 210 °C TL peak where it is used for the dosimetry. The extent of this effect depends on the thermal history of the volume from which the granular quartz was extracted, and consequently it is expected to be greatest where brickwork is exposed to a high levels of insolation. As discussed further in the following section, the use of OSL measurement procedures provides a means of circumventing this problem.

An initial examination of the variation of DX with height had indicated a systematic reduction in DX from 6 m to 1 m on the SW wall of the mill (Bougrov et al., 1998). However, subsequent analysis by Taranenko et al. (2003), which included the testing of additional samples, concluded that there was no significant difference between

the best estimates of D_x at 6 m and 4 m (3.1 ± 0.4 vs 2.9 ± 0.4 Gy, respectively; 95% confidence interval). This revised outcome supported a dosimetry model with a dominant contribution to the dose in brick from sources on the river banks, and with a minor contribution from the post-evacuation reservoir source geometry (0.35 Gy). For the sampled depth range in brick (5–15 mm), the calculated conversion factor to a reference location within the river bank zone was ~0.1 (i.e., about 10% of the dose at the reference location is registered in this depth range). Employing the median value of D_x obtained at a height of 6 m, and after subtracting the estimated contribution to the cumulative dose from the reservoir stage, a best estimate of 32 Gy (2σ range, 21–45 Gy) was obtained for the cumulative dose in air at the reference location during the period 1949–56, and this value compares well with the TDRS estimate of 26.6 Gy (Jacob et al., 2003). The experimental and computational steps leading to this comparison are instructive, not only because of the complexity of the radiation 'scenario', but because a detailed account is provided of the assessment of uncertainty in the experimental data and modelling calculations, using both deterministic and stochastic approaches (Jacob et al., 2003 and Tarenenko et al., 2003). Given the ten-fold factor applied to obtain the dose at the reference location, the analysis of the propagation of uncertainties is of particular importance for a study of this type where the source geometry history is uncertain.

In addition to the examination of variation of D_x with height, depth-dose profiles can be used as additional means of testing experimentally the robustness of a modelled source configuration. While determinations of D_x were also obtained at a depth of 20 mm in the later work referred to above, a deeper profile (>100 mm) enables different source configurations to be more readily distinguished. It is interesting to note that the deeper depth-dose profiles that had been obtained in the earlier work of Göksu et al. (1996) and Bougrov et al. (1998) for bricks from the SW of the Old Mill are closer to that calculated for ^{137}Cs sources uniformly distributed on flat ground (30 g cm^{-2}; Meckbach et al., 1996) than that calculated for the prototype 'river' stage model where the main contribution to the dose registered in brick was along the riverbanks (1 m-wide strips; Bougrov et al., 1998). Although the lower heights of the sample locations (1 m and 2 m above the reservoir level) in this earlier work lead to a higher dose contribution from the 'reservoir' configuration of sources, the comparisons suggest that the area of activity during 1949–1956 could have been spatially dispersed to a greater extent beyond the riverbanks than assumed in the river stage of the model.

Several dose determinations have also been obtained with bricks from the NNW walls of the Old Mill and Granary facing that face Metlinski Pond. The intervening fabric of the two buildings shields these two locations from radiation emitted by the Reservoir deposits and consequently are potentially of greatest relevance to the

environment experienced by residents inhabiting the settlement between 1949 and 1956. Dose determinations had been obtained with bricks at lower heights in the wall of the Old Mill and Granary but these locations were additionally shielded by the dam mound, and in 2008 further samples were obtained from the upper reaches of these walls (Degteva et al., 2008). Once completed, with conversion factors calculated for a Metlinsky Pond source model, a second – and critically important - comparison with the TRDS can be completed by employing data from these three locations. In addition, dose determinations obtained with bricks taken from various positions on the walls of the church (Degteva et al., 2008) and at three heights of the belfry walls are expected to provide further information of the time-averaged source configuration when published in full (Hiller et al., 2014).

3.3.3.2. Muslymovo

A substantial mill and a nearby water tower, both built in brick and located on the banks of the Techa River in Muslymovo, provided well-positioned sampling locations for monitoring the effects of the fluvially transported releases located ~70 km downstream of the point of release. The age of the mill reported in Bougrov et al. (1998) as 105 ± 10 years (and to a lesser extent the water tower, 55 ± 10 years) gave rise a cumulative background dose that accounts for a much higher proportion of the total dose than was the case for the buildings in Metlino. Bricks collected from three locations were used to form the basis of an intercomparison involving five laboratories (Göksu et al., 2002a) where both TL (210 °C peak) and OSL measurement procedures were applied to determine the cumulative dose (D_T, denoted DL in Göksu et al., 2002a) with coarse quartz grains extracted from a common depth range (10 ± 2.5 mm). Estimates of the cumulative background dose (D_{BG}) were obtained for two heavily shielded sample locations within the massive walls by applying TL and OSL procedures to determine D_T and calculating D_{BG} using the dose rate and the reported age of the building. These estimates were found to be in agreement within measurement uncertainty, although it was noted that the values of D_T determined using TL were systematically lower than those obtained using OSL by ~10%. The average values of D_T obtained for bricks from the three locations exposed to the contaminated riverbanks and floodplain agreed within 21%, with uncertainties of less than 10% obtained for individual determinations of D_T. The values of DX ranged from 146 ± 29 mGy (mill) to 195 ± 26 mGy (water tower), where the background dose amounted to 60% and 40% of D_T, respectively. However, unlike the samples from the heavily shielded locations, an analysis of the D_T values indicated no overdispersion, suggesting the absence of a significant systematic difference between OSL and TL determinations of the dose in this case. Following up this work, Woda et al. (2011a) tested further samples from the mill and focused on making a more detailed assessment of D_{BG}. Recognizing that care should be taken to

avoid making uncritical use of published geometry factors to estimate the gamma dose rate, they applied MC radiation transport simulations to calculate the gamma dose rate as a function of depth in the wall of the mill arising from lithogenic sources located in the ground adjacent to the sampled wall and within the wall fabric. In the case of the mill, the former makes a relatively minor contribution to the total dose rate (~3%), and in the case of the latter, a geometry factor of 0.63 (i.e., 63% of the infinite medium dose rate) was calculated for their selected sample depth (10 ± 5 mm) from the exposed surface of the wall. At this depth, and at a height of 4 m, the calculated total dose rate (1.98 mGy a^{-1}) comprised ~63% beta, ~26% gamma and 11% cosmic radiation. The walls of the Muslymovo and Metlino mills exceed 1 m in thickness at their base and within such massive walls the gamma dose rate increases with depth, from the surface towards infinite matrix (IM) conditions within ~50 cm. However, it should be noted that the form of the calculated dose rate profile varies according to the thickness of the wall and for thinner walls, as typically found in domestic buildings, the thickness may be insufficient to achieve IM conditions at the center. At depths of 1 cm and 12.5 cm in a double-wythe wall of ~25 cm thickness, for example, the gamma dose rate is predicted to be ~52% and ~79% of the IM dose rate by calculation (Bailiff, 2001) and the geometry factor at a depth of 1 cm is consequently predicted to be lower than is the case for a thick wall (e.g., > 50 cm).

Using bricks from four heavily shielded locations within the Mill walls luminescence dates were obtained and found (A.D. 1867–1887; 2σ) to be broadly consistent with the documentary sources for the date (A.D. 1899) reported by Bougrov et al. (1998). With the exception of one brick, there were no significant differences between the cumulative dose determined using OSL and TL measurement procedures applied to samples extracted from these locations. However, as argued by Woda et al. (2011b), the warming of bricks by exposure to solar radiation may lead to an underestimate of the cumulative dose when applying procedures that are based on the measurement of the 210 °C TL peak of quartz. OSL techniques have tended to be preferred when dating of bricks from ancient structures and within NW Europe they have been found to produce reliable and accurate results for buildings of the last 1000 years (Bailiff, 2007) in a temperate climatic region.

Woda et al. (2011a) also examined the issue of variation in dose registered by bricks at different heights to glean more information regarding the time-averaged source configuration that is required when calculating a dose conversion factor. Applying a SAR OSL measurement procedure, they obtained good precision (average overall uncertainty in D$_T$ of ~4%) and excellent concordance (2.5% standard deviation) between four adjacent bricks at the same height (4 m), contrasting the variability encountered at Metlino when using a TL procedure (Jacob et al., 2003). The dose registered in brick (10 mm depth) at a height of 12.5 m was found to be double that

at 3.0 m. While a trend of increasing dose with height had been predicted by radiation transport simulations (ICRU, 2002) for sources (662 keV) distributed on the ground surface between 35 and 100 m from the wall (i.e., an absence of contamination near to the building), the calculated increase between heights of 1 and 10 m was only 10%. Moreover, the measured depth-dose profile obtained with brick at a height of 4 m more closely resembled the calculated profile for a semi-infinite distribution of sources on the ground (ICRU, 2002), but for such a source distribution the dose in brick is predicted to decrease with height on the wall. Although no quantitative survey data were presented, a survey of ^{137}Cs in the ground between the mill wall and up to 20 m towards the riverbanks had indicated relatively low contamination, compared with the ground at greater distances. In the absence of more detailed Monte Carlo radiation transport simulations for this site, a general-purpose modelling tool (Bailiff and Slim, 2008) has been used for the purposes of this review to examine the predicted changes in dose with source configuration and height. A significantly stronger increase (~2) in dose with height (comparing 1 and 10 m) was obtained for sources distributed between 50 and 100 m in 'strips' of ground oriented parallel to the wall to a depth of 9 g cm^{-2}; the extent of the increase (with height) progressively reduces as the area of a contaminated strip facing the building is moved further from the wall.

By comparing their measured depth-dose profiles obtained with bricks at a height of 4 m with calculated profiles, Woda et al. (2011a) concluded that their measured profiles, with a half-depth of ~6 cm, more closely resembled a calculated profile for a semi-infinite distribution of sources (662 keV) on the ground (6 g cm^{-2}) than the calculated profile for sources distributed within a strip 16–18 m from the wall (simulating deposition on the riverbanks) that has a half-depth of ~8 cm. It is worth noting here that the calculated profiles for a riverbank distribution of sources (662 keV) and a semi-infinite distribution on the ground of higher energy sources (1600 keV) are similar (Göksu et al., 2002a), and the latter is potentially relevant in view of the presence of short-lived isotopes such as ^{140}Ba/^{140}La within the inventory of releases from the Mayak facility (Mokrov, 2004).

To further explore the time-averaged source configuration, the depth-dose profiles may contain further information. Whereas for a semi-infinite distribution of sources the (normalized) profile is predicted not to change significantly over a height range of 1–10 m, a change in depth-dose profile is predicted for a strip source configuration. Using the modelling tool, the calculated profile at a height of 1 m is relatively shallow where the sources are distributed between 15 and 20 m from the wall, compared with that for a semi-infinite distribution of sources of the ground (i.e., as found by Göksu et al., 2002a), but for sources distributed at slightly greater distances (20–50 m), the profile approaches that for a semi-infinite ground source

configuration. At a brick height of 10 m, similar behavior is predicted, but a reversion to the profile for a semi-infinite ground source configuration is approached as the source strips are moved to greater distances from the wall (e.g., 100 m). Such changes in dose registered in brick are likely to reflect the variation in solid angle subtended by the source area from the sample location underlining the importance of radiation transport modelling where there is a complex history of source distribution within ~100 m of a sampled wall. As the distribution of sources moves to greater distances from the sampled wall, as in this case, the details of the spatial distribution become increasingly important in the calculation of the dose conversion factor and uncertainty in its value, with the conversion factor for a sub-surface sample in brick at a height of 10m exceeding ~15 where the sources are distributed in a strip beyond ~20 m from the wall, for example, and significantly higher values predicted at lower heights. This accounts for the cautious approach taken regarding the conversion of cumulative dose from brick to the reference location in this case. While a definitive account of the dosimetry and modelling has yet to be published, the various studies of the Muslymovo Mill present an unfolding of the practical issues that are relevant to cases where the cumulative background dose represents a substantial proportion of the total dose registered in the brick.

3.3.3.3. Ozyorsk

The studies undertaken in Ozyorsk (Woda et al., 2009b) are interesting because they present a different radiological aspect to pollution from the MPA facility, being related to gaseous releases and consequently aerial dispersal within a cloud-source geometry. A high proportion of the releases to the atmosphere occurred before 1956, with gaseous ^{41}Ar (1.29 MeV primary γ-emission) accounting for about half of the total emissions. Four brick structures that had been constructed in 1948 and 1949 were sampled and tested, two of which were boundary walls and the other two were buildings. All the walls had been rendered with 1–1.5 cm of mortar and this was assumed to have been applied at the time of construction. The finding of a relatively high porosity of the brick fabric (by measuring water uptake) suggests that this treatment is likely to have been necessary to protect the brick. Although quartz extracted from some of the bricks were found to exhibit poor luminescence characteristics, determinations of the cumulative dose, D_T (denoted D_L in Woda et al., 2009b), were obtained for all samples, with one exception, and ranged from 117 ± 4 mGy to 163 ± 8 mGy (TL) and 96 ± 4 mGy to 146 ± 7 mGy (OSL). Following subtraction of the background dose (estimated by a combination of gamma spectrometric analysis of relevant materials and calculation), the weighted average values of DX for all the samples were 10 ± 9 mGy and 1 ± 9 mGy using TL and OSL techniques respectively, which are not significantly different from a value of zero. Calculations by Glagolenko et al. (2008) using an atmospheric dispersion model had

produced an estimated range of the cumulative external dose of 9–13 mSv for the period 1949–1989, at least 85% of which was attributed to [41]Ar. Using the monitoring data gathered between 1959 and 1992, an upper limit of ~1 mSv for the external dose at the sampling locations within the city was estimated for this period. In assessing the outcome of the luminescence results against the computational estimate, the issue of the detection limits for the application of the method in these particular circumstances was examined. On the basis of taking the upper limit of the highest estimate (TL) for D_X of 19 mGy, applying a conversion factor to obtain the kerma in air at the reference location (1–10 m from the wall) of 2.1 ± 0.2 and a conversion coefficient of 0.4 Sv Gy−1 derived for [41]Ar from previously published dose coefficients, a value of ~21 mSv was obtained as an upper limit for the effective dose derived from the luminescence measurements, and is taken to compare favorably with the predictions of the dispersion model. In considering various sensitivities of the uncertainties in the various measured quantities the authors conclude that the detection limit of D_X in this application was about 24 mGy and they note that this is comparable to the findings of two other studies (Ramzaev et al., 2008 and Bailiff et al., 2004a). This is a useful marker when planning further applications of the method, should they be needed, and it is also worth noting that where residual contamination is absent, the use of dosimeters (e.g., using Al_2O_3:C OSL dosimeters) to register the contemporary in-situ gamma dose in walls provides a means of reducing the uncertainty in the determination of D_{BG}.

3.3.4. Semipalatinsk Nuclear Test Site

The 1949 above-ground nuclear bomb test at the Semipalatinsk Nuclear Test Site (SNTS) led to substantial releases of radioactive fallout and its dispersal along a relatively narrow corridor extending to the NNE for hundreds of kilometers. This test has been the subject of much debate and concern regarding contradictory evidence for potential radiological effects to populations living in the path of the fallout (e.g., Simon and Bouville, 2002 and Bouville et al., 2002) and, of all the tests performed at the site, the 1949 test is considered to be the main source of radiation dose from fallout affecting populations located NE of Semipalatinsk. Preliminary luminescence work by Takada et al., 1999 and Takada et al., 2002 had demonstrated the suitability of ceramic building materials from several cities and settlements within Kazakhstan located downwind of the 1949 test fallout, including Dolon which had become the focus of epidemiological study because of the high estimated cumulative dose in the settlement. Calculated estimates of cumulative dose at the location of a former church in Dolon, based on dose rate and radionuclide concentration measurements, were of the order of 1 Gy, and this was supported by the luminescence results (~1.4 Gy air kerma) obtained by Takada et al., 1999 and Takada et al., 2002 for Dolon. However, in parallel with this work, EPR dosimetry

applied to tooth enamel obtained from residents of affected settlements indicated much lower values for Dolon (~200 mGy), although subsequently they were later revised (300–440 mGy; Ivannikov et al., 2006). Further application of luminescence was undertaken in a study that examined buildings located along the central axis of the fallout plume extending from Kazahkstan into Russia, and also within the lateral peripheral regions of the plume to examine for an expected strong gradient in cumulative dose. A collaborative team of laboratories (Bailiff et al., 2004b) undertook this work in Dolon, at the same former church as that sampled by Takada et al. (2002), and in nine other settlements (Fig. 47).

Fig. 47

Unlike the regions downwind of Chernobyl, the fallout from the 1949 test was dominated by relatively short-lived radionuclides (90% of the cumulative dose is estimated to have been delivered within the first year). Although ^{137}Cs associated with SNTS fallout has been detected in soil in some locations, its occurrence appears to be sporadic and dose-rate monitoring and soil sampling undertaken following the test was sparse. Consequently the scope for comparisons between building dosimetry and conventional dose reconstruction has been limited so far to those where sufficient historical dosimetry data are available. In Dolon, a value of the cumulative dose in air, $_{RL}D_X$, obtained by luminescence of 475 ± 110 mGy (Bailiff et al., 2004b) was obtained. In the absence of extant fallout within the adjacent ground (and also access to it because of subsequent alterations), the sources were assumed to have been uniformly distributed in the ground (to a depth of 5 g cm^{-2}) and a value of C_{RL} of 2.6 ± 0.25 calculated by MC simulation for the particular building geometry and a source energy of 662 keV. The form of the depth-dose profile obtained in brick from the former church was consistent with a time-averaged source energy of at least several hundred keV, and the results from the profile also confirmed the reliability of the estimates of D_{BG} (Equation (4b)) by testing of brick from highly shielded depths in the thick wall.

This estimate of cumulative dose is substantially lower than the previous estimates, with the exception of the EPR results, and the luminescence determination is expected to represent an upper limit for the latter assuming the dose is attributed to external gamma sources. By completing a detailed re-examination of the location of the original monitoring data relative to the former church, and scaling according to extant ^{137}Cs activity measured in soil at the two locations, a scaling of the official dose reconstruction value of cumulative dose for Dolon to the cumulative dose at the sampled building was obtained, yielding an estimated range of 460–630 mGy. This range compares very well with the luminescence result and estimates of whole body dose of ~500 mGy derived from chromosome aberration techniques obtained by

Salomaa et al. (2002) add further support to a cumulative dose in air of much less than 1 Gy.

Further downwind along the main axis of the plume (~65 km, Fig. 47), the testing of a substantial four-storey grain mill constructed in brick at Leshoz Topolinsky provided the opportunity to obtain samples at both ground (1m) and elevated height (12 m). Comparison of the ratio of the values of D_T obtained at these two heights with Monte Carlo radiation transport simulations for ground- and cloud-based source configurations indicated that the cumulative dose was due predominantly to a ground-based source distribution at this site. The pattern of dose determinations for all ten locations tested within the region indicate a degree of spatial heterogeneity that is significantly greater than had been previously assumed on the basis of the calculated estimates of fallout distribution (Shoikhet et al., 1998). For example, within a span of 100 km along the main axis of the plume (Fig. 47), the central values of $_{RL}D_X$ obtained for Dolon (475 ± 110 mGy) and Leshoz Topolinsky (230 ± 70 mGy) were in contrast to the results obtained for Izvestka (D_X = 2 ± 28 mGy), Laptev Log (D_X = 0 ± 19 and −17 ± 23 mGy) and Bol'shaya Vladimirovka (D_X = −5 ± 26 mGy), the values of D_X for which could not be resolved above the cumulative background dose, D_{BG}. Also, slightly to the south of the main axis of the plume, the values of $_{RL}D_X$ obtained at Akkol' (D_X = 2 ± 28 mGy) and Kanonerka (240 mGy) appear similarly enigmatic since Akkol' is located closer to central axis. Providing the assumptions concerning the emplacement of the sampled bricks before the 1949 tests are reliable, this suggests that there is a consequent risk that such spatial variation will not be reflected in a generalized dose distribution produced by a computational model without spatially dispersed determinations of dose to constrain/validate them.

Further progress towards resolving the various dosimetry issues was made at the 3rd Dosimetry Workshop on the SNTS (Semipalatinsk Research, 2006), at which the outcome of an inter-laboratory comparison of retrospective dosimetry measurements was reported (Stepanenko et al., 2006a, Stepanenko et al., 2006b and Stepanenko et al., 2006c) and evaluated in terms of their potential contribution to dose reconstruction for populations in affected settlements. The techniques applied included luminescence, EPR, biological (dicentric chromosome aberration in lymphocytes) dosimetry and computational modelling based on soil radionuclide contamination data. The luminescence measurements were performed on four bricks taken from three buildings in Dolon, two from the (large) former church that had been sampled previously, a school and a small church, all three within the same vicinity; whole bricks were subdivided and distributed between six laboratories. A

consensus value of 220 mGy was calculated for the average value of D_x (10 mm depth) for the three locations, and a conversion factor of 2 applied, obtaining a value of 440 mGy for the 'local' air kerma. This result compared well with the consensus value of the cumulative dose of 500 mGy for the settlement estimated by the (four) computational modelling groups. A calculated estimate of ~2300 mGy for the cumulative dose on the central axis of the plume, located 1.82 km north of Dolon settlement, underlines the potential for significant uncertainty in dose estimation where such strong gradients of activity are present in the distributed fallout. In the same way that ceramics within buildings have the advantage of performing dosimetry at a fixed point within the environment, tooth enamel similarly performs a dosimetry function within the relevant environment of the EPR samples (i.e., the body), but the history of movement of individuals some 60 years earlier than the measurements within a non-uniform radiation environment presents immense complications in the interpretation of the cumulative dose determined by EPR (Zhumadilov et al., 2013). In addition to the technical issues associated with the condition of the enamel at the time of extraction, the radiological history of such samples is complex, being dependent on the behavioral movements of the individual, and potentially further compounded where the deposition of fallout was heterogeneous.

While a full quantitative assessment of the radiological impact on the affected communities affected by the 1949 test may be difficult to obtain because of the considerable time that has elapsed, the various intercomparisons conducted have contributed to testing the reliability of the experimental methods and obtaining improved convergence as components of a comprehensive system of dose reconstruction (Simon et al., 2006).

4. Retrospective EPR dosimetry with teeth

The clear advantage of EPR dosimetry with teeth is that this technique reconstructs the doses to individuals, which could be used directly in any related epidemiological study as well as benchmark tests for verification and validation of corresponding analytical methods. For the latter application, EPR dosimetry may play a similar role as luminescent techniques with quartz and other materials. Below we describe results obtained with EPR dosimetry with teeth for large radiation-involved accidents.

4.1. Chernobyl liquidators (clean-up workers)

According to Chumak (2013), about 300,000 individuals are officially certified in Ukraine as liquidators (clean-up workers). Two large epidemiological studies were conducted by the common US-Ukrainian teams for leukemia and cataracts among

Chernobyl liquidators (Chumak et al., 2007 and Chumak et al., 2008). Both these studies required knowledge of Chernobyl-related doses for targeted individuals, which were either unknown (especially for liquidators who participated in the clean-up activity during the first days/weeks after the accident when the dose rates were the highest) or had unacceptable uncertainties (such as those liquidators whose doses were recorded in the Ukrainian National Dose Registry, but without any details how these doses were obtained). A few approaches were proposed and tested in order to develop the dosimetric methods which could be used for dose reconstruction for the liquidators. It should be noted that analytical methods developed with the help of luminescent techniques for A-bomb survivors, inhabitants of the SNTS, as well as residents of territories contaminated due to the Chernobyl accident were unsuitable in the case of the Chernobyl liquidators due to the peculiarity of the liquidators' exposure since the dose to the liquidators was accumulated from several clean-up activities fulfilled at different locations. While luminescent techniques can, in principle, be applied to building materials to measure the cumulative doses for the specific locations, its use is not appropriate because the temporal relationship between the cumulative dose registered in ceramic building materials and the liquidator's partial dose obtained during clean-up activities at that location is not known. Therefore, EPR doses of teeth were used in the case of the Chernobyl liquidators for verification of doses obtained by calculation methods. In fact, EPR doses could be used directly in any epidemiological study of the liquidators, but calculations or other alternative techniques are still required because of the invasive nature of the EPR technique has prevented dose determinations for all members of the study. Although EPR doses were reconstructed for 770 Chernobyl liquidators within the leukemia project (Chumak et al., 2005), only 61 liquidators (those whose doses were higher than 50 mGy, who responded to contact and who satisfied some extra requirements) participated in the verification test for the calculation technique. Nevertheless, the study of the liquidators resulted in a few important consequences. It was found that the analytical dose reconstruction method (Nossovsky, 1996), which was widely used before 1998, produced significant overestimation of the dose. Another calculation technique – the so-called "soft expert assessment of dose" (SEAD; Krjuchkov et al., 1998 and Krjuchkov et al., 2012) – also gave dose estimates that disagreed with the reference EPR doses. It was concluded that the SEAD method could not be used for dosimetric support of epidemiological studies. Finally, another estimation method, known as the RADRUE method ("realistic analytical dose reconstruction with uncertainty estimation") was developed and refined through comparison with EPR dose estimates. This method was widely used for dose assessment for the liquidators within the leukemia study (Chumak et al., 2008).

4.2. Chernobyl populations

These studies have been conducted by a research team from the Medical Radiological Research Center (Obninsk, Russia) since 1993 (Skvortsov et al., 2000). Skvortzov et al. (1995) report approximately 1500 reconstructed doses. It was noted in this study that the mean value of the EPR doses for some regions correlates with the level of 137Cs contamination in the ground. More than 3000 teeth were measured by the year 2000, mainly from the Bryansk region, which has the highest levels of Chernobyl-related contamination in Russia. Only back teeth (premolars, molars and wisdom teeth) were used for EPR analysis due to the effect of UV solar exposure on the front teeth (Ivannikov et al., 1997). This analysis was complicated by the frequent migration of the population after the Chernobyl accident, as well as by the application of effective countermeasures (e.g., soil removal) against overexposure in many settlements. Nevertheless, the Chernobyl component of the cumulative dose to teeth was found to be linearly correlated with the areal activity of 137Cs contamination in the ground, with a slope of 0.068 ± 0.010 mGy per kBq m^{-2} in the range 0–1000 kBq m^{-2} and for an integration period 1986–1994. This correlation coefficient was close to the value 0.061 mGy per kBq m^{-2} calculated for the same integration period according to an analytical method described by Balonov et al. (1996). At higher values of ^{137}Cs contamination some reduction of the Chernobyl dose component to teeth was observed, which was explained as the result of countermeasures undertaken, mainly to those settlements with high levels of contamination.

A comparison of the measured and calculated doses were reported by Ivannikov et al. (2004b) for the inhabitants of Zaborie (Russia), the most contaminated settlement that remained inhabited following the Chernobyl accident. Determinations of the dose to teeth were obtained with high precision using a specially developed EPR spectrum processing procedure. Calculated doses were obtained using the local radioactive contamination activity levels, dose rates and information about individual behavior. It was found that mean-square variation between the results of the EPR and calculated values of dose was 34 mGy, which is consistent with the known uncertainties of both methods. In this way, the methodology of individual dose calculation was validated against EPR dosimetry using teeth.

This finding has been confirmed in a more-recent publication from this research team (Ivannikov et al., 2014). Both individual and average (over a settlement) doses measured with EPR of teeth and estimated with an acknowledged analytical method were compared for some settlements of the Bryansk region (Russia). A linear regression analysis was used in which the sum-of-the-squares of the differences between the regression line and experimental points, inversely weighted by their

uncertainties, was minimized. As a result of this analysis, the regression line constructed had a slope close to unity and an intercept close to zero. The mean-square difference between the EPR and calculated doses was 35 mGy for the individual doses and 15 mGy for the average doses. This is consistent with the known uncertainties for the dose estimates obtained with the individual methods. It was concluded that the results of this analysis validated both methods and verified the reconstructed doses.

4.3. Semipalatinsk Nuclear Test Site

Most EPR doses for inhabitants of areas near the Semipalatinsk Nuclear Test Site have been determined by a common team of Kazakh, Russian and Japanese researchers (Ivannikov et al., 2002, Ivannikov et al., 2006, Stepanenko et al., 2007, Zhumadilov et al., 2006, Zhumadilov et al., 2007, Zhumadilov et al., 2009, Zhumadilov et al., 2011a, Zhumadilov et al., 2011b, Zhumadilov et al., 2013 and Zhumadilov et al., 2016). The first published work reported doses for 26 adult individuals residing in the vicinity of the SNTS (Ivannikov et al., 2002). EPR doses for 25 persons were below 250 mGy; one person from Semipalatinsk city was found to have a dose of 2.8 Gy. It was noted that higher doses were observed in residents whose teeth were formed before the end of the atmospheric nuclear tests in 1962, which was consistent with dose estimations based on the officially registered data. In subsequent studies by this research team (Ivannikov et al., 2006 and Zhumadilov et al., 2006) the dose estimates for residents of the three most contaminated villages (Dolon, Boden and Mostik) were reconstructed using EPR. It was found that the nuclear-test-related EPR doses could be as high as 440 mGy, with a mean dose of 74.1 ± 45.5 mGy, for those residents of Dolon whose enamel was formed before 1949 (the time of the most contaminating nuclear test, the radioactive fallout cloud from which passed over Dolon and some other settlements). Conversely, the doses for younger residents were below 120 mGy, with an average of 11.5 ± 37.7 mGy.

An attempt to compare three dose reconstruction methods has been undertaken by Stepanenko et al. (2007) for Dolon. The methods of choice were: (a) dose calculations based on the available archival data and on individual questionnaire responses from the inhabitants, (b) EPR dosimetry with teeth, and (c) retrospective luminescence dosimetry (RLD) with quartz from bricks, as discussed in Section 3.3.4. While doses calculated for the south-eastern part of Dolon (the location of the RLD sampling points) correlated with the corresponding measured RLD doses (645 ± 70 mGy and 460 ± 92 mGy, respectively), the average EPR dose obtained for 16 inhabitants of Dolon was much lower (156 ± 37 mGy). Using this value, a "shielding and behavior" factor was calculated for residents of Dolon and was found to be 0.28 ± 0.068. This factor is the reduction of the calculated average dose due to shielding from exposure,

which occurred when residents stayed indoors or were out of the village. For some residents of Dolon, calculations of individual external doses were also performed (based on the data derived from individual questioning), which demonstrated a much better correlation with corresponding EPR doses.

An average EPR dose 222 ± 131 mGy was obtained for 13 residents of Dolon by another research team (Sholom et al., 2007a). In that study, tooth doses were reconstructed for 103 people from 9 settlements with all studied teeth having been formed before the first nuclear test in 1949. The average doses (calculated only using the EPR doses of lateral teeth) were in the range 24.5 mGy–230 mGy, while the maximum individual doses were between 44 mGy and 1790 mGy. Some EPR doses for inhabitants of Dolon and three other settlements are also reported in Pivovarov et al. (2007); all data in this latter work are presented in the form of dose distributions and do not include average or individual doses. Maximum individual doses for all tested settlements were reported to be below 1 Gy, however.

The doses due to another significant surface nuclear test conducted on 24 August 1956 have been estimated for residents of Ust-Kamenogorsk, Znamenka and some other settlements located close to radioactive fallout plume (Zhumadilov et al., 2009, Zhumadilov et al., 2011b and Zhumadilov et al., 2013). The average nuclear-test-related EPR doses were in the range 17–41 mGy, which is consistent with estimations based on the official registered data. Maximum individual doses were between 47 mGy and 268 mGy.

4.4. Techa River

EPR dosimetry with teeth has recently been used (together with FISH-based dose estimates) for verification of doses of Techa riverside residents caused by radioactive releases into the Techa River from the Mayak Production Association between 1949 and 1956. The determined values were compared with doses reconstructed using the most-recent Techa River Dosimetry System (TRDS) (Degteva et al., 2015). The main issue in EPR dosimetry with teeth for the Techa River residents is related to strontium radioisotopes incorporated in teeth during enamel formation (Shishkina et al., 2011). A special approach was developed to account for possible contributions by strontium to the cumulative EPR dose (Shishkina et al., 2014) where concentrations of ^{90}Sr in the dental tissues were measured using passive TL beta dosimeters (Göksu et al., 2002b), and then concentration-to-dose conversion factors were calculated for different teeth using a Monte Carlo method (Shishkina et al., 2006).

Taking into account the time of the radioactive-waste release, as well as the potential issues with ^{90}Sr contribution, 79 individuals were selected for dose reconstruction by

applying EPR to samples of teeth. All populated settlements located within 70 km of the release site since 1950 and until at least 1952 (the time when the maximum external dose was predicted) and had teeth of age 6 or older in September 1950, when a massive intake of ^{90}Sr had begun. (Teeth of such an age are considered, according to Tolstykh et al. (2011), to be appropriate for EPR dose reconstruction taking into account the possible ^{90}Sr contribution to the cumulative absorbed dose.). 181 teeth were obtained from these 79 individuals and measured repeatedly in different laboratories as a test of reliability. As noted above, concentrations of ^{90}Sr in dental tissues were measured (for 49% of teeth) using thin-layer, beta dosimeters (Göksu et al., 2002b). For other samples, these concentrations were evaluated according to the method of Shishkina et al. (2014). The ^{90}Sr-corrected doses were split into four groups, depending on the distance from the release site: group I included the residents of Metlino located at 7 km from the site while group IV represented the residents of Ibragimovo and Isaevo located at 54 and 60 km from the release site, respectively. The first finding was that EPR doses were comparable to the corresponding FISH-based estimates within the same groups (Degteva et al., 2005 and Degteva et al., 2015). This allowed use of the both EPR and FISH dose estimates for the comparison with the dose estimates produced by the TRDS. This comparison was undertaken for doses calculated using two versions of the TRDS code (TRDS-2009 and the latest version of the TRDS). The newest version of TRDS contains an improvement in the dose rate data for the river shorelines and in the use of individual household-location data. (For the latter, an outdoor-to-riverbank ratio of 43% is estimated for the EPR donors.) As a consequence of these improvements the newest TRDS demonstrated better agreement with the EPR doses, but the latter values were still higher than the corresponding TRDS doses. It was assumed that 137Cs incorporated in soft tissues may contribute to the cumulative dose and be the cause of the difference. This component depends on the 137Cs intake and was maximal for those settlements located at ~50–60 km from the release site. When this component of the total dose was taken into account, the TRDS and EPR doses were the same, within measurement uncertainties.

5. Summary and conclusions

The intent of this review has been to summarize the latest developments in the use of physical dosimetry techniques – namely EPR, TL and OSL – to applications in emergency and retrospective dosimetry following large-scale, radiological exposure events, either accidental or intentional. The organization of the review has divided the discussion into two broad segments; (a) emergency dosimetry for dose estimations immediately after the event, primarily for triage purposes, and (b) retrospective dosimetry which contributes to the reconstruction of dose to populations and individuals following external exposure, and contributes to the

long-term study of stochastic processes and their consequential epidemiological effects, the measurements often being made many years after the onset of the radiation incident. As the review has shown, the development of emergency dosimetry techniques is much more immature than the use of EPR, TL or OSL in retrospective dosimetry, with much technique development still required. EPR (of teeth and nails) and TL and/or OSL (of fortuitous materials) is still under experimental development for emergency dosimetry. There have been precious few applications or field trials of the methods, either following small-scale accidents or in carefully controlled laboratory intercomparisons. The latter is urgently needed to compare methods and techniques using carefully monitored and controlled samples and a variety of either laboratory or semi-realistic, field exposure scenarios. For most of the techniques, and technique-material combinations, no universally agreed-upon measurement protocols have yet emerged.

There is, however, much to be optimistic about. Based on the procedural developments that have been published, and the modest success has been obtained in single-person accidents or standardized intercomparisons, there are clear directions for the needed research to proceed and much has been learned from research to date. Nevertheless, there is still a long way to go before the community can settle upon truly universal, fully accepted protocols for, for example, EPR of fingernails, OSL from SMRs or TL from smartphone screen glass. Essential in this quest will be carefully controlled intercomparisons in which the primary goals should be technique harmonization and an understanding of the limitations and uncertainties of the various techniques.

In retrospective dosimetry, however, decades of research – in model development and technique development – are beginning to yield, or have already yielded, accepted protocols. Furthermore, an understanding of the discrepancies between the results of the various radiation transport models and the different measurement modalities has emerged. The various techniques have developed to the point of being essentially universally accepted and reliably applied. This has been demonstrated in this review by examining the results of multiple studies on the doses to buildings (TL/OSL) and people (EPR) following the World War II atomic-bomb detonations, and radiation pollution from the SNTS and MPA and from the Chernobyl accident.

Even here, however, further research is called for in terms of experimental methodology and the application radiation transport modelling. The most recent developments in the Japanese studies, using single grain OSL measurement techniques, open up a new avenue of research by enabling the measurement of external beta dose in the sub-surface layers of ceramics. While the attendant

complications of heterogeneity will need to be tackled, this approach should prove to be particularly interesting. As radiation transport modelling software and training for researchers has become more widely available, and also the access to high performance computing facilities, we can expect the potential of the computational techniques to be more deeply tapped, and its interactive use with the experimental work can be expected to yield benefits in terms of guiding sample selection in the field. Much of the methodological work conducted so far has been driven by application to specific radiological problems; Fukushima is clearly a candidate for application of retrospective techniques and making use of experiences gained in the previous applications will be important (Barletta et al., 2016 and Chumak, 2013).

For EPR dosimetry with teeth, continued development is needed of either a high-sensitivity in-vivo (L band) or quasi-in-vivo (Q band, when just a small 1–2 mg piece of the tooth could be enough for EPR measurement) dosimetric technique. Such development would allow the use of the EPR technique for reconstruction of doses of all targeted individuals – whether they are individuals requiring emergency dosimetry or whether they are part of a retrospective dosimetry campaign for epidemiology purposes. Also with EPR, study of UV-induced EPR signals in teeth is required in order to develop a reliable dosimetric technique for front teeth (currently such teeth are rejected from retrospective dosimetry consideration).

Acknowledgements

References

Ainsbury, A.E., Bakhanova, E., Barquinero, J.F., Brai, M., Chumak, V., Correcher, V., Darroudi, F., Fattibene, P., Gruel, G., Guclu, I., Horn, S., Jaworska, A., Kulka, U., Lindholm,C., Lloyd, D., Longo,A., Marrale, M., Monteiro Gil, O., Oestreicher, U., Pajic, J., Rakic, B., Romm, H., Trompier, F., Veronese, I., Voisin,P., Vral,A., Whitehouse, C.A., Wieser, A., Woda, C., Wojcik, A., Rothkamm, A., 2011. Review of retrospective dosimetry techniques for external ionizing radiation exposures. Radiat. Prot. Dosim. 147, 573-592.

Aitken, M.J., 1985. Thermoluminescence Dating. Academic Press, London.

Aitken, M.J., 1998. An introduction to optical dating. Oxford University Press, Oxford.

Aldrich, J.E., Pass, B., 1988. Determining radiation exposure from nuclear accidents and atomic tests using dental enamel. Health Phys. 54, 469–471.

Alexander, G.A., Swartz, H.H., Amundson, S.A., Blakely, W.F., Buddemeier, B., Gallez, B., Dainiak, N., Goans, R.E., Hayes, R.B., Lowry, P.C., Noska, M.A., Okunieff, P., Salner, A.L., Schauer, D.A., Rompier, F., Turtletaub, K.W., Voisin, P., Wiley, A.L., Wilkins, R., 2007. BiodosEPR 2006: Acute dosimetry consensus committee recommendations on biodosimetry applications in events involving uses of radiation by terrorist and radiation accidents. Radiat. Meas. 42, 972-996.

Aragno, D., Fattibene, P., Onori, S., 2000. Dental radiography: tooth enamel EPR dose assessment from Rando phantom measurements. Phys. Med. Biol. 45 , 2671–2683.

Bailey, R.M., Smith, B.W., Rhodes, E.J., 1997. Partial bleaching and the decay form characteristics of quartz OSL. Radiat. Meas. 27, 123-136.

Bailiff, I. K., 1994. The pre-dose technique. Radiat. Meas. 23, 471-479.

Bailiff, I.K., 1997. Retrospective dosimetry with ceramics. Radiat. Meas. 27, 923-941.

Bailiff, I.K., 1999. The development of retrospective luminescence dosimetry for dose reconstruction in areas downwind of Chernobyl. Radiat. Protect. Dosim. 84, 411-419.

Bailiff IK., 2001. Fallout dose evaluation: gamma dose-rate geometry factors for brick walls. In: Bailiff IK and Stepanenko V, eds. Dose reconstruction for populations in areas contaminated by Chernobyl fallout, Final Report. European Commission, Contract IC15-CT96-0315.

Bailiff. I.K., Stepanenko, V.F. (eds) 2001. Dose reconstruction for populations in areas contaminated by Chernobyl fallout, Final Report. Durham: University of Durham; European Commission, Contract IC15-CT96-0315.

Bailiff, I.K., 2006. Development of single grain OSL dating of ceramic materials: spatially resolved measurement of absorbed dose. Radiat. Meas. 41, 744–749.

Bailiff, I.K., 2007. Methodological developments in the luminescence dating of brick from English late-medieval and post-medieval buildings. Archaeometry 49, 827–851.

Bailiff, I.K., Bøtter-Jensen, L., Correcher, V., Delgado, A., Göksu, H.Y., Jungner, H., Petrov, S.A., 2000. Absorbed dose evaluations in retrospective dosimetry: methodological developments using quartz. Radiat. Meas. 32, 609-613.

Bailiff, I.K., Correcher, V., Delgado, A., Göksu, Y., Hübner, S., 2002. Luminescence characteristics of dental ceramics for retrospective dosimetry: A preliminary study. Radiat. Prot. Dosim. 101, 519-524.

Bailiff, I. K., Mikhailik, V. B., 2004. The use of calcium silicate bricks for retrospective dosimetry. Radiat. Meas. 38, 91–99.

Bailiff, I.K., Slim, H.A., 2008. Development of reference database for gamma dose assessment in retrospective luminescence dosimetry. Radiat. Meas. 43, 859-863.

Bailiff, I.K., Stepanenko, V.F., Göksu, H.Y., Boetter-Jensen, L., Brodsky, L., Chumack, V., Correcher, V., Delgado, A., Golikov, V., Jungner, H., Khamidova, L.G., Kolizshenkov, T.V., Likhtarev, I., Meckbach, R., Petrov, S.A., Sholom, S., 2004a Comparison of retrospective luminescence dosimetry with computational modeling in two highly contaminated settlements downwind of the Chernobyl NPP. Health Phys. 86, 25–41.

Bailiff, I.K., Stepanenko, V.F., Göksu, H.Y., Jungner, H., Balmukhanov, S.B., Balmukhanov, T.S., Khamidova,, L.G., Kisilev, V.I., Kolyado, I.B., Kolizshenkov, T.V., Shoikhet, Y.N., Tsyb, A.F.,

2004b. The application of retrospective dosimetry in areas affected by fallout from the Semipalatinsk Nuclear Test Site: an evaluation of potential. Health Phys. 87, 625–641.

Bailiff, I. K., Stepanenko, V.F., Göksu, H.Y., Bøtter-Jensen, L., Chumak, V., Correcher, V., Delgado, A., Jungner, H., Khamidova, L.G., Meckbach, R., Petrov, S.A., Sholom, S., 2005. Luminescence retrospective dosimetry: development of approaches to application in populated areas downwind of the Chernobyl NPP. Health Phys. 89, 233-246.

Banerjee, D., Bøtter-Jensen, L., Murray, A. S., 1999. Retrospective dosimetry: preliminary use of the single-aliquot regeneration (SAR) protocol for the measurement of quartz dose in young house bricks. Radiat. Protect. Dosim. 84, 421-426.

Balonov, M.I., Bruk, G.Ya, Golikov, V.Yu, Shutov, V.N., Savkin, M.N., Pitkevich, V.A., Stepanenko, V.F., Vakulovskiy, S.M., Perminova, G.S., 1996. Reconstruction of the mean effective dose accumulated in 1986-1995 for inhabitants of settlements in Russian Federation affected by radioactive contamination as a result of the Chernobyl NPP accident in 1986 year: Methodical Instructions. Methodical Instructions MI 2.6.1. 579–96. Moscow. Ministry of Health of Russian Federation. Official Issue.

Banerjee, D., Bøtter-Jensen, L., Murray, A. S., 1999. Retrospective dosimetry: preliminary use of the single-aliquot regeneration (SAR) protocol for the measurement of quartz dose in young house bricks. Radiat. Protect. Dosim. 84, 421-426.

Barkyoumb, J.H., Mathur, V.K., 2008. Epoxy encapsulant as serendipitous dosimeters during radiological/nuclear events. Radiat. Meas., 43, 841-844.

Barletta, W.A., Stoop, J., O'Hara, C., Bailiff, I.K., Hermanspahn, N., Hugtenburg, R., Alcock, R., Covaci, A., Barceló, D., Gan, J., Karlsson, A. (Eds), 2016. 5 years after Fukushima — insights from current research. Virtual Special Issue, Elsevier. Accessed 7 June 2016. https://www.elsevier.com/connect/5-years-after-fukushima-insights-from-current-research?sf22311273=1

Barthe, J., Kamenopoulou, V., Catoire, B., Bermann, F., Portal, G., 1992. Electron spin resonance spectra of irradiated textiles: Applications to the dosimetry of ionizing radiations. Proceedings of the First European Meeting on Electron Spin Resonance (ESR) Applications in Organic and Bioorganic Materials. Editor: Catoire, B. Springer-Verlag, Berlin, Heidelberg.

Barthe, J., Kamenopoulou, V., Catoire, B., Portal, G., 1989. Dose evaluation from textile fibers: A post-determination of initial ESR signal. Appl. Radiat. Isotopes 40, 1029-1033.

Bartolotta, A., Brai, M., Caputo, V., D'Oca, M.C., Longo, A., Marrale, M., 2011. Thermoluminescence response of sodalime glass irradiated with photon and electron beams in the 1-20 Gy range. Radiat. Meas. 46, 975-977.

Bassinet, C., Pirault, N., Baumann, M., Clairand, I., 2014a. Radiation accident dosimetry: TL properties of mobile phone screen glass. Radiat. Meas. 71, 461-465.

Bassinet, C., Trompier, F., Clairand, I., 2010a. Radiation accident dosimetry on glass by TL and EPR spectrometry. Health Phys. 98, 400-405.

Bassinet, C., Trompier, F., Clairand, I., 2010b. Radiation accident dosimetry on electronic components by OSL. Health Phys. 98, 440-445.

Bassinet, C., Woda, C., Bortolin, E., Della Monaca, S. Fattibene, P., Quattrini, M.S., Bulanek, B., Ekendahl, D., Burbidge, C., Cauwels, V., Kouroukla, E., Geber-Bergstrand, T., Piasjkowski, A., Marczewska, B., Bilksi, P., Sholom, S., McKeever, S.W.S., Smith, R., Veronese, I., Gallim, A., Panzeri, L., Martini, M., 2014b. Retrospective radiation dosimetry using OSL from electronic components: results of an inter-laboratory comparison. Radiat. Meas. 71, 475-479.

Beerten, K., Reekmans, F., Schroeyers, W., Lievens, L., Vanhavare, F., 2011. Dose reconstruction using mobile phones. Radiat. Prot. Dosim., 144, 580-583.

Beerten, K., Vanhavare, F., 2008. The use of portable electronic device in accident dosimetry. Radiat. Prot. Dosim. 140, 294-299.

Beerten, K., Vanhavare, F., 2010. Photon energy dependence of three fortuitous dosemeters from personal electronic devices, measured by optically stimulated luminescence. Radiat. Prot. Dosim. 131, 509-512.

Beerten, K., Woda, C. Vanhavare, F., 2009.Thermoluminescence dosimetry of electronic components from personal objects. Radiat. Meas. 44, 620-625.

Bennet, B.G., 2002. Worldwide dispersion and deposition of radionuclides produced in atmospheric tests. Health Phys. 82, 644-655.

Black, P.J., Swarts, S.G., 2010. Ex vivo analysis of irradiated finger nails: Chemical yields and properties of radiation-induced and mechanically-induced radicals. Health Phys. 98, 301-308.

Blakely, W.F., Salter, C. A., Prasanna, P.G.S., 2005. Early response biological dosimetry – recommended countermeasure enhancements for mass-casualty radiological incidents and terrorism. Health Phys. 89, 494-504.

Bøtter-Jensen, L., McKeever, S.W.S., Wintle, A.G., 2003. Optically stimulated luminescence dosimetry. Elsevier Science, Amsterdam.

Bøtter-Jensen, L., Murray, A.S., 2001. Optically stimulated luminescence techniques in retrospective dosimetry. Radiat. Phys. Chem. 61, 181-190.

Bøtter-Jensen, L., Solongo, S., Murray, A.S., Banerjee, D., Jungner, H., 2000. Using the OSL single-aliquot regenerative-dose protocol with quartz extracted from building materials in retrospective dosimetry. Radiat. Meas. 32, 841-845.

Bortolin, E., Boniglia, C., Della Monica, S., Gragiulo, R., Fattibene, P., 2011. Silicates collected from personal objects as a potential fortuitous dosimeter in radiological emergency. Radiat. Meas. 46, 967-970.

Bortolin, E., Boniglia, C., Della Monica, S., Gragiulo, R., Onori, R., Fattibene, P., 2010. Is dust a suitable material in retrospective personal dosimetry? Radiat. Meas. 45, 753-755.

Bos, A.J.J., Wallinga, J., 2012. How to visualize quartz OSL signal components, Radiat. Meas. 47, 752-758.

Bougrov, N.G., Göksu, H.Y., Haskell, E.H., Degteva, M.O., Meckbach, R., Jacob, P., 1998. Issues in the reconstruction of environmental doses on the basis of thermoluminescence measurements in the Techa Riverside. Health Phys. 75, 574-583.

Bougrov, N.G., Vlasov, V.K., Kiryukhin, O.V., Fatkulbayanova, N.L., 1995. Thermoluminescence measurements of ceramic samples from accidentially polluted territory of South-Urals. Radiat. Meas. 24, 493-498.

Bouville, A., Simon, S.L., Miller, C.W., Beck, H.L., Anspaugh, L.R., Bennett, B.G., 2002. Estimates of doses from global fallout. Health Phys. 82, 690-705.

Brady, J., Aarestad, N., Swartz, H., 1968. In vivo dosimetry by electron spin resonance spectroscopy. Health Phys. 15, 43-47.

Breen, S.L., Battista, J. J., 1995. Radiation dosimetry in human bone using electron paramagnetic resonance. Phys. Med. Biol. 40, 2065-2077.

Brik, A., Haskell, E., Brik, V., Scherbina, O., Atamanenko, O., 2000. Anisotropy effects of EPR signals and mechanisms of mass transfer in tooth enamel and bones. Appl. Radiat. Isot. 52, 1077-1083.

Callens, F., Vanhaelewyn, G., Matthys, P., Boesman, E., 1998. EPR of carbonate derived radicals: Applications in dosimetry, dating and detection of irradiated Food. Appl. Magn. Reson. 14, 235-254.

Chandra, H., Symons, M.C.R., 1987. Sulphur radicals formed by cutting ⍺-keratin. Nature 328, 833-834.

Chen, R., McKeever, S.W.S., 1997. Theory of thermoluminescence and related phenomena. World Scientific Publishers, Singapore.

Christoudlides, C, Fremlin, J.H., 1971. Thermoluminescence of biological materials. Nature 232, 257-258.

Chumak, V.V., 2012. The Chernobyl experience in the area of retrospective dosimetry. J. Radiol. Prot. 32, N59–N63.

Chumak, V.V., 2013. Retrospective dosimetry of populations exposed to reactor accident: Chernobyl example, lesson for Fukushima. Radiat. Meas. 55, 3-11.

Chumak, V., Bailiff, I., Baran, N., Bugap, A., Dubovsky, S., Fedesov, I., Fini, V., HaskelL, E., Hayes, R., Ivannikov, A., Kenner, G., Kirillov, V., Khamidova, L., Kolesnik, S., Liidja, G., Likhatarev, I., Lippmaa, E., Maksimenko, V., Meijer, A., Minenk, V., Pasalskaya, L., Pas, J., Puskar., Radchuk, V., Sholom, S., Skvortzov, V., Stepanenko, V., Vaher, U., Wieser, A., 1996. The First International Intercomparison of EPR-dosimetry with Teeth: First Results. Appl. Radiat. Isot. 47, 1281-1286.

Chumak, V., Likhtarev, I., Sholom, S., Meckbach, R., Krjuchkov, V., 1998. Chernobyl experience in field of retrospective dosimetry: reconstruction of doses to the population and liquidators involved in the accident. Radiat. Protect. Dosim. 77, 91-95.

Chumak, V.V., Romanenko, A.Y., Voillequé, P.G., Bakhanova, E.V., Gudzenko, N., Hatch, M., Zablotska, L.B., Golovanov, I.A., Luckyanov, N.K., Sholom, S.V., Kryuchkov, V.P., Bouville A., 2008. The Ukrainian-American study of leukemia and related disorders among Chornobyl cleanup workers from Ukraine: II. Estimation of bone marrow doses. Radiat. Res. 170, 698-710.

Chumak, V.V., Sholom, S.V., Bakhanova, E.V., Pasalskaya, L.F., Musijachenko, A.V., 2005. High precision EPR dosimetry as a reference tool for validation of other techniques. Appl. Radiat. Isot. 62, 141-146.

Chumak, V., Sholom, S., Pasalskaya, L., 1999. Application of high precisions EPR dosimetry with teeth for reconstruction of doses to Chernobyl populations. Radiat. Prot. Dosim. 84, 515-520.

Chumak, V. V., Worgul, B. V., Kundiyev, Y. I., Sergiyenko, N. M., Vitte, P. M., Medvedovsky, C., Bakhanova, E. V., Junk, A. K., Kyrychenko, O. Y., Musijachenko, N. V., Sholom, S. V., Shylo, S. A., Vitte, O. P., Xu, S., Xue, X., Shore R. E., 2007. Dosimetry for a study of low-dose radiation cataracts among Chernobyl clean-up workers. Radiat. Res. 167, 606-614.

Ciesielski, B., Karaszewska, A., Penkowski, M., Schultka, K., Junczewska, M., Nowak., R., 2007. Reconstruction of doses absorbed by radiotherapy patients by means of EPR dosimetry in tooth enamel. Radiat. Meas. 42, 1021-1024.

Ciesielski, B., Krefft, K., Pankowski, M., Kinisnka, J., Drogoszewska, B., 2014. Effects of water treatment and sample granularity of radiation sensitivity and stability of EPR signals in x-ray irradiated bone samples. Radiat. Prot. Dosim., 159, 141-148.

Ciesielski, B., Marciniak, A., Zientek, A., Krefft, K., Cieszyński, M., Boguś, P., Prawdzik-Dampc, A., 2016. The effect of background signal and its representation in deconvolution of EPR spectra on accuracy of EPR dosimetry in bone. Radiat. Prot. Dosim., doi:10.1093/rpd/ncw171.

Clairand, I., Huet, C., Trompier, F., Bottollier-Depois, J.-F., 2008. Physical dosimetric reconstruction of a radiological accident due to gammagraphy equipment that occurred in Dakar and Abidjan in summer, 2006. Radiat. Meas. 43, 698-703.

Clairand, I., Trompier, F., Bottollier-Depois, J.-F., Gourmelon, P., 2006. Ex vivo ESR measurements associated with Monte Carlo calculations for accident dosimetry: Application to the 2001 Georgian accident. Radiat. Prot. Dosim. 119, 500-505.

Cogliati, J.J., Derr, K.W., Wharton, J., 2014. Using CMOS sensors in a cellphone for gamma detection and classification. http://arxiv.org/pdf/1401.0766v1.pdf.

Çolak, S., Özbey, T., 2011. An ESR study on biological dosimeters: Human hair. Radiat. Meas. 46, 465-472.

Coleman, C.N., Sullivan, J.M., Bader, J.L., Murrain-Hill, P., Koerner, J.F., Garret, A.L., Weinstock, D.M., Case, C., Hrdina, C., Adams, S.A., Whitcomb,. R.C., Graeden, E., Shankman, R., Lant, T., Maidment, B.W. and Hatchett, R.C., 2015. Public health and medical prepardness for a nuclear detonation: The nuclear incident medical enterprise. Health Phys. 108, 149-160.

Crespo, R.H., Domene, M.M., Rodríguez, M.J.P. , 2011. Biodosimetry and assessment of radiation dose. Rep. Pract. Oncology & Radiotherapy, 16. 131-137.

Cullings, H.M., Egbert, S.D., Maruyama, T., Hoshi, M., Fujita, S., 2005. Thermoluminescence dosimetry for gamma rays, Chap. 7 Part B. In Young, R.W., Kerr, G.D., (Eds)., 2005. Reassessment of the

Atomic Bomb Dosimetry for Hiroshima and Nagasaki—Dosimetry System 2002 (DS02). Hiroshima: Radiation Effects Research Foundation, 395-453.

Cullings, H.M., Fujita S., Funamoto S., Grant, E.J., Kerr, G.D., Preston, D.L., 2006. Dose estimation for atomic bomb survivor studies: its evolution and present status. Radiat. Res. 166, 255-270.

Da Costa, Z.M., Pontuschka, W.M., Campos, L.L., 2005. A comparative study based on dosimetric properties of different sugars. Appl. Radiat. Isot. 62, 331-336.

Dalgarno, B.G., McClymont, J.D., 1989. Evaluation of ESR as a radiation accident dosimetry technique. Appl. Radiat. Isot. 40, 1013-1020.

Dauer, L.T., Zanzonico, P., Tuttle, R.M., Quinn, D.M., Strauss, H.W., 2014. The Japanese tsunami and resulting nuclear emergency at the Fukushima Daiichi power facility: Technical, radiologic, and response perspectives. J. Nucl. Med., 52, 1423–1432.

Davies, J.E., 1979. On the use of dental ceramics as a possible second-line approach to accident irradiation dosimetry. Radioprotection, 14, 89-97.

De, T., Romanyukha, A., Trompier, F., Pass, B., Misra, P., 2013. Feasibility of Q-band EPR dosimetry in biopsy. Appl. Magn. Reson. 44, 375–387.

Degteva, M.O., Anspaugh, L.R., Akleyev, A.V., Jacob, P., Ivanov, D.V., Weiser, A., Vorobiova, M.I., Shishkina, E.A., Shved, V.A., Vozilova, A.V., Bayankin, S.N., Napier, B., 2005. Electron paramagnetic resonance and fluorescence in situ hybridization-based investigations of individual doses for persons living at Metlino in the upper reaches of the Techa River. Health Phys. 88, 139–153.

Degteva, M.O., Bougrov, N.G., Vorobiova, M.L., Jacob, P., Göksu, H.Y., 2008. Evaluation of anthropogenic dose distribution amongst building walls at the Metlino area of the upper Techa River region. Radiat. Environ. Biophys. 47, 469-479.

Degteva, M.O., Kozheurov, V.P., Vorobiova, M.I., 1994. General approach to dose reconstruction in the population exposed as a result of the release of radioactive wastes into the Techa River. Sci. Total Env. 142, 49-62.

Degteva, M.O., Shagina N.B., Shishkina, E.A., Vozilova, A.V., Volchkova, A.Y., Vorobiova, M.I., Wieser, A., Fattibene, P., Della Monaca, S., Ainsbury, E., Moquet, J., Anspaugh, L.R., Napier, B.A., 2015. Analysis of EPR and FISH studies of radiation doses in persons who lived in the upper reaches of the Techa River. Radiat. Environ. Biophys. 54, 433-444.

Degteva, M. O., Shagina, N. B., Vorobiova, M. I., Anspaugh, L. R., Napier, B. A., 2012. Re-evaluation of waterborne releases of radioactive materials from the Mayak Production Association into the Techa River in 1949–1951. Health Phys. 102, 25-38.

Degteva, M.O., Vorobiova, M.I., Kozheurov, V.P., Tolstykh, E.I., Anspaugh, L.R., Napier, B.A., 2000. Dose reconstruction system for the exposed population living along the Techa River. Health. Phys. 78, 542–554.

Degteva, M.O., Vorobiova, M.I., Tolstykh, E.I., Shagina, N.B., Shishkina, E.A., Anspaugh, L.R., Napier, B.A., Bougrov, N.G., Shved, V.A., Tokareva, E.E., 2006. Development of an improved dose reconstruction system for the Techa River population affected by the operation of the Mayak Production Association. Radiat. Res. 166, 255–270.

Demidenko, E., Williams, B.B., Sucheta A., Dong, R., Swartz, H.M., 2007. Radiation dose reconstruction from L-band in vivo EPR spectroscopy of intact teeth: Comparison of methods. Radiat. Meas. 43, 1089-1093.

Deperas-Kaminska, M., Bajinskis, A., Marczyk, M., Polanska, J., Wersall, P., Lidbrink, E., Ainsbury, E.A., Guipaud, O., Benderitter, M., Haghdoost, A., Wojcik, A., 2014. Radiation-induced changes in levels of selected proteins in peripheral blood serum of breast cancer patients as a potential triage biodosimeter for large-scale radiological emergencies. Health Phys. 107, 555-563.

Derr, K., Benjamin, M., Kutsche, C., 2012. Cellphone-based radiation warning system. Idaho National Laboratory Research Fact Sheet. 2012. URL http:// www.inl.gov/research/cellphone-based-radiation-warning-system/. 12-GA50627.

Desmet, C. M., Levêque, P., Gallez, B., 2016. Factors affecting the quality of tooth enamel for in vivo EPR-based retrospective biodosimetry. Prot. Dosim., doi:10.1093/rpd/ncw212.

Desrosiers, M.F., 1993. EPR bone dosimetry: A new approach to spectral deconvolution problems. Appl. Radiat. Isot. 44, 81-83.

Desrosiers, M.F, Schauer, D.A., 2001. Electron paramagnetic resonance (EPR) biodosimetry. Nucl. Instrum. Meth. Phys. Res. B 184, 219-228.

Desrosiers, M., Wadley, S., 2006. Time dependence of the radiation-induced EPR signal in sucrose. Radiat. Prot. Dosim. 118, 479-481.

DeWitt, R., Klein, D.M., Yukihara, E.G., Simon, S.L., McKeever, S.W.S., 2010. Optically stimulated luminescence (OSL) of tooth enamel and its potential use in post-irradiation exposure triage. Health Phys. 98, 432-439.

Discher, M., Bortolin, E., Woda, C., 2016. Investigations of touchscreen glasses from mobile phones for retrospective and accident dosimetry. Radiat. Meas. 89, 44-51.

Discher, M., Greiter, M., Woda, C., 2014. Photon energy dependence and angular response of glass display used in mobile phones for accident dosimetry. Radiat. Meas. 71, 471-474.

Discher, M., Woda, C., 2013. Thermoluminescence of glass displays from mobile phones for retrospective and accident dosimetry. Radiat. Meas. 53-54, 12-21.

Discher, M., Woda, C., 2014. Thermoluminescence emission spectrometry of glass display in mobile phones and resulting evaluation of the dosimetric properties of a specific type of display glass. Radiat. Meas. 71, 480-484.

Discher, M., Woda, C., Fiedler, I., 2013. Improvement of dose determination using glass display of mobile phones for accident dosimetry. Radiat. Meas. 56, 240-243.

Eakins, J. S. Hager, L. G. Kouroukla E., Smith, R.W. and Tanner, R. J., 2016. The PHE fortuitous dosimetry capability based on optically stimulated luminescence of mobile phones. Radiat. Prot. Dosim., doi:10.1093/rpd/ncv520.

Eakins, J.S., Kouroukla, E., 2015. Luminescence-based retrospective dosimetry using Al_2O_3 from mobile phones: a simulation approach to determine the effects of position. J. Radiol. Protect. 35, 343-381.

Egbert, S.D., Kerr, G.D., 2012. Gamma-ray thermoluminescence measurements: a record of fallout deposition in Hiroshima? Radiat. Environ. Biophys. 51,113-131.

Egbert, S.D., Kerr, G.D., Cullings, H.M., 2007. DS02 fluence spectra for neutrons and gamma rays at Hiroshima and Nagasaki with fluence-to-kerma coefficients and transmission factors for sample measurements. Radiat Environ. Biophys. 46, 311–325.

Egersdorfer, S., Wieser, A., Miller, A., 1996. Tooth Enamel as a Detector Material for Retrospective EPR Dosimetry. Appl. Radiat. Isot. 47, 1299-1303.

Eisler, R., 2013. The Fukushima 2011 disaster. ISBN 978-1-4665-7782-4. CRC Press, Boca Raton, USA.

Ekendahl, D., Judas, L., 2012. Retrospective dosimetry with alumina substrate from electronic components. Radiat. Prot. Dosim. 150, 134-141.

Ekendahl, D., Judas, L., Sukupova, L., 2013. OSL and TL retrospective dosimetry with a fluorapatite glass-ceramic used for dental restoration. Radiat. Meas. 58, 138-144.

El-Faramawy, N.A., 2005. Comparison of γ- and UV-light-induced EPR spectra of enamel from deciduous molar teeth. Appl. Radiat. Isot. 62, 191-195.

Fattibene, P., Callens, F., 2010. EPR dosimetry with tooth enamel: a review. Appl. Radiat. Isot. 68, 2033-2116.

Fattibene, P., Duckworth, T.L., Desrosiers, M.F., 1996. Critical evaluation of the sugar-EPR dosimetry system. Appl. Radiat. Isot. 47, 1375-1379.

Fattibene , P., Trompier , F., Wieser , A., Brai , M., Ciesielski , B., De Angelis, C., Della Monaca, S., Garcia , T., Gustafsson, H., Hole , E.O., Juniewicz , M., Krefft, K., Longo, A., Leveque, P., Lund, E., Marrale,, M., Michalec, B., Mierzwin'ska , G., Rao, J.L., Romanyukha , A.A., Tuner, H., 2014. EPR dosimetry intercomparison using smart phone touch screen glass. Radiat. Environ. Biophys. 53, 311–320.

Fattibene, P., Wieser, A., Adolfsson, E., Benevides, L.A., Brai, M., Callens, F., Chumak, V., Ciesielski, B., Della Monaca, S., Emerich, K., Gustafsson, H., Hirai, Y., Hoshi, M., Israelsson, A., Ivannikov, A., Ivanov, D., Kaminska, J., Ke, Wu., Lund, E., Marrale, M., Martens, L., Miyazawa, C., Nakamura, N., Panzer, W., Pivovarov, S., Reyes, R.A., Rodzi, M., Romanyukha, A.A., Rukhin, A., Sholom, S., Skvortsov, V., Stepanenko, V., Tarpan, M.A., Thierens, H., Toyoda, S., Trompier, F., Verdi , E., Zhumadilov, K., 2011. The 4th international comparison on EPR dosimetry with tooth enamel Part 1: Report on the results. Radiat. Meas. 46, 765-771.

Fenech, M., 2011. Current status, new frontiers and challenges in radiation biodosimetry using cytogenic, transcriptomic and proteomic techniques. Radiat. Meas. 46, 737-741.

Fiedler, I., Woda, C., 2011. Thermoluminescence of chip inductors from mobile phones for retrospective accident dosimetry. Radiat. Meas. 46, 1862-1865.

Flood, A.B., Boyle, H.K., Du, G., Demidenlo, E., Nicolade, R.J., Williams, B.B., Swartz, H.M., 2014. Advances in a framework to compare bio-dosimetry methods for triage in large-scale radiation events. Radiat. Prot. Dosim. 159, 77-86.

Fujita, H. Jain, M. Murray, A.S., 2011. Retrospective dosimetry using Japanese brick quartz: A way forward despite an unstable fast decaying OSL signal. Radiat. Meas. 46, 565-572.

Galbraith, R.F., Roberts, R.G., 2012. Statistical aspects of equivalent dose and error calculation and display in OSL dating: an overview and some recommendations. Quat. Geochron. 11, 1-27.

Geber-Bergstand, T., Berhardsson, C., Mattsson, S., Rääf, C.L., 2012 Retrospective dosimetry using OSL of tooth enamel and dental repair materials irradiated under wet and dry conditions. Radiat. Environ. Biophys. 51, 443-449.

Glagolenko, Y.V., Drozhko, E.G., Mokrov, Y.G., Rovny, S.I., Beregich, D.A., Stukalov, P.M., Ivanov, I.A., Aleksakhin, A., Anspaugh, L.R., Napier, B.A. (2008) Reconstruction of external doses to Ozyorsk residents due to atmospheric releases of inert radioactive gases from the stacks of the ''Mayak'' PA reactor plant from 1948 to 1989. Special issue of Radiation Safety Problems (Voprosy Radiatsionnoy Bezopasnosti), ''Mayak'' Production Association Journal, 20–32.

Godfrey-Smith, D.I., 2008. Towards in vivo OSL dosimetry of human tooth enamel. Radiat. Meas. 45, 854-858.

Godfrey-Smith, D.I, Pass, B., 1997. A new method of retrospective radiation dosimetry: optically stimulated luminescence in dental enamel. Health Phys. 72, 744-749.

Göksu, H.Y., 2003. Telephone chip-cards as individual dosemeters. Radiat. Meas. 37, 617-620.

Göksu, H.Y., Bailiff, I.K., 2006. Luminescence dosimetry using building materials and personal objects. Radiat. Protect. Dosim. 119, 413-420.

Göksu, H.Y., Bailiff, I.K., Bøtter-Jensen, L., Hütt, G., 1995. Interlaboratory beta source calibration using TL and OSL on natural quartz. Radiat. Meas. 24, 479-483.

Göksu, H. Y., Bailiff, I. K., Mikhailik, V. B., 2003. New approaches to retrospective dosimetry using cementitious building materials. Radiat. Meas. 37, 323–327.

Göksu, H. Y., Bougrov, N.G., Dalheimer, A.R., Heide, L.M., Jacob, P., Meckbach, R., 1996.Dose depth distribution in a brick from South Ural by using thermoluminescence. Appl. Radiat. Isot. 47, 433-440.

Göksu, H.Y., Degteva, M.O., Bougrov, N.G., Meckbach, R., Haskell, E.H., Bailiff, I.K., Bøtter-Jensen, L., Jungner, H., Jacob, P., 2002a. First international intercomparison of luminescence techniques using samples from the Techa River valley. Health Phys. 82, 94-101.

Göksu, H.Y., Heide, L.M., Bougrov, N.G., Dalheimer, A.R., Meckbach, R., Jacob, P., 1996. Depth-dose distribution in bricks and by Monte Carlo calculation for external -dose reconstruction. Appl. Radiat. Isotopes 47, 433–440.

Göksu, H.Y., Semiochkina, N., Shishkina, E.A., Wieser, A., El-Faramawy, N.A., Degteva, M.O., Jacob, P., Ivanov, D.V., 2002b. Thin layer α-Al$_2$O$_3$:C beta dosemeters for the assessment of current dose rate in teeth due to ^{90}Sr intake, and comparison with electron paramagnetic resonance dosimetry. Radiat. Prot. Dosim. 101, 507–513.

Göksu, H.Y., Stoneham, D., Bailiff, I.K., Adamiec, G., 1998. A new technique in retrospective dosimetry: pre-dose effect in the 230°C TL glow peak of porcelain. Appl. Radiat. Isotopes 49, 99-104.

Göksu, H.Y., Wieser, A., Ulanovsky, A., 2007. Retrospective individual dosimetry using luminescence and EPR after radiation accidents. Report abstract, IAEA/INIS, vol. 40. Reference number 40103753. Reihe Umweltpolitik; v. 696; 2007; 83 p; BMU--2007-696; ISSN 1612-6386.

Gold, R., 1995. The DS86 Neutron Enigma. Radiat. Meas. 24, 9-29.

Golikov, V. Yu., Balanov, M.I., Jacob, P., 1999. Model Validation for External Doses Due to Environmental Contamination by the Chernobyl Accident. Health Phys. 77, 654-661.

Golikov, V. Yu., Balanov, M.I., Jacob, P., 2002. External exposure of the population living in areas of Russia contaminated due to the Chernobyl accident. Radiat Environ Biophys. 41, 185-193.

González, A.S., 2007. An international perspective on radiological threats and the need for retrospective biological dosimetry of acute radiation overexposure. Radiat. Meas. 42, 1053-1062.

Gordy, W., Ard, W.B., Shields, H., 1955. Microwave spectroscopy of biological substances. I. Paramagnetic resonance of x-irradiated amino acids and proteins. Proc. Natl. Acad. Sci. USA 41, 983-996.

Gougelet, R.M., Rea, M.E., Nicolalde, R.J. Geiling, J.A., Swartz, H.M., 2010. The view from the trenches: Part I – Emergency medical response plans and the need for EPR screening. Health Phys. 98, 118 –127.

Grace, M. B., Cliffer, K.D., Moyer, B.R., Coleman, C.N., Prasher, J.M., Hatchett, R., Mercier, J., Manning, R.G., Bader, J.L., Disbrow, G.L., Kovac, G.R., 2011. The US Government's medical countermeasure portfolio management for nuclear and radiological emergencies: Synergy from interagency cooperation. Health Phys. 101, 238-247.

Grinberg, O., Sidabras, J.W., Tipikin, D., Krymov, V., Mariani, M., Feldman, M., Kmiec, M., Petryakov, S., Brugger, S., Carr, B., Schreiber, W., Swarts, S.G., Swartz, H.M., 2016. Dielectric-backed aperture resonators for X-Band in vivo EPR nail dosimetry. Radiat. Prot. Dosim., doi:10.1093/rpd/ncw163.

Guo, J., Zou, J., Dong, G., Ma, L., Cong, J., Fan, K., Yang, G, Wu, K., 2016. The application and distribution of magnetic field modulation in the detection apertures of X-band EPR cavities for in vivo tooth dosimetry. Radiat. Prot. Dosim., doi:10.1093/rpd/ncw173.

Guskova, A.K., Barabanova, A.V., Baranov, A.Y., Gruszdev, G.P., Pyatkin, Y.K., Nadezhina, N.M., Metlyaeva, N.A., Selidovkin, G.D., Moiseev, AA., Gusef, I.A., Dorofeeva, E.M., Zykova, I.E.,1988. Acute radiation effects in victims of the Chernobyl accident, in Appendix to Annex G of "Early effects in man of high radiation doses", UNSCEAR 1988.

Güttler, A., Wieser, A., 2008. EPR-dosimetry with tooth enamel for low doses. Radiat. Meas. 43, 819-822.

Haskell, E.H., Bailiff, I.K., Kenner, G.H., Kaipa, P.L., Wrenn, M.E., 1994. Thermoluminescence measurements of gamma-ray doses attributable to fallout from the Nevada Test Site using building bricks as natural dosemeters. Health Phys. 66, 380-391.

Haskell, E.H., Hayes, R.B., Kenner, G.H., Sholom, S.V., Chumak, V.V., 1997. EPR techniques and space biodosi-metry. Radiat. Res. 148, S51-S59.

Hayes, R.B., Haskell, E.H., Romanyukha, A.A., Kenner, G.H., 1998. Techniques for increasing reproducibility in EPR dosimetry of tooth enamel. Meas. Sci. Technol. 9, 1994-2006.

He, X., Gui, J., Matthews, T.P., Williams, B.B., Swarts, S.G., Grinberg, O., Sidabras, J., Wilcox, D.E., Swartz, H.M., 2011. Advances towards using finger/toenail dosimetry to triage a large population after potential exposure to ionizing radiation. Radiat. Meas. 46, 882-887.

He, X., Swarts, S.G., Demidenko, E., Flood, A.B., Grinberg, O., Gui, J., Mariani, M., Marsh, S.D., Ruuge, A.E., Sidabras, J.W., Tipikin, D., Wilcox, D.E., Swartz, H.M., 2014. Development and validation of an ex vivo electron paramagnetic resonance fingernail biodosimetric method. Radiat. Prot. Dosim. 159, 172-181.

Hervé, M.L., Trompier, F., Tikunov, D.D., Amouroux, V., Clairand, I., 2006. Study of materials for mixed field dosimetry by EPR spectroscopy. Radiat. Prot. Dosim. 120, 205-209.

Higashimura, T., Ichikawa, Y., Sidei, T., 1963. Dosimetry of atomic bomb radiation in Hiroshima by thermoluminescence of roof tiles. Science 139, 1284-1285.

Hiller, M.M., Woda, C., Bougrov, N., Degteva, M., Ivanov, O., Romanov, S., 2014. Dose reconstruction in the former village of Metlino in the contaminated Techa River region, Southern Urals, Russia. ANS RPSD 2014 - 18th Topical Meeting of the Radiation Protection & Shielding Division of ANS. September 14–18, 2014, American Nuclear Society, Knoxville, TN, USA.

Hirose, K, 2012. 2011 Fukushima Dai-ichi nuclear power plant accident: summary of regional radioactive deposition monitoring results. J. Environ. Radioactivity 111, 13-17.

Hoshi, M; Sawada, S; Ichikawa, Y; Nagatono, T., Uehara S, Kondo S., 1989. Thermoluminescence dosimetry of gamma-rays from the Hiroshima atomic-bomb at distances 1.91-2.05 km from the hypocentre. Health Phys. 57, 1003-1008.

Hoshi, M., Shibata, Y., Okajima, S., Takatsuji, T., Yamashita, S., Namba, H., Yokoyama, N., Izumi, M., Nagataki, S., Fujimura, K., Kuramoto, A., Krupnik, T.A., Dolbeshkin, N.K., Danilchik, S.A., Derzhitsky, V.E., Wafa, K.A., Kiikuni, K., Shigematsu, I., 1994. ^{137}Cs concentration among children in areas contaminated with radioactive fallout from the Chernobyl accident: Mogilev and Gomel oblasts, Belarus. Health Phys 67, 272–275.

Hoshi, M.,Toyoda, S., Ivannikov, A., Zhumadilov, K., Fukumura, A., Apsalikov, K., Zhumadilov, Zh. S., Bayankin, S., Chumak, V., Ciesielski, B., DeCoste,V., Endo, S., Fattibene, P., Ivanov, D., Mitchell, C. A., Onori, S., Penkowski, M., Pivovarov, S.P., Romanyukha, A., Rukhin, A.B., Schultka, K., Seredavina,T.A., Sholom, S., Skvortsov, G., Stepanenko,V., Tanaka, K., Trompier, F., Wieser, A., Wolakiewicz, G., 2007. Interlaboratory comparison of tooth enamel dosimetry on Semipalatinsk region: Part1, general view. Radiat. Meas. 42, 1005–1014.

Hübner, S., Göksu, H. Y., 1997. Retrospective dosimetry using the pre-dose effect in porcelain. Appl. Radiat. Isotopes 48, 1231-1235.

Huntley, D.J., Lamothe, M., 2001. Ubiquity of anomalous fading in K-feldspars and the measurement and correction for it in optical dating. Canadian J. Earth Sci. 38, 1093-1106.

IAEA, 2002. Use of electron paramagnetic resonance dosimetry with tooth enamel for retrospective dose assessment: Report of a co-ordinated research project. IAEA-TECDOC-1331.

Ichikawa, Y., Higashimura, T., Sidei, T., 1966. Thermoluminescence dosimetry of gamma rays from atomic bombs in Hiroshima and Nagasaki. Health Phys. 12, 395-405.

Ichikawa, Y., Nagatomo, T., Hoshi, M., Kondo, S., 1987. Thermoluminescence dosimetry of γ rays from the Hiroshima bomb at distances of 1.27 to 1.46 kilometers from the hypocentre. Health Phys. 52, 443-451.

ICRP, 2007. The 2007 recommendations of the International Commission on Radiological Protection. ICRP Publication 103. Ann. ICRP 37 (2-4).

ICRU, 2002. International Commission on Radiation Units and Measurements. Retrospective assessment of exposures to ionising radiation. ICRU Report 68. International Commission on Radiation Units and Measurements, Bethesda, USA, 2002.

Ikeya, M., Ishii, H., 1989. Atomic bomb and accident dosimetry with ESR natural rocks and human tooth in vivo spectrometer. Appl. Radiat. Isot. 40, 1021–1027.

Ikeya, M., Miyajima, J., Okajima, S, 1984. ESR dosimetry for atomic bomb survivors using shell buttons and tooth enamel. Jap. J. Appl. Phys. 23, L697-L699.

Inrig, E.L., Godfrey-Smith, D.I., Khanna, S., 2008. Optically stimulated luminescence of electronic components for forensic, retrospective, and accident dosimetry. Radiat. Meas. 43, 726-730.

Inrig, E.L., Godfrey-Smith, D.I., Larsson, C.L., 2010. Fading corrections to electronic component substrates in retrospective accident dosimetry. Radiat. Meas. 45, 746-748.

Ishigaki, Y., Matsumoto, Y., Ichimiya, R., Tanaka, K., 2013. Development of mobile radiation monitoring system utilizing smartphone and its field tests in Fukushima. IEEE Sensors Journal 13, 3520-3526.

Ishii H., Ikeya M., Okano M., 1990. ESR dosimetry of teeth of residents close to Chernobyl reactor accident. J. Nucl. Sci. Tech. 27, 1153-1155.

Ivanov, D.V., Wieser, A., Shishkina, E.A., Ustinov, V.V., 2014. Effect of spectrum processing procedure on the linearity of the EPR dose reconstruction in tooth enamel. Radiat. Meas. 68, 7-13.

Ivannikov, A.I., Gaillard-Lecanu, E., Trompier, F., Stepanenko, V.F., Skvortsov, V.G., Borysheva, N., Tikunov, D.D., Petin, D.V., 2004b. Dose reconstruction by EPR spectroscopy of tooth enamel: application to the population of Zaborie village exposed to high level of radiation after the Chernobyl accident. Health Phys. 86, 121–134.

Ivannikov, A.I., Skvortsov, V.G., Stepanenko, V.F Tikunov, Tsyb, A.F., Khamidova, L.G., 2000. Tooth enamel EPR dosimetry: sources of errors and their correction. Appl. Radiat. Isotop. 52, 1291-1296.

Ivannikov, A.I., Skvortsov, V.G., Stepanenko, V.F., Tikunov, D.D., Romanyukha, A.A., Wieser, A., 1997. Wide scale EPR retrospective dosimetry. Results and problems. Radiat. Prot. Dosim. 71, 175–180.

Ivannikov A.I., Skvortsov V.G., Stepanenko V.F., Zhumadilov K. Sh., 2014. Comparative analysis between radiation doses obtained by EPR dosimetry using tooth enamel and established analytical methods for the population of radioactively contaminated territories. Radiat. Prot. Dosim. 159, 125-129.

Ivannikov, A.I., Tikunov, D.D., Borysheva, N.B., Trompier, F., Skvortsov, V.G., Stepanenko, V.F., Hoshi, M., 2004a. Calibration of EPR signal dose response of tooth enamel to photons: Experiment and Monte Carlo simulation. Radiat. Prot. Dosim. 108, 303–315.

Ivannikov, A., Toyoda, S., Hoshi, M., Zhumadilov, K., Fukumura, A., Apsalikov, K., Zhumadilov, Zh., Bayankin, S., Chumak, V., Ciesielski, B., De Coste, V., Endo, S., Fattibene, P., Ivanov, D., Mitchell, C., Nalapko, M., Onori, S., Penkowski, M., Pivovarov, S., Romanyukha, A., Rukhin, A.B., Schultka, K., Seredavina, T., Sholom, S., Skvortsov, V., Stepanenko, V., Tanaka, K., Trompier, F., Wieser, A., Wolakiewicz, G., 2007. Interlaboratory comparison on tooth enamel dosimetry on Semipalatinsk region: Part 2, effects of spectra processing. Radiat. Meas. 42, 1015–1020.

Ivannikov, A.I., Zhumadilov, Zh., Gusev, B.I., Miyazawa, Ch., Jiao, L., Skvortsov, V.G., Stepanenko, V.F., Takada, J., Hoshi, M., 2002. Individual dose reconstruction among residents living in the vicinity of the Semipalatinsk Nuclear Test Site using EPR spectroscopy of tooth enamel. Health Phys. 83, 183-196.

Ivannikov, A., Zhumadilov, K., Tieliewuhan, E., 2006. Results of EPR dosimetry for population in the vicinity of the most contaminating radioactive fallout trace after the first nuclear test in the Semipalatinsk Test Site. J. Radiat. Res. 47, Suppl. A39-A46.

Ivannikov, A., Zhumadilov, K., Tieliewuhan, E., Jiao, L., Zharlyganova, D., Apsalikov, K.N., Berekenova, G., Zhumadilov, Zh., Toyoda, Sh., Miyazawa, C., Skvortsov, V., Stepanenko, V., Endo, S., Tanaka, K., Hoshi, M., 2006. Results of EPR dosimetry for population in the vicinity of the most contaminating radioactive fallout trace after the first nuclear test in the Semipalatinsk Test Site. J. Radiat. Res. 47, A39-A46.

Ivannikov, A.I., Khailov, A.M., Orlenko, S.P., Skvortsov, V.G., Stepanenko, V.F., Zhumadilov, K.S., Williams, B.B., Flood, A.B., Swartz, H.M., 2016. Determination of the average native background and the light-induced EPR signals and their variation in the teeth enamel based on large-scale survey of the population. Radiat. Prot. Dosim., doi:10.1093/rpd/ncw150.

Iwasaki, A., Grinberg, O., Walczak, T., Swartz, H.M., 2005a. In vivo measurements of EPR signal in whole human teeth. Appl. Radiat. Isotop. 62, 187-190.

Iwasaki, A., Walczak, T., Grinberg, O., Swartz, H.M., 2005b. Differentiation of the observed low frequency (1200 MHz) EPR signals in whole human teeth. Appl. Radiat. Isotop. 62, 133-139.

Jacob, P. (Ed), 2000. Radiation Fields, Dosimetry, Biokinetics and Biophysical Models for Cancer Induction by Ionising Radiation: 1996 - 1999; EC-GSF Association Contract F14P-CT95-0011; Final Report; Dose Reconstruction (Ed. P. Jacob). GSF-Forschungszentrum für Umwelt und Gesundheit, Oberschleissheim, Germany.

Jacob, P., Göksu, H.Y., Taranenko, V., Meckbach, R., Bougrov, N.G., Degteva, M.O., Vorobiova, M.I., 2003. On an evaluation of external values in the Techa River Dosimetry System (TRDS) 2000. Radiat. Environ. Biophys. 42, 169-174.

Jacob, P., Likhtarev, I. (Eds), 1996. Pathway analysis and dose distributions. Joint Study project No. 5. Final report EUR 16541 EN. European Commission Directorate General XII, Brussels.

Jacob, P., Meckbach, R., 1987. Shielding factors and external dose evaluation. Radiat. Protect. Dosim. 21, 79-85.

Jain, M., Bøtter-Jensen, L., Murray, A. S., Jungner, H., 2002. Retrospective dosimetry: dose evaluation using unheated and heated quartz from a radioactive waste storage building. Radiat. Prot. Dosim. 101, 525–530

Jain, M., Choi, J. H., Thomas, P. J., 2008. The ultrafast OSL component in quartz: Origins and implications. Radiat. Meas. 43, 709-714.

Jain, M., Murray, A.S., Bøtter-Jensen, L., 2003. Characterisation of blue-light stimulated luminescence components in different quartz samples: implications for dose measurement. Radiat. Meas. 37, 441-449.

Jasińka, M., Niewiadomski, T., 1970. Thermoluminescence of biological materials. Nature 227, 1159-1160.

Jaworska, A., 2009. Types of radiation mass casualties and their management. Ann Ist Super Sanità 45, 246-250.

Jaworska, A., Ainsbury, E.A., Fattibene, P., Lindholm, C., Oestreicher, U., Rothkamm, K., Romm, H., Thierens, H., Trompier, F., Voisin, P., Vral, A., Woda, C., Wijcek. A., 2014a. Operational guidance for radiation emergency response organizations in Europe for using biodosimetric tools developed in EU MULTIBIODOSE project. Radiat. Prot. Dosim. 164, 165-169.

Jaworska, A., Wojcik, A. , Ainsbury, E.A., Fattibene, P., Lindholm, C., Oestreicher, U., Rothkamm, K., Romm, H., Thierens, H., Trompier, F., Voisin, P., Vral, A., Woda, C, 2014b. Guidance for using MULTIBIODOSE tools in emergencies – for radiation emergency response organisations in Europe. http://www.multibiodose.eu/

Jiao, L., Takada, J., Endo, A., Tanaki, K., Zhang, W., Ivannikov, A., Hoshi, M., 2007. Effects of Sunlight Exposure on the Human Tooth Enamel ESR Spectra Used for Dose Reconstruction. J. Radiat. Res. 48, 21–29.

JIWG, 2005. Technology assessment and roadmap for emergency radiation dose assessment program. Joint Interagency Working Group, US Department of Homeland Security, Washington DC; UCRL-TR-215887. www.dhs.gov/xlibrary/assets/S_T_TechAssess_ERDAP_June05.pdf.

Kamenopoulou, V., Barthe, J., Hickman, C., Portal, G., 1986. Accidental gamma irradiation dosimetry using clothing. Radiat. Prot. Dosim. 17, 185-188.

Karaoglou, A., Desmet, G., Kelly, G. N., Menzel, H.G., 1996. The Radiological Consequences of the Chernobyl Accident. European Commission Directorate General XII. Brussels.

Kerr, G.D., Egbert, S.D., Al-Nabulsi, I., Bailiff, I.K., Beck, H.L., Belukha, I.G., Cockayne, J.E., Cullings, H.M., Eckerman, K.F., Granovskaya, E., Grant, E.J., Hoshi, M., Kaul, D.C., Kryuchkov, V., Mannis, D., Ohtaki, M., Otani, K., Shinkarev, S., Simon, S.L., Spriggs, G.D., Stepanenko, V.F., Stricklin, D., Weiss, J.F., Weitz, R.L., Woda, C., Worthington, P.R., Yamamoto, K., Young, R.W., 2015. Workshop Report on Atomic Bomb Dosimetry--Review of Dose Related Factors for the Evaluation of Exposures to Residual Radiation at Hiroshima and Nagasaki. Health Phys. 109, 582-600.

Kerr, G.D., Egbert, S.D., Al-Nabulsi, I., Beck, H.L., Cullings, H.M., Endo, S., Hoshi, M., Imanaka, T., Kaul, D.C., Maruyama, S., Reeves, G.I., Ruehm, W., Sakaguchi, A., Simon, S.L., Spriggs, G.D., Stram, D.O., Tonda, T., Weiss, J.F., Weitz, R.L., Young, R.W., 2013. Workshop report on atomic bomb dosimetry—residual radiation exposure: recent research and suggestions for future studies. Health Phys. 105, 140–149.

Khailov, A.M., Ivannikov, A.I., Skvortsov, V.F., Stepanenko, V.F., Orlenko, S.P., Flood, A.B., Williams, B.B., Swatrz, H.M., 2015. Calculation of dose conversion factors for doses in fingernails to organ doses at external gamma irradiation in air. Radiat. Meas. 82, 1-7.

Khvostunov, I.K., Ivannikov, A.I., Skvortsov, V.G., Nugis, V. Yu., Golub, E.V., 2015. Review of the correlation between results of cytogenetic dosimetry from blood lymphocytes and EPR dosimetry from tooth enamel for victims of radiation accidents. Radiat. Prot. Dosim. 163, 399-408.

Kim, M.J., Lee, Y.L., Lee, J.I., Kim, J.L., Hong, D.G., 2015. Fading test using the SAAD-POSL method for retrospective accidental dosimetry of building materials. Radia. Phys. Chem. 116, 373-376.

Kinoshita, A., Guzman, C., Sandra, C., Sakamoto-Hojo, E., Camparato, M.L., Picon, C., Baffa, O., 2003. Evaluation of a high dose to a finger from a ^{60}Co accident. Health Phys., 84, 477-482.

Kitis, G., Charalambous, S., Tuyn, J.W.N., 1993. Thermoluminescence response of heavy concrete used in the shielding of the CERN 600 MeV synchrocyclotron. Radiat. Protect. Dosim. 47, 589-593.

Kleinerman, R.A., Romanyukha, A.A., Schauer, D.A., Tucker, J.D., 2006. Retrospective assessment of radiation exposure using biological dosimetry: Chromosome painting, electron paramagnetic resonance and glycophorin A mutation assay. Radiat. Res. 166, 287-302.

Kolberg, S., Prydz, S., Dahm, S., 1974. Thermally stimulated luminescence in dental hard tissues and bone. Calcif. Tiss. Res. 17, 9-23.

Kohn, S., Eaton, J.L., Feroz, S., Bainbridge, A.A., Hoolachan, J., Barnett, D.J., 2012. Personal disaster preparedness: An integrative review of the literature. Disaster Medicine and Public Health Preparedness. 6, 217-231.

Kouroukla, E.C., Bailiff, I.K., Terry, I., 2014. Emergency dosimetry using ceramic components in personal electronic devices. Int. J. Modern Phys: Conf. Series. 27, 1460155-1 – 1460155-10.

Krefft, K., Drogoszewska, B., Kaminska, J., Juniewicz, M., Wołakiewicz, G., Jakacka, I., Ciesielski, B., 2014. Application of EPR dosimetry in bone for ex vivo measurements of doses in radiotherapy patients. Radiat. Prot. Dosim., 162, 38-42.

Krjuchkov, V.P., Chumak, V.V., Kosterev, V.V., 1998. The problem of dose reconstruction for liquidators of ChNPP accident and the possibility of its decision by fuzzy sets method. Proceedings of 1998 ANS Radiation Protection and Shielding Division Topical Conference ''Technologies for the New Century'', Nashville (USA), Vol. 1, 562–567.

Krjuchkov, V.P., Kochetkov, O.A., Tsovijanov, A.G., 2012. Mitigation of accident consequences at Chernobyl NPP: radiation and dosimetry issues. Ed. By Asmolov, V.G. and Kochetkov, O.A. Moscow, IzdAT. – 208.

Kulka, U., Ainsbury, L., Atkinson, M., Barquinero, J.F., Barrios, L., Beinke, C., Bognar, G., Cucu, A., Darroudi, F., Fattibene, P., Gil, O., Gregoire , E., Hadjidekova, V., Haghdoost, S., Herranz, R., Jaworska, A., Lindholm, C., Mkacher, R., Mört, S., Montoro, A., Moquet, J., Moreno, M., Ogbazghi, A., Oestreicher, U., Palitti, F., Pantelias, G., Popescu, I., Prieto, M.J., Romm, H., Rothkamm, K., Sabatier, L., Sommer, S., Terzoudi, G., Testa, A., Thierens, H., Trompier, F., Turai, I., Vandersickel, V., Vaz, P., Voisin, P., Vral, A., Ugletveit, F., Woda, C., Wojcik, A., 2012. Realising the European Network of Biodosimetry (RENEB). Radiat. Prot. Dosim. 151, 621-625.

Lanjanian, H., Ziale, F., Modarresi, M., Nikzad, M., Shahvar, A., Durrani, S.A., 2008. A technique to measure the absorbed dose in human tooth enamel using EPR method. Radiat. Meas. 43, S648-S650.

Lee, J.I., Chang, I., Kim, J.L., Pradhan, A.S., Kim, B.H., Chung, K.S., 2016. Dose re-estimation using thermoluminescence of chip inductors and resistors following the dose estimation by using optically stimulated luminescence readout for retrospective accident dosimetry. Radiat. Meas. 90, 257-261.

Lee, J.I., Chang, I., Pradhan, A.S., Kim, J.L., Kim, B.H., Chung, K.S., 2015. On the use of new generation mobile phone (smart phone) for retrospective accident dosimetry. Radiat. Phys. Chem. 116, 151-154.

Liidja, G., Past, J., Puskar, J., Lippmaa, E., 1996. Paramagnetic resonance in tooth enamel created by ultra-violet light. Appl. Radiat. Isotopes 47, 785–788.

Likhtarev, I.A., Kovgan, L.N., Jacob, P., Anspaugh, L.R. 2002. Chernobyl accident: retrospective estimates of external dose of the population of Ukraine. Health Phys., 82, 290-303.

Likhtarev, I.A., Kovgan, I., Novak, D., Vavilov, S., Jacob, P., Paretzke, H.G., 1996. Effective doses due to external irradiation from the Chernobyl accident for different population groups of Ukraine. Health Phys. 70, 87-98.

Lubenau, J.O., Strom, D.J., 2002. Safety and Security of radiation sources in the aftermath of 11 September 2001. Health Phys. 83, 155-164.

LUMINATE, 2003. The Development of New Techniques for Retrospective Luminescence Dosimetry (LUMINATE), Final Report. Nuclear Science and Technology, European Commission. 41 pp. Accessed 18 April 2016: http://cordis.europa.eu/publication/rcn/8199_en.html

Marciniak, A., Ciesielski, B., 2016. EPR dosimetry in nails – A review. Appl. Spectrosc. Rev. 51, 73-92.

Marrale, M., Longo, A., Bartolotta, A., D'Oca, M.C., Brai, M., 2013. Preliminary application of thermoluminescence and single aliquot regeneration method for dose reconstruction in soda lime glass. Nucl. Instrum Meth Phys. Res. B. 27, 58-63.

Marrale, M., Longo, A., D'Oca, M.C., Bartolotta, A., Brai, M., 2011. Watch glasses exposed to 6MV photons and 10 MeV electrons analysed by means of ESR technique: A preliminary study. Radiat. Meas. 46, 822-826.

Maruyama, T., Cullings, H.M., Hoshi, M., Nagatomo, T., Kumamoto, Y., Kerr, G.D., 2005. Thermoluminescence dosimetry for gamma rays, Chap. 7 Part B. In: Young, R.W., Kerr, G.D. (eds) Reassessment of the atomic bomb radiation dosimetry for Hiroshima and Nagasaki—Dosimetry System 2002 (DS02), Vol 1. Radiation Effects Research Foundation, Hiroshima, Japan, 362–394.

Maruyama, T.; Kumamoto, Y.; Ichikawa, Y.; Nagatomo, T.; Hoshi, M.; Haskell, E.; Kaipa, P., 1987. Thermoluminescence measurements of gamma rays. In: US-Japan Joint Reassessment of Atomic Bomb Radiation Dosimetry in Hiroshima and Nagasaki, Final Report, Vol. 1, 143-184 (Roesch, W.C.; ed.). Hiroshima, Japan: Radiation Effects Research Foundation.

Mathur, V.K., Barkyoumb, J.H., Yukihara, E.G., Göksu, H.Y., 2007. Radiation sensitivity of memory chip module of an ID card. Radiat. Meas. 42, 43-48.

Mauz, B., Lang, A., 2004. Removal of the feldspar-derived luminescence component from polymineral fine silt samples for optical dating applications: evaluation of chemical treatment protocols and quality control procedures. Ancient TL 22, 1-8.

Meckbach, R., Bailiff, I.K., Göksu, H.Y., Jacob, P., Stoneham, D., 1996. Calculation and measurement of dose-depth distribution in bricks. Radiat. Protect. Dosim. 66,183-186.

Meckbach, R., Jacob, P. 1988. Gamma exposures due to radionuclides deposited in urban environments. Part II: Location Factors for different deposition patterns. Radiat. Protect. Dosim. 25, 181-190.

McDonald, J.C., 2010. The top ten list of challenges for radiation protection dosimetry in 2011. Radiat. Prot. Dosim. 141, 105-105.

McKeever, S.W.S., 1985. Thermoluminescence of solids. Cambridge University Press, Cambridge.

McKeever, S.W.S., Moscovitch, M., Townsend, P.D., 1995. Thermoluminescence dosimetry materials: Properties and uses. Nuclear Technology Publishing, Ashford.

McKeever, S.W.S., Sholom, S., 2016. Biodosimetry versus physical dosimetry for emergency dose assessment following large-scale radiological exposures. Radiat. Meas. 92, 8-18 (2016).

Milton, R.C., Shohoji, T., 1968. Tentative 1965 radiation dose (T65D) estimation for atomic bomb survivors. Hiroshima: Radiation Effects Research Foundation, ABCC report TR 1-68.

Miyake, M., Liu, K.J., Walczak, T.M., Swartz, H.M., 2000. In vivo EPR dosimetry of accidental exposures to radiation: experimental results indicating the feasibility of practical use in human subjects. Appl. Radiat. Isot. 52, 1031-1038.

Mokrov, Y., 2004. External radiation exposure of residents living close the Mayak facility: main sources, dose estimates and comparison with earlier assessments. Radiat. Environ. Biophys. 43, 127-139.

Moscovitch, M., 2012. Dosimetry system based on optically stimulated luminescence. US patent US20120292532 A1. United States Patent and Trademark Office.

Mrozik, A., Marczewska, B., Bilski, P., Gieszczyk, W., 2014b. Investigation of OSL signal of resistors from mobile phones for accidental dosimetry. Radiat. Meas. 71, 466-470.

Mrozik, A., Marczewska, B., Bilski, P., Kłosowksi, M., 2014a. Investigation of thermoluminescence properties of mobile phone screen displays as dosimeters for accidental dosimetry. Radiat. Phys. Chem. 104, 88-92.

Nagatomo, T., Hoshi, M., Ichikawa, Y., 1992. Comparison of the measured gamma-ray dose and the DS86 estimate at 2.05 km ground distance in Hiroshima. J. Radiation Research 33, 211-217.

Nagatomo, T., Hoshi, M., Ichikawa, Y., 1995. Thermoluminescence dosimetry of the Hiroshima atomic-bomb gamma-rays between 1.59 km and 1.63 km from the hypocentre. Health Phys. 69, 556-559.

Nakajima, T., 1986. The use of organic substances as emergency dosimeters. Int. J. Radiat. Isot. 33, 1077-1084.

Nakamura, N., Miyazawa, C., Sawada, S., Akiyama, M., Awa, A.A., 1998. A close correlation between electron spin resonance (ESR) dosimetry of tooth enamel and cytogenetic dosimetry from lymphocytes of Hiroshima atomic-bomb survivors. Int. J. Radat. Bio. 73, 619-627.

Narayan, P., Vaijuapurkar, S.G., Senwar, K.R., Kumar, D., Bhatnagar, P.K., 2008. Accidental gamma dose measurement using commercial glass. Radiat. Prot. Dosim. 130, 319-324.

NCRP, 2000. Radiation protection guidance for activities in low-Earth orbit, Report 132, National Council on Radiation Protection and Measurements, 2000.

Nicolalde, R.J., Gougelet, R.M., Rea, M., Williams, B.B., Dong, R., Kmiec, M., M., Lesniewski, P.N., Swartz, H.M., 2010. The view from the tranches: Part 2 – Technical considerations for EPR screening. Health Phys. 98, 128-135.

Nilsson, J., Lund, E., Lund, A., 2001. The effects of UV-irradiation on the ESR-dosimetry of tooth enamel. Appl. Radiat. Isotop. 54, 131-139.

Nossovsky, A. (Ed.), 1996. Retrospective dosimetry of participants of clean-up after Chornobyl accident. Seda-stil, Kiev (in Russian).

NRC, 2006. Facing Hazards and Disasters: Understanding Human Dimensions. Committee on disaster research in the social sciences: Future challenges and opportunities. National Research Council ISBN: 0-309-65985-X. http://www.nap.edu/catalog/11671.html.

Ohnishi, T., 2012. The disaster at Japan's Fukushima-Daiichi nuclear power plant after the March 11, 2011 earthquake and tsunami, and the resulting spread of radioisotope contamination. Radiat. Res. 177, 1-14.

Oks, H., Spooner, N.A., Smith, B.W., Prescott, J.R., Creighton, D.F., McCulloch, I., Adamiec, G., 2011. Assessment of thermoluminescence peaks in porcelain for use in retrospective dosimetry. Radiat. Meas. 46, 1873-1877.

Ozasa, K., Shimizu, Y., Suyama, A., Kasagi, F., Soda, M., Grant, E. J., Sakata, R., Sugiyama, H., Kodama, K., 2012. Studies of the mortality of atomic bomb survivors, Report 14, 1950-2003: an overview of cancer and noncancer diseases. Radiat Res. 177, 229-243.

Pascu, A., Vasiliniuc, S., Zeciu-Dolha, M., Timar-Gabor, A., 2013. The potential of luminescence signals from electronic components for accident dosimetry. Radiat. Meas. 56, 384-388.

Pass, B., 1997. Collective radiation biodosimetry for dose reconstruction of acute accidental exposures: A review. Environ. Health Persp. 105, 1397-1402.

Pass, B., Aldrich, J.E., Scallion, P.L., 1990. An analysis of paramagnetic centers in irradiated dentin using electron spin resonance. Calcif. Tissue Int. 46, 166–168.

Petrov, S. A., Bailiff, I. K., 1997. Determination of trap depths associated with TL in synthetic quartz (359K-550K). Radiat. Meas. 27, 185–191.

Petryakov, S., Schreiber, W., Tseytlin, M., Kmiec, M., Williams, B., Swartz, H., 2016. Surface dielectric resonators for X-band EPR spectroscopy. Radiat. Prot. Dosim., doi:10.1093/rpd/ncw167.

Pivovarov, S., Rukhin, A., Seredavina, T., Sushkova, N., Hill, P., Peterson, L.E., 2007. Exposure subpopulations and peculiarities of individual dose distributions among inhabitants of the Semipalatinsk region. Radiat. Meas. 42, 1033-1036.

Pivovarov, S., Rukhin A., Seredavina T., Zhdanov A., 2002. Retrospective EPR-dosimetry in Semipalatinsk nuclear test site region. In: Kawamori, A., Yamauchi, J., Ohta, H. (Eds.), EPR in the 21st century: basics and applications to material, life and earth sciences. Proceedings of the Third Asia-Pacific EPR/ESR Symposium, Kobe, Japan, pp. 634–639.

Pradhan, A.S., Lee, J.L., Kim, J.L., 2014. Use of OSl and TL of electronic components of portable devices for retrospective accident dosimetry. Defect and Diffusion Forum, 347, 229-245.

Ramzaev, V., Bøtter-Jensen, L., Thomsen, K.J., Andersson, K.G., Murray, AS., 2008. An assessment of cumulative external doses from Chernobyl fallout for a forested area in Russia using the optically stimulated luminescence from quartz inclusions in bricks. J Environ. Radioact. 99, 1154-1164.

Rea, M.E., Gougelet, R.M., Nicolalde, R.J., Geiling, J.A., Swartz, H.M., 2010. Proposed triage categories for large-scale radiation incidents using high-accuracy biodosimetry methods. Health Phys. 98, 136-144.

Regulla, D.F., 2005. ESR spectrometry: a future-oriented tool for dosimetry and dating. Appl. Radiat. Isotopes. 62, 117-127.

Report, 2011. Report of Japanese government to the IAEA ministerial conference on nuclear safety: the accident at TEPCO's Fukushima nuclear power stations. http://www.kantei.go.jp/foreign/kan/topics/201106/iaea_houkokusho_e.html.

RERF, 2012. Views on residual radiation. Radiation Effects Research Foundation, December 8. Available at http://www.rerf.or.jp/news/pdf/residualrad_ps_e.pdf.

Reyes, R.A., Romanyukha, A., Olsen, C., Trompier, F., Benevides, L.A., 2009. Electron paramagnetic resonance in irradiated fingernails: variability of dose dependence and possibilities of initial dose assessment. Radiat. Environ. Biophys. 48, 295-310.

Reyes, R.A., Romanyukha, A., Trompier, F., Mitchell, C.A., Clairand, I., Benevides, L.A., Swartz, H.M., 2008. Electron paramagnetic resonance in Human fingernails: the spong model implication. Radiat. Environ. Biophys. 47, 515-526.

Roesch, W. C., (Ed.), 1987. US-Japan Joint Reassessment of Atomic Bomb Radiation Dosimetry in Hiroshima and Nagasaki. Radiation Effects Research Foundation, Hiroshima.

Romanyukha, A.A., Degteva, M.O., Kozheurov, V.P., Wieser, A., Jacob, P., Ignatiev, E.A., Vorobiova, M.I., 1996. Pilot study of the Urals population by tooth electron paramagnetic resonance dosimetry. Radiat. Environ. Biophys. 35, 305–310.

Romanyukha, A.A., Desrosiers, M.F. and Regulla, D.F., 2000a. Current issues on EPR dose reconstruction in tooth enamel. Appl. Radiat. Isotopes. 52, 1265-1273.

Romanyukha, A.A., Hayes, R.B., Haskell, E.H., Kenner, G.H., 1999. Geographic variations in the EPR spectrum of tooth enamel. Radiat. Prot. Dosim. 84, 445–449.

Romanyukha, A.A., Ignatiev, E.A., Vasilenko, E.K., Drozhko, E.G., Wieser, A., Jacob, P., Keriim-Markus, I.B., Kleschenko, E.D., Nakamura, N., Miyazawa, C., 2000b. EPR dose reconstruction for Russian nuclear workers. Health Phys. 87, 15-20.

Romanyukha, A., Mitchell, C. A., Schauer, D. A., Romanyukha, L., Swartz, H M., 2007a. Q-band EPR biodosimetry in tooth enamel microsamples: Feasibility test and comparison with X-band. Health Phys. 93, 631-635.

Romanyukha, A., Regulla, D.F., 1996. Aspects of retrospective ESR dosimetry. Appl. Radiat. Isot. 47, 1293-1297.

Romanyukha, A.A., Regula D., Vasilenko E. and Wieser A., 1994. South Ural nuclear workers: comparison of individual doses from retrospective EPR dosimetry and operational personal monitoring. Appl. Radiat. Isotopes. 45, 1195-1199.

Romanyukha, A., Reyes, R.A., Trompier, F., Benevides, L.A., 2010. Fingernail dosimetry: Current status and perspectives. Health Phys., 98, 296-300.

Romanyukha, A.A., Schauer, D.A., Thomas, J.A. and Regulla D.F., 2005. Parameters affecting EPR dose reconstruction in teeth. Appl. Radiat. Isot. 62, 147-154.

Romanyukha, A., Trompier, F., LeBlanc, B., Calas, C., Clairand, I., Mitchell, C.A., Smimotopoulos, J.G., Swartz, H.M., 2007b. EPR dosimetry in chemically treated fingernails. Radiat. Meas. 42, 1110-1113.

Romanyukha, A., Trompier, F., Reyes, R.A., Christensen, D.M., Iddins, C.J., Sugarman, S.L., 2014. Electron paramagnetic resonance radiation dose assessment in fingernails of the victim exposed to high dose as result of an accident. Radiat. Environ. Biophys. 53, 755-762.

Romanyukha, A., Trompier, F., Reyes, R.A., Melanson, M.A., 2011. EPR measurements of fingernails in Q-band. Radiat. Meas. 46, 888-892.

Rossi, A.M., Wafcheck, C.C., De Jesus, E.F., Pelegrini, F., 2000. Electron spin resonance dosimetry of teeth of Goiânia radiation accident victims. Appl. Radiat. Isotopes. 52, 1297–1303.

Rudko, V.V., Vorona, I.P., Baran, N.P. and Ishchenko, S.S., 2007. γ- and UV-induced CO_2^-, radicals in tooth enamel. Radiat. Meas. 42, 1181–1184.

Salomaa, S., Lindholm, C., Tankinmanova, M.K., Mamyrbaeva, Zh., Koivistonen, A., Hulten, M., Mustonen, R., Dubrova, Y. E., Bersimbaev, R.I., 2002. Stable Chromosome aberrations in the lymphocytes of population living in the vicinity of the Semipalatinsk nuclear test site. Radiation Research 158, 591-596.

Santos, A.B., Rossi, A.M., Baffa, O., 2005. Study of dental enamel and synthetic hydroxyapatite irradiated by EPR at K-band. Appl. Radiat. Isot. 62, 213-217.

Sato, H., Filas, B.A., Eaton, S.S. , Eaton, G.R., Romanyukha, A. A., Hayes, R., Rossi, A., 2007. Electron spin relaxation of radicals in irradiated tooth enamel and synthetic hydroxyapatite. Radiat. Meas. 42, 997 – 1004.

Sato, H., Takatsuji, T., Takada, J., Endo, S., Hoshi, M., Sharifov, V.F., Veselkina. I.I., Pilenko, I.V., Kalimullin, W.A., Masyakin, V.B., Yoshikawa, I., Nagatomo, T., Okajima, S., 2002. Measuring the external exposure dose in the contaminated area near the Chernobyl nuclear power station using the thermoluminescence of quartz in bricks. Health Phys. 83, 227-236.

Schauer, D.A., Desrosiers, M.F., Kuppusamy, P., Zweier, J.L., 1996. Radiation dosimetry of an accidental overexposure using EPR spectrometry and imaging of human bone. Appl. Radiat. Isotopes 47, 1345-135.

Schauer, D. A., Desrosiers, M. F., Le, F. G., Seltzer, S. M., Links, J. M., 1994. EPR Dosimetry of Cortical Bone and Tooth Enamel Irradiated with X and Gamma Rays: Study of Energy Dependence. Radiat. Res. 138, 1-8.

Schreiber, W., Petryakov, S., Kmiec, M., Feldman, M., Brugger, S., Williams, B., Boyle, H., Satinsky, V., Dong, R., Flood, A.B., Swartz, H., 2016. Flexible, wireless, inductively coupled surface coil resonators for EPR tooth dosimetry. Radiat. Prot. Dosim., doi:10.1093/rpd/ncw153.

Semipalatinsk Research, 2006. Proc. 3rd Dosimetry Workshop on the Semipalatinsk Nuclear Test Site Area, Hiroshima University, 9-11 March 2005. J. Radiation Research 47, Suppl. A, A1-A224.

Serezhenkov V. A., Domracheva E. V., Klevezal G. A., Kulikov S. M., Kuznetsov S. A., Mordvincev P. I., Sukhovskaya L. I., Schklovsky-Kordi, Vanin A. F., Voevodskaya N. V. and Vorobiev A. I., 1992. Radiation dosimetry for residents of the Chernobyl region: a comparison of cytogenetic and electron spin resonance methods. Radiat. Prot. Dosim. 42, 33-36.

Shagina, N.B., Vorobiova, M.I., Degteva, M.O., Peremyslova, L.M., Shishkina, E.A., Anspaugh, L.R., Napier, B.A., 2012. Reconstruction of the contamination of the Techa River in 1949–1951 as a result of releases from the "MAYAK" Production Association. Radiat. Environ. Biophys. 51, 349-366. doi: 10.1007/s00411-012-0414-0

Shimano, T., Iwasaki, M., Miyazawa, C., Miki, T., Kai, A., Ikeya, M., 1989. Human tooth dosimetry for gamma-rays and dental X-rays using ESR. Appl. Radiat. Isot. 40, 1035–1038.

Shishkina, E.A., Degteva, M.O., Tolstykh, E.I., Shved, V.A., Tokareva, E.E., Ivanov, D.V., Bayankin, S.N., Wieser, A., Goksu, H.Y., Anspaugh, L., 2006. Results of dosimetric studies of teeth for Techa riverside residents. Radiat. Safety Problems, 1, 26–44 (in Russian).

Shishkina, E.A., Degteva, M.O., Tolstykh, E.I., Volchkova, A., Ivanov, D.V., Wieser, A., Della Monaca, S., Fattibene, P., 2011. Extra high doses detected in the enamel of human teeth in the Techa riverside region. Radiat. Meas. 46, 760–764

Shishkina, E.A., Tolstykh, E.I., Verdi, E., Volchkova, A.Y., Veronese, I., El-Faramawy, N.A., Goksu, H.Y., Degteva, M.O. (2014) Concentrations of ^{90}Sr in the tooth tissues 60 years after intake: results of TL measurements and applications for Techa River dosimetry. Radiat. Environ. Biophys. 53, 159–173.

Shoikhet, Y.N., Kisilev, V.I., Loborev, V.M., Sudakov, V.V., Algazin, A.I., Demin, V.F., Lagutin, A.A., 1998. The 29 August 1949 nuclear test. Radioactive impact on the Altai Region population. Barnaul, Russia: Institute of Regional Medico-Ecological Problems.

Sholom, S.V., Chumak, V., 2008. Age-related peculiarities of tooth enamel as a natural EPR biodosimeter. Radiat. Meas. 43, 823-826.

Sholom, S., Chumak, V., 2010. EPR emergency dosimetry with plastic components of personal goods. Health Phys. 98, 395-399.

Sholom, S.V., Chumak, V.V., Bakhanova, E.V., 2002. Assessment of contribution of confounding factors to cumulative dose determined by EPR of enamel. In: Kawamori, A., Yamauchi, J., Ohta, H. (Eds.), EPR in the 21st century: basics and applications to material, life and earth sciences. Proceedings of the Third Asia-Pacific EPR/ESR Symposium, Kobe, Japan, pp. 628–633.

Sholom, S.V., Chumak, V.V., Pasalskaja, L.F., 2000b. Some aspects of EPR dosimetry of liquidators. Appl. Radiat. Isotopes 52, 1283-1286.

Sholom, S., Chumak, V., Pavlenko, Y., 1997. The doses from diagnostic X-ray exposure in the EPR-spectroscopy technique with tooth enamel. In: The IRPA regional symposium on radiation protection in neighboring countries of Central Europe, September 8-12, Prague, Proceedings, 571-574.

Sholom, S., Desrosiers, M.F., 2014. EPR and OSL emergency dosimetry with teeth: A direct comparison of two techniques. Radiat. Meas. 71, 494-497.

Sholom, S., Desrosiers, M., Bouville, A., Luckyanov, N., Chumak, V., Simon, S. L., 2007a. EPR tooth dosimetry of SNTS area inhabitants. Radiat. Meas. 42, 1037 – 1040.

Sholom S.V., Desrosiers, M., Chumak, V., Luckyanov, N., Simon, S.L., Bouville, A., 2010. UV effects in tooth enamel and their possible application in EPR dosimetry with front teeth. Health Phys. 98, 360–368.

Sholom, S., DeWitt, R., Simon, S.L., Bouville, A., McKeever, S.W.S., 2011a. Emergency dose estimation using optically stimulated luminescence from human tooth enamel. Radiat. Meas. 46, 778-782.

Sholom, S., DeWitt, R., Simon, S.L., Bouville, A., McKeever, S.W.S., 2011b. Emergency optically stimulated luminescence dosimetry using different materials. Radiat. Meas. 46, 1866-1869.

Sholom, S.V., Haskell, E.H., Hayes, R.B., Chumak, V.V., Kenner, G.H., 1998a. Properties of light induced EPR signals in enamel and their possible interference with gamma-induced signals. Radiat. Meas. 29, 113-118.

Sholom, S.V., Haskell, E.H., Hayes, R.B., Chumak, V.V., Kenner, G.H., 1998b. Influence of crushing and additive irradiation procedures on EPR dosimetry of tooth enamel. Radia. Meas. 29, 105-111.

Sholom, S.V., Haskell, E.H., Hayes, R.B., Chumak, V.V., Kenner, G.H., 2000a. EPR- dosimetry with carious teeth. Radiat. Meas. 32, 799–803.

Sholom, S., McKeever, S.W.S., 2014a. Emergency OSL dosimetry with commonplace materials. Radiat. Meas. 61, 33-51.

Sholom, S., McKeever, S.W.S., 2014b. Emergency OSL/TL dosimetry with integrated circuits from mobile phones. Proc. SPIE 9213, 921319-1 – 021319-10.

Sholom, S., McKeever, S.W.S., 2016. Emergency EPR dosimetry technique using vacuum-stored dry nails. Radiat. Meas. 88, 41-47.

Sholom, S., McKeever, S.W.S., 2015. Integrated circuits from mobile phones as possible emergency OSL/TL dosimeters. Radiat. Prot. Dosim., doi:10.1093/rpd/ncv446.

Sholom, S., O'Brien, M., Bakhanova, E., Chumak, V., Desrosiers, M., Bouville, A. 2007b. X-ray and gamma-ray absorbed dose profiles in teeth: An EPR and modeling study. Radiat. Meas. 42, 1196-1200.

Simon, S.L., Bailiff, I.K., Bouville, A., Fattibene, P., Kleinerman, R.A., Lloyd, D.C., McKeever, S.W.S., Romanyukha, A., Sevan'kaev, A.V., Tucker, J.D., Wieser, A., 2007. BiodosEPR 2006: Consensus committee report on biodosimetric methods to evaluate radiation doses at long times after exposure, Radiat. Meas., 42, 948-971.

Simon, S.L., Bouville, A., 2002, Radiation doses to local populations near nuclear weapons test sites worldwide. Health Phys. 82, 706-725.

Simon, S.L., Bouville, A., Kleinerman, R., 2010. Current use and future needs of biodosimetry in studies of long-term Health risk following radiation exposure. Health Phys. 98, 109-117.

Simon, S.L., Bouville, A., Kleinerman, R., Ron. E., 2006. Dosimetry for epidemiologic studies: learning from the past, looking to the future. Radiat. Res. 166, 313–318.

Sirota, K., Twig, Y., Blank, A., 2013. Pulsed electron spin resonance ex situ probe for biodosimetry. Appl. Magn. Reson. 44, 671-689.

Skvortzov, V.G., Ivannikov, A.I., Eichoff, U., 1995. Assessment of individual accumulated irradiation doses using EPR spectroscopy of tooth enamel. J. Molecular Struct. 347, 321-330.

Skvortzov, V.G., Ivannikov, A.I., Stepanenko, V.F., Tsyb, A.F., Khamidova, L.H., Kondrashov, A.E., Tikunov, D.D., 2000. Application of EPR retrospective dosimetry for large-scale accidental situations. Appl. Radiat. Isotopes 52, 1275-1282.

Soni, A., Mishra, D.R., Polymeris, G.S., Bhatt, B.C., Kulkarni, M.S., 2014. OSL and thermally assisted OSL response in dental enamel for its possible application in retrospective dosimetry. Radiat. Environ. Biophys. 53, 763-774.

Stepanenko, V.F., Hoshi, M., Bailiff, I.K., Ivannikov, A.I., Toyoda, S., Yamamoto, M., Simon, S.L., Matsuo, M., Kawano, N., Zhumadilov, Z., Sasaki, M.S., Rosenson, R.I., Apsalikov, K.N., 2006a. Around Semipalatinsk nuclear test site: progress of dose estimations relevant to the consequences of nuclear tests (a summary of 3rd Dosimetry Workshop on the Semipalatinsk nuclear test site area, RIRBM, Hiroshima University, Hiroshima, 9-11 March, 2005). J Radiat. Res. 47, Suppl. A, A1-13.

Stepanenko, V.F., Hoshi, M., Dubasov, Y.V., Sakaguchi, A., Yamamoto, M., Orlov, M.Y., Bailiff, I.K., Ivannikov, A.I., Skvortsov, V.G., Iaskova, E.K., Kryukova, I.G., Zhumadilov, K.S., Endo, S., Tanaka, K., Apsalikov, K.N., Gusev, B.I., 2006c. A gradient of radioactive contamination in Dolon village near the SNTS and comparison of computed dose values with instrumental estimates for the 29 August, 1949 nuclear test. J Radiat. Res. 47 Suppl. A, A149-A158.

Stepanenko, V.F., Hoshi, I.K., Ivannikov, M., Bailiff, I.K., Zhumadilov, Z., Skvortsov. V.G., Argembaeva, R., Tsyb, A.F., 2007. The 1st Nuclear Test in the former USSR of 29 August 1949: Comparison of individual dose estimates by modeling with EPR retrospective dosimetry and luminescence retrospective dosimetry data for Dolon village, Kazakhstan. Radiat. Meas. 42, 1041-1048.

Stepanenko, V.F., Hoshi, M., Yamamoto, M., Sakaguchi, A., Takada, J., Sato, H., Iaskova, E.K., Kolizshenkov, T.V., Kryukova, I.G., Apsalikov, K.N., Gusev, B.I., Jungner, H., 2006b. International intercomparison of retrospective luminescence dosimetry method: sampling and distribution of the brick samples from Dolon' village, Kazakhstan. J Radiat. Res. 47, Suppl. A, A15-21.

Stepanenko, V., Kolyzshenkov, T.V., Dubov, D.V., Ohtaki, M., Hoshi, M., 2014. Evaluation of residual exposure at Hiroshima and Nagasaki: Possibility of the measurements of beta-particle dose using the retrospective luminescence dosimetry technique. Abstracts of the Fifty-Ninth Annual

Meeting of the Health Physics Society. Baltimore, Maryland, 13-17 July 2014. Health Phys. 107, 1 , Supplement, S43-S44.

Straume, T., Anspuagh, L.R., Haskell, E.H., Lucas, J.N., Marchetti, A.A., Haskell, E.H., Likhtarev, I.A., Chumak, V.V., Romanyukha, A.A., Khrouch, V.T., Gavrilin, Yu.I., Minenko, A.F., 1997. Emerging technological bases for retrospective dosimetry. Stem Cells 15, 183-193.

Straume, T., Egbert, S.D., Woolson, W.A., Finkel, R.C., Kubik, P.W., Gove, H.E., Sharma, P., Hoshi, M., 1992. Neutron discrepancies in the DS86 Hiroshima dosimetry system. Health Phys. 63, 421-426.

Strzelczak, G., Sadło, J., Marek Danilczuk, M., Stachowicz, W, Callens, F., Vanhaelewyn, G., Goovaerts, E., Michalik, J., 2007. Multifrequency electron paramagnetic resonance study on deproteinized human bone. Spectrochimica Acta Part A 67, 1206–1209.

Strzelczak, G., Sterniczuk, M., Sadło, J., Kowalska, M., Michalik, J., 2013. EPR study of g-irradiated feather keratin and human fingernails concerning retrospective dose assessment. Nukleonika 58, 505-509.

Sullivan, J.M., Prasanna, P.G.S., Grace, M.B., Wathen, L.K., Wallace, R.L., Koerber, J.F., Coleman, C.N., 2013. Assessment of biodosimetry methods for a mass-casualty radiological incident: Medical response and management considerations. Health Phys. 105, 540-554.

Swartz, H.M., 1965. Long-lived electron spin resonances in rats irradiated at room temperature. Radiat. Res. 24, 579-586.

Swartz, H.M., Burke, G., Coey, M., Demidenko, E., , Dong, R., Grinberg, O., Hilton, J., Iwasaki, A., Lesniewski, P., Kmiec, M., Lo, K.-M., Nicoldale, N., Ruuge, A., Sakata, Y., Sucheta, A., Walczak, T., Williams, B.B., Mitchell, C.A., Romanyukha, A., Schauer, D.A., 2007. In vivo EPR for dosimetry. Radiat. Meas. 42, 1075-1084.

Swartz, H.M., Williams, B.B., Nicolade, R.J., Demidenko, E., Flood, A.B., 2011. Overview of biodosimetry for management of unplanned exposures to ionizing. Radiation. Radiat. Meas. 46, 742-748.

Takada, J., Hoshi, M., Nagatomo, T., Yamamoto, T., Yoshikava, I., Gusev, B.I., Sekerbaev, A.K., Tchaijunosova, N.I., 1999. External doses for residents near Semipalatinsk Nuclear Test Site. Journal of Radiation Research 40, 337-344.

Takada, J., Hoshi, M., Yamamoto, M., 2002. External doses in residential areas around Semipalatinsk nuclear test site. In: Lindholm, C., Simon, S., Makar, B., Baverstok, K. (eds.) Proceedings of a workshop on dosimetry of the population living in the proximity of the Semipalatinsk atomic weapons test site. Finnish Radiation and Nuclear Safety Authority, Helsinki, STUK-A187, 69-77. http://www.julkari.fi/handle/10024/123593 31 Jan 2016.

Takahashi, F. Sato, K., 2012. Organ dose conversion from ESR measurements using tooth enamel of atomic bomb survivors. Radiat. Prot. Dosim. 149, 67-70.

Takahashi, F., Yamaguchi, Y., Iwasaki, M., Miyazawa, C., Hamada, T., 2001. Relations between tooth enamel dose and organ doses for electron spin resonance dosimetry against external photon exposure. Radiat. Prot. Dosim. 95, 101-108.

Takahashi, F., Yamaguchi, Y., Iwasaki, M., Miyazawa, C., Hamada, T., Kimiaki, S., 2002. Conversion of tooth enamel dose to organ doses for electron spin resonance dosimetry. J. Nucl. Sci. Technol. 39, 964-971.

Tarenenko, V., Meckbach, R., Degteva, M.O. Bougrov, N.G., Göksu, H.Y., Vorobiova, M.I. and Jacob, P., 2003. Verification of external exposure assessment for the upper Techa riverside by luminescence measurements and Monte Carlo photon transport modelling. Radiat. Environ. Biophys. 42, 17-26.

Teixeira, M.I., Da Costa, Z.M., Da Costa, D.C.R., Pontuschka, W.M., Caldas, L.V., 2008. Study of gamma radiation response of watch glasses. Radiat. Meas. 43, 480-482.

Tepe Çam, S., Polat, M., Seyhan, N., 2014. The use of human hair as a biodosimeter. Appl. Radiat. Isotopes 94, 272-281.

Thomsen, K. J., Bøtter-Jensen, L., Murray, A. S., Solongo, S., 2002. Retrospective dosimetry using unheated quartz: a feasibility study. Radiat. Prot. Dosim. 101, 345–348

Thomsen, K. J., Jain, M., Bøtter-Jensen, L., Murray, A. S., Jungner, H., 2003. Variation with depth of dose distributions in single grains of quartz extracted from an irradiated concrete block. Radiat. Meas. 37, 315–321

Thomsen, K.J., Kook, M., Murray, A.S., Jain, M., Lapp, T. 2015. Single-grain results from an EMCCD-based imaging system. Radiat. Meas. 81, 185-191.

Thomsen, K.J., Murray, A.S., Bøtter-Jensen, L. 2005. Sources of variability in OSL dose measurements using single grains of quartz. Radiat. Meas. 39, 47-61

Tolstykh, E.I., Degteva, M.O., Peremyslova, L.M., Shagina, N.B., Shishkina, E.A., Krivoschapov, V.A., Anspaugh, L.R., Napier, B.A., 2011. Reconstruction of long-lived radionuclide intakes for Techa riverside residents: strontium-90. Health Phys. 101, 28–47.

Tominaga, T., Hachiya, M., Tatsuzaki, H, Akashi, M., 2014. The Accident at the Fukushima Daiichi Nuclear Power Plant in 2011. Health Phys. 106, 630-637.

Townsend, P.D., Kelly, J.C., 1973. Colour centres and imperfections in insulators and semiconductors. Sussex University Press, London.

Trapeznikov, A.V.; Pozolotina, V.N.; Chebotina, M.Y.; Chukanov, V.N.; Trapeznikova, V.N.; Kulikov, N.V.; Nielsen, S.P.; Aarkrog, A., 1993. Radioactive contamination of the Techa River, The Urals. Health Phys. 65, 481-488.

Trevedi, A. Greenstock, C.L., 1993. Use of sugars and hair for ESR emergency dosimetry. Appl. Radiat. Isotopes 44, 85-90.

Trompier, F., Bassinet, C., Clairand, I., 2010b. Radiation accident dosimetry on plastics by EPR spectrometry. Health Phys. 98, 388-304.

Trompier, F., Bassinet, C., Della Monica S., Romanyukha, A., Reyes, R, Clairand, I., 2010a. Overview of physical and biophysical techniques for accident dosimetry. Radiat. Prot. Dosim. 144, 571-574.

Trompier, F., Bassinet, C., Wieser, A., De Angelo, C., Viscomi, D., Fattibene, P., 2009a. Radiation-induced signals analysed by EPR spectrometry applied to fortuitous dosimetry. Ann 1st Super Sanita 45, 287-296.

Trompier, F., Della Monica, S., Fattibene, P., Clairand, I., 2011. EPR dosimetry of glass substrate of mobile phone LCDs. Radiat. Meas. 46, 827-831.

Trompier, F., Fattibene P., Woda C., Bassinet C., Bortolin E., De Angelis C., Della Monaca S.,Viscomi D., Wieser A., 2012. Retrospective dose assessment in a radiation mass casualty by EPR and OSL in mobile phones. Proceedings of the 13th IRPA International Congress, May, 13-18, 2012, Glasgow, IRPA13 2358609.

Trompier, F., Kornak, L., Calas, C., Romanyukha, A., LeBlanc, B., Mitchell, C.A., Swartz, H.M., Clairand, I., 2007b. Protocol for emergency EPR dosimetry in fingernails. Radiat. Meas. 42, 1985-1088.

Trompier, F., Queinnec, F., Bey, E., De Revel, T., Lataillade, J.J., Clairand, .I, Benderitter, M., Bottollier-Depois, J.F., 2014b. EPR retrospective dosimetry with fingernails: report on first application cases. Health Phys. 106, 798-805.

Trompier, F., Romanyukha, A., Kornalk, L., Calas, C., LeBlanc, B., Mitchell, C., Swartz, H. Clairand, I., 2009b. Electron paramagnetic resonance radiation dosimetry in fingernails. Radiat. Meas. 44, 6-10.

Trompier, F., Romanyukha, A., Reyes, R., Vezin, H., Queinnac, F., Gourier, D., 2014a. State of the art in nail dosimetry: free radicals identification and reaction mechanisms. Radiat. Environ. Biophys. 53, 291–303.

Trompier, F., Sadlo, J., Michalik, J., , W., Mazal, A., Clairand, I., Rostkowska, J., Bulski, W., Kulakowsk, W., Sluszniak, J., Gozdz, S., Wojcik, A., 2007a. EPR dosimetry for actual and suspected overexposures during radiotherapy treatments in Poland. Radiat. Meas. 42, 1025 – 1028

Ulanovsky, A., Wieser, A., Zankl, M., Jacob, P., 2005. Photon dose conversion coefficients for human teeth in standard irradiation geometries. Health Phys. 89, 645-659.

United Nations Scientific Committee on the Effects of Atomic Radiation (UNSCEAR), 2000. Report to the General Assembly, with Scientific Annexes, Vol II, Annexe J, Exposures and effects of the Chernobyl accident. United Nations Publications, New York.

Vanhaelewyn, G., Goovaerts, E. Callens, F., 2002. Multi-frequency EPR study of radiation-induced radicals in tooth enamel. Radiat. Eff. Defects Solids 157, 1127–1131.

Veronese. I., Galli. A., Cantone, M.C., Martini. M., Vernizzi, F., Guzzi, G., 2010. Study of TSL and OSL properties of dental ceramics for accidental dosimetry applications. Radiat. Meas. 45, 35-41.

Veronese, I., Giussani, A., Göksu, H.Y., Martini, M., 2004a. Isothermal decay studies of intermediate energy levels in quartz. Radiat. Environ. Biophys. 43, 51–57.

Veronese, I., Giussani, A., Göksu, H. Y., Martini, M., 2004b. The trap parameters of electrons in intermediate energy levels in quartz. Radiat. Meas. 38, 743–746

Viscomi, D., De. Angelis, C., Fattibene, P., 2011. Cotton as a fortuitous dosimeter in radiological emergency: An EPR preliminary study. Radiat. Meas. 46, 978-983.

Volchkova, A., Shishkina, E.A., Ivanov, D.V., Timofeev, Yu., Fattibene, P., Wieser, A., Degteva, M.O., 2011. Harmonization of dosimetric information obtained by different EPR methods: experience of Techa River study. Radiat. Meas. 46, 801–807.

von Hippel, F.N., 2011. The radiological and psychological consequences of the Fukushima Daiichi accident. Bull. of Atomic Scientists 67, 27-36.

Wagner, E, Sorom, R, Wiles, L., 2016. Radiation monitoring for the masses. Health Phys. 110, 37-44.

Waller, E.J., van Maanen, J., 2015. The role of the Health Physicist in nuclear safety. Health Phys. 108, 468-476.

Wang, L, Wang, X, Zhang, W, Zhang, H, Ruan, S, Jiao, L., 2015. Determining Dosimetric Properties and Lowest Detectable Dose of Fingernail Clippings from their Electron Paramagnetic Resonance Signal. Health Phys. 109, 10-14.

Wieser, A., 2012. Review of reconstruction of radiation incident air kerma by measurement of absorbed dose in tooth enamel with EPR. Radiat. Prot. Dosim. 149, 71-78.

Wieser, A., Aragno, D., El-Faramawy, N., Fattibene, P., Jacob, P., Meckbach., R., Onori, S., Pressello, M.C., Ulanovsky, A., Zankl, M., 2002. Monte Carlo calculations and experimental verification of the photon energy response of tooth enamel in a head size plexiglas phantom. Radiat. Prot. Dosim. 101, 549–552.

Wieser, A., Debuyst, R., Fattibene, P., Meghzifene, A., Onori, S., Bayankin, S.N., Blackwell, B., Brik, A., Bugay, A., Chumak, V., Ciesielski, B., Hoshi, M., Imata, H., Ivannikov, A., Ivanov, D., Junczewska, M., Miyazawa, C., Pass, B., Penkowski, M., Pivovarov, S., Romanyukha, A., Romanyukha, L., Schauer, D., Scherbina, O., Schultka, K., Shames, A., Sholom, S., Skinner, A., Skvortsov, V., Stepanenko, V., Tielewuhan, E., Toyoda, S., Trompier, F., 2005. The 3rd international intercomparison on EPR tooth dosimetry: Part 1, general analysis. Appl. Radiat. Isotopes 62, 163-171.

Wieser, A., Debuyst, R., Fattibene, P., Meghzifene, A., Onori, S., Bayankin, S.N., Brik, A., Bugay, A., Chumak, V., Ciesielski, B., Hoshi, M., Imata, H., Ivannikov, A., Ivanov, D., Junczewska, M., Miyazawa, C., Pass, B., Penkowski, M., Pivovarov, S., Romanyukha, A., Romanyukha, L., Schauer, D., Scherbina, O., Schultka, K., Sholom, S., Skvortsov, V., Stepanenko, V., Thomas, J.A., Tielewuhan, E., Toyoda, S., Trompier, F., 2006. The 3rd international intercomparison on EPR tooth dosimetry: part 2, final analysis. Radiat. Prot. Dosim. 120, 176-183.

Wieser, A., Fattibene, P., Shishkina, E.A., Ivanov, D.V., De Coste, V., Güttler, A., Onori S., 2008. Assessment of performance parameters for EPR dosimetry with tooth enamel. Radiat. Meas. 43, 731 – 736.

Wieser, A., Göksu, H.Y., Regulla, D.F., Vogenauer, A., 1996. Limits of Retrospective accident dosimetry by EPR and TL with natural materials. Radiat. Meas. 23, 509-514.

Wieser, A., Haskell, E., Kenner G., Bruenger, F., 1994. EPR dosimetry of bone gains accuracy by isolation of calcified tissue. Appl. Radial. Isotopes 45, 525-526.

Wieser, A., Mehta, K., Amira, S., Aragno, D., Bercea, S., Brik, A., Bugai, A., Callens, F., Chumak, V., Ciesielski, B., Debuyst, R., Dubovsky, S., Duliu, O.G., Fattibene, P., Haskell, E.H., Hayes, R.B., Ignatiev, E.A., Ivannikov, A., Kirillov, V., Kleschenko, E., Nakamura, N., Nather, M., Nowak, J., Onori, S., Pass, B.P., Pivovarov, S., Romanyukha, A., Scherbina, O., Shames, A.I., Sholom, S., Skvortsov, V., Stepanenko, V., Tikounov, D.D., Toyoda, S., 2000a. The 2nd International Intercomparison on EPR Tooth Dosimetry. Radiat. Meas. 32, 549–557.

Wieser , A., Onori, S., Aragno, D., Fattibene , P., Romanyukha, A., Ignatievc, E., Koshta A., Skvortzov, V., Ivannikov, A., Stepanenko , V., Chumak, V., Sholom S., Haskell E., Hayes, R., Kenner, G., 2000b. Comparison of sample preparation and signal evaluation methods for EPR analysis of tooth enamel. Appl. Radiat. Isotopes 52, 1059-1064.

Wieser, A., Vasilenko, E., Zankl, M., Greiter, M., Ulanovsky, A., Sabayev, A., Knyazev, V., Zahrov, P., 2011. Evaluation of dose to tooth enamel from medical diagnostic X-ray examinations at Mayak PA. Radiat. Meas. 46, 808–812.

Wilcox, D.E., He, X., Gui, J., Ruuge, A.E., Li, H., Williams, B.B., Swartz, H.M., 2010. Dosimetry based on EPR spectral analysis of fingernail clippings, Health Phys. 98, 309-317.

Wilkins, R.C., Romm, H., Oestreicher , U., Marro, L., Yoshida, M.A., Suto, Y., Prasanna, P.G.S., 2011. Biological dosimetry by the triage dicentric chromosome assay - Further validation of international networking. Radiat. Meas. 46, 923-928.

Wilkinson, D., Waruszynski, B., Mazurik, L., Szymczak, A.-M., Redmond, E., Lichacz, F., 2010. Radiat. Prot. Dosim. 142, 8-11.

Williams, B.B., Dong, R., Kmiec, M., Burke, G., Demidenko, E., Gladstone, D., Nicolade, R.J., Sucheta, A., Lesniewski, P., Swartz, H.M., 2010. Development of in vivo tooth EPR for individual radiation dose estimation and screening. Health Phys. 98, 327-338.

Williams, B.B., Dong, R., Flood, A.B., Grinberg, O., Kmiec, M., Lesniewski, P.N., Matthews, T.P., Nicolade, R.J., Raynolds, T., Salikhov, I.K., Swartz, H.M., 2011. A deployable in vivo EPR tooth dosimeter for triage after a radiation event involving large populations. Radiat. Meas. 46, 772-777.

Williams, B.B., Flood, A.B., Salikov, I., Kobayashi, K., Dong, R., Rychert, K., Du, G., Schrieber, W., Swartz, H.M., 2014. In vivo EPR tooth dosimetry for triage after a radiation event involving large populations. Radiat. Environ. Biophys. 53, 335-346.

Williams, B.B., Sucheta, A., Dong, R., Sakata, Y., Iwasaki, A., Burke, G., Grinberg, O., Lesniewski, P., Kmiec, M., Swartz, W.M., 2007. Experimental procedures for sensitive reproducible in situ EPR tooth dosimetry. Radiat. Meas. 42, 1094-1098.

Wintle, A.G., Murray, A.S., 2006. A review of quartz optically stimulated luminescence characteristics and their relevance in single-aliquot regeneration dating protocols. Radiat. Meas. 41, 369-391.

Woda, C., Bassinet, C., Trompier, F., Bortolin, E., Della Monica, S., Fattibene, P., 2009. Radiation-induced damage analyzed by luminescence methods in retrospective dosimetry and emergency response. Ann. Ist. Super. Sanita. 45, 297-306.

Woda, C., Fieldler, I., Spottl, T., 2012. On the use of OSL of chip card modules with molding for retrospective and accident dosimetry. Radiat. Meas. 47, 1068-1073.

Woda, C., Greilich, S., Beerten, K., 2010. On the OSL curve shape and preheat treatment of electronic components from portable electronic devices. Radiat. Meas. 45, 746-748.

Woda, C., Jacob, P., Ulanovsky, A., Fiedler, L., Mokrov, Y., Rovny, S., 2009. Evaluation of external exposures of the population of Ozyorsk, Russia, with luminescence measurements of bricks. Radiat. Environ. Biophys. 48, 405-417.

Woda, C., Spöttl, T., 2009. On the use of OSL of wire-bonded chip card modules for retrospective and accident dosimetry. Radiat. Meas. 44, 548-553.

Woda, C., Ulanovsky, A., Bougrov, N.G., Fiedler, I., Degteva, M.O., Jacob, P., 2011a. Luminescence dosimetry in a contaminated settlement of the Techa River valley, Southern Urals, Russia. Radiat. Meas. 46, 277-285.

Woda, C., Ulanovsky, A., Bougrov, N.G., Fiedler, I., Degteva, M.O., Jacob, P., 2011b. Potential and limitations of the 210°C TL peak in quartz for retrospective dosimetry. Radiat. Meas. 46, 485-493.

Woflson, H., Ahmad, R., Twig, Y., Williams, B., Blank, A., 2015. A magnetic resonance probehead for evaluating the level of ionizing radiation absorbed in human teeth. Health. Phys. 108, 326-335.

Wu, K., Sun, C.P., Shi, Y.M., 1995. Dosimetric properties of watch glass: A potential practical ESR dosimeter for nuclear accidents. Radiat. Protect. Dosim., 59, 223-225.

Yordanov, N.D., Georgieva, E., 2014. EPR and UV spectral study of gamma-irradiated white and burned sugar, fructose and glucose. Spectrochimica Acta Part A 60, 1307-1314.

Young, R.W., Kerr, G.D., (Eds)., 2005. Reassessment of the Atomic Bomb Dosimetry for Hiroshima and Nagasaki - Dosimetry System 2002 (DS02). Hiroshima: Radiation Effects Research Foundation.

Yüce, Ü.R., Meriç, N., Atakol, O., Yasar, F., 2010. Dose response of hydrazine-deproteinated tooth enamel under blue light stimulation. Radiat. Meas. 45, 797-800.

Yukihara, E.G., McKeever, S.W.S., 2011. Optically Stimulated Luminescence: Fundamentals and Applications. John Wiley & Sons.

Yukihara, E.G., McKeever, S.W.S., Simon, S., 2007. Investigation on the potential of the Optically Stimulated Luminescence (OSL) from dental enamel for retrospective assessment of radiation exposure. Radiat. Meas. 42, 1256-1260.

Zdravkova, M., Vanhaelewyn, G., Callens, F., Gallez, B. Debuyst, R., 2005. Multi-frequency electron paramagnetic resonance study of irradiated human finger phalanxes. Spectrochimica Acta Part A 6, 3131–3138.

Zhumadilov, K., Ivannikov, A., Apsalikov, K.N., Zhumadilov, Zh., Toyoda, S., Zharlyganova, D., Tieliewuhan, E., Endo, S., Tanaka, K., Hoshi, M., 2006. Radiation dose estimation by tooth enamel EPR dosimetry for residents of Dolon and Bodene. J. Radiat. Res. 47, A47-A53.

Zhumadilov, K., Ivannikov, A., Apsalikov, K., Zhumadilov, Zh., Zharlyganova, D., Stepanenko, V., Skvortsov, V., Berekenova, G., Toyoda, S., Endo, S., Tanaka, K., Miyazawa, C., Hoshi, M., 2007. Results of tooth enamel EPR dosimetry for population living in the vicinity of the Semipalatinsk nuclear test site. Radiat. Meas. 42, 1049-1052.

Zhumadilov, K., Ivannikov, A., Stepanenko, V., Zharlyganova, D., Toyoda, S., Zhumadilov, Z., Hoshi, M., 2013. ESR dosimetry study of population in the vicinity of the Semipalatinsk Nuclear Test Site. J Rad. Res. 54, 775–779.

Zhumadilov, K., Ivannikov, A., Zharlyganova, D., Stepanenko, V., Abralina, Sh., Zhumadilova, Z., Apsalikov, K., Toyoda, S., Endo, S., Tanaka, K., Miyazawa, C., Okamoto, T., Hoshi, M., 2011a. The influence of the Lop Nor Nuclear Weapons Test Base to the population of the Republic of Kazakhstan. Radiat. Meas. 46, 425-429.

Zhumadilov, K., Ivannikov, A., Zharlyganova, D., Zhumadilov, Zh., Stepanenko, V., Abralina, Sh., Sadvokasova, L., Zhumadilova, A., Toyoda, S., Endo, S., Okamoto, T., Hoshi, M., 2011b. ESR dosimetry study for the residents of Kazakhstan exposed to radioactive fallout on 24, August 1956. Radiat. Meas. 46, 793–796.

Zhumadilov, K., Ivannikov, A., Zharlyganova, D., Zhumadilov, Z., Stepanenko, V., Apsalikov, K., Rodzi, M., Zhumadilova, A., Toyoda, S., Endo, S., Tanaka, K., Okamoto, T., Hoshi, M., 2009. ESR dosimetry study on population of settlements nearby Ust-Kamenogorsk city, Kazakhstan. Radiat. Environ. Biophys. 48, 419-425.

Zhumadilov, K., Ivannikov, A., Stepanenko, V., Toyoda, S., Skvortsov, V., Hoshi, M., 2016. EPR dosimetry study for population residing in the vicinity of fallout trace for nuclear test on 7 August 1962. Radiat. Prot. Dosim., doi:10.1093/rpd/ncw178.

TABLES & FIGURES

Table 1

Radiation dose triage levels for symptoms and medical care (Jaworska et al., 2014a and Jaworska et al., 2014b). For deterministic effects the critical quantity to be measured is the absorbed dose.

Category	Triage Dose	Symptoms and Care
Low	<1 Gy	Unlikely to develop symptoms of acute radiation syndrome (ARS); no immediate care required
Medium	1-2 Gy	May experience mild or delayed ARS symptoms; follow-up care may be necessary
High	>2Gy	Moderate-to-urgent care may be required

Table 2

Required characteristics of PoC and HT dosimetry devices or methods (Sullivan et al., 2013).

	Point of Care (PoC) Device	High-Throughput (HT) Device
Type of result	Qualitative	Quantitative (accuracy ±0.5Gy)
Concept of operations	Initial triage and sorting	Injury assessment/treatment
Exposure level	2 Gy threshold	Range; 0.5 – 10.0 Gy
Ease of operation	Easy to operate; minimal complexity; requires minimal training	Laboratory instrument; more labor intensive; requires training
Device characteristics	Integrated components; no sample preparation	May include separate components, as needed; High automation desired
Intended use	In field (tents, shelters, open settings)	Labs., hospitals, fixed facilities
Number of patients/event	~1 million in 6 days	Up to 400,000
Time to result	15 – 30 minutes per individual	Up to 24 hr

Table 3

Summary of the materials potentially useful in emergency triage dosimetry, showing the likely stability of the signal and the possible MMD values that may be obtained.

Materials Examined	Method(s) Used	Typical MMD	Notes[1]	Representative Citations
Bone	EPR	1-2 Gy	Stable	1-8
Tooth enamel	EPR, OSL	<100 mGy (EPR); < 1Gy (OSL)	Stable (EPR); unstable (OSL); RIS, MIS and BG EPR signals	8-20, 35
Finger nails	EPR, OSL	<0.1-1 Gy (EPR); 0.1-5 Gy (OSL)	Unstable; humidity dependent; RIS, MIS and BG EPR signals	21-26, 35
Phone glass	EPR, TL	1-2 Gy (EPR); 300-400 mGy (TL)	Unstable	27-29
Watch glass	EPR, TL	1-2 Gy (EPR); <1 Gy (TL)	Unstable	30-32
Plastic buttons	EPR, OSL	~5 Gy (EPR); 30-300 mGy (OSL)	Unstable	33-35
Plastic eye glasses	EPR	<1 Gy	Unstable	33
Cotton clothing	EPR	>1 Gy	Unstable	36
Chip cards	TL, OSL	100 mGy (TL), <10 mGy (OSL)	Unstable plus stable components	37-40
Electronic components	TL, OSL	<10 mGy (OSL; SMRs), 0.13-0.26 Gy (OSL; ICs)	SMRs – unstable; ICs approx. stable with preheat	40- 45
Dental ceramics	TL, OSL	mGy – tens mGy	Unstable	46,47
Synthetic clothing	OSL	45 mGy – 1.2 Gy	Unstable; strong native signal in some cases	48
Shoes	OSL	55 – 550 mGy	Unstable; strong native signal in some cases	48
Paper money	OSL	40 mGy to 240 mGy	Unstable; strong native signal in some cases	48
Coins	OSL	30 mGy – 2 Gy	Unstable	48, 49
Plastic Cards	OSL	8 mGy and 1.5 Gy	Unstable; strong native signal in some cases	48
Business Cards	OSL	40 mGy – 1 Gy	Unstable	35
Dust from Personal Objects	TL	100 mGy (keys, tobacco)	Stable	49

Citations:

1. Callens *et al*. (1998)
2. Brik *et al*. (2000)
3. Desrosiers (1993)
4. Wieser *et al*. (1994)
5. Breen and Battista (1995)
6. Pass (1997)
7. Zdravkova *et al*. (2005)
8. Desrosiers and Schauer (2001)
9. Romanyukha and Regulla (1996)
10. Straume *et al*. (1997)
11. Hayes, *et al*. (1998)
12. Sholom *et al*. (1998b)
13. Sato *et al*. (2007)
14. Lanjanian *et al*. (2008)
15. Romanyukha, *et al*. (2005)
16. Miyake *et al*. (2000)
17. Godfrey-Smith and Pass (1997)
18. Godfrey-Smith (2008)
19. DeWitt *et al*. (2010)
20. Sholom *et al*. (2011a)
21. Reyes *et al*. (2009)
22. He *et al*. (2011)
23. Romanyukha *et al*. (2014)
24. Trompier *et al*. (2014a)
25. Wang *et al*. (2015)
26. Sholom and McKeever (2016)
27. Trompier *et al*. (2009a)
28. Trompier *et al*. (2010a, 2011)
29. Discher and Woda (2013)
30. Wu *et al*. (1995)
31. Bassinet *et al*. (2010a)
32. Woda *et al*. (2009)
33. Trompier et al. (2010b)
34. Sholom and Chumak (2010)
35. Sholom *et al*. (2011b)
36. Viscomi *et al*. (2011)
37. Göksu (2003)
38. Mathur *et al*. (2007)
39. Barkyoumb and Mathur (2008)
40. Woda *et al*. (2012)
41. Inrig *et al*. (2008)
42. Beerten *et al*. (2009)
43. Woda *et al*. (2010)
44. Bassinet *et al*. (2014b)
45. Sholom and McKeever (2014b, 2015)
46. Ekendahl *et al*. (2013)
47. Veronese et al. (2010)
48. Sholom and McKeever (2014a)
49. Bortolin *et al*. (2011)

---

[1] Includes notes on stability of the radiation-induced signals. Stability varies widely. A signal is classified here as "unstable" if it displays enough fading within the first 24 hours to require a correction algorithm to be used.

Table 4

Summary of the key factors relevant to the use of ceramic building materials within standing structures for application to retrospective dosimetry measurements

Primary measured quantity	Absorbed dose in crystalline minerals with luminescent properties.
Retrospective application	Determination of past absorbed dose due to external gamma radiation incident on ceramic materials used in buildings and structures.
Conversion of primary measured quantities	Calculation, based on Monte Carlo simulations of absorbed dose in ceramic medium to dose in air at an external Reference Location.
Requirements	Fired ceramic materials in place before the onset of irradiation by artificial sources of radiation.
Other Factors	Absorbed dose due to natural sources of radiation must be taken into account
Stability	High stability providing appropriate luminescence signals are measured; absorbed dose determination may be made decades after the event of interest providing samples are not accidentally heated, e.g., by fire.
Dose range	~10 mGy - >100 Gy
Examples of output	Time-integrated gamma dose in the vicinity of buildings in populated areas; benchmark values for use in dose reconstruction to derive dose to populations; Time-averaged shielding factors for buildings; Location factors, populated areas; Configuration and average energy of artificial sources of external gamma radiation; Accidental exposure to gamma-ray emitting radiation sources within buildings; Characterization of gamma radiation field.

Figure 1

The common elements of all disaster/mass-casualty events have led to several specialist research topics. The overlap between assessment of hazards and development of response is generally known as "preparedness". (Redrawn from NRC, 2006)
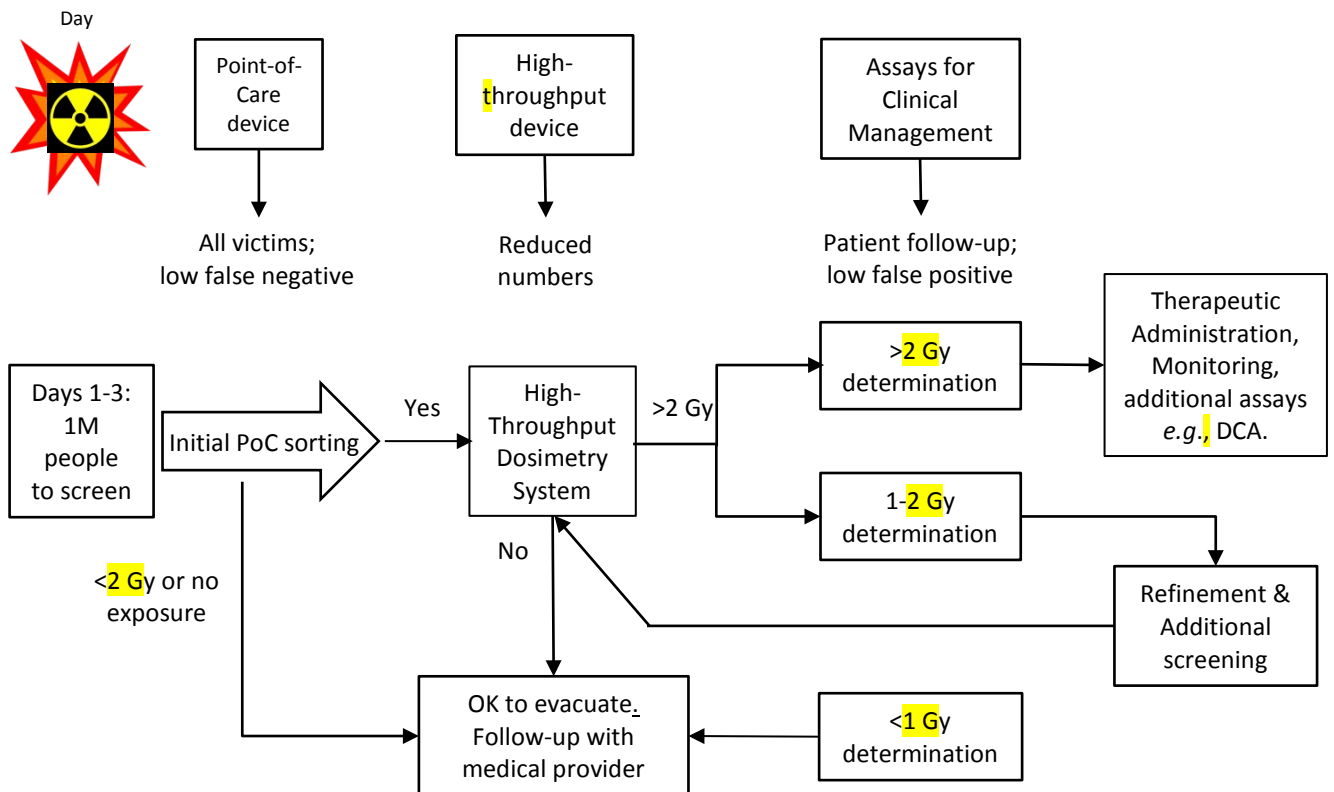
Figure 2

Model for triage screening of large numbers of potentially exposed people following a large-scale radiological event. Two screening levels are envisioned. The initial sorting is performed at Point-of-Care locations in which the screening is rapid and qualitative. Those believed to be exposed to doses >2 Gy are passed on to a High-Throughput, quantitative screening process. Only those verified as having been exposed to levels >2 Gy are processed further for possible immediate therapy and additional assays. (Based on the model shown in Sullivan et al., 2013.)
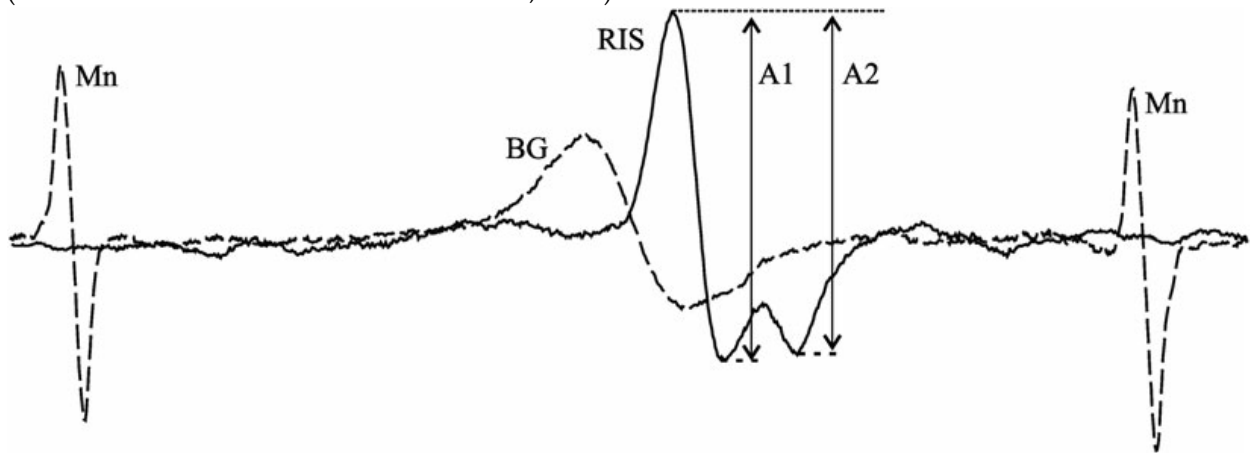
Figure 3

Radiation-induced (RIS) and non-radiation-induced background (BG) X-band EPR signal from irradiated bone. (Reproduced from Ciesielski et al., 2014)
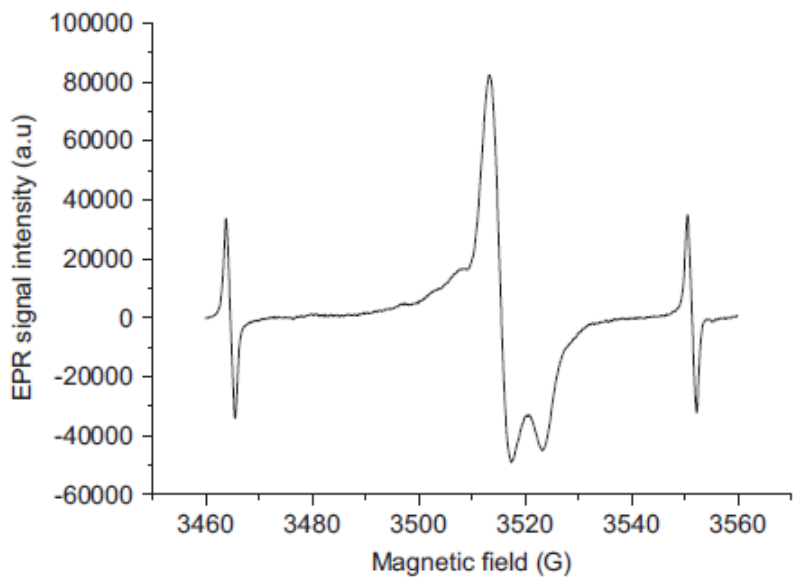
(a)
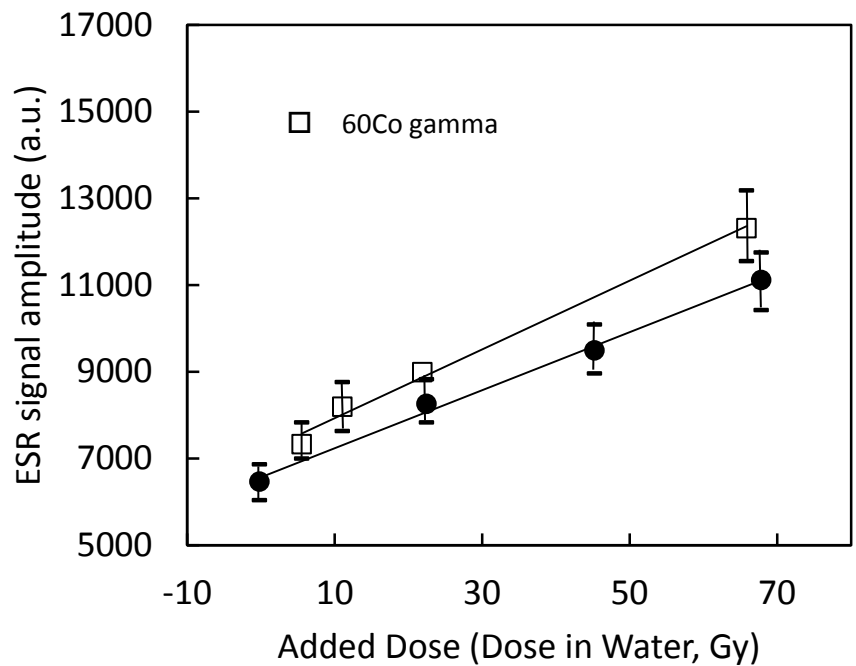
Figure 4

(a) EPR spectrum from rib bone for a radiotherapy patient. The applied dose was 120 Gy. (Note: 10 G corresponds to 1 mT.) (b) RIS dose response. (Reproduced from Trompier et al., 2007a
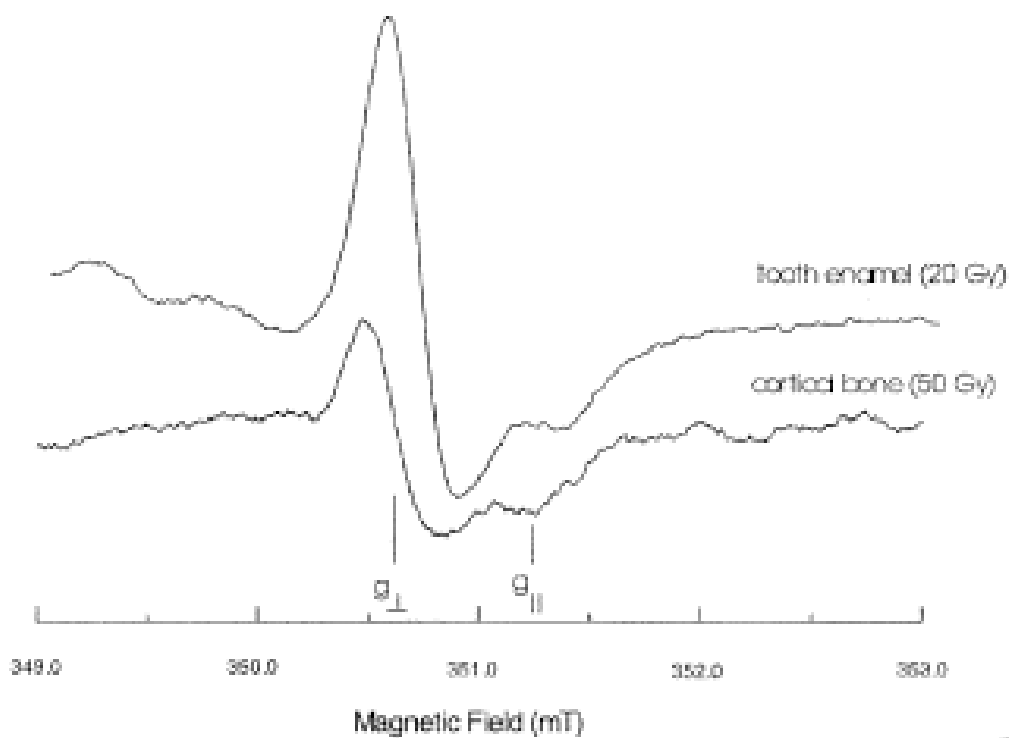
Figure 5

A comparison of the EPR spectrum, due to CO_2^- radicals, from irradiated tooth enamel and cortical bone. (Reproduced from Desrosier and Schauer, 2001)
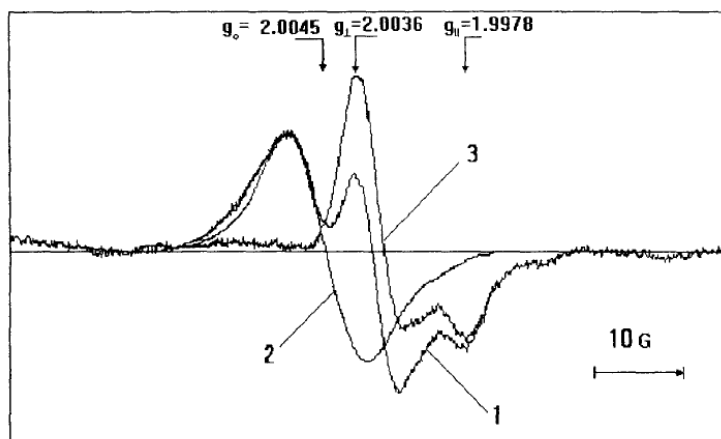
Figure 6

Composite EPR spectrum (1) from irradiated (2 Gy gamma) tooth enamel, consisting of the isotropic native signal at g=2.0045 (2) and the anisotropic radiation-induced signal at g = 2.0036 and g = 1.9978 (3). (Reproduced from Skvortzov et al.,1995)
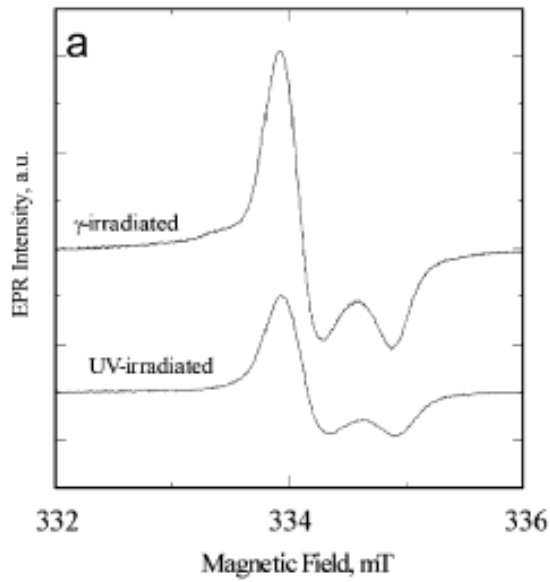
Figure 7
Comparison of gamma-induced and ultraviolet-induced EPR signals in tooth enamel. (Reproduced from Rudko *et al.*, 2007)
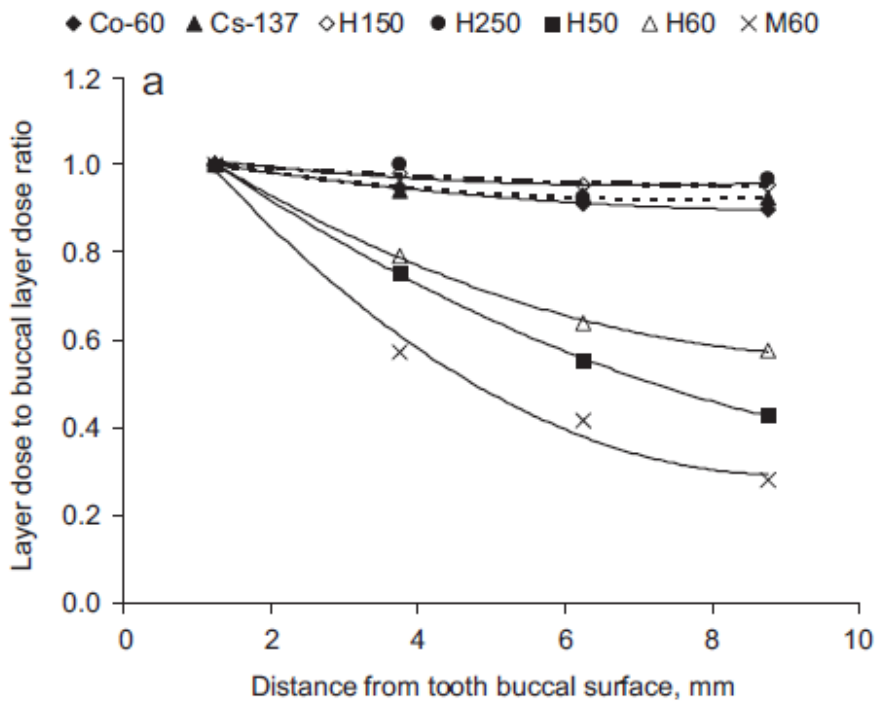
Figure 8
Dose-depth profiles, normalized to the first 1 mm, for different gamma and x-ray exposures. (Reproduced from Sholom *et al.*, 2007b)
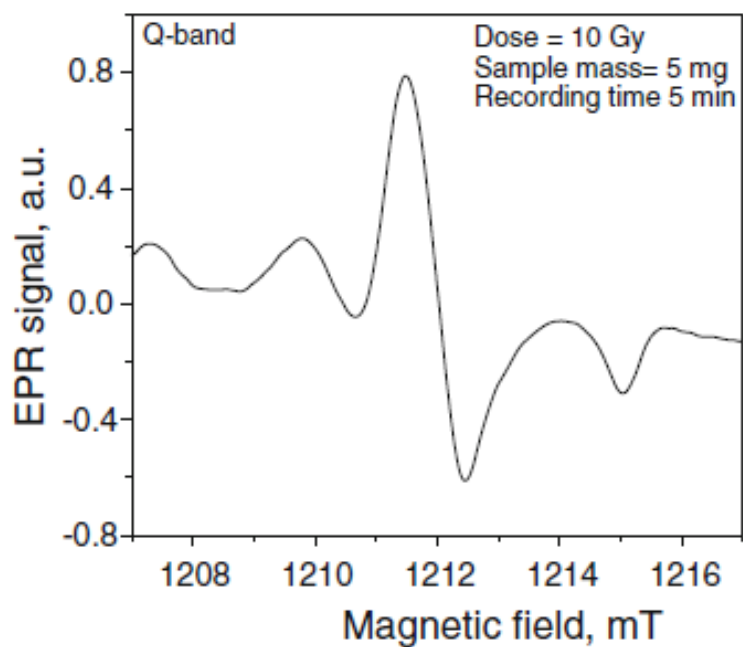
Figure 9

Q-band spectrum from irradiated tooth enamel showing the CO_2^- radical. (Reproduced from De et al., 2013)
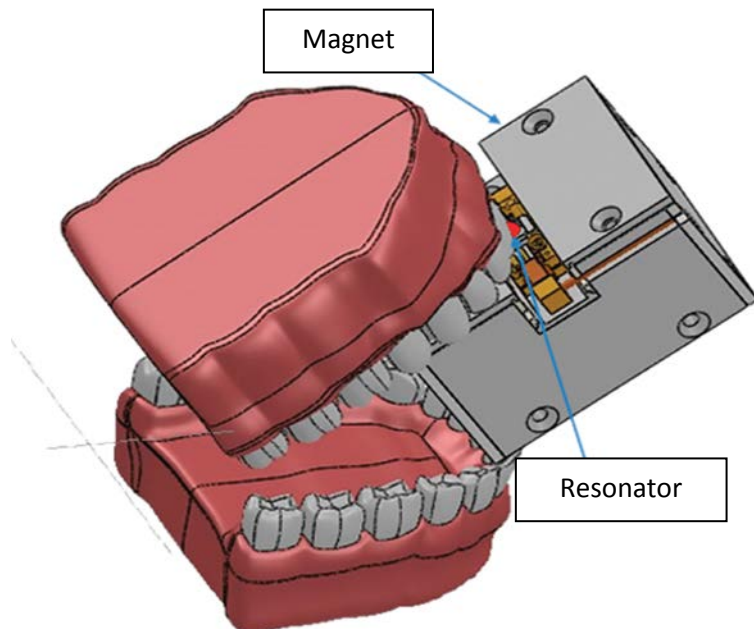
Figure 10

Schematic of the pulsed EPR probehead for X-band *in-vivo* dosimetry of teeth, showing the permanent magnet and resonator assembly. (Reproduced from Woflson et al., 2015)
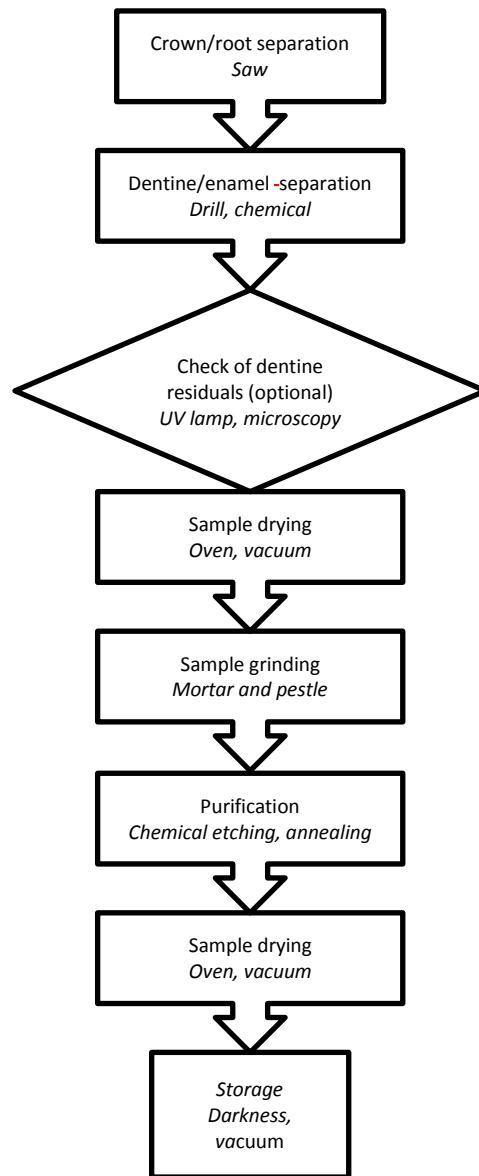
Figure 11

Flow diagram for the typical steps in preparing an extracted tooth for EPR measurements. (Adapted from Fattibene and Callens, 2010.)
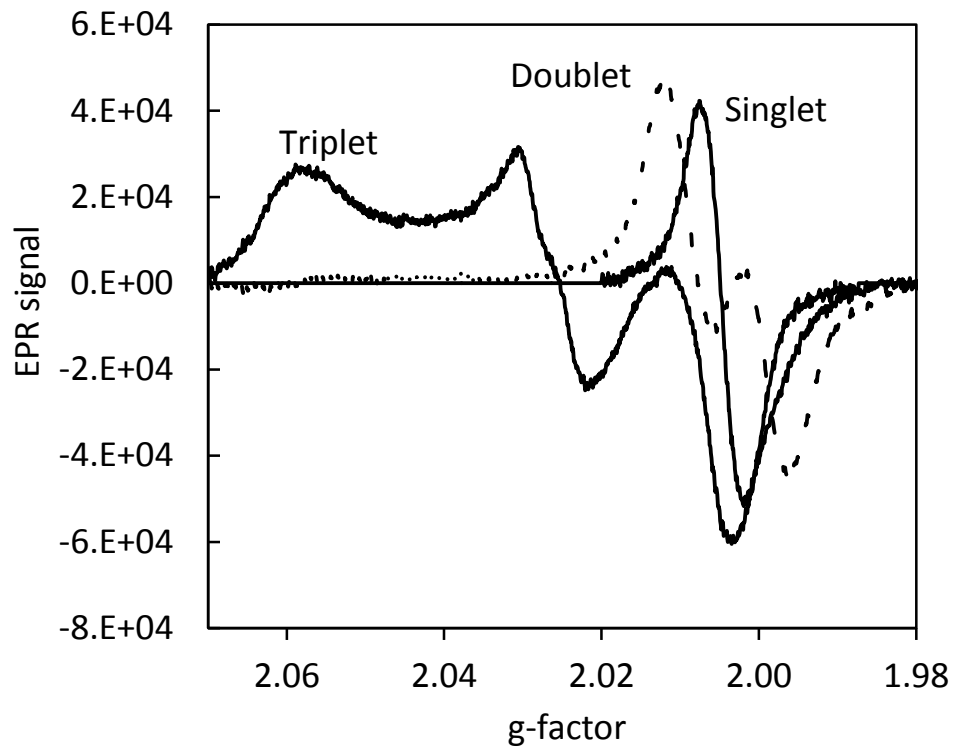
Figure 12

X-band EPR signals from human fingernails, showing the singlet, doublet and triplet signals.
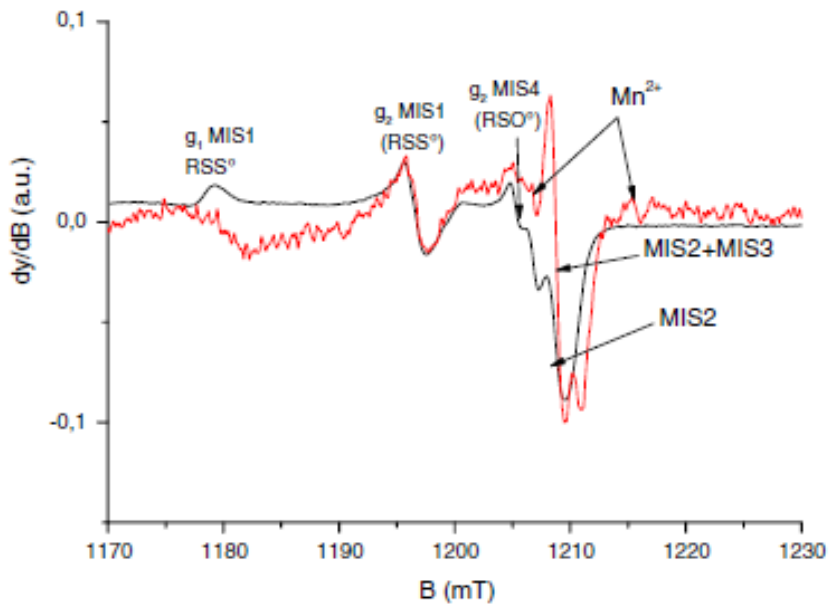
Figure 13

Q-band EPR spectra of nails mechanically stressed and measured under an ambient atmosphere (black line) and under a nitrogen atmosphere (red line). (Reproduced from Trompier et al., 2014a)
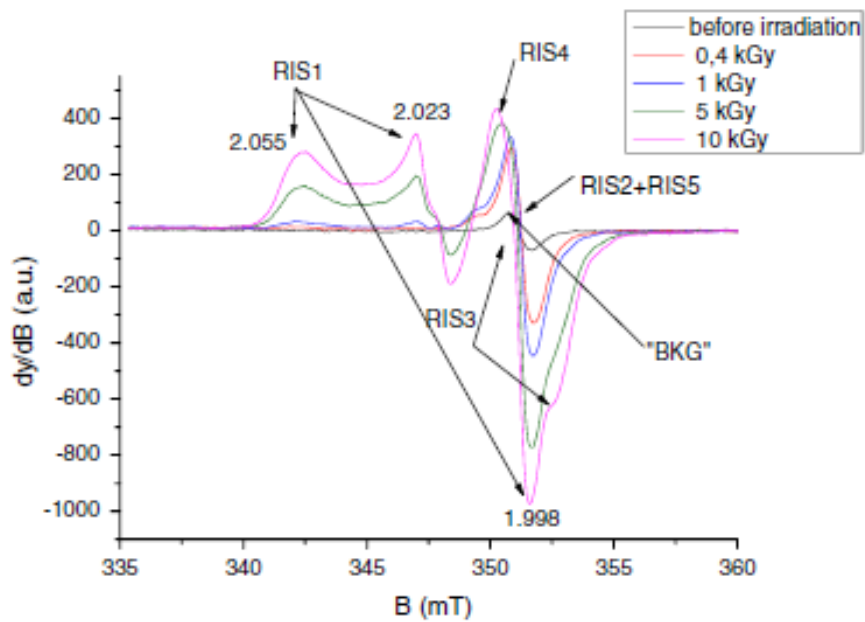
Figure 14

Dose dependence of the RIS signals, identified in the X-band. (Reproduced from Trompier et al., 2014a)

(a)
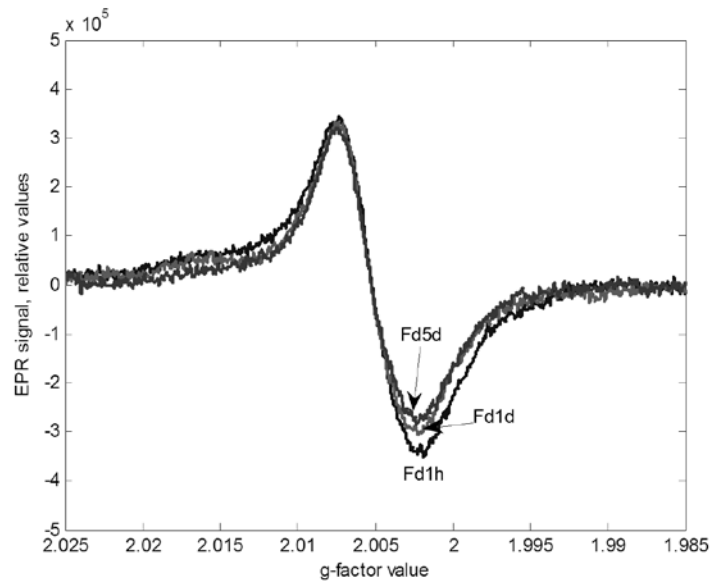
(b)
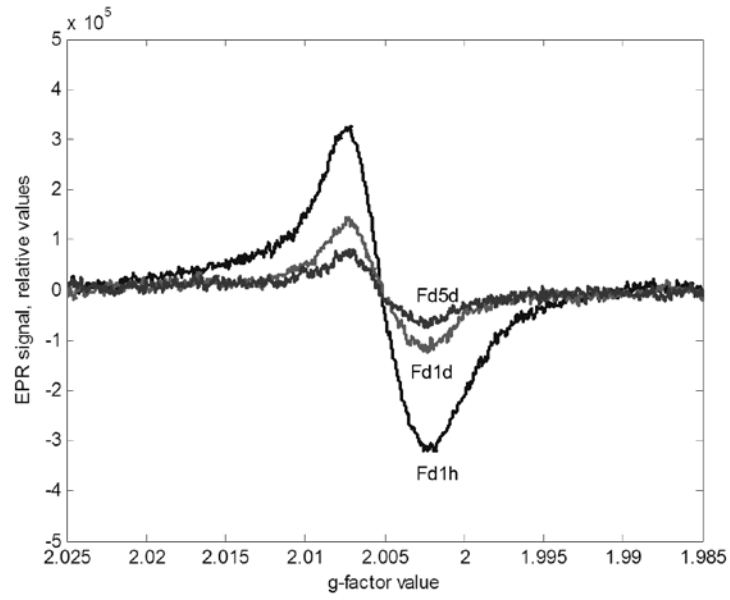
(c)
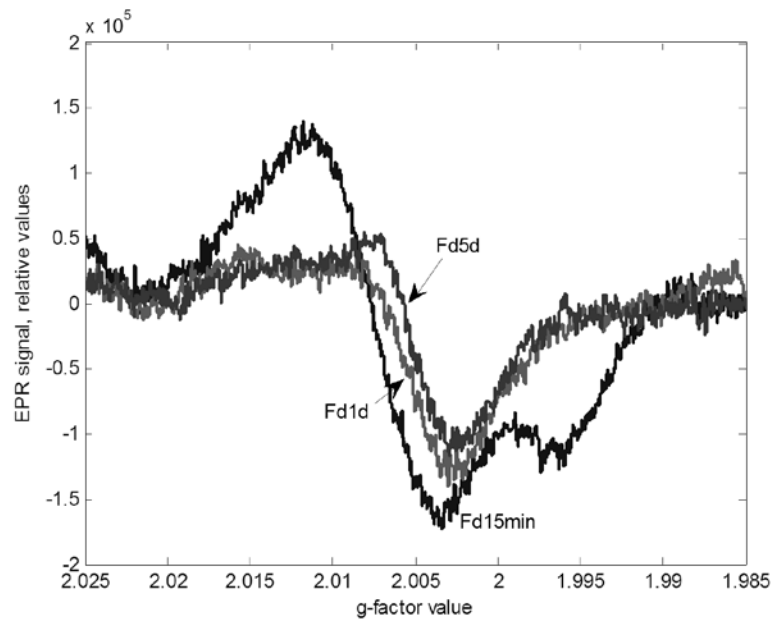
(d)
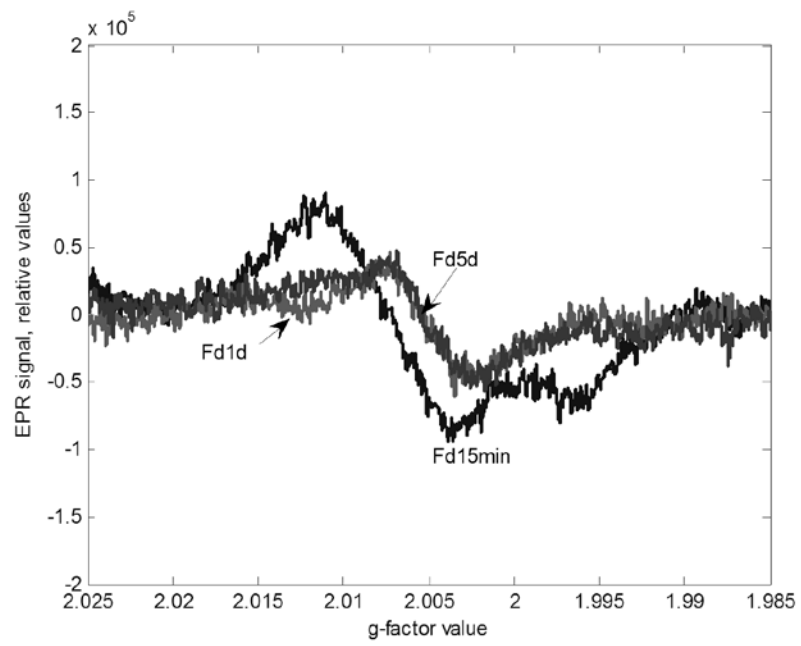
(e)
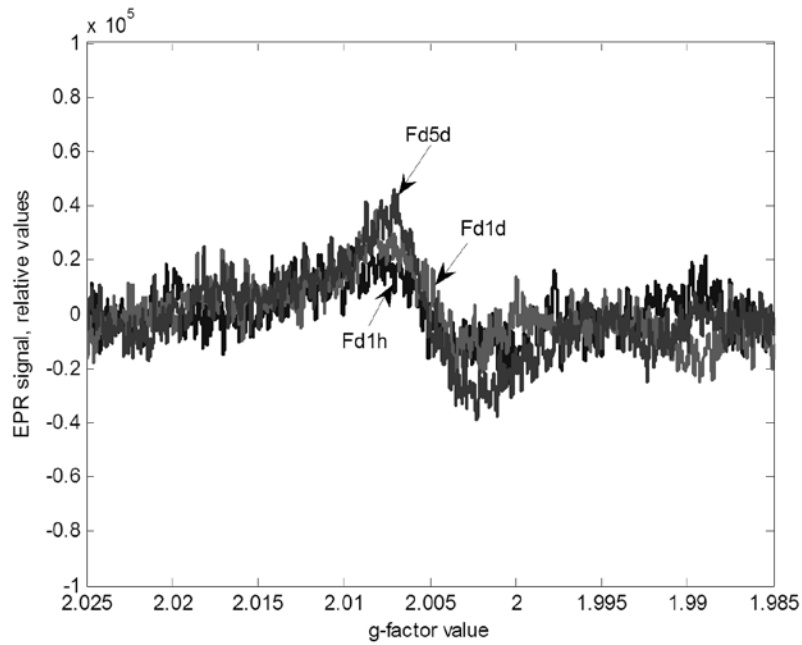
(f)
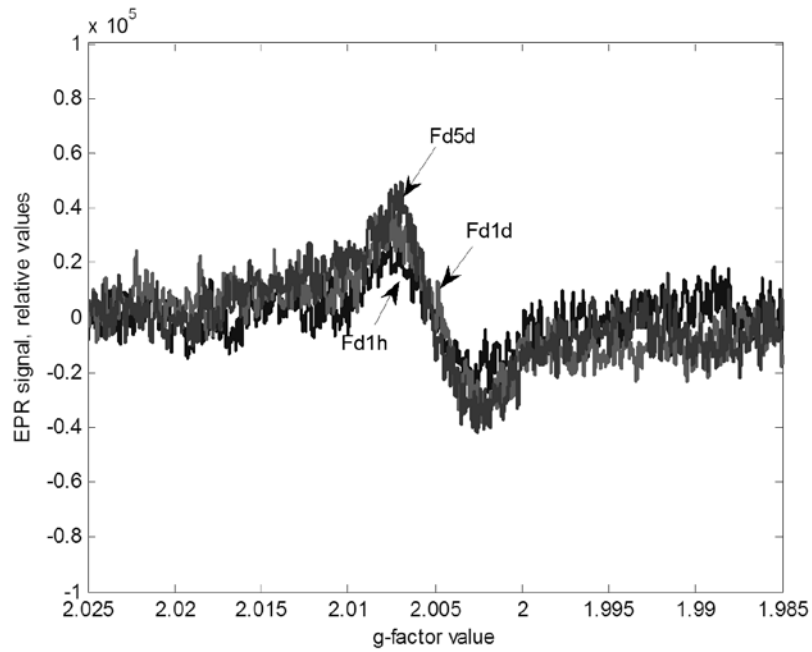
Figure 15

Evolution with time of the RIS ((a) and (b), MIS ((c) and (d)) and BG ((e) and (f) EPR signals from human fingernails for storage in vacuum ((a), (c) and (e)) and at 62 % humidity ((b), (d) and (f)). All storage temperatures were 20 °C. The notation "Fd1h" means fading (or storage) for 1 hour, *etc*. (Reproduced from Sholom and McKeever, 2016)
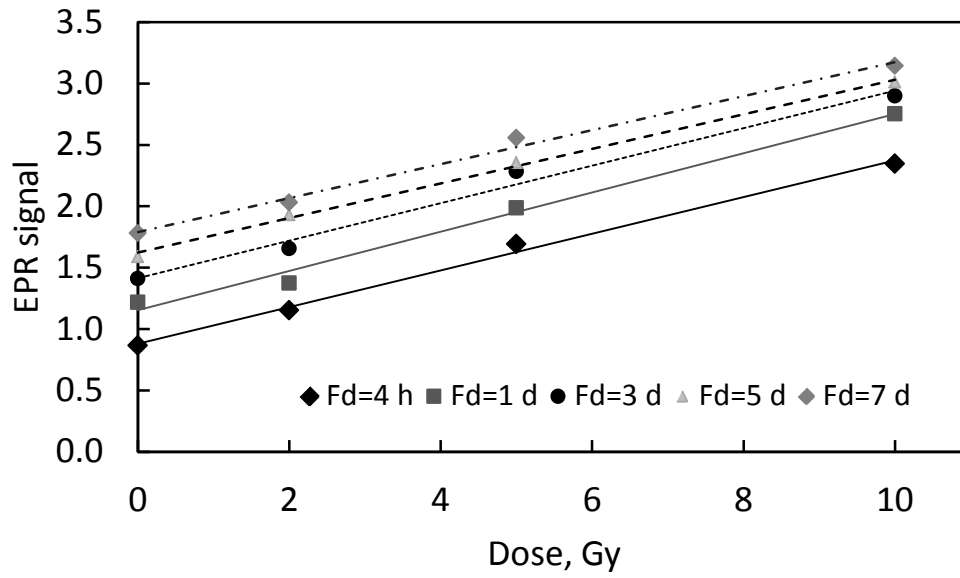
Figure 16

Dose response curves for vacuum-stored samples obtained at different times after exposure and cutting. Fd = fading time. Each data set is fitted with a linear function of the type y = mx + c, with m = slope and c = intercept, corresponding to the BG signal. (Reproduced from Sholom and McKeever, 2016)
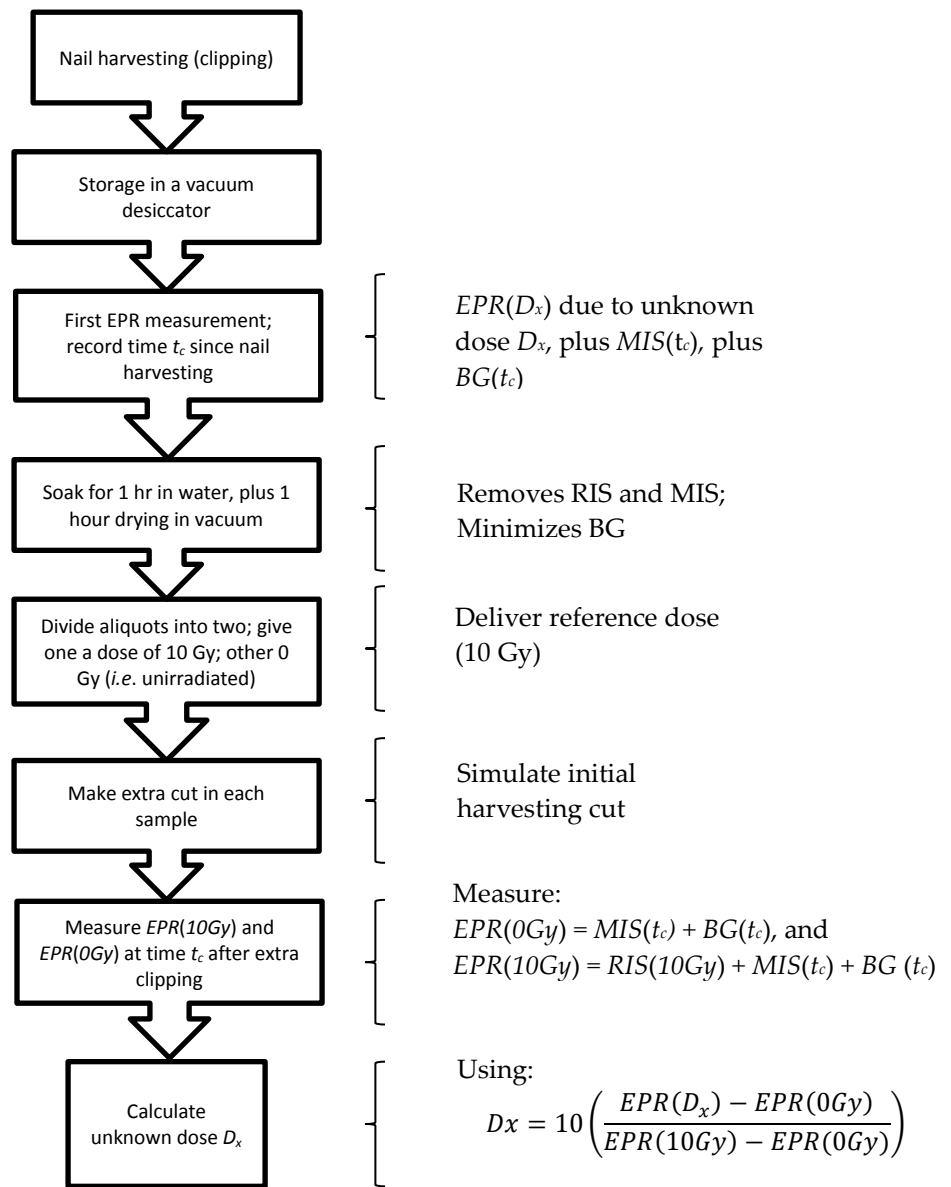
Figure 17

Summary of proposed protocol by Sholom and McKeever (2016) for evaluating an unknown dose D_x, using X-band EPR analysis. All storage conditions are in a vacuum.
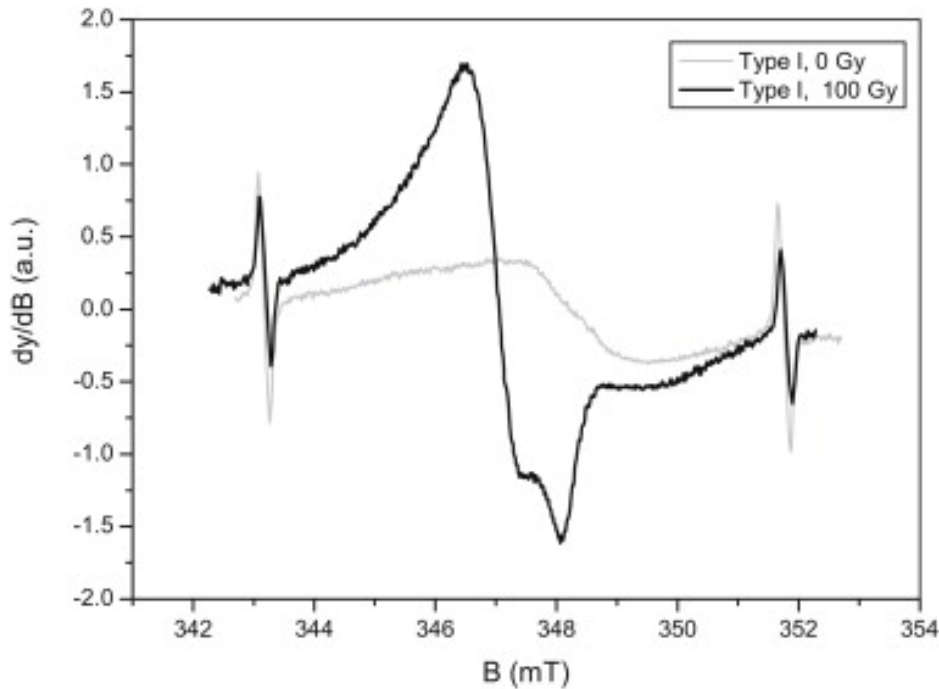
Figure 18

EPR spectra from "Type I" phone glass. (Reproduced from Trompier et al., 2011)
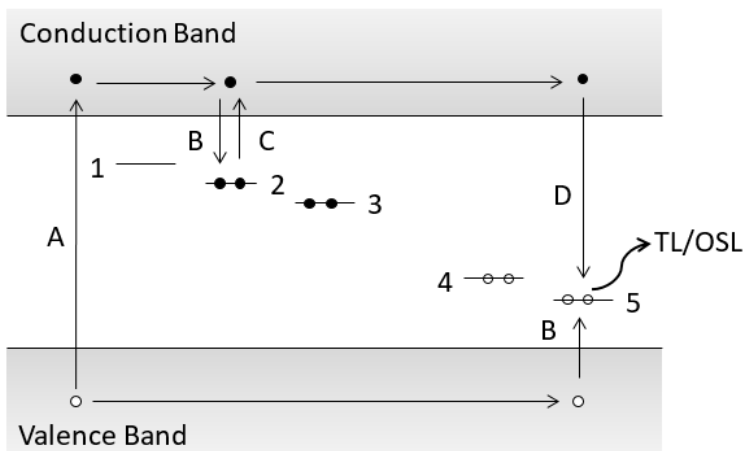
Figure 19

Schematic representation of the TL/OSL process. Upon irradiation free electrons and holes are created (transition A). Movement of the free charge leads to trapping at defects within the crystal such that the energy of the trapped charge is to be found in the band gap between the conduction and valence bands (transitions B). Thermal (for TL) or optical (for OSL) stimulation frees an electron (transition C), leading to recombination (transition D) and the subsequent emission of light. Levels 1, 2 & 3 are electron-trapping levels (normally empty of electrons before irradiation); 4 and 5 are hole trapping levels (normally full of electrons before irradiation). Shallow traps (1) do not hold trapped charge for long; deep traps (3) may remain full after stimulation, depending upon temperature (for TL) or stimulation wavelength (for OSL).
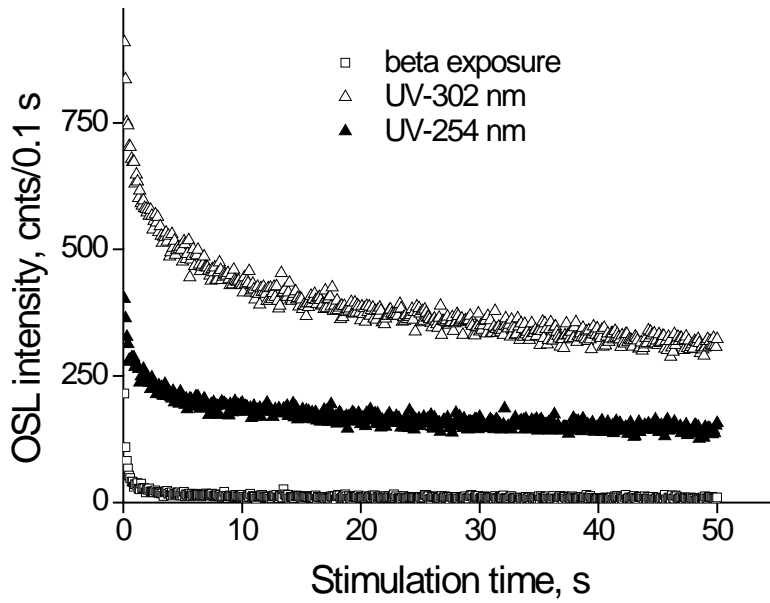
a)
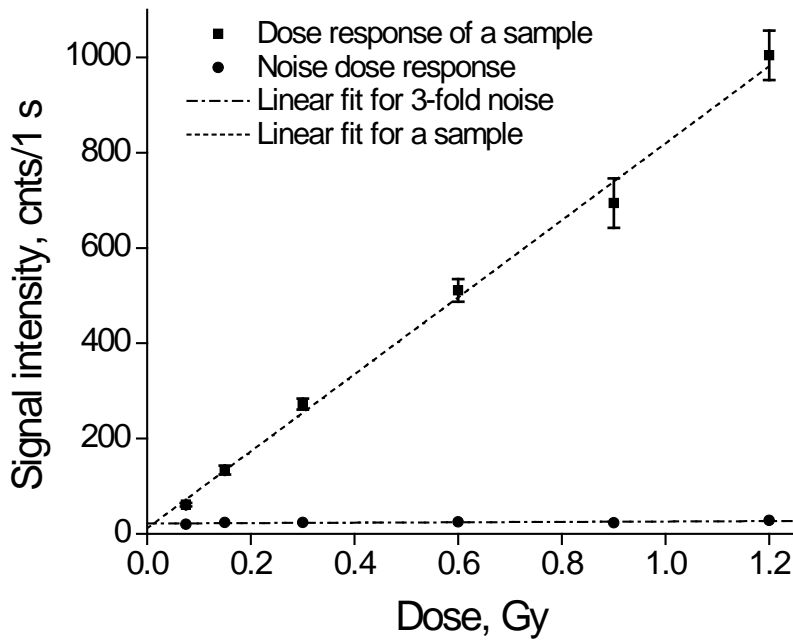
b)

Figure 20

(a) OSL decay curves from human tooth enamel following irradiations with different sources, as shown.

(b) Dose response curve: OSL as a function of beta dose. The MMD for this example is 0.27 Gy.

(Reproduced from Sholom et al., 2011a)
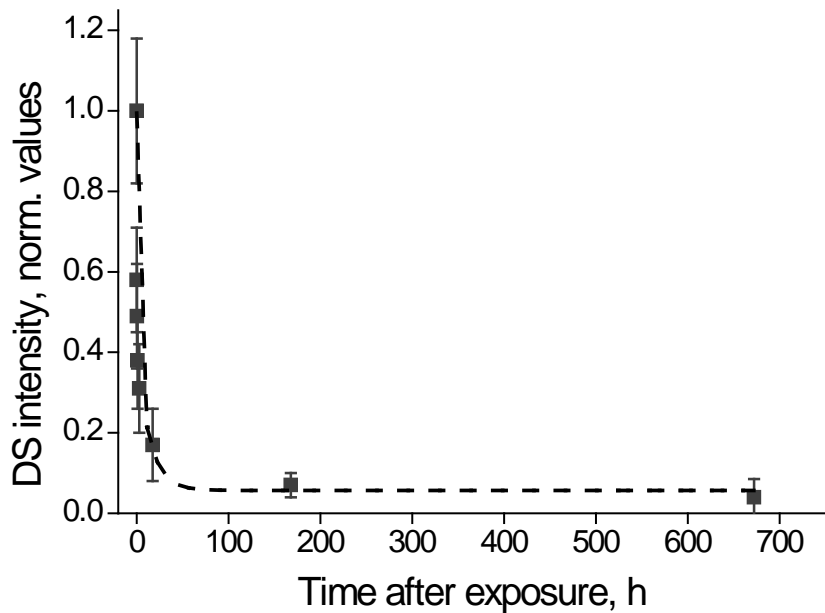
Figure 21

Fading of the OSL signal from human tooth enamel after irradiation. (Reproduced from Sholom and McKeever, 2011a)
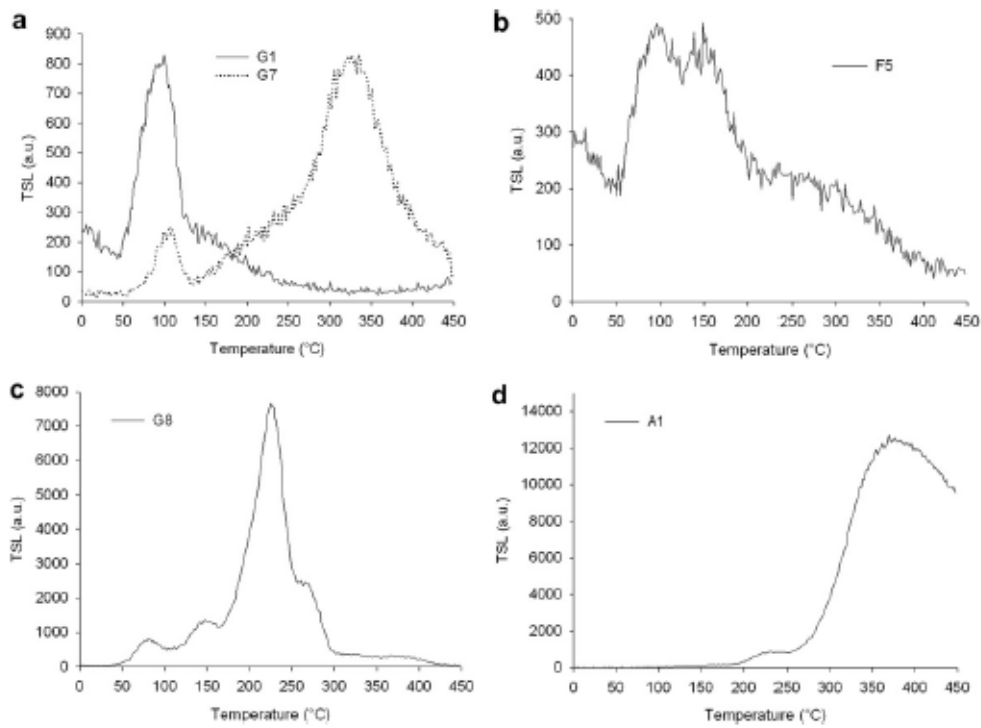
Figure 22

TL glow curves from (a) glass ceramic veneer; (b) feldspathic ceramic veneer; (c) glass ceramic core; (d) alumina-based ceramic core. (Reproduced from Veronese et al., 2010)
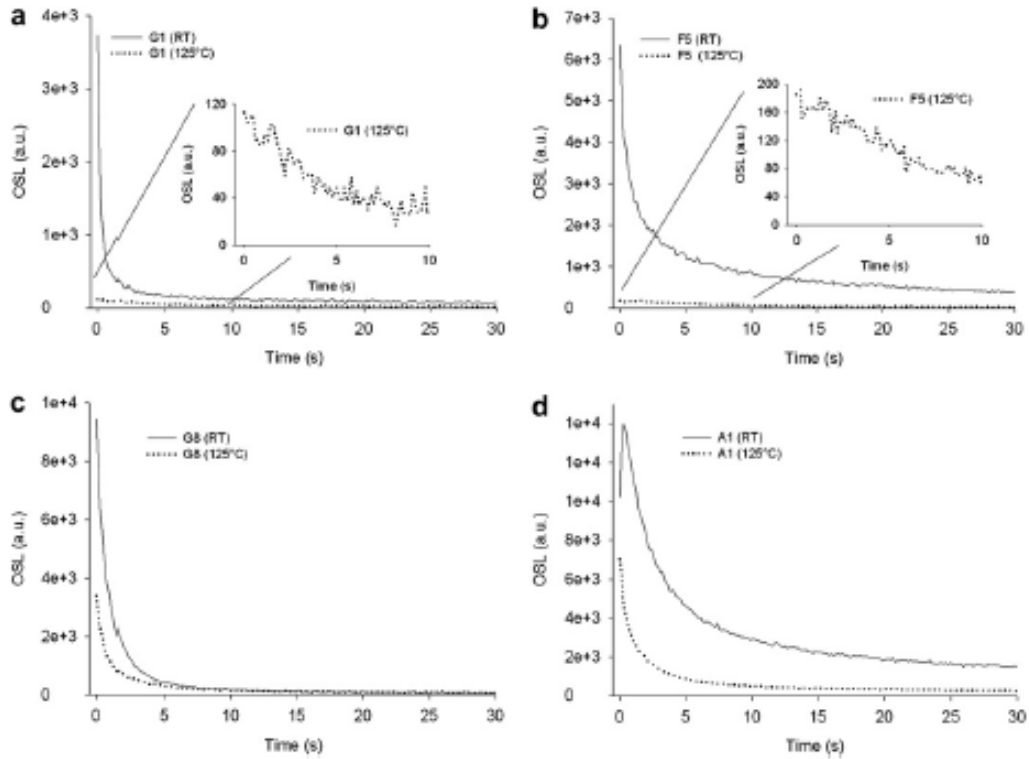
Figure 23

OSL glow curves from: (a) glass ceramic veneer; (b) feldspathic ceramic veneer; (c) glass ceramic core; (d) alumina-based ceramic core. The insets in figures 23(a) and (b) show the initial parts of the decay. (Reproduced from Veronese et al., 2010)
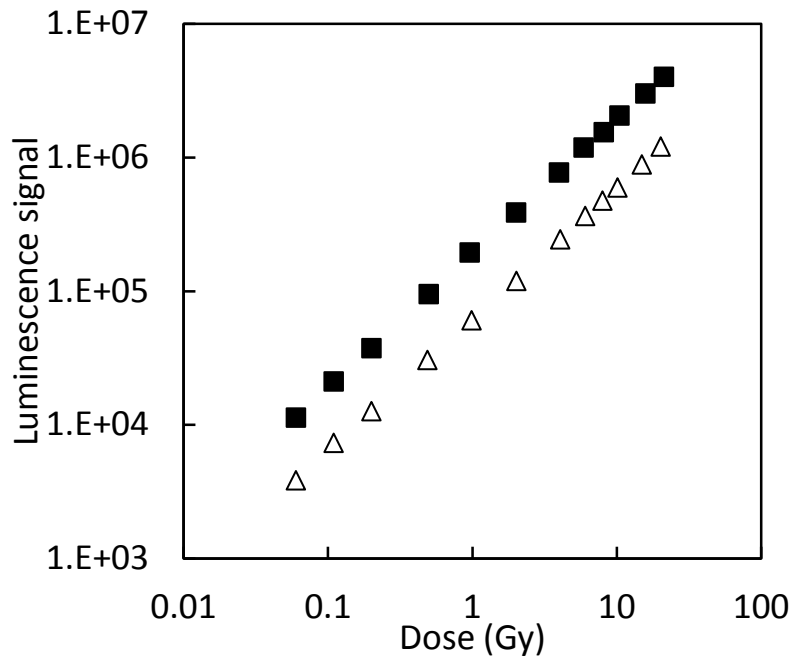
Figure 24. Linear dose responses for OSL and TL from fluorapatite glass dental ceramics. (Reproduced from Ekendahl et al., 2013)
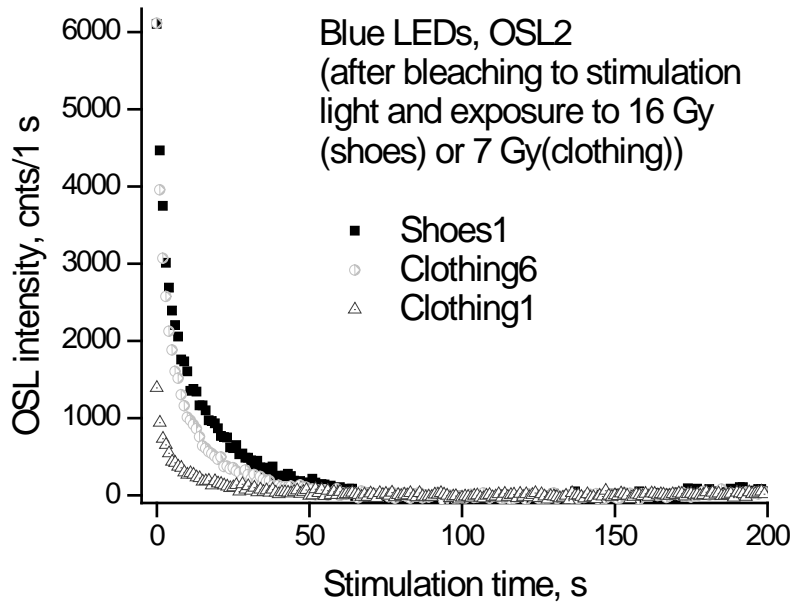
Figure 25

Blue-light (470 nm) stimulated OSL (recorded at 340 nm) from irradiated clothing and shoes. (From Sholom and McKeever, 2014a; reproduced with permission.)
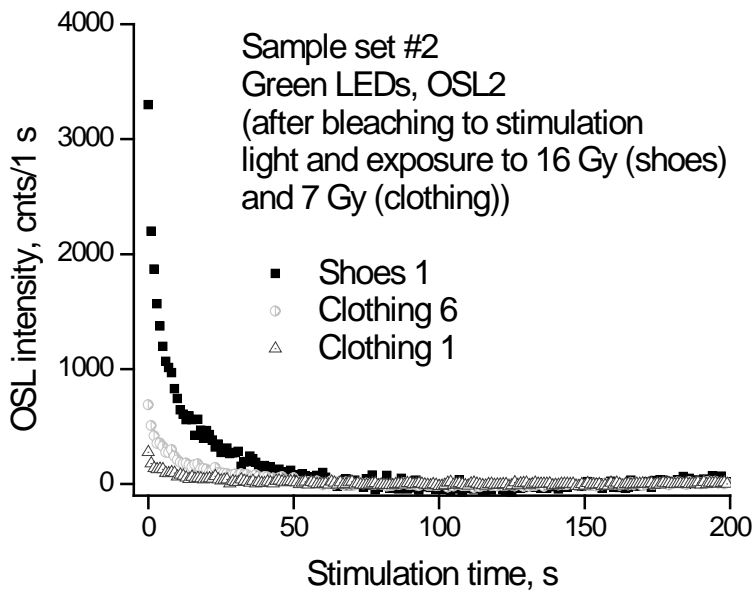
Figure 26

Green-light (530 nm) stimulated OSL (UV range) from irradiated clothing and shoes. (Reproduced from Sholom and McKeever, 2014a)
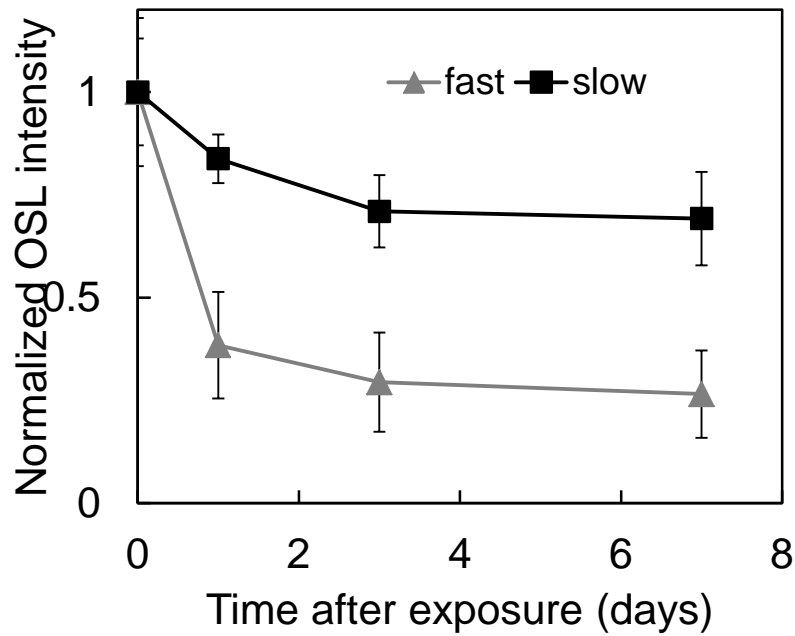
Figure 27

Representative fading curves for clothing, showing the "fast" and "moderate" fading curves obtained for the materials examined. (Re-plotted data from Sholom and McKeever, 2014a.)
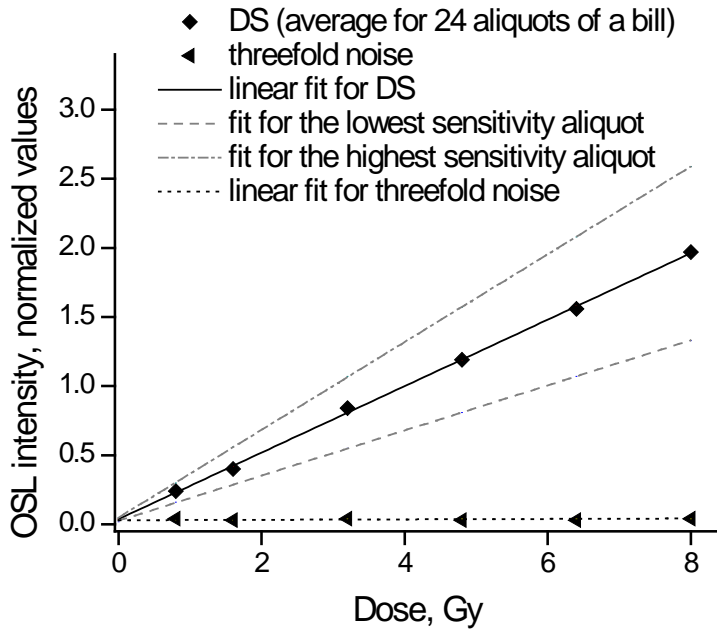
a)
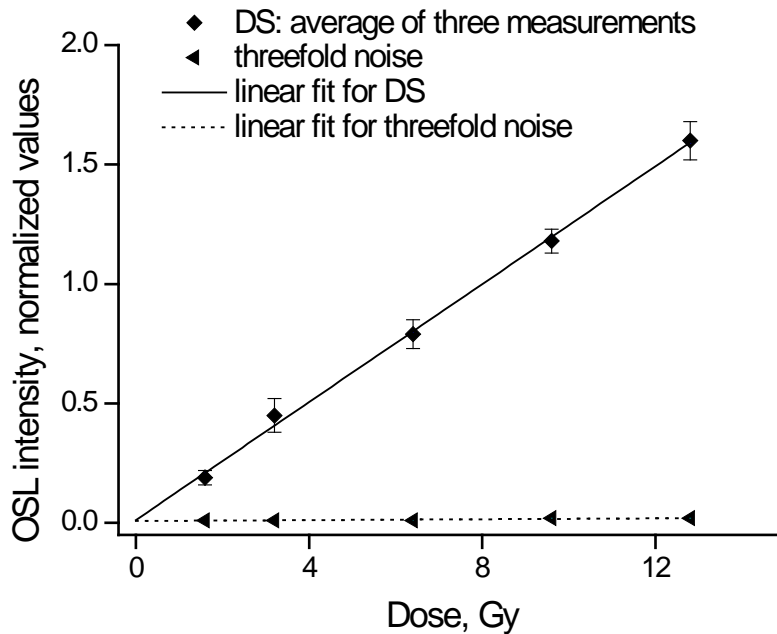
b)

Figure 28

(a) Dose response for a US $1 bill. The average of all aliquots is plotted with a linear fit (full line). Also, shown are the linear fits but for the highest (dotted line) and lowest (dashed line) sensitivities, illustrating the spread in sensitivities for the samples – all taken from the same $1 bill. Also shown is the linear fit for the 3σ-noise. (b) Dose response for an example plastic card. A linear fit through the data s shown, along with a fit of the 3σ-noise. (Reproduced from Sholom and McKeever, 2014a)
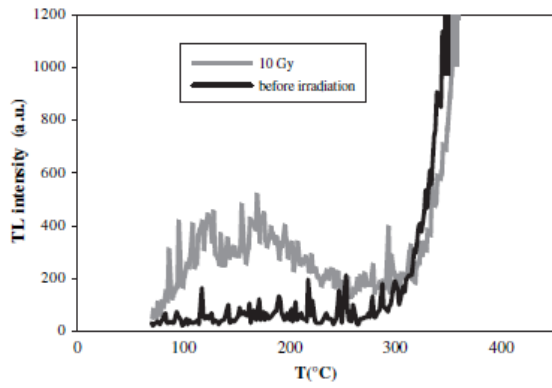
a)
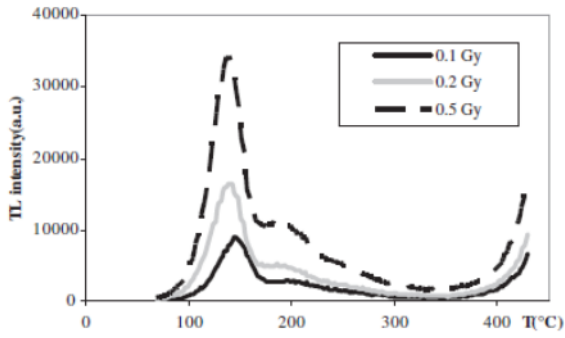
b)
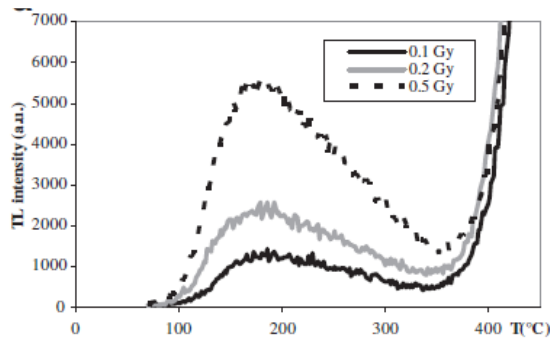
c)

Figure 29

TL glow curves for irradiated dust from (a) a hairband, (b) tobacco, and (c) keys. A variety of curve shapes is seen, suggesting different minerals. (Reproduced from Bortolin et al., 2010 (curve a) and Bortolin *et al*, 2011 (curves b and c).
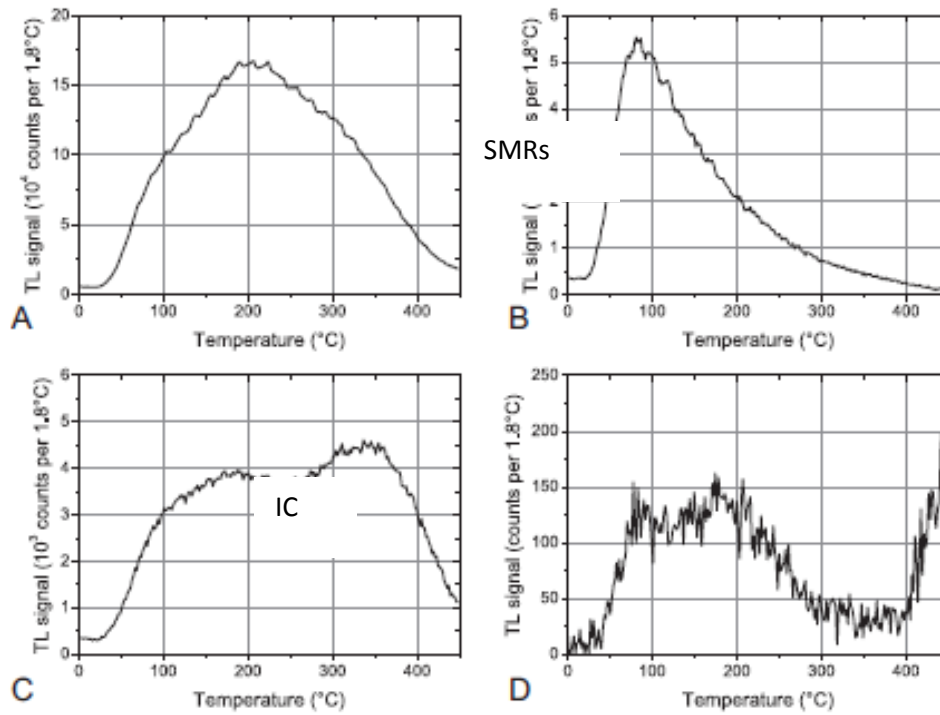
Figure 30

TL glow curves from pre-heated smartphone glass displays, after irradiation with 1 Gy ^{90}Sr/^{90}Y beta particles, showing four typical and different glow curve shapes. (Reproduced from Discher and Woda, 2013)
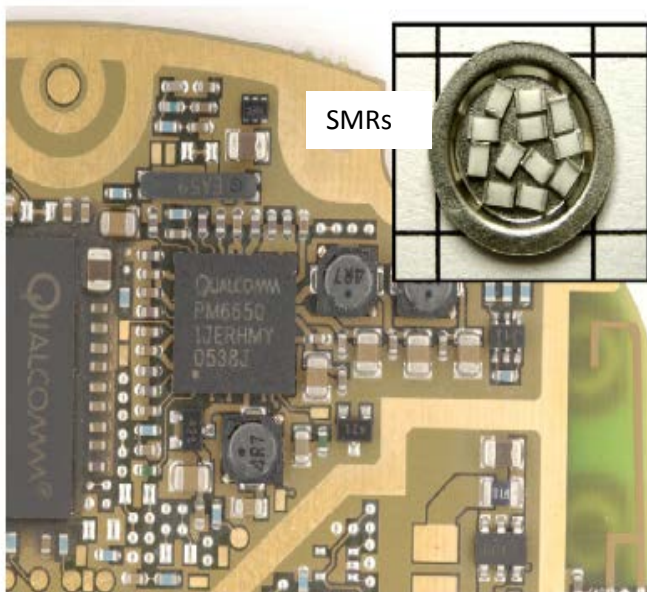
Figure 31

Surface-mount resistors (SMRs) from a mobile phone. (Reproduced from Inrig et al., 2008)
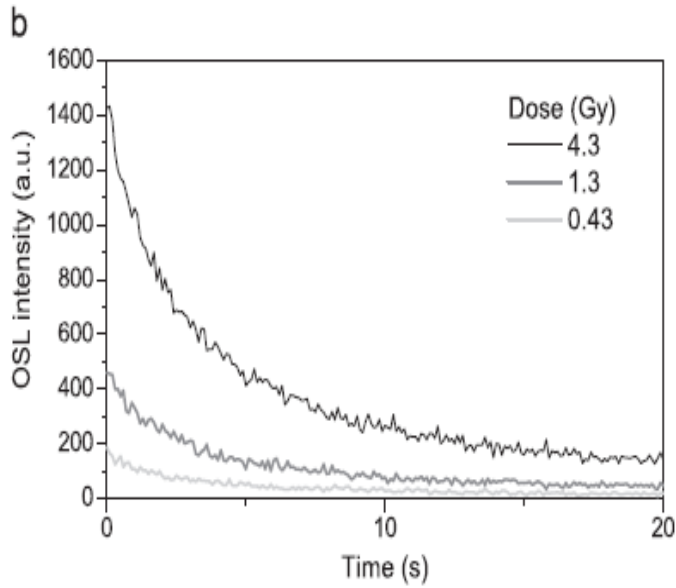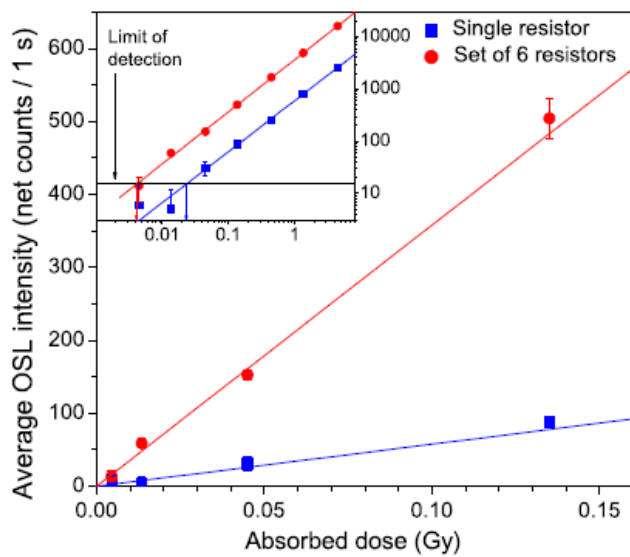
Figure 32

OSL decay curves (a) and dose response curves (b) for SMRs from mobile phones. (Reproduced from Inrig et al., 2008)
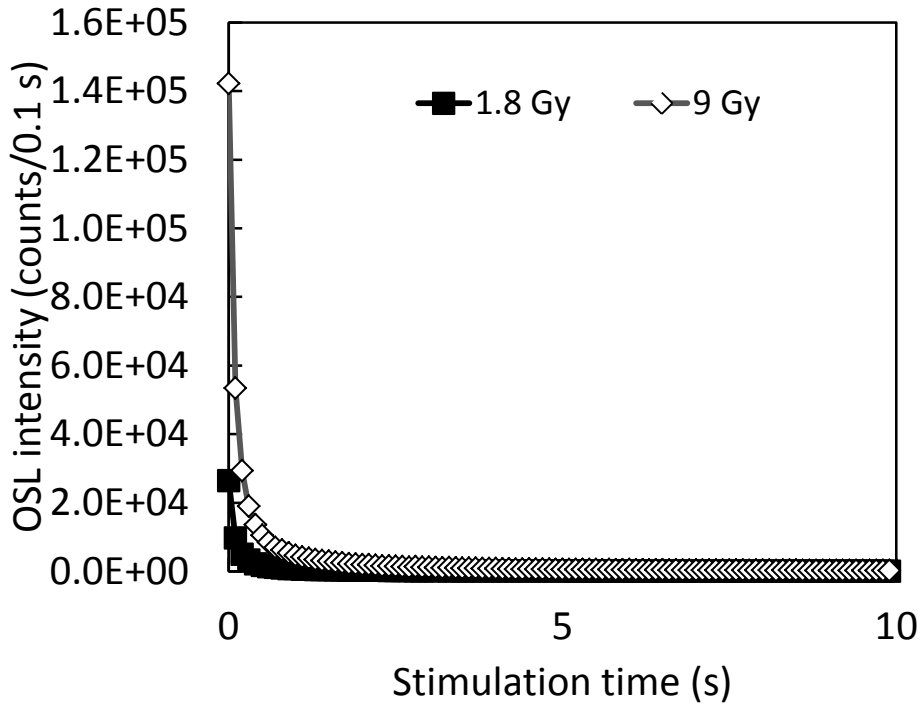
a)
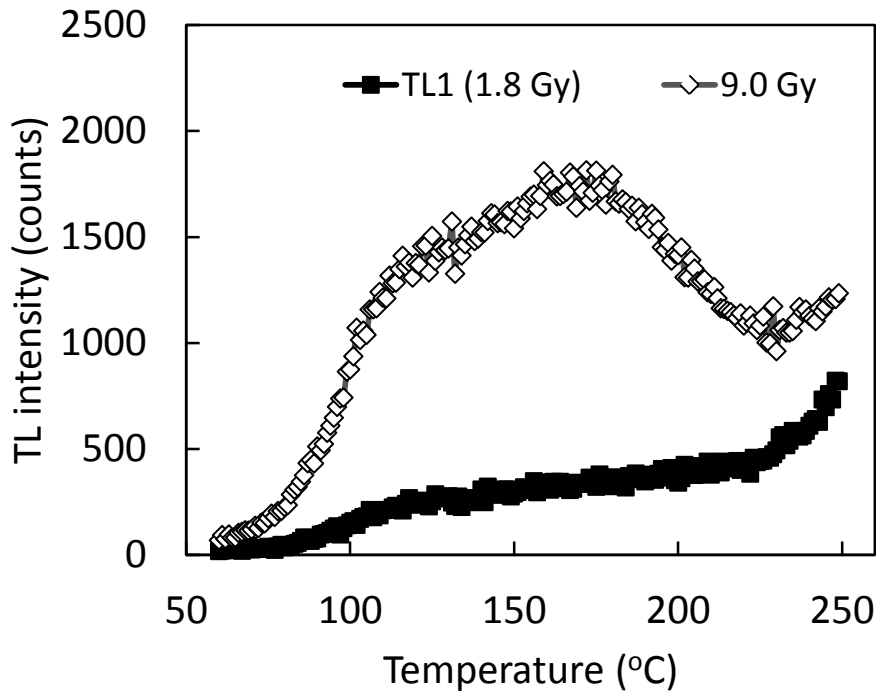
b)

Figure 33

OSL (a) and TL (b) signals from ICs extracted from mobile phones. (Re-plotted data from Sholom and McKeever, 2014b.)
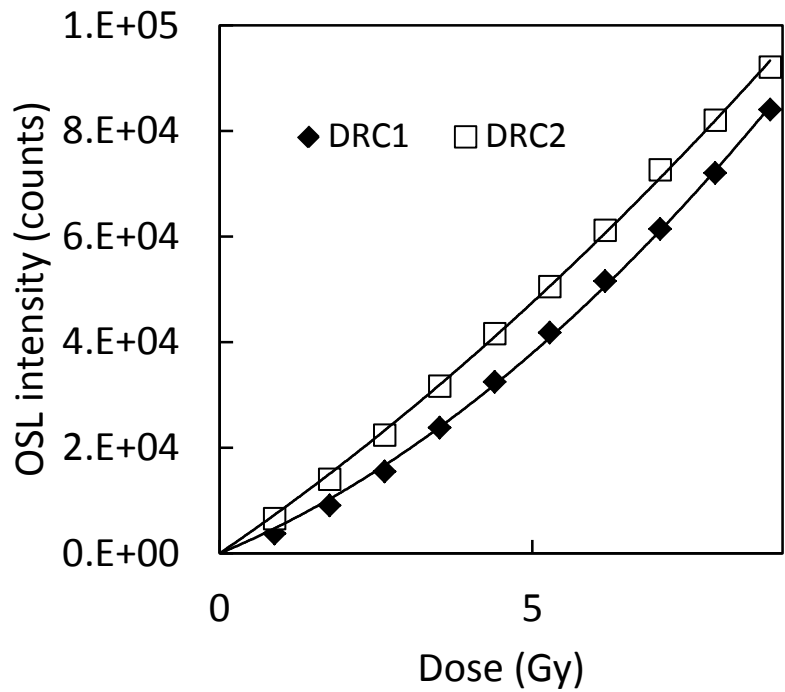
a)
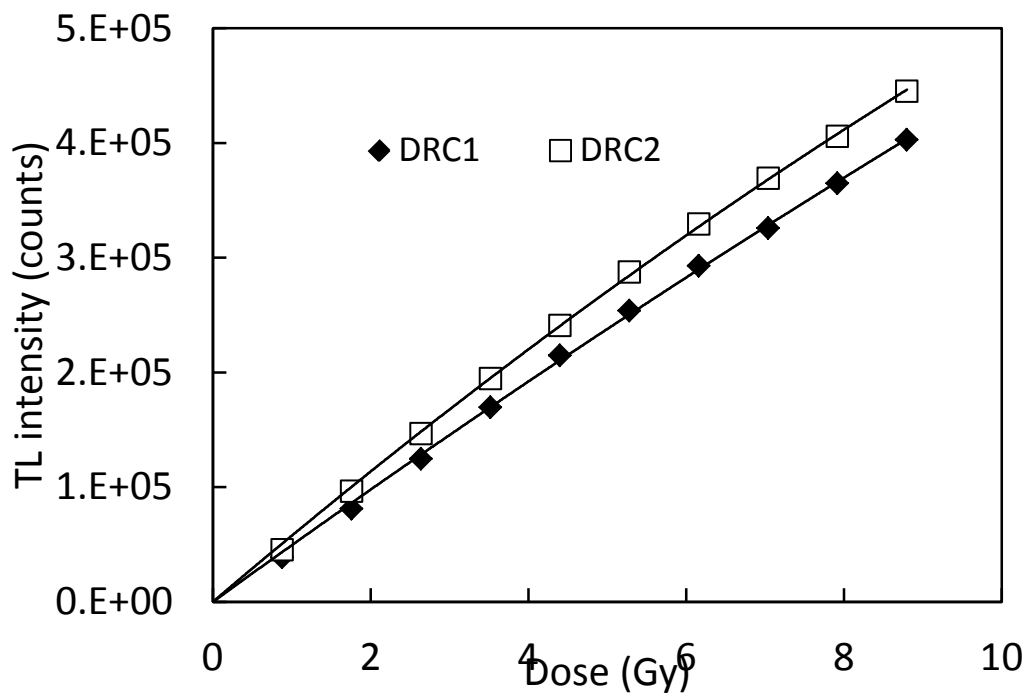
b)

Figure 34

OSL (a) and TL (b) dose response curves (DRC) from ICs extracted from mobile phones. The non-linear nature of the curves reflect sensitivity changes which are observed when the dose response is repeated a second time. (Re-plotted data from Sholom and McKeever, 2014b.)
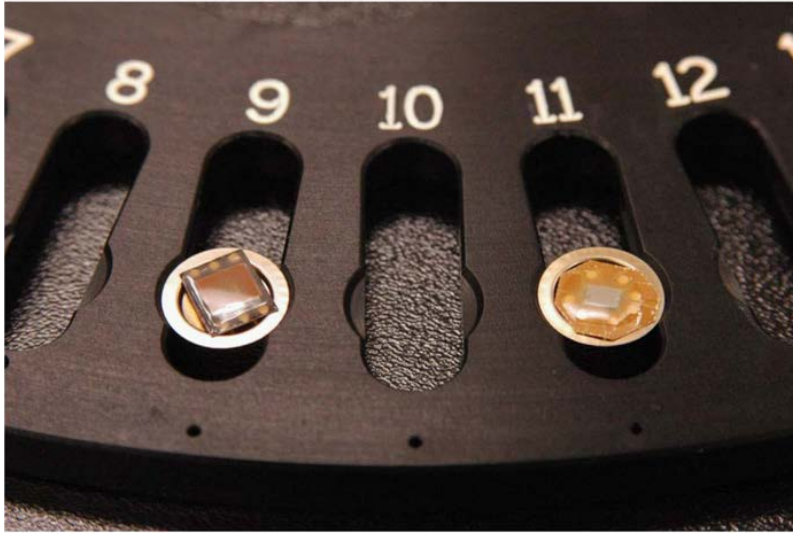
Figure 35

Epoxy encapsulated memory chips from chip cards, showing the epoxy resin that contains the silicate filler materials used to give the OSL signal. (Reproduced from Mathur et al., 2007)
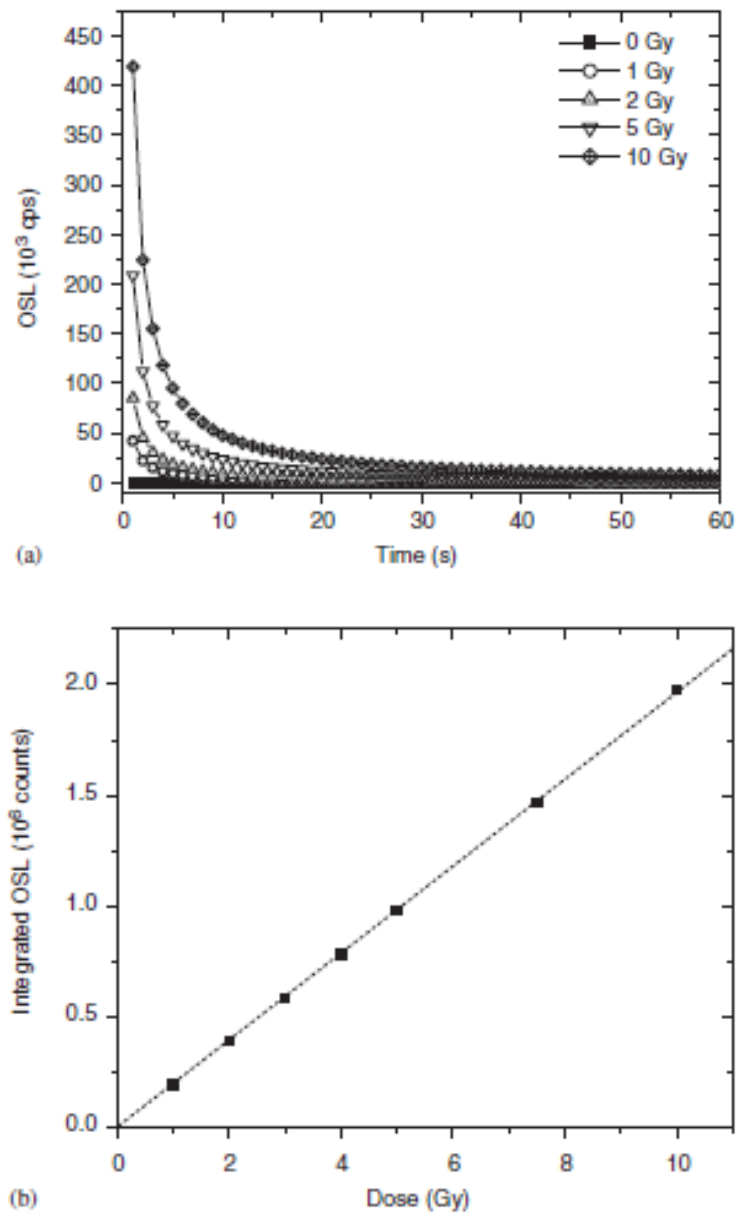
Figure 36

(a) Blue-stimulated OSL curves from epoxy-encapsulated chip cards, and (b) dose response curve for a beta-irradiated sample. (Reproduced from Mathur et al., 2007)
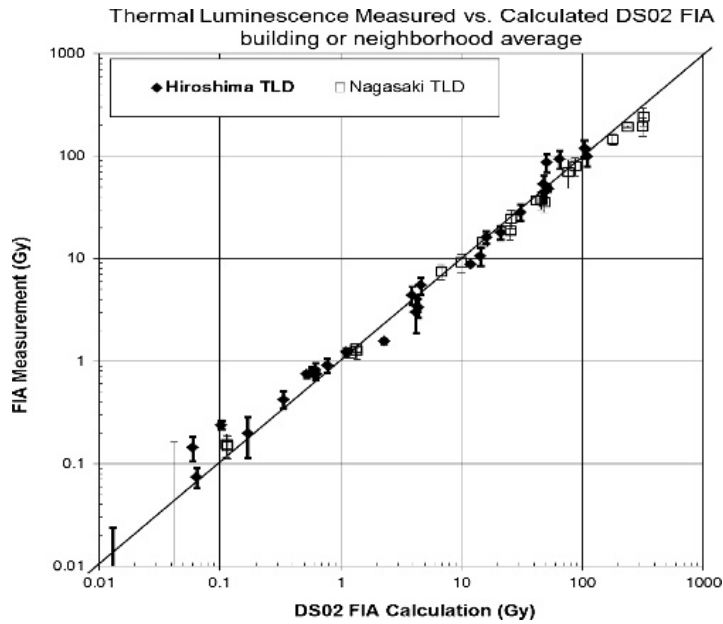
Figure 37

Comparison of measured values (TL) with DS02 calculated values of free-in-air (FIA) absorbed dose from gamma-rays at 1 m above ground at Hiroshima and Nagasaki. At ground ranges of 0, 500, 1000, 1500, 2000, 2500 m, the dose values for Hiroshima are 120, 35.7, 4.22, 0.527, 0.0764, 0.0125 Gy, and for Nagasaki they are 328, 83.0, 8.62, 0.983, 0.138, 0.0228 Gy. (Reproduced from Kerr *et al.*, 2015)
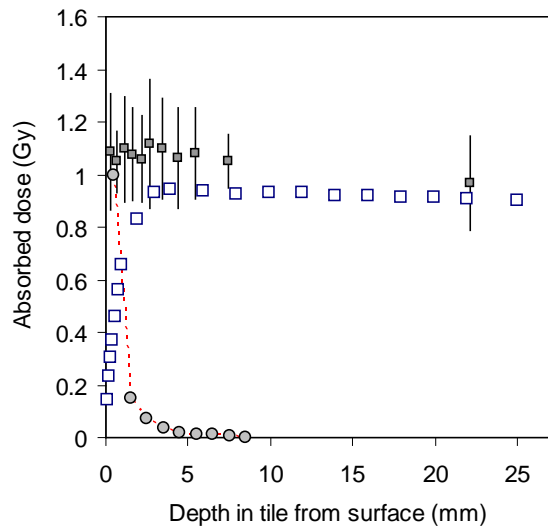
Figure 38

Depth-dose profiles. Comparison of a) measured depth-dose profile in a tile sample taken from an old Hiroshima University building (H4 at 1324 m ground range), using a single-grain OSL technique applied to coarse quartz crystals extracted from the ceramic (filled squares). A high-density glazed opaque surface layer was removed from the tile prior to measurements; b) measured relative profile in Al_2O_3:C crystals exposed to beta particles from a $^{90}Sr/^{90}Y$ source (filled circles); c) calculated profile obtained by Monte Carlo radiation transport simulation of dose due to photon irradiation (^{60}Co) of the tile (open squares). (From Workshop presentation by Prof. V. Stepanenko; replotted data from Kerr et al., 2015.)
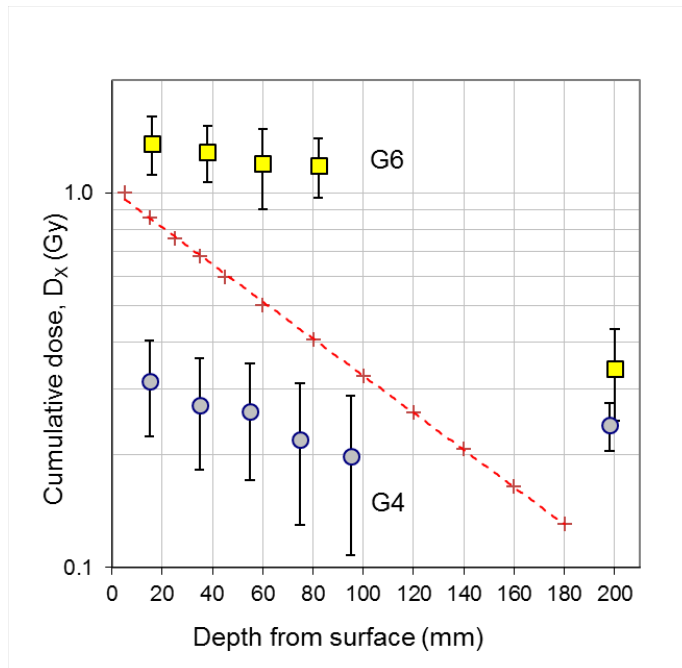
Figure 39

Depth-dose profiles for external bricks from locations in Belarus in the distal settlement G4 (filled circles) and the proximal settlement G6 (filled squares); for locations see map in Supplementary Material (Figure SM1). The bricks were taken at a height of 1 m above ground from single storey brick dwellings. The cumulative natural background dose due to lithogenic sources were subtracted from the values of cumulative dose due to fallout, D_X, shown in the plot. The dotted line represents the calculated reduction in dose with depth for ^{137}Cs sources distributed uniformly on flat ground facing the wall. The values of D_X plotted on the RHS of the graph were obtained with the interior brick and assumed to be located at the depth equivalent to a typical double wythe wall (~200 mm). (Replotted data from Sato et al., 2002.)

Figure 40

Map showing the location of settlements referred to in this review, including Zaborie, Vesnianoje and Stary Vishkov, relative to Chernobyl.
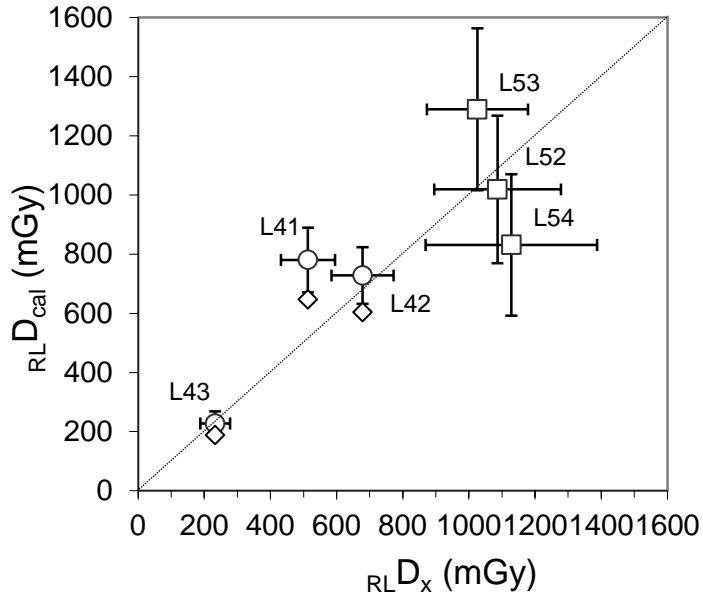
Figure 41

Relationship between estimates of cumulative dose (1986-1997) at the Reference Location obtained by luminescence, $_{RL}D_x$ and by computation, $_{RL}D_{cal}$, for locations in Zaborie (open circles, Inst. Radiation Health model; open diamonds, Medical Radiological Research Centre model) and Vesnianoje (open squares). The dotted line represents a line of concordance. For clarity the error bars for the MRRC model data are not shown. (Data replotted from Bailiff et al., 2004a.)
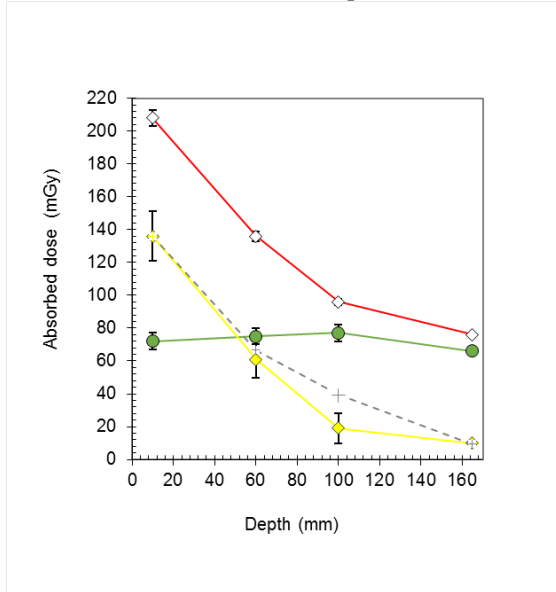
Figure 42

Depth-dose profiles in brick for Location 55, Stary Vishkov, showing values of D_T (open diamonds), D_{BG} (filled circles) and D_x (filled diamonds) at three or more depths from the surface of the exposed brick. The calculated depth profile (small cross), calculated by MC simulations for E=662 keV and assuming that the sources were distributed on the ground to a depth of 1-6 g cm^{-2}, normalised to the value of D_x for the outermost sample, is also shown for comparison. Where the depth is greater than ~125 mm, the sample was extracted from an inner wall. (Data replotted from Bailiff et al., 2005.)
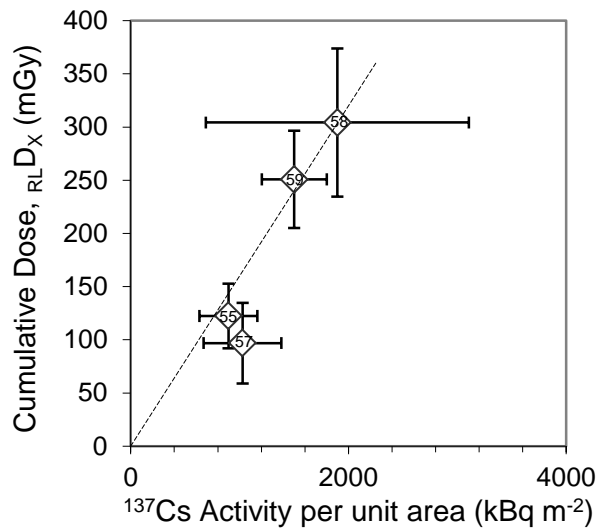
a)
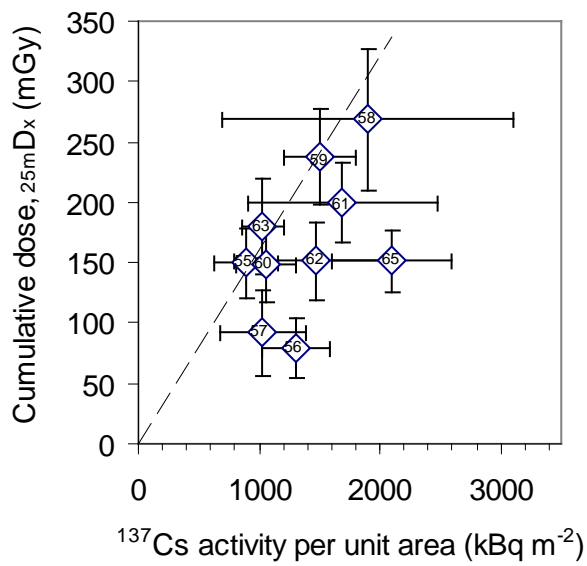
b)

Figure 43

Relationship between estimates of cumulative dose obtained by luminescence at (a) the Reference Location, $_{RL}D_X$, and (b) averaged over 25 m adjacent to the sampled wall, $_{25m}D_X$, and the average ^{137}Cs areal activity (kBq m[-2]), A_a, adjusted to 1986, in the vicinity of the sampled building for selected locations in Stary Vishkov. The line represents the predicted values of cumulative dose obtained using a value of 0.16 mGy per kBq m[-2] for the coefficient D_Σ. The location numbers are indicated within the plot symbols. (Redrawn from Bailiff et al., 2005.)
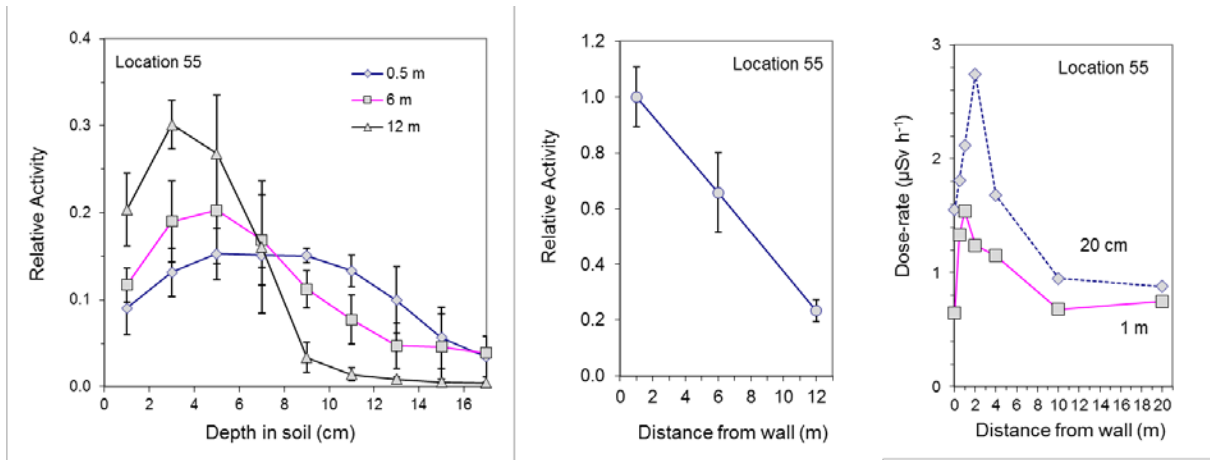
Figure 44

Characteristics of the deposition of ^{137}Cs in soil in the areas adjacent to the sampled building at Location 55, in Stary Vishkov, showing (1) the ^{137}Cs activity profile at different distances from the sampled wall, (2) the activity transect and (3) the dose-rate transect. (Redrawn from Bailiff et al. , 2005.)
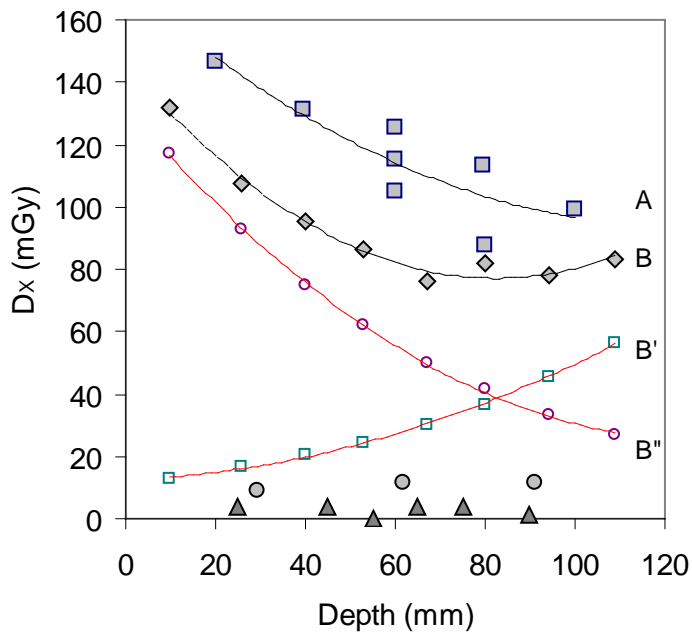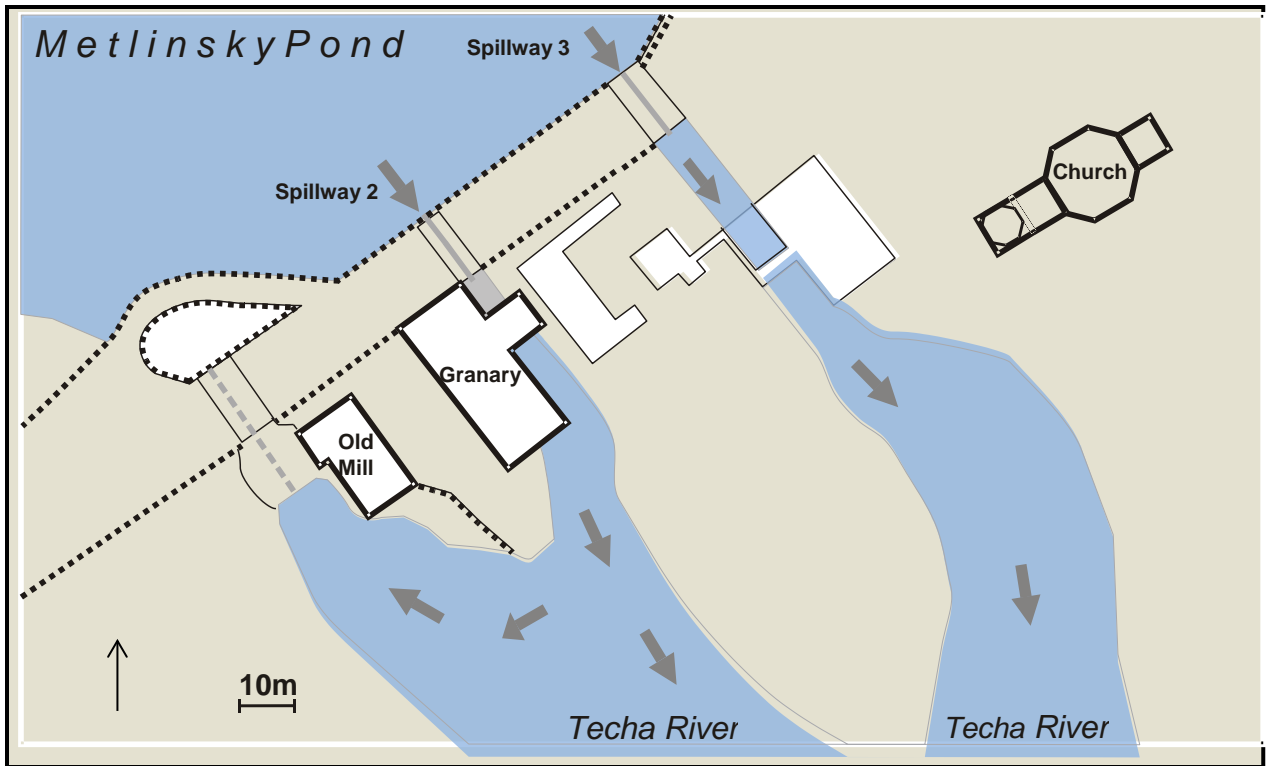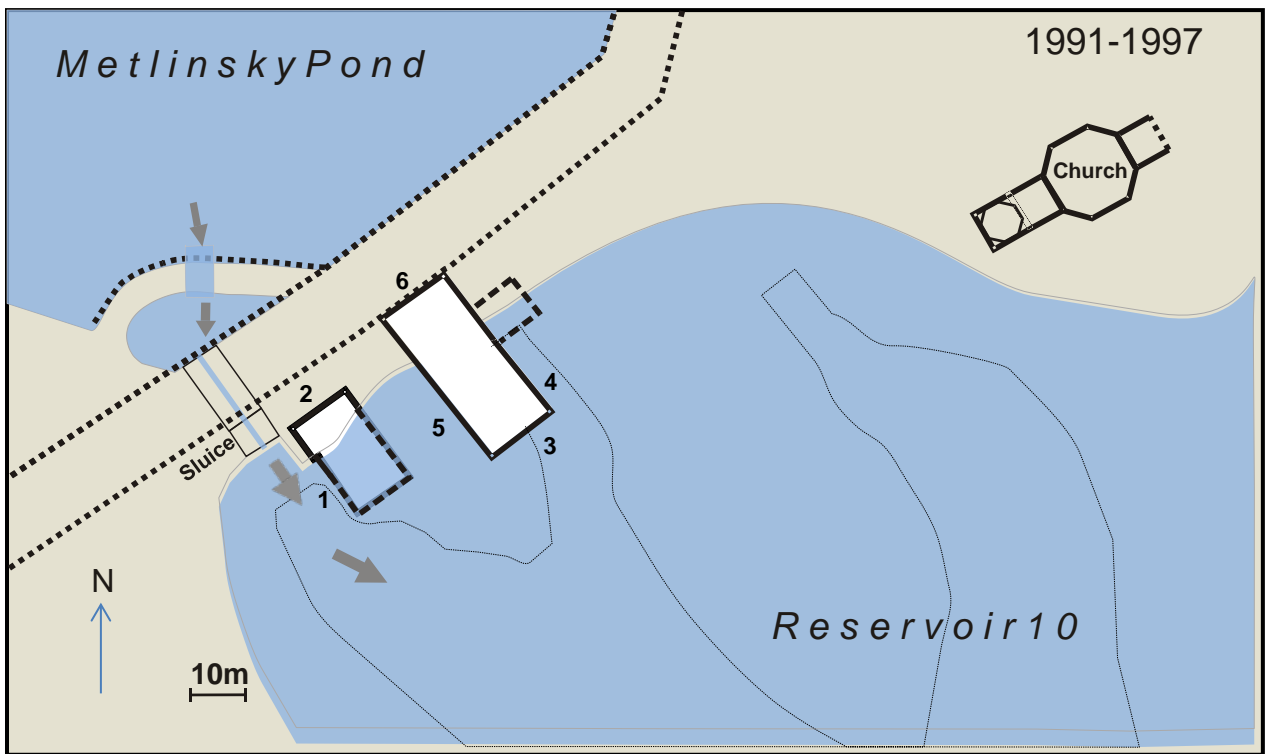

Figure 45

Depth-dose profiles obtained with a) exposed bricks in the walls of the hut (A, filled squares, corner; B, filled diamonds, mid-wall) and shielded bricks in the basement of a wooden house (filled circles and triangles) in Novie Bobovichi. The broken line fitted to the measured values of D_X for the hut mid-wall brick (filled diamonds) corresponds to the sum of two component depth-dose fitted to calculated data points indicated by B' (open squares) and B'' (open circles) related to ^{137}Cs sources distributed externally on the ground and on the hut roof, respectively, as discussed in the main text. (The measured data values are replotted from Ramzaev et al., 2008.)

a)

MetlinskyPond

Spillway 3

Spillway 2

Church

Granary

Old
Mill

10m

Techa River

Techa River

b)

MetlinskyPond

1991-1997

Church

6

2

4

5

3

Sluice

1

N

10m

Reservoir 10

Figure 46

Schematic maps illustrating the contamination history of the Metlino settlement during the periods a) 1949-1957 when the releases occurred, and b) 1991-1997, when brick sampling was performed; the locations of the sampled walls are indicated numerically (1-6) and discussed in the main text.

a) **1949-1957**. From 1949 to 1954 effluent from the Mayak Production Facility was directed downstream via the Techa River into the Metlinski Pond; the river flowed downstream via Spillways 2 and 3 since Spillway 1 had been blocked in 1949, accompanied by the construction of a 'crosspiece' barrier. This routing of water flow caused contamination to be transported past the E wall of the Granary via the W channel and past the church via the E channel. Fluvial sediment containing radionuclides was also transported into a catchment formed by what had become a backwater lying to the W of the Old Mill after closure of Spillway 1, and notably the section of river channel in this area was found to have the highest concentration of contamination (~500 Bq kg^{-1} of wet sediment; Degteva et al., 2008).

b) **1991-1997**. Following evacuation of the settlement in 1956, Reservoir 10 was created by constructing another dam further downstream, closing Spillways 2 and 3, and creating a sluice in the position of the old Spillway 1, which diverted all water flow from the pond past the Old Mill. At the time of brick sampling in 1997, two buildings and part of the Old Mill walls had collapsed, but most of the walls of the Granary were standing (shown in outline). The two riverbed channels and their associated banks with contaminated sediments were submerged by the creation of the reservoir, and presumably there was the potential for fluvial sediments to be gradually dispersed from the submerged riverbanks, along the floor of the reservoir, and towards its shores (Bougrov et al., 1995). Following evacuation, the installation of the sluice reintroduced a pathway for water flow past the SW facing wall of the Old Mill and the construction of a causeway N of Spillway 1 changed the source geometry for the NNW facing wall of the Old Mill since it is distanced further from the pond shore compared with the NNW facing wall of the Granary.

(After Fig. 4 in Degteva et al., 2008; redrawn using graphic elements kindly supplied by Dr. N.G. Bougrov.)
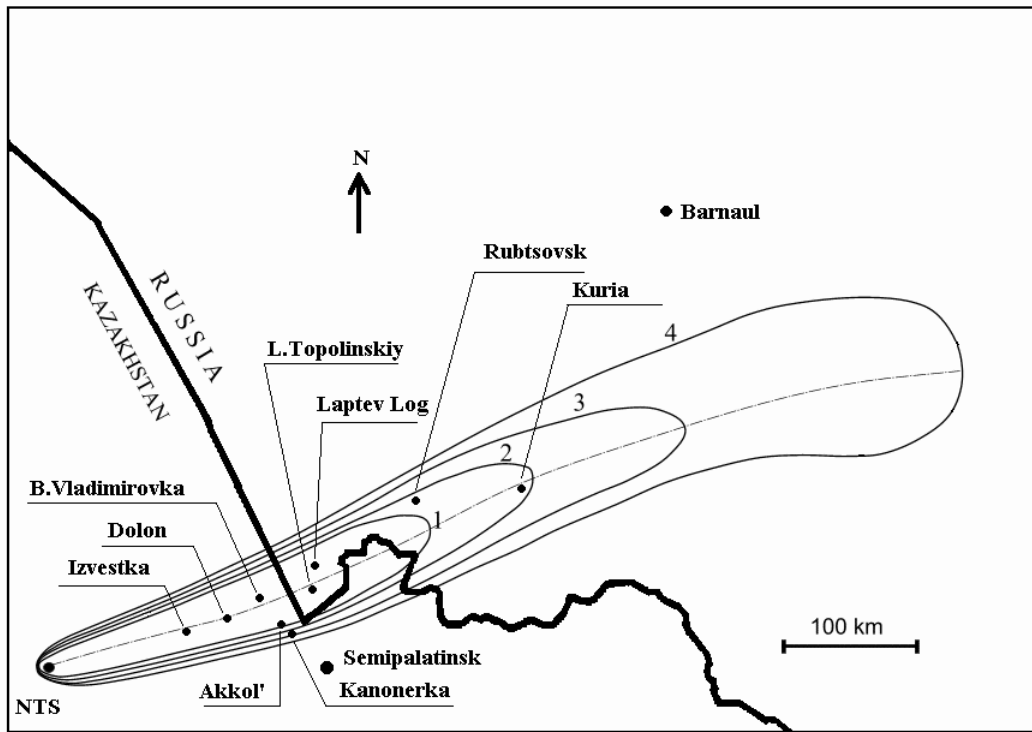
Figure 47

Regional map showing the relationship between the Semipalatinsk Nuclear Test Site (NTS) major cities and sampled settlements. The dose contours associated with the plume from the 1949 tests are based on calculations by Shoikhet et al. (1998); the contour values correspond to the following levels of cumulative dose: 1 (250 mSv); 2 (50 mSv); 3 (10 mSv); 4 (1 mSv). (Reproduced from Bailiff et al., 2004b)

Figure SM.1

Map showing the location of the sampling sites and the surface ground contamination levels. This map is a simplified version of the Surface Contamination Maps published by the International Advisory Committee. (Reproduced from Sato et al., 2002.)

Figure SM.2

Cumulative dose determinations at the surface of interior and exterior bricks, expressed as tissue dose, plotted against cumulative dose calculated for the period 1986-1994 on the basis of glass dosimeter measurements at exterior and interior sample locations. The dotted line represents linear regression line for the exterior samples (filled circles). (Reproduced from Sato et al., 2002)

Supplementary Material

Figure SM1.

Map showing the location of the sampling sites and the surface ground contamination levels. This map is a simplified version of the Surface Contamination Maps published by the International Advisory Committee. (Reproduced with permission from Sato et al., 2002.)
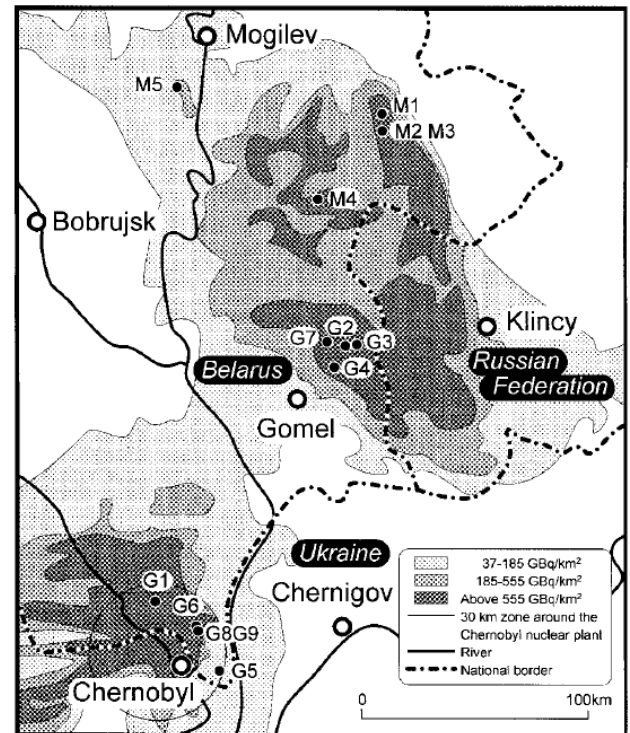

Figure SM.2

Cumulative dose determinations at the surface of interior and exterior bricks, expressed as tissue dose, plotted against cumulative dose calculated for the period 1986-1994 on the basis of glass dosimeter measurements at exterior and interior sample locations. The dotted line represents linear regression line for the exterior samples (filled circles). (Reproduced with permission from Sato et al., 2002)
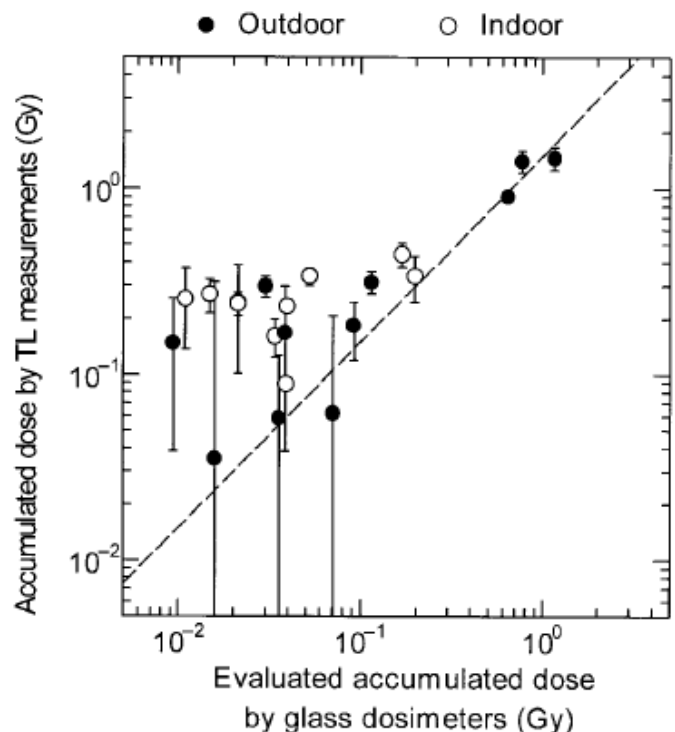
Table SM.1

Values of cumulative dose due to fallout, D_X, expressed as tissue dose, determined by applying an additive dose TL measurement procedure to quartz coarse grains, and identifying a plateau within the temperature range 180-300 °C of the glow curve. Corrections for attenuation were applied to the experimental values to obtain values of D_X at the exposed surface of the brick. The location of the settlements from which the samples were obtained are shown in Figure SM.1.

(Data from Sato et al., 2002.)

Sample Location	Exterior (Gy)	Interior (Gy)
M1	-	0.089±0.005
M2	0.058±0.069	0.699±0.079
M3	0.298±0.039	0.230±0.029
M4	0.313±0.043	0.161±0.037
M5	0.148±0.109	-
G1	0.183±0.064	0.338±0.035
G2	0.062±0.146	0.207±0.095
G3	0.067±0.140	0.244±0.143
G4	0.333±0.040	0.241±0.035
G5	0.035±0.280	0.256±0.120
G6	1.453±0.203	0.340±0.094
G7	0.168±0.129	0.270±0.055
G8	1.394±0.188	0.444±0.065
G9	0.908±0.052	0.232±0.014